Biofluid Analysis to Differentiate Brain Disease

Alex Dickens

New College, University of Oxford



A thesis submitted for the degree of Doctor of Philosophy
Gray Institute for Radiation Oncology and Biology
University of Oxford

Michaelmas Term 2011

Abstract

It has been demonstrated that by using ^{1}H NMR spectroscopy in combination with multivariate statistical modelling (PLS) it is possible, using urine samples obtained from rats, to distinguish between different types of CNS lesions. Against this background this thesis will explore whether the combination of ^{1}H NMR and PLS modelling on biofluids can be used to identify biomarkers in different neurological diseases and in clinically relevant animal models of neurologic disease. The results in this thesis demonstrate that it is possible to separate sets of animals at different stages of disease in models of multiple sclerosis and to identify the presence of early brain metastasis. The same methodology was also applied to human biofluids. In MS patient cohorts (RR-MS, PP-MS and SP-MS) it was also possible to differentiate between RR-MS and SP-MS as well between MS and healthy controls. Therapy for these two stages of MS are very different and therefore a rapid test to determine a patient's stage of MS would be hugely beneficial in the clinic. Further investigation revealed that it is possible to separate MS patients from individuals with Alzheimer's disease. Metabolomics was then combined with other co-variants in a study of cerebrospinal fluid obtained from patients with HIV associated dementia (HAD) to discover whether disease progression could be followed in this manner. The results show that it is possible to detect neurocognitive changes in patients with HAD. Indeed, the results demonstrate that metabolomics is a far more sensitive tool for the following progression than other non-PLS biomarker techniques and should provide a useful method for early diagnosis of CNS disease and the evaluation of therapy in prospective studies.

Acknowledgements

I am extremely grateful for this opportunity to pursue my DPhil studies, and I have many people that I would like to thank.

First, I wish to say thank you to my two supervisors Dr. Nicola Sibson and Dr. Daniel Anthony, without whom this thesis would not have been possible. Their help and supervision have been invaluable throughout the whole course of my DPhil studies. I would also like to thank them for all their patience and support during the writing of this thesis. I have immensely enjoyed being a member of both laboratories.

A special thanks must go Professor Ben Davis, Dr. Jacqueline Palace, and Dr. Norman Haughey. To Ben for allowing me to occasionally work in his laboratory during my studies, and to Jackie and Norman, for providing me with all the human samples used in this thesis.

I would like to thank Dr. Tim Claridge and Dr. Julian Griffin for their technical expertise and guidance. The NMR experiments would not have been possible without Tim's help, and I also wish to thank him for all his advice during the analysis of the spectra in this thesis. Jules initially taught me how to use SIMCA, and therefore, all the modelling in this thesis would not have been possible without his help.

A big thank you must go to the Medical Research Council for funding my 3 years of DPhil study at Oxford. I would also like to thank the members and fellows of New College for a memorable seven years at Oxford.

I would also like to thank all the members of the Anthony, Davis and Sibson labs for making these last three years enjoyable. Specifically I would like to thank Yvonne Couch for her figure drawing skills, and Matthew Evans, Emma O'Brien, Dr. Sandra Campbell, and Dr. Sebastien Serres for their friendship and putting up with me on daily basis. A big thank you must also go to Dr. James Larkin for trying to pick through my work. I would like to say a special thank you to Dr. Helen Stolp for proofreading this thesis and for providing invaluable advice and guidance.

Finally, this thesis would not have been possible without the support of my family and my girlfriend Annie. Their help and support during this thesis has been vital and I would not have finished this thesis without them.

Presentations related to this thesis

Publications

Dickens A.M., Anthony D.C., Claridge T. D. W., Mardiguian S., Cavey A., Davis B.G., Griffin J.L., Campbell S.J., Palace J., Sibson N.R. PLS models discriminate types of MS from spectroscopic analysis of plasma and urine. Multiple Sclerosis. 2009 Sep;15(9)S275.

Sibson N.R., Anthony D.C., van Kasteren S., **Dickens A. M.,** Perez-Balderas F., McAteer M.A., Choudhury R.P., Davis B.G. Molecular MRI approaches to the detection of CNS inflammation. Methods in Molecular Biology. 2011; 7111:379.

Dickens A.M., Anthony D. C., Griffin J. L., Cavey A., Matthews L., Davis B.G., Claridge T.D.W., Palace J., Sibson N.R. 2011. A reliable method for differentiating between different disease states in an animal model of multiple sclerosis and in multiple sclerosis patients. (under review).

Posters

Dickens A.M., Anthony D.C., Claridge T.D.W., Mardiguian S., Cavey A., Davis B.G., Griffin J.L., Campbell S.J., Palace J., Sibson N.R. Partial least squares models discriminate stages of multiple sclerosis from spectroscopic analysis of plasma. 7th FENS forum in Amsterdam, Netherlands, 2010 and Young Physiologists Society meeting, Oxford, UK 2011 (poster prize).

Dickens A.M., Claridge D.C., Larkin, J.R., Hamilton A., O'Brien E., Anthony D.C., Sibson N.R. A metabolomics approach for the early diagnosis of brain metastasis. NCRI Cancer Conference 2011. Liverpool, UK.

Table of Contents

Abstract ..... **i**

Acknowledgements ..... **ii**

Presentations related to this thesis ..... **iii**

Table of Contents ..... **iv**

Table of Figures ..... **xiii**

Table of Tables ..... **xvi**

List of Abbreviations ..... **xviii**

Chapter 1 : Introduction **1**

1.1. General introduction 1

1.1.1. Aims of this Thesis 2

1.2. Biomarkers 4

1.2.1. General 4

1.2.2. Overview of techniques used for biomarker identification 7

1.3. Metabolomics 13

1.3.1. General 13

1.3.2. Analytical techniques used in metabolomics 14

1.4. NMR Spectroscopy 17

1.4.1. General 17

1.4.2. Principles of NMR 17

1.4.3. NMR techniques for metabolomics 20

1.4.4. Previous NMR studies in metabolomics 23

1.5. Overview of Multiple Sclerosis 26

1.5.1. Prevalence of MS 26

1.5.2. Aetiology of MS 27

1.5.3. Clinical course of MS 30

1.5.4. Current diagnostic criteria for MS 37

1.5.5. Animal models of MS 48

1.5.6. Previous biomarker studies in MS 49

1.6. Alzheimer's disease 51

1.6.1. General 51

1.6.2. Prevalence of AD 51

1.6.3. Clinical course of AD 52

1.6.4. Current diagnostic criteria for AD 56

1.6.5. Previous biomarker studies in AD 60

1.7. Human immunodeficiency virus associated dementia 62

1.7.1. General 62

1.7.2. Prevalence of HIV associated dementia 62

1.7.3. Clinical course of HIV associated dementia 63

1.7.4. Neuropathology and pathogenesis of HIV associated dementia 64

1.7.5. Diagnosis of HIV associated dementia 66

1.8. Cancer metastases to the brain 67

1.8.1. General 67

1.8.2. Prevalence of brain metastases 67

1.8.3. Formation of brain metastases 67

1.8.4. Clinical symptoms of brain metastases 71

1.8.5. Treatment of brain metastases 71

1.8.6. Current diagnostic tools for brain metastases 75

1.8.7. Previous biomarker studies for brain metastasis 75

1.9. Overview of thesis 78

Chapter 2 : Materials and Methods 80

2.1. Animals 80

2.2. Human samples 80

2.3. Reagents 80

2.4. Cancer cell lines 80

2.5. *In vivo* protocols 81

2.5.1. Anaesthesia 81

2.5.2. Killing *via* overdose of an anaesthetic agent 81

2.5.3. Sample Collection 81

2.6. NMR spectroscopy 82

2.6.1. NMR phosphate buffer 82

2.6.2. Sample preparation 82

2.6.3. NMR experiments 82

2.7. Statistical analysis 83

2.7.1. Bucket integration 83

2.7.2. PLS modelling 84

2.7.3. Reasons for spectral exclusions 84

2.7.4. Model validation 85

2.7.5. Metabolite identification 87

2.7.6. Exclusion of regions within the spectra 92

2.7.7. Spiking experiments 92

Chapter 3 : Metabolomic changes in Multiple Sclerosis 93

3.1. Introduction 93

3.1.1. Aims of Chapter 94

3.2. Materials and Methods 95

3.2.1. Animal Experimental Design 95

3.2.2. Human Experimental Design 97

3.2.3. NMR Spectroscopy and Data Analysis 97

3.2.4. Metabolite identification 98

3.2.5. Spiking experiments 100

3.3. Results 101

3.3.1. Cr-EAE: Animal Model 101

3.3.2. Initial Models 101

3.3.3. Cr-EAE: Urine analysis 104

3.3.4. Cr-EAE: Plasma analysis 110

3.3.5. Human MS: Urine analysis 119

3.3.6. Human MS: Serum analysis 122

3.3.7. Spiking experiments 126

3.4. Discussion 130

3.4.1. Preclinical urine analysis 130

3.4.2. Preclinical blood analysis 134

3.4.3. Clinical studies 135

3.4.4. Chapter Summary 138

Chapter 4 : Metabolomic changes in Alzheimer's Disease 140

4.1. Introduction 140

4.1.1. Aims of Chapter 141

4.2. Methods 144

4.2.1. Sample collection 144

4.2.2. NMR sample preparation 144

4.2.3. NMR Spectroscopy 144

4.2.4. Statistical analysis 144

4.2.5. Metabolite identification 145

4.3. Results 146

4.3.1. Alzheimer's disease results 146

4.3.2. Addition of clinical data 151

4.4. Discussion 153

4.4.1. MS and AD comparison 154

4.4.2. Addition of EDSS scores 155

4.4.3. Chapter Summary 156

Chapter 5 : Metabolic changes in HIV-associated dementia 157

5.1. Introduction 157

5.1.1. Aims of chapter 158

5.2. Methods 159

5.2.1. Sample collection 159

5.2.2. Sample pre-treatment 159

5.2.3. NMR sample preparation 159

5.2.4. Statistical analysis 160

5.2.5. Metabolite identification 161

5.3. Results 162

5.3.1. Initial results 162

5.3.2. Model improvements 164

5.3.3. Clinical data 169

5.3.4. Incorporation of clinical data into models 170

5.4. Discussion 172

5.4.1. Initial models 173

5.4.2. Metabolite identification 174

5.4.3. Clinical data 175

5.4.4. Chapter summery 175

Chapter 6 : Metabolic changes in brain cancer metastasis.....176

6.1. Introduction 176

6.1.1. Aims of chapter 178

6.2. Methods 179

6.2.1. Animal experimental design 179

6.2.2. *In vivo* procedures 180

6.2.3. Intracardiac injection of tumour cells 182

6.2.4. Sample collection 182

6.2.5. Statistical analysis and metabolite identification 183

6.2.6. Histological analysis 183

6.3. Results 188

6.3.1. 4T1-GFP model 188

6.3.2. Intracerebral model 188

6.3.3. Comparison of different tumour induction routes 199

6.3.4. Additional intracerebral models 205

6.4. Discussion 210

6.4.1. Intracerebral injections 210

6.4.2. Variation in distribution of tumour burden 215

6.4.3. Different tumour cell lines 219

6.4.4. Chapter Summery 220

Chapter 7 : General Discussion 221

7.1. Principal findings of this thesis 221

7.2. Biofluids used in this thesis 222

7.3. Biomarker technology 225

7.4. Limitations of metabolomics 227

7.5. Biology of neurodegenerative diseases 229

7.6. Future Directions 232

7.6.1. Multiple Sclerosis 232

7.6.2. HIV-associated dementia 234

7.6.3. Cancer Metastasis 235

7.7. Summary 236

Bibliography 237

Table of Figures

Figure 1.1: Principles of NMR. 19

Figure 1.2: Principles of water suppression..... 22

Figure 1.3: Clinical course of MS. 36

Figure 1.4: MRI brain scans of MS patients. 39

Figure 1.5: Clinical features of AD over time. 55

Figure 1.6: PET as a tool for AD diagnosis. 59

Figure 1.7: Clinical course of HIV associated dementia. 65

Figure 1.8: Formation of brain metastases. 70

Figure 1.9: Diagnosis of brain metastases. 74

Figure 2.1: PLS model validation. 86

Figure 2.2: A sample S-Plot. 89

Figure 2.3: Demonstration of how NMR assignments are derived. 91

Figure 3.1: A sample plasma COSY spectra 99

Figure 3.2: Cr-EAE animal model results. 102

Figure 3.3: Initial PLS-DA plot of human serum samples 103

Figure 3.4: Cr-EAE animal PLS urine results. 105

Figure 3.5: Overlaid ^{1}H NMR spectra 111

Figure 3.6: Plasma Cr-EAE animal PLS results. 112

Figure 3.7: Schematic to show the metabolite changes over time in the animal models. 116

Figure 3.8: Human MS plasma results. 124

Figure 3.9: A sample box-and-whisker plot 125

Figure 3.10: First spiking experiments. 128

Figure 3.11: Urine NMR spiking experiments. 129

Figure 4.1: PLS-DA model between the PP-MS patients and RR-MS patients 142

Figure 4.2: Table showing the EDSS scale for classify the progression of MS. 143

Figure 4.3: PLS-DA plots of PP v SP MS patients. 149

Figure 4.4: PLS models with the inclusion of EDSS data. 152

Figure 5.1: : Initial HIV PLS model results. 163

Figure 5.2: NMR spectra comparison. 166

Figure 5.3: PLS plots of HIV samples with the baseline removed. 167

Figure 5.4: Clinical data results. 171

Figure 6.1: Immunohistochemical analysis of brain metastasis induced *via* the injection of 4T1-GFP cells. 189

Figure 6.2: 4T1 intracerebral injection urine results. 190

Figure 6.3: 4T1 intracerebral injection plasma results. 197

Figure 6.4: PLS plots of differing tumour burdens within the CNS. 203

Figure 6.5: Additional intracerebral models results. 207

Figure 6.6: PLS plots of additional intracerebral models. 208

Table of Tables

Table 1.1: Relative cost of imaging techniques. 9

Table 1.2: Table of key metabolites in various neurodegenerative diseases... 25

Table 1.3: McDonald criteria for diagnosis of MS 47

Table 2.1: Full literature assignments for all compounds within this thesis..... 90

Table 3.1: Table showing the clinical scoring system in Cr-EAE animals..... 96

Table 3.2: q^2 values of the PLS models generated from the Cr-EAE animals. 106

Table 3.3: Metabolite changes in Cr-EAE urine models. 109

Table 3.4 q^2 values from the plasma Cr-EAE animals. 113

Table 3.5: Plasma metabolites which varied during the Cr-EAE time course. 117

Table 3.6: Plasma metabolites which varied in the Cr-EAE compared to the control groups. 118

Table 3.7: q^2 values from human MS samples..... 120

Table 3.8: Metabolite changes in the Human MS samples..... 121

Table 4.1: Table showing the metabolite differences between AD patients and PP- and SP-MS patients. 150

Table 5.1: Metabolites causing separations between the PLS-DA models for the HIV samples..... 168

Table 6.1: Table showing the clinical scoring system used for assessing the animals within the tumour cell models. 181

Table 6.2: Table to show the different antibodies used in this thesis. 186

Table 6.3: 4T1 Intracerebral q^2 values. 191

Table 6.4: Significant metabolites in the 4T1 animal models. 194

Table 6.5: Intracerebral injection of 4T1-GFP plasma results. 198

Table 6.6: Urine metabolites responsible for the separation in the different routes of injection models. 204

Table 6.7: Additional intracerebral models metabolite identification. 209

List of Abbreviations

^{11}C	Carbon-11
^{13}C	Carbon-13
^{18}F	Fluorine-18
^{1}H	Hydrogen
ABC	Avidin-Biotin Complex
ABH	Antibody-High
AD	Alzheimer's Disease
AIDS	Acquired Immunodeficiency Syndrome
ANOVA	Analysis of Variance
Aβ	Amyloid Beta
B_0	Fixed magnetic field
BBB	Blood Brain Barrier
CD	Cluster of Differentiation
CFA	Complete Freund's Adjuvant
CIS	Clinically Isolated Syndrome
CNS	Central Nervous System
COSY	Correlation Spectroscopy
CPMG	Carr–Purcell–Meiboom–Gill
Cr-EAE	Chronic Experimental Allergic Encephalomyelitis
CRP	C-reactive protein
CSF	Cerebrospinal Fluid
CT	X-Ray Computed Tomography
d. H_2O	Distilled Water
DAB	Diaminobenzidine Hydrochloride
DSM-IV-TR	Diagnostic and Statistical Methods of Mental Disorders, fourth edition
EAE	Experimental Allergic Encephalomyelitis

EDSS	Expanded Disability Status Scale
GABA	Gamma-Aminobutyric Acid
Gd	Gadolinium
GFP	Green Fluorescent Protein
Gy	Gray
HAART	Highly Active Antiretroviral Therapy
HAD	HIV Associated Dementia
HepC	Hepatitis C
HIV	Human Immunodeficiency Virus
HPLC	High Pressure Liquid Chromatography
HTS	High Throughput Screening
IFA	Incomplete Freund's Adjuvant
IFN-γ	Interferon
IgG	Immunoglobulin G
IL	Interleukin
K	Kelvin
MCI	Mild Cognitive Impairment
MHC II	Major histochemical complex class II
MHz	Megahertz
MRI	Magnetic Resonance Imaging
MRS	Magnetic Resonance Spectroscopy
MS	Multiple Sclerosis
M-S	Mass Spectrometry
mSv	Milli-Sieverts
NMO	Neuromyelitis Optica
NMR	Nuclear Magnetic Resonance
NOESY	Nuclear Overhauser Effect Spectroscopy

ns	Non Significant model
NSE	Neuron-Specific Enolase
OPLS	Orthogonal Partial Least Squares
PBS	Phosphate Buffered Saline
PCA	Principle Component Analysis
PFA	Paraformaldehyde
PiB	Pittsburgh compound B
PLP	Periodate Lysine Parafomaldehyde
PLS	Partial Least Squares
PLS-DA	Partial Least Squares-Discriminate Analysis
ppm	Parts Per Million
PP-MS	Primary Progresive
PSA	Prostate-Specific Antigen
RF	Radio Frequency
RR-MS	Relapse Remitting
SCID	Severe Combined Immunodeficiency
SP-MS	Secondary Progressive
T	Tesla
TMA	Trimethylamine
TMAO	Trimethylamineoxide
TR	Relaxation Delay
VCAM-1	Vascular Adhesion Molecule-1
VEP	Visual Evoked Potential
δ	Chemical Shift
$\delta_{x\text{-}y}$	Centre of chemical shift as identified by SIMCA

Chapter 1: Introduction

1.1. General introduction

The overall aim of this thesis is to identify disease-specific biomarkers for neurological diseases. The study of biofluids using metabolomics has shown promise for diagnosis and treatment both in animal models of central nervous system (CNS) diseases and certain specific human diseases (Griffin*, et al.*, 2007; Salek*, et al.*, 2008). Hitherto, this approach has been applied in a limited way to a study of multiple sclerosis (MS), but not within the field of cancer metastasis, Alzheimer's disease (AD) or human immunodeficiency virus (HIV) associated dementia (HAD). Early diagnosis in these diseases is critical, because irreversible brain damage can occur long before the onset of clinical symptoms. Clinically, MS is one of the leading causes of disability in the western world (Noseworthy*, et al.*, 2000) and brain metastasis is one of the leading causes of death within cancer patients (Klos*, et al.*, 2004). AD is the most common cause of dementia in the world with an estimated 33.9 million sufferers worldwide (Barnes*, et al.*, 2011). Despite the introduction of highly active retroviral therapy (HAART) there is a growing number of HIV patients developing HAD, currently around 10% of all HIV patients (Marle*, et al.*, 2005). In all cases, innovative diagnostic techniques involving the study of biofluids could enable patients to receive treatment at an earlier stage, and thus dramatically improve outcome. The specific goal of my work, therefore, is to identify sets of biomarkers that can be used as an early diagnostic tool for these important neurological diseases.

The principal aim of this thesis is to explore the use of metabolomics as a tool for diagnosing MS and describe its usefulness in sub-typing MS. The same technique will also be used in a clinically relevant mouse model of MS, the

chronic experimental autoimmune encephalomyelitis (Cr-EAE) model (described in Section 1.5.6). Metabolomics analysis, involving ^{1}H NMR and PLS modelling, will be conducted on plasma and urine samples. This approach enables serial or temporal identification of changes in potential biomarkers that can be correlated with disease progression. Using this combination of ^{1}H NMR and PLS modelling on MS patients' biofluids has the potential to enable both early diagnosis of the disease and, most critically, accurate staging of disease. PLS modelling is a class-based modelling technique that allows the spectral variation to be modelled so as to reduce the effects of random metabolite changes within the sample set. Subsequently, the specificity of this approach for MS neuropathology is tested by applying it to analysis of biofluid samples from MS patients and patients with another common, but distinct, neurological condition, AD. CSF samples obtained from HIV patients will be examined in order to identify metabolites which can separate out different neurocognitive states within these patients. Finally, application of this metabolomics tool to a different neurological disease, brain metastasis, will be explored in murine models.

1.1.1. Aims of this Thesis

Against this background, this thesis will investigate the following hypotheses:

1. The use of ^{1}H NMR and pattern recognition on biofluids can distinguish between animal models of different neurological diseases.
2. Metabolomics analysis of biofluids can enable identification of type-0 biomarkers, which give an indication of the staging of certain neurodegenerative disease in both animal models and human patients.

3. Metabolomics analysis of biofluids can separate distinct neurodegenerative diseases from each other and from a healthy control cohort.
4. Clinical data can be used to enhance the metabolomics models to provide a more robust tool for the staging and diagnosis of neurodegenerative diseases.

1.2. Biomarkers

1.2.1. General

The search for biomarkers has been a key area for disease diagnostics since at least the 14th century. Doctors at that time would examine the chemical composition of a patient's urine in order to identify pathology, with limited success (as discussed by Nicholson*, et al.*, 2008). Biomarkers are becoming an increasingly common focus of scientific research because they have a wide range of applications within the field of disease diagnostics (Bales*, et al.*, 1984). Despite this, the use of the word 'biomarkers' is relatively new within the scientific community (discussed by Sahu*, et al.*, 2011). Until ten years ago there was confusion over what constituted biomarkers, surrogate markers, and clinical endpoints. The first attempts to define them were made by Lesko *et al.* (Lesko*, et al.*, 2001). The different biomarkers are defined below, including how they differ from clinical endpoints and surrogate markers.

The current accepted definition of a biomarker is:

'A characteristic that is objectively measured and evaluated as an indicator of normal biological processes, pathogenic processes or pharmacological responses to a therapeutic intervention' (Frank*, et al.*, 2003).

A clinical endpoint is defined as a characteristic or variable that reflects how a patient feels or functions, or as how long a patient survives (Lesko*, et al.*, 2001). For example, the clinical endpoint of a person receiving antihypertensive drugs in order to reduce the risk of a stroke is whether or not they suffer a stroke (Atkinson, 2007). The potential advantage of biomarkers is that, if chosen well, they could represent an earlier marker of disease, reducing the necessity of taking studies to the clinical endpoint. This is especially relevant during clinical trials, in which such markers can be used to monitor the effectiveness of the

new treatment. The possibility of an early diagnosis may help to arrest disease progression at an earlier timepoint, which could preserve patients' function for longer.

The term used for this type of biomarker is 'surrogate marker', meaning a biomarker that is intended as a substitute for a clinical endpoint. A clinical investigator uses epidemiological, therapeutic, pathophysiological, or laboratory evidence to select a surrogate marker that is expected to predict clinical benefit, harm, or lack of benefit or harm (Lesko*, et al.*, 2001). Cholesterol level has been found to be a reliable surrogate marker in the testing of novel drugs designed to lower the risk of heart attacks. The higher a patient's cholesterol level, the greater the chance of him suffering a heart attack, and therefore if a drug lowers the cholesterol level, it is assumed that the drug is effective at reducing the risk of subsequent heart attack (Pedersen*, et al.*, 1998).

However, several of the early drug trials, which used surrogate markers as their endpoint, have been shown not to improve patient survival (Fleming*, et al.*, 1996). There were several reasons for this (reviewed by Fleming *et al.*), but in the majority of cases the authors of the clinical trials were using the incorrect type of biomarker (Fleming*, et al.*, 1996). For example, when assessing the effects of quinidine as a treatment for atrial fibrillation the maintenance of sinus rhythm was used as the endpoint for the trial (Normand*, et al.*, 1976). However, a meta-analysis study later revealed that although quinidine did maintain sinus rhythm it also increased the mortality rate from 0.8% to 2.9% (Coplen*, et al.*, 1990). Therefore, a distinction between biomarkers which occur naturally during the disease time course and biomarkers which are induced by intervention such as drug therapy was deemed necessary (Rolan*, et al.*, 2003).

Type 0 biomarkers are the markers of the natural history of a disease, and the subsequent changes in concentration over time correlate longitudinally with

clinical indices, such as symptoms over the full range of disease states. There are several examples of type 0 biomarkers within the literature, as the need to understand the natural progression of a disease is the key to developing future drugs for its treatment. One such example of a type 0 biomarker is vascular adhesion molecule-1 (VCAM-1) which has been shown to be expressed on the surface endothelium of cells in a mouse model of intracerebral ischemia (Hoyte*, et al.*, 2010). The authors of this study show that the area of VCAM-1 binding was around 25% of the total brain volume compared to the 3% of brain volume change using a more traditional, diffusion measurement in the MRI. This shows that following a stroke there is a significant increase in the inflammatory response around the injury site (Hoyte*, et al.*, 2010).

In contrast, a type I biomarker captures the effect of an intervention in accordance with the mechanism of action of the drug, even though the mechanism may not be known to be associated with clinical outcome. Prostate-specific antigen (PSA) is an example of a biomarker in this category, that has been shown to be a marker of the presence of prostate carcinoma (Oesterling, 1991). The authors of this study also used this marker to assess how effective various radiotherapies and chemotherapies were in reducing the PSA expression and hence the tumour burden in these patients. This is a type I, and not a type II biomarker (see below), as the link between PSA and reduction in tumour size has not been categorically proven. Therefore, regulators of drug trials will not allow this biomarker to be used as an endpoint marker (Lesko*, et al.*, 2001).

Type II biomarkers are considered to be surrogate markers. This is because a change in them predicts clinical benefit. In the case of prostate carcinoma described above, the authors used a biopsy of the prostate 7 years after the start of treatment as a type II ‘biomarker’. If the tumour reduced in size or

disappeared then the drug was deemed to be a success (Lesko*, et al.*, 2001). This is an invasive procedure which requires surgical intervention, and therefore the hunt for a non-invasive biomarker continues (Kline*, et al.*, 2006).

The need to identify biomarkers, and in particular non-invasive type II biomarkers, is crucial within drug trials because of the potential cost saving which arises when using biomarkers rather than clinical endpoints (Frank*, et al.*, 2003; Lesko*, et al.*, 2001). It also allows for the possibility of diagnosis before the clinical endpoint of a disease, greatly reducing patient suffering with the potential to terminate trials of drugs which are not effective at an earlier stage.

1.2.2. Overview of techniques used for biomarker identification

Recently, the number of tools available to researchers to identify biomarkers has expanded considerably. Initially, biomarkers were identified using simple techniques in biofluids such as blood, urine, and saliva. However, the development of a variety of imaging modalities has more recently enabled the identification of imaging biomarkers. Improvements in analytical techniques have also led a resurgence in biomarker identification within biofluids. A common example of this was the monitoring of HIV sufferers using counts of their viral loads and CD4 levels in plasma and CSF samples (Fischl*, et al.*, 1987). The discovery of the viral load biomarker led to the research and development, and then to the clinical assessment of, the Highly Active Antiretroviral Therapy (HAART) which is now the central treatment for HIV patients (Sahu*, et al.*, 2011). In this example, data sets could be obtained with relative ease, a factor which is vital for the utility of a biomarker (Ilyin*, et al.*, 2004).

1.2.2.1. Molecular imaging

The invention of molecular imaging led to the idea that biomarkers could be monitored using various imaging modalities in both clinically relevant animal models and human diseases (Rudin*, et al.*, 2003; Sahu*, et al.*, 2011). Advances in human imaging techniques have allowed this technology to emerge as a potential tool for the identification of novel biomarkers. Nevertheless, a greater driving force is that the downsizing of these modalities to the scale of small animals has allowed models of disease to be studied (Rudin*, et al.*, 2003). There are, however, several issues surrounding the increased use of molecular imaging techniques for biomarker identification. The primary problem is cost, as can be seen in Table 1.1, where, in animal models of disease, the hardware required to perform the imaging studies can be prohibitively expensive. In addition to this, not all the imaging modalities are translatable into human studies (Table 1.1). The need to inject contrast agents or to submit patients to ionising radiation is also another potential issue with molecular imaging, especially if the biomarker in question needs to be followed serially.

Technique	Resolution	Depth	Time	Target	Cost
MRI	10-100 μm	No limit	Minutes to hours	A, M, P	$$
CT	50 μm	No limit	Minutes	A, P	$
Ultrasound	50 μm	Milimeters	Minutes	A, P	$
PET	1-2 mm	No limit	Minutes	P, M	$$
SPECT	1-2 mm	No limit	Minutes	P, M	$

Table 1.1: Relative cost of imaging techniques. Table to show the relative merits and cost of imaging techniques. Key: A - anatomical, M - molecular, P - physiological $$ - greater than $300,000 $ - $100,000-300,000. (Adapted from Rudin*, et al.*, 2003).

1.2.2.2. 'omics' techniques

Genetic biomarkers have been used since the 1960s, when Nowell and Hungerford reported a genetic abnormality in patients suffering from chronic granulocytic leukaemia (Nowell*, et al.*, 1960). The sequencing of the human genome (Venter*, et al.*, 2001) has increased the focus on genomics as a tool for identifying biomarkers (Frank*, et al.*, 2003; Ilyin*, et al.*, 2004). However, in recent years it has become clear that the use of the human genome covers only a fraction of the knowledge required to understand disease progression (Bonetta, 2010; Oliver*, et al.*, 1998; Wasinger*, et al.*, 1995). This is partly due to the many post-translational modifications to the proteins following transcription from DNA (van Kasteren*, et al.*, 2007). The use of tests to examine genetic predisposition to important diseases would have major clinical, social, and economic ramifications. However, the great majority of the newly identified risk-marker alleles discovered in genome wide association studies (GWAS) are predictive of very small relative risks, ranging from 1.1 to 1.5 even though such analyses meet stringent statistical criteria. Even when alleles that are associated with a modest increase in risk are combined, they have low discriminatory and predictive ability (Janssens*, et al.*, 2008). The realisation of this has prompted the development of a new set of tools to investigate biomarkers with the opportunity to develop diagnostic techniques which include proteomics, transcriptomics, and metabolomics (Frank*, et al.*, 2003).

The principal advantage of the 'omics' techniques is that biofluids can be used. This allows the sample collection for trials to become simpler and less expensive than in molecular imaging studies (Griffin*, et al.*, 2004b). Another advantage is that one can apply a multiple 'omics' approach to the same set of samples in order to improve the reliability of the models. These advantages could allow a fuller understanding of the biological processes involved in the

changes as compared to the changes observed when using only one technique. For example, it has been shown that it is possible to correlate metabolite changes to the transcriptomic changes of rats exposed to phenobarbital poisoning (Waterman*, et al.*, 2010).

1.2.2.3. Multivariate analysis

It was soon realised that with the acquisition of large datasets associated with 'omics' studies, standard statistical tests were not adequate. In 1901, Karl Pearson described a form of statistics which could represent multidimensional data on a straight line or a plane (Pearson, 1901). In order to do this the data are placed into principal components, and then the components which contain the greatest variance within the data set are used to create the two dimensional model. This is known as principal component analysis (PCA) and is a useful tool for identifying any outliers within a given dataset. In nature, however, there are often factors that can cause great variance within a dataset in a manner that is unrelated to the factor of study. For example, in order to investigate potential markers for disease, urine samples may be acquired randomly throughout the day from both healthy and diseased cohorts. When carrying out PCA analysis of the Nuclear Magnetic Resonance (NMR) spectra obtained from these samples the separation between the groups may not be caused by disease but by diurnal variation in the amount of urine produced (Giovannoni*, et al.*, 1998).

In order to exclude any variance that occurs naturally within a biological system it is necessary to utilise a class based approach to building models for separating data sets. Partial least squares (PLS) regression analysis is a tool for such modelling. The aim of PLS is to find the greatest variance in the primary dataset that gives the greatest separation within the secondary dataset. In a simple class based model, such as diseased patient *versus* healthy patient, the secondary dataset is determined by the disease state. This is known as

partial least squares-discriminate analysis (PLS-DA) and is a commonly used statistical tool for metabolomics. The advantage of using PLS-DA modelling over PCA is that PLS-DA mitigates any factors within the models that are unknown. These factors include variations in diet or gender effects which could mask the disease-specific metabolite changes. These variations may be important when studying other aspects of disease, such as an individual's response to therapy. However, this thesis will attempt to identify type 0 biomarkers associated with neurodegenerative diseases, and therefore, these unrelated disease factors needed to be excluded. In addition, PLS modelling can also be used to model such things as gender differences within the sample set. The use of PLS-DA as a modelling technique biases the models towards the separation between the classes over and above the noise generated by other clinical factors.

1.3. Metabolomics

1.3.1. General

The concept of studying the metabolic composition of biofluids has its roots in early diagnostic medicine, as mentioned above (1.2.1). The term metabolomics can be defined as the study of the metabolite profile in biofluids. The idea that it is possible to separate biofluids into their constituent metabolites was introduced by Roger Williams in the 1940's. Williams demonstrated that it was possible to use paper chromatography to show a unique metabolite profile from the saliva of schizophrenic patients (Williams, 1951). This study showed that there was variation in creatinine and magnesium ions in the urine of schizophrenic patients (Williams, 1951). The idea that saliva could be used to separate schizophrenic patients from healthy controls led to the idea that other analytical techniques could be used to study the metabolite concentrations within biofluids.

It was not until the invention of modern analytical techniques in the 1950s that it was possible to quantify the concentrations of metabolites within biofluids. During the 1960's and 1970's, however, focus on biomarker research shifted away from studying the metabolite composition in biofluids, because the fundamental composition of them was considered too complex (Holmes*, et al.*, 1994; Preti, 2005). Advances in analytical techniques have allowed greater resolution in the data obtained from the biofluids (Lynch*, et al.*, 1994; Want*, et al.*, 2005), which has led to a resurgence of metabolomics research in recent years. The idea of combining multivariate statistics with these analytical techniques was first pioneered by Nicholson in the 1980's using proton NMR to analyse the biofluid samples (Nicholson*, et al.*, 1989).

1.3.2. Analytical techniques used in metabolomics

Several analytical techniques are used for the identification of biomarkers from biofluids. In recent years, two techniques ^{1}H NMR and mass spectrometry have come to the forefront of metabolomics research. However, several other techniques can be used. These include capillary electrophoresis, HPLC and laser spectroscopy. There are several drawbacks when using these techniques. In particular, it has been reported that certain metabolites have been missed using capillary electrophoresis when studying complex biological mixtures (Ramautar*, et al.*, 2006). HPLC, especially when used in conjunction with mass spectrometry, is good way of performing targeted metabolomics where specific metabolites are to be studied. For example, HPLC has been used to study the baseline expression of eight phthalate metabolites in human urine with a view to study any associations of changes in these specific metabolites during cancers (Blount*, et al.*, 2000). However due to the complex nature of biofluids it is often difficult to find conditions to fully separate out all metabolites from a complex mixture, thus it is difficult to study all the metabolites which change in one single sample using HPLC (Blow, 2008).

1.3.2.1. Mass spectrometry in metabolomics

Mass spectrometry allows the vast number of the metabolites within biofluids to be analysed. Several techniques have been developed within the field of mass spectrometry, however the basic underlying principle is the same for all of them. In order to acquire a spectrum of the mass composition of a sample the metabolites have to be vaporised, ionised, and then sorted into mass/charge ratio prior to being detected. However, a degree of contention surrounds the use of mass spectrometry within the field of metabolomics due to the need to pre-treat the biofluids in order to assist with the data acquisition (Lindon*, et al.*, 2007; Want*, et al.*, 2005). The ionisation of molecules within the original mass

spectrometers is dependent on the chemical composition of the sample. Therefore, if the composition of the sample changed, the quantity of the metabolite of interest reaching the detector would vary between samples. Biofluids by their nature vary between samples and, thus, quantification of metabolites was difficult. The vaporisation and the detection of the particles are not affected by the composition of the samples.

There have been many recent technological advances within the field of mass spectrometry. These advances are beginning to overcome the problems described above and have allowed researchers to fully quantify the spectra acquired (Want*, et al.*, 2005). Surface based loading techniques which then use a laser to vaporise and ionise the sample simultaneously are beginning to show promise within the field of metabolomics (Woo*, et al.*, 2008). These advances allow greater control of the ionisation of the samples and, therefore, more accurate quantification of the metabolites present. However, this quantification is only relative, and it is not possible to fully quantify the metabolite changes using mass spectrometry.

The major drawback to mass spectrometry, however, is the fact that it is a destructive process and often the metabolites themselves are fragmented during the acquisition of the spectra. This means that only one experiment can be performed per sample.

1.3.2.2. NMR spectroscopy in metabolomics

As stated previously (1.3.1) NMR has been at the forefront of metabolomics research since the 1980's. There are several reasons for this: principally, unlike mass spectrometry, NMR is a non-destructive technique and, therefore, multiple sets of analysis can be carried out on each sample. Another key advantage of NMR is the minimal amount of sample preparation required to acquire the

spectra. The principles of NMR spectroscopy are outlined below (1.4). Other benefits include the cost, after the initial cost of the spectrometer; a single NMR spectrum is estimated to cost around $1 including all the processing required (Griffin*, et al.*, 2004b). With the invention of fully automated robots to load samples into the NMR magnet it is possible to process up to 300 samples per 24 hour period, with each NMR spectrum taking between 4 and 7 minutes to run (Holmes*, et al.*, 2002).

One of the major drawbacks of NMR as a technique for metabolomics is the relative sensitivity of NMR when compared to mass spectrometry. Using NMR, it is possible to detect metabolites in the low nmol concentrations when using a high field magnet (Pan*, et al.*, 2007). whereas, using mass spectrometry, it is possible to detect metabolites with a concentration of 1 ppm or lower (Brown*, et al.*, 2005).

1.4. NMR Spectroscopy

1.4.1. General

One of the fundamental physical characteristics of all atomic particles is a property called spin, a measure of its orbital angular momentum (Noyes, 1957). In 1924 Pauli predicted that certain isotopes would have a magnetic moment due to their spins. However, this theory was not experimentally proven until 1938 when Isidor Rabi managed to measure this phenomenon in a beam of particles (Rabi*, et al.*, 1938). It was not until 1946 that the technique was applied to solids and liquids. Bloch and Purcell, working independently, noted that if certain elements were placed in a magnetic field they would absorb radio frequency (RF) energy at a specific frequency. Therefore, they concluded that this must be the magnetic resonance frequency for that nucleus at a given magnetic field strength (Bloch*, et al.*, 1946; Purcell*, et al.*, 1946). It was also noted that when the RF pulse was switched off it was still possible to detect an RF signal from the nuclei in the sample. This allowed Bloch to patent the first NMR machine as a means of analysing the composition of materials using nuclear magnetic inductions (Bloch, 1955).

1.4.2. Principles of NMR

The absorption of RF energy at the magnetic frequency arises from the fact that when you place nuclei within a fixed magnetic field (B_0) the spins form two discrete energy levels. These energy levels arise from the spin of the nuclei aligning themselves either in the direction of the magnetic field or in the opposite direction to the magnetic field. These energy states are commonly referred to as spin up and spin down, where spin down is the lower energy state in which the spins are aligned with the main magnetic field (Figure 1.1). The energy of the radiation required to promote a nucleus from the spin down state

to the spin up state falls within the RF of the electromagnetic spectrum. Hence the magnetic resonance frequency of nuclei falls within the MHz range. Application of an RF pulse will promote a small number of nuclei from a spin down state to a spin up state and, thus, energy will be put into the system. When the RF pulse is switched off the system will restore itself to the baseline energy level. In doing this it will emit an RF pulse that can be detected and recorded on a spectrum (Figure 1.1). The reason NMR is such a powerful tool in the elucidation of structure of molecules is that the chemical environment of individual protons, or indeed any other non-zero spin isotope such as carbon 13, within a compound changes the local magnetic field. Therefore, each unique chemical environment will have its own chemical shift within an NMR spectrum.

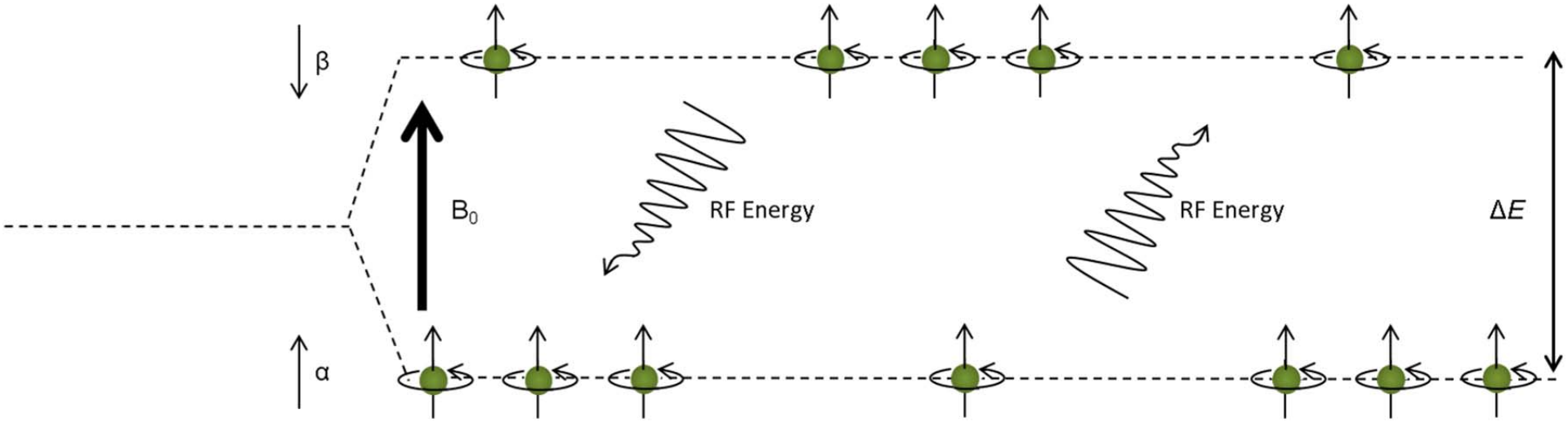


Figure 1.1: Principles of NMR.

In order for an isotope to be 'NMR active' (have a magnetic resonance) the total value for the spin of that isotope must not be zero. For example, hydrogen (^{1}H) and carbon 13 (^{13}C) both have a spin of ½ and, therefore, are commonly used in NMR experiments. ^{1}H is the most commonly used nucleus for NMR experiments, owing to its natural abundance, of around 99.98% (Bleakney*, et al.*, 1933). Hydrogen is also a key element in organic molecules and, therefore, NMR has become a vital tool for characterising compounds. Carbon is another common element in organic molecules, however, the natural abundance of the NMR active isotope, ^{13}C, is only 1.11%. Consequently, a greater number of scans or a greater concentration of the compound is needed to achieve the same signal from ^{13}C as compared to ^{1}H.

1.4.3. NMR techniques for metabolomics

As mentioned above, there is little need for sample preparation owing to the wide range of water suppression sequences available. Water suppression is necessary because the majority of biofluids are primarily composed of water. As a consequence, the water signal saturates the RF receiver and the metabolites, which are at significantly lower concentrations, are not visible without a suppression sequence (Nicholson*, et al.*, 1989). Several techniques exist for water suppression, but the basic principle is that an RF pulse is applied at the resonant frequency of water to saturate the signal and eliminate it from the acquired spectrum. To do this, the RF pulses used to excite the water protons are orientated and timed in such a way that the direction of the nuclear spins becomes orthogonal to the receiving coils and, therefore, these are not measured in the spectrum (Hore, 1983). The water suppression used in this thesis will be the NOESY presaturation sequence. The name NOESY is slightly misleading, as no nuclear Overhauser effects are measured during the NMR experiment. The name is derived from the fact that the same pulse sequence to

measure the nuclear Overhauser effect is used to suppress the water signal. This pulse sequence works by applying two 90° pulses of RF energy, in quick succession, at the resonant frequency of water which inverts the direction of the vector of the spins of water (Figure 1.2 i). The spins are then allowed to relax towards the direction of the magnetic field (Figure 1.2 ii). After a period of time, where the vector of the spin direction is realigning to the magnetic field, a further 90° pulse is applied at the resonant frequency of water. This second 90° pulse aligns the spin vector in the orthogonal plane to the receiving coil and, thus, removes the signal due to water (Figure 1.2 iii). The reason this water suppression is used over other techniques is that it has been shown to provide a more consistent suppression in biofluid samples where ionic concentrations may vary. Therefore, the water suppression generated by this technique is less varied than other techniques (Mckay, 2011). In order to fully elucidate the specific structures of the compounds identified by the PLS modelling (as demonstrated in Figure 2.3) 2D COSY spectroscopy will be used. This form of spectroscopy reveals the correlations between adjacent hydrogens within a chemical structure.

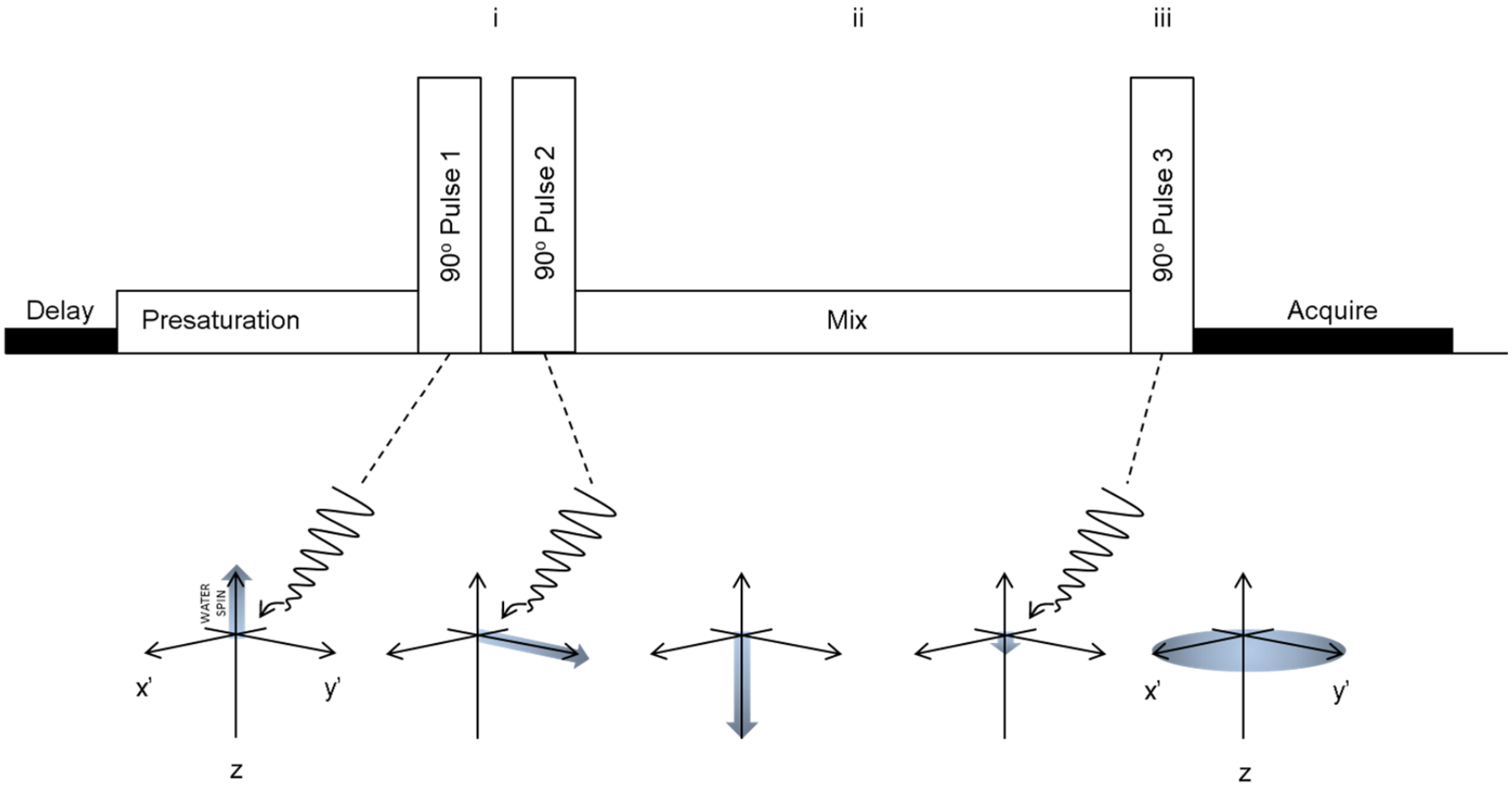


Figure 1.2: Principles of water suppression.

Recent technical developments in NMR machines such as increased magnetic field strength and cryoprobes have improved the quality of the spectra obtained from biofluids. These developments overcame some of the criticisms of earlier metabolomics studies in which the spectra were of insufficient resolution to identify specific metabolites with a high degree of accuracy (Weljie*, et al.*, 2006). Cryoprobes are becoming increasingly common on modern NMR spectrometers. The difference between a cryoprobe and a normal probe is that the RF coil and associated electronics, which record the spectra from the sample, are cooled to 4 Kelvin (K) using liquid helium, whilst keeping the samples at room temperature. This reduction in temperature of the probe reduces the noise generated by the machine and fewer scans are needed to achieve the same signal-to-noise ratio (Serber*, et al.*, 2000; Styles*, et al.*, 1984). There is some debate as to the usefulness of cryoprobes for ^{1}H NMR spectroscopy of biofluids, because the energy required for water suppression can warm the probe slightly during acquisition. This warming leads to a broadening of the line widths of the proton signals and, thus, reduces the resolution of the spectrum acquired (Aran ´ bar*, et al.*, 2006). However, with an increased magnetic field strength it is possible to suppress the NMR signal from water and still obtain good resolution on the metabolites which are at a lower concentration. Therefore, the effective use of a cyroprobe relies on achieving a balance between time needed to run a sample and the water suppression that can be achieved on any individual system.

1.4.4. Previous NMR studies in metabolomics

The use of ^{1}H NMR has been demonstrated to be sensitive enough to differentiate kidney function between different strains of wild rodents and laboratory rats using PLS-DA analysis (Griffin*, et al.*, 2000). However, this difference can be identified purely by the gross visual differences within the

spectra. It has also been demonstrated that it is possible to separate groups of rats that have been injected in the striatum with two different adenoviruses (Griffin*, et al.*, 2004a) using urine obtained from the animals. These adenoviruses induced expression of two different cytokines IL-1β and TNF-α, respectively, leading to markedly different inflammatory infiltrates in the brain. In the case of IL-1β a neutrophil-mediated lesion was induced, while TNF-α evoked purely macrophage recruitment to the brain. More recently, it has been reported that it possible to distinguish between the plasma obtained from stroke patients and healthy people (Jung*, et al.*, 2011). This study reported that metabolites such as lactate, glycolate, pyruvate, and formate could be used to distinguish between the two groups. These metabolites were identified using a combination of ^{1}H NMR coupled with PLS-DA modelling (Jung*, et al.*, 2011). There have also been several articles published in the literature profiling the metabolomic changes in other neurodegenerative disease such as Alzheimer's disease and Huntingdon's disease. Several biomarkers have been addressed, and the key biomarkers identified in these studies are: N-acetyl aspartate, lactate, choline and phosphocholine. These metabolites will be discussed in detail later in this thesis (Section 7.5). For a more comprehensive list of previous metabolomic studies of neurodegenerative diseases, see Table 1.2. These findings led to the first hypothesis to be addressed in this thesis, that biofluids could be used to diagnose and stage different neurodegenerative diseases such as MS and brain metastasis.

Neurological Disease	Sample used in study	Analysis technique used	Biomarkers identified						Reference
Stroke	Plasma	^{1}H NMR and PLS-DA	Lactate	Glycolate	Pyruvate	Formate			(Jung, *et al.*, 2011)
Amyotrophic lateral sclerosis	Serum	^{1}H NMR and Univariate modeling	Glutamate	β–Hydroxybutyrate	Formate	Glutamine	Histidine	N-acetyl derivatives	(Kumar, *et al.*, 2010)
	CSF	^{1}H NMR and PCA	No specfic metabolites identified						(Blasco, *et al.*, 2010)
Parkinsons Disease	Whole brain	MRS	Glucose	N-acetyal aspartate					(Lucetti, *et al.*, 2001)
	Whole brain	MRS/PET	Lactate	Choline	N-acetyal aspartate				(Brownell, *et al.*, 1998)
	Whole brain	MRS	N-acetyal aspartate						(Burt, *et al.*, 2006)
Huntingdon's Disease	Whole brain	MRS	N-acetyal aspartate	*myo*-Inositol					(Hoang, *et al.*, 1998)
	Whole brain	MRS	N-acetyal aspartate	Lactate					(Jenkins, *et al.*, 1998)
	Brain sections, plasma and urine	^{1}H NMR and PLS-DA	Glucose	Unsaturated lipids	Creatine	Glutamate	Acetate	Citrate	(Tsang, *et al.*, 2006)
	Serum	GC -MS-TOF and PLS-DA	Glycerol	Monosaccharides	Alanine	Leucine	Valine	Malonate	(Underwood, *et al.*, 2006)
Alzheimer's disease	Whole brain	MRS	N-acetyl compounds	Creatine	Choline				(Pfefferbaum, *et al.*, 1999)
	Whole brain	MRS	Phosphocholine	Choline	Other choline species	N-acetyl compounds			(Cheng, *et al.*, 2002)
Schizophrenia	Whole brain	MRS and PCA	Phosphocholine	Uridine	*myo*-Inositol	Adenosine	Taurine	Acetate	Prabakaran (Prabakaran, *et al.*, 2004)

Table 1.2: Table of key metabolites in various neurodegenerative diseases.

1.5. Overview of Multiple Sclerosis

Multiple Sclerosis (MS) is primarily an autoimmune disease of the central nervous system (CNS) which results in the demyelination of axons (Compston, *et al.*, 2008). The exact cause of the initial inflammatory response is not fully understood (Compston, *et al.*, 2002), but it is known to be mediated by T-cells and macrophages and to cause demyelination, axon loss, and blood-brain-barrier breakdown (BBB). This inflammatory process can lead to a wide range of clinical signs, which makes the diagnosis of MS difficult in the early stages of the disease.

There is some debate over who first described MS-type lesions. Initially a French anatomist named Jean Cruveilhier was credited as the first person to describe the lesions present in MS in 1842 (Cruveilhier, 1842). However, a Scottish illustrator named Robert Carswell is now believed to have published his illustrations of MS slightly earlier (Carswell, 1838). Both Carswell and Cruveilhier presented their work in Paris at roughly the same time and, despite the fact they were not looking at the same patients, their illustrations were remarkably similar (Compston, 1988). The first full description of MS as a separate disease was published by the French pathologist Jean Charcot in 1868 (Charcot, 1868).

1.5.1. Prevalence of MS

It is estimated that 2.5 million people worldwide suffer from MS (Compston, *et al.*, 2002). The prevalence of MS varies greatly across the world, but it is higher in certain communities, for example the rates of MS within England and Wales are reported to be between 72 and 112 cases per 100,000, while, the prevalence is higher in Scotland and is thought to be around 190 cases per 100,000 (Rosati, 2001). Lower risk areas include Japan, where the prevalence

is believed to be as low as 9 to 13 cases per 100,000 (Houzen*, et al.*, 2008). These geographical differences may be explained by the environmental contribution to disease aetiology or by genetic factors, and these will be discussed in section 1.5.3. Typically the age of onset of MS is between 20 and 40 years and females are affected to a greater extent than males by a factor of 2.17 (Krökki*, et al.*, 2011).

1.5.2. Aetiology of MS

The exact cause of MS still remains a mystery to researchers, but there is growing evidence that it is caused by a combination of factors. These factors appear to be both environmental and genetic. The search for type-0 biomarkers could prove a key step in understanding the mechanisms that lead to a patient developing MS.

1.5.2.1. Environmental factors

The different rates of MS within the population appear to be roughly correlated with distance from the equator, but the significance of this is not fully understood (Pugliatti*, et al.*, 2002; Taylor*, et al.*, 2010). This pattern can occur over a relatively small geographical distance, as demonstrated in a study of French farmers that showed higher numbers of cases in the north of the country (Vukusic*, et al.*, 2007). One of the environmental factors thought to be responsible for this phenomenon is exposure to UV light. It has been reported that there is an inverse link between UV exposure and the rate of MS within a population (Sloka*, et al.*, 2008). The link between UV exposure and vitamin D production within the body has been widely reported within the literature (Holick, 2002). It has, therefore, been hypothesised that a reduced amount of vitamin D increases the risk of contracting MS (Hanwell*, et al.*, 2011). The mode of action of this effect is not clear, however, vitamin D has been shown to have

immunoregulatory properties through the vitamin D receptor, which is expressed on both activated T-cells and antigen presenting cells (Hayes, 2000). Vitamin D has been shown to regulate cytokine expression within the immune system in two ways. Directly, by targeting transcription initiation and regulation, for example by reducing interleukin-12 (IL-12), or by inhibiting the expression of surface major histocompatibility complex class II (MHC II). Indirectly, Vitamin D also affects the immune system indirectly by inhibiting intracellular signalling pathways through interference with the transcription factors NF-AT and NF-κB. Another possible explanation for the inverse correlation between UV light levels and MS incidence could be the increased levels of melatonin, which is produced after prolonged non-exposure to UV light (Max*, et al.*, 1992). This increase in melatonin has been shown to augment the production of Th1 type immune cells and, therefore, could increase the likelihood of contracting MS (Kidd, 2003; Ponsonby*, et al.*, 2005).

1.5.2.2. Infectious agents as triggers of MS

Foreign bodies, such as viruses or bacteria, have long been thought to play a role in MS. There is considerable debate about whether the immune response to these organisms is beneficial or detrimental in determining the risk of contracting MS. One theory, which could potentially explain the geographical distribution of MS, is the hygiene hypothesis. This hypothesis states that the risk of diseases such as hay fever is related to an increase in standards of hygiene within the population. If a young child is not exposed to unhygienic conditions early in life the immune system does not develop tolerance to foreign bodies (Strachan, 2000). It has been shown that the rates of MS diagnosis are inversely correlated with the infection rate of *Trichuris trichiura*, which is a marker of relative hygiene within a community (Holmøy*, et al.*, 2008). This infection has been shown to be a marker of poor hygiene within a community

(Bundy*, et al.*, 1989) and therefore the authors of this study hypothesised that being exposed to infectious agents at an early stage of life could reduce a person's chances of developing MS (Fleming*, et al.*, 2006). Several viruses have been identified which may increase the risk of contracting MS, including the Epstein Barr virus (EBV). This virus, while asymptomatic in most of the population, develops into infectious mononucleosis in some individuals, and this has been correlated with the development of MS. The correlation with EBV does not fully explain the geographical distribution of MS cases unless it is coupled with the exposure to vitamin D correlation mentioned above (1.5.2.1) (Ramagopalan*, et al.*, 2011). However, vitamin D levels cannot be used as a biomarker for MS as there are many diseases where vitamin D varies, such as prostate cancer (Corder*, et al.*, 1995), and osteoporosis (Lips*, et al.*, 2001). Vitamin D levels in patients could be used as a covariant in future MS biomarker studies to enhance any diagnostic models.

1.5.2.3. Genetic factors

It is becoming increasingly clear that there is a genetic factor involved in susceptibility to contracting MS. It has been shown that there is an increased risk of both monozygotic twins contracting MS when compared to dizygotic twins (Dyment*, et al.*, 2004). Dyment *et al*. also showed that there is a 20-50 fold increase in the risk of developing MS if a first degree relative has MS (Dyment*, et al.*, 2004), whilst Hemminki *et al.* reported a significant genetic link between all autoimmune diseases and MS (Hemminki*, et al.*, 2009). It has been reported that the common risk factor is mutations in MHC on chromosome 6p21 (Sawcer*, et al.*, 2005). Other studies have identified 20 additional risk loci, however, this does not fully explain the genetic link to MS. This number of risk loci has been doubled recently with the publication of a genome-wide association study (Sawcer*, et al.*, 2011). This study confirmed the original 20

loci and added a further 29 sites of risk, implicating a large number of genes that code for the cytokine pathway (such as *CXCR5, IL2RA, IL7R, IL7, IL12RB1, IL22RA2, IL12A, IL12B, IRF8, TNFRSF1A, TNFRSF14, TNFSF14*). They also discovered links to genes encoding for the vitamin D pathway which supports the environmental theory set out in 1.5.2.1 (Sawcer*, et al.*, 2011).

1.5.3. Clinical course of MS

MS is the most common cause of progressive disability in the Western world (Noseworthy*, et al.*, 2000). A wide range of common symptoms are associated with the onset of MS, such as difficulties with balance, dizziness, blurred vision, muscle weakness and fatigue (Janardhan*, et al.*, 2002; Kurtzke, 1983; White, 1997). Other symptoms which can develop during the disease time course include depression (Sadovnick*, et al.*, 1996) and a decline in cognitive ability (Bobholz*, et al.*, 2003). These symptoms can result from one single demyelinating event in the patient. If no further clinical symptoms develop over time then the disease is classed as clinically isolated syndrome (CIS). If the patient then goes on to suffer a further period of neurological symptoms or there is evidence of further lesions within the CNS (see 1.5.4.2 for a full introduction to MS diagnosis) then a diagnosis of MS can be made (McDonald*, et al.*, 2001; Polman*, et al.*, 2005; Polman*, et al.*, 2011). Therefore, for a diagnosis of MS it is necessary for lesions to be disseminated in both time and space as discussed in section 1.5.4. It has been reported that within a 6 year period 51% of CIS cases progress to clinically defined MS, while 15% of CIS patients appear to have clinically silent MS that is, nevertheless, diagnosable using radiological imaging techniques (Chard*, et al.*, 2011). As the disease progresses the level of disability tends to increase, with the majority of patients finally loosing motor, autonomic and cognitive function. Death due to MS tends to be from complications, such as infections arising in severely disabled patients

(Compston, *et al.*, 2008), and occurs on average 30 years after the onset of symptoms (Brønnum-Hansen, *et al.*, 2004). Corticosteroids are used to alleviate some of the symptoms during an attack (Filippini, *et al.*, 2000). There are four main stages of MS and these are described below.

1.5.3.1. Relapse Remitting MS

Around 80% of all MS suffers will initially be diagnosed with relapse remitting MS (RR-MS) (Compston, *et al.*, 2008). This stage of the disease is characterised by patients exhibiting periods of clinical symptoms interspersed with periods of complete or partial remission (Lublin, *et al.*, 1997), as depicted in Figure 1.3 A. There is a wide variation in the length of time a patient can suffer from RR-MS before it develops to Secondary Progressive Multiple Sclerosis (SP-MS) (1.5.2.2), but the median time is 19 years (Rovaris, *et al.*, 2006). There is also variation in the number of relapses per year that can occur in an individual patient. It has been reported that if a patient suffers frequent attacks during the initial two to five years after diagnosis then the chances of progressing to SP-MS are increased (Confavreux, *et al.*, 2003; Kantarci, *et al.*, 1998; Weinshenker, *et al.*, 1989).

However, it has recently been reported that the number of relapses during the total time that a patient is in the RR-MS phase does not correlate to the time taken to enter the SP-MS phase (Scalfari, *et al.*, 2010). Thus, the main goal in the treatment of RR-MS is to prolong the intervals between relapses (Kappos, *et al.*, 2006). Interferon-1β was the first drug to be approved for the treatment of RR-MS, in 1993, and is still in common use today. It was shown in a random placebo controlled trial to reduce the number of annual relapses (Paty, *et al.*, 1993). Recently, MS treatments have focused on RR-MS as this appears to provide the largest benefit to the patient. To this end a number of new treatments, including glatiramer acetate and Natalizumab and Mitoxantrone

have been trialled. Glatiramer acetate has been shown to be as effective as interferon-β at reducing MS lesions on MRI, however, 39% of patients receiving this treatment suffered from a reaction to the injection such as swelling around the injection site (Comi*, et al.*, 2001). Glatiramer acetate is thought to work by activating the Th2 pathway in the CNS by promoting the excretion of pro-inflammatory cytokines (Comi*, et al.*, 2001).

Natalizumab was the first monoclonal antibody treatment for RR-MS which passed into clinical use. It was reported that the number of annual relapses of patients was 0.26 as opposed to 0.81 in the placebo group (Polman*, et al.*, 2006). Natalizumab works by binding to two different integrins (α1β4 and α4β7) on leukocytes. These intergrins are responsible in the binding of VCAM-1 and mucosal addressin-cell adhesion molecule-1. This binding reduces the inflammatory response by these leukocytes and hence reduces the number of relapses (Polman*, et al.*, 2006). Mitoxantrone reduces the DNA and RNA synthesis of B and T cells (Mauch*, et al.*, 1992). Mitoxantrone has been shown to be an effective therapy in RR-MS and SP-MS (Edan*, et al.*, 1997; Mauch*, et al.*, 1992; Noseworthy*, et al.*, 1993), however, there are several side effects such as cardiotoxicity and acute leukaemia which means the use of this treatment is limited in the clinic (Goodin*, et al.*, 2003; Voltz*, et al.*, 2004). More recently the focus of MS therapy has been on creating an oral treatment for MS. This has led to the development of cladribine which is an oral anti-inflammatory drug which works by causing the death of activated T and B cells. Cladrabine has shown to be effective treatment for RR-MS patients, with a reduction of lesion load as measured by MRI after 18 months (Beutler*, et al.*, 1996). However, there is evidence of side effects from cladarbine, which have been reported following a phase III clinical trial. These side effects include mild ones such as an increase in lymphocytopenia (25% increase over controls) and headaches (5% increase over controls), to more serious adverse effects such

as 4 deaths from a population of 884 as compared to 2 in the placebo group (n = 435) (Giovannoni*, et al.*, 2010).

Two further drugs are currently undergoing clinical trials. These are Fingolimod, which internalises sphingosine-1 receptors (Brinkmann*, et al.*, 2010) and Ocrelizumab, a humanised anti CD-20 antibody (Hutas, 2008). The internalisation of the sphingosine-1 receptors caused by Fingolimod, depletes the number of circulating T-cells due to their inability to leave the lymph nodes or the thymus once these receptors are blocked (Hiestand*, et al.*, 2008). Clinical trials of Fingolimod has shown a significant reduction in Gd-enhanced lesions in RR-MS patients (Kappos*, et al.*, 2006). However, there are a number of serious side effects to this drug including 2 reported deaths from opportune infections (Spain*, et al.*, 2009). Ocrelizumab causes depletion of $CD20^+$ B cells by interfering with the lipid rafts associated with these cells (Kasper*, et al.*, 2010). This drug is currently undergoing a phase III clinical trial, however, the non-humanised form rituximab has shown promise in reducing Gd-enhanced lesions in RR-MS patients (Hauser*, et al.*, 2008), but with significant side effects following multiple doses, hence the need for humanisation (Stuve*, et al.*, 2009).

1.5.3.2. Secondary Progressive MS

Approximately 65% to 80% of RR-MS patients will enter a second stage of disease (Compston*, et al.*, 2008; Lublin*, et al.*, 1996; Weinshenker*, et al.*, 1989) which is known as secondary progressive MS (SP-MS). The defining feature of this stage of disease is that progress toward permanent disability becomes steadier and there are no longer periods of complete remission. It is possible for the patient to suffer small bouts where the disease worsens and then recovers slightly, but this is not as common as in RR-MS (Lublin*, et al.*, 1996). Defining the transition between RR-MS and SP-MS has become a key feature in MS research in recent years. This is due to the different treatment regimes that the

two stages of the disease require (Jones*, et al.*, 2010). The difficulty with differentiating between these two stages of the disease arises primarily from the fact that the mechanisms underlying each stage of disease are not fully understood. There is often a wide disparity between clinical symptoms, MRI visible lesions (McFarland, 1999) and immunohistochemical analysis (Raine*, et al.*, 1988) in the two stages of disease (Figure 1.3 B). The duration of the SP-MS stage of disease is again highly variable, but it has been reported that the median time for patients to reach severe disability is 6 years (Runmarker*, et al.*, 1993).No effective disease-modifying therapies are available for SP-MS and any treatments are purely palliative. However, it remains important to identify the transition from RR to SP-MS and, at present there is no effective biomarker. This is because the treatments for RR-MS generally modulate the immune system within the patient, which increases the risk of opportune infections or developing certain cancers. Thus, it is vital for clinicians to stop these medications when they cease to be effective. There is also considerable research work being invested into finding therapies which slow down or stop the progression of the disease, and therefore being able to monitor a patient's transition from RR-MS to SP-MS is critical to their receiving the correct treatment.

1.5.3.3. Primary Progressive MS

The remaining 20% of patients who contract MS suffer from progressive disability throughout the disease course (similar to SPMS, Compston*, et al.*, 2002). This stage of disease is known as primary progressive MS (PP-MS). Like SP-MS patients, PP-MS patients can also have small plateaus in disease progression, but there is a clear underlying trend to permanent disability (Scalfari*, et al.*, 2010), (Figure 1.3 C). The me6dian time for a patient to reach

severe disability is the same as for SP-MS, 6 years (Runmarker*, et al.*, 1993). Again there are no effective disease-modifying treatments for PP-MS.

1.5.3.4. Primary Relapsing MS

A fourth type of MS has also been described, that of primary relapsing MS (PRMS). However, PRMS is a very rare form of the disease (Tullman*, et al.*, 2004), and it is estimated that only 6% of MS patients suffer from PRMS (Oshinsky*, et al.*, 1998). This type of MS is similar to PP-MS, but with periods of acute attacks which then relapse back to the original PP-MS disease course (Oshinsky*, et al.*, 1998), (Figure 1.3 D). Disease progression in PRMS follows closely that of PP-MS (Confavreux*, et al.*, 2000).

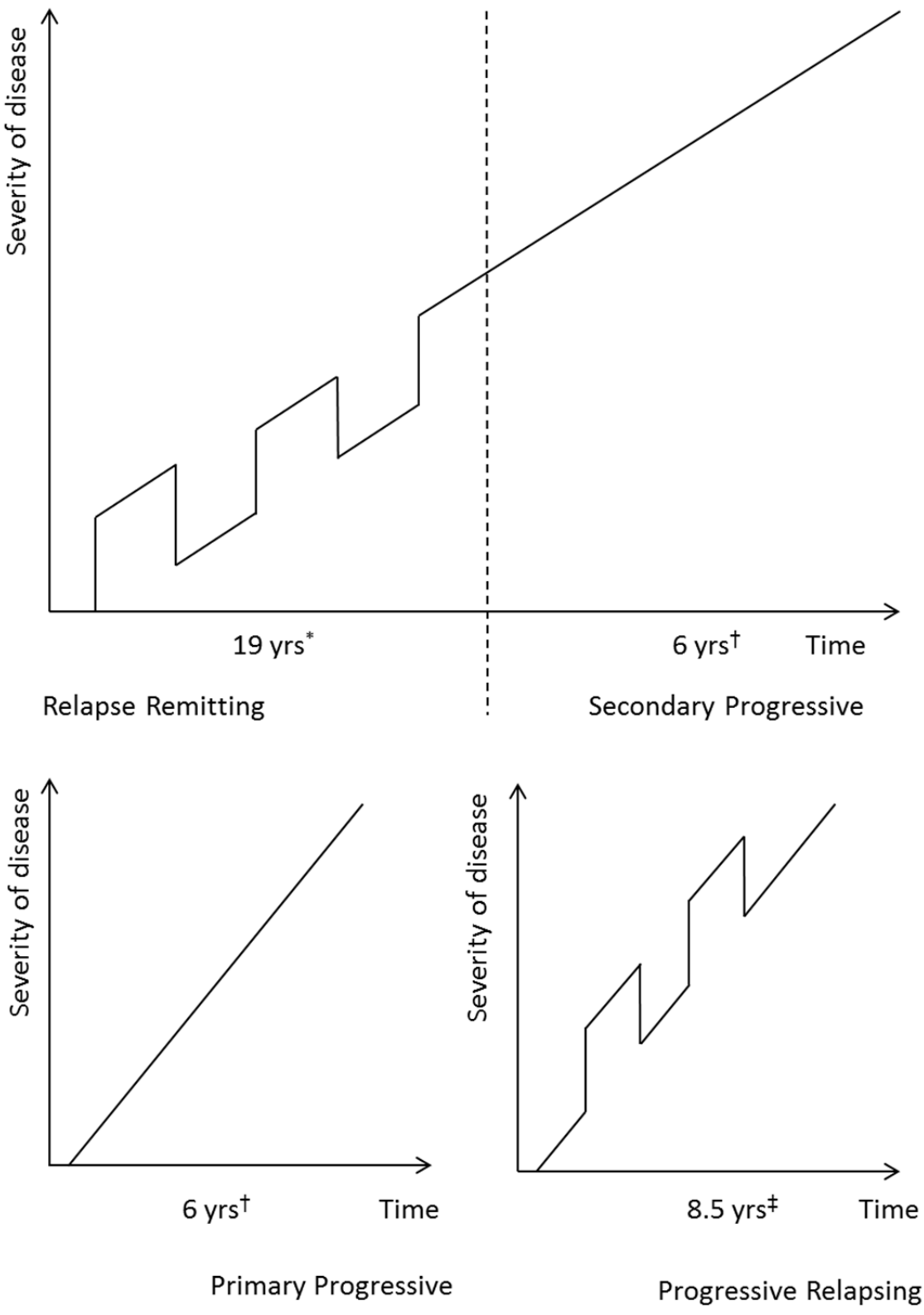


Figure 1.3: Clinical course of MS. (A) Relapse remitting MS, showing periods of clear clinical symptoms followed by a complete or partial remission. (B) Secondary Progressive MS, showing the steady progress towards complete disability. (C) Primary Progressive MS, showing patients steady progress towards complete disability. (D) Primary Relapsing MS, showing the underlying progress to complete disability with acute attacks superimposed onto the top. Key: * Median time, reported by Rovaris, et al., 2006; † Median time, reported by Runmarker, et al., 1993; ‡ Median time, reported by Tullman *et al. 2004*.

1.5.4. Current diagnostic criteria for MS

There are several different guidelines for the diagnosis of MS including the Schumacher (Schumacher*, et al.*, 1965) and the Poser (Poser*, et al.*, 1983) criteria. However, these have mostly been superseded by the gold standard criteria for MS diagnostics, which is known as the McDonald criteria. An international panel of experts chaired by McDonald published the following set of guidelines in 2001 (McDonald*, et al.*, 2001).

1.5.4.1. Definitions required for the McDonald criteria

McDonald *et al*. identified key areas where the definition of clinical symptoms was not clear. The authors describe an 'attack of MS' as either a relapse or an exacerbation of the disease which can be attributed to a demyelination event caused by inflammation. These could be a wide range of attacks, such as blurred vision (optical neuritis) or dizziness. The time between separate attacks was also a key issue that needed to be defined in order to distinguish between early cases of PP-MS and RR-MS. The authors determined that there has to be a gap of 30 days in order for attacks to be considered separate (McDonald*, et al.*, 2001).

McDonald *et al*. also incorporated MRI as a key tool in the diagnosis of MS, owing to its utility in identifying lesions in both time and space. With this information, it is possible to determine whether a sufferer has a singular lesion or several disseminated lesions in the CNS. To ensure the accuracy of a positive diagnosis of MS by MRI, three out of four of the following markers must be present in the MRI scan (Barkhof*, et al.*, 1997; Tintore*, et al.*, 2000):

1. One Gadolinium (Gd)-enhanced lesion or nine T2 hyperintense lesions
2. At least one lesion in the infratentorial region within the brain
3. At least one juxtacortical lesion

4. At least 3 periventricular lesions

If there is a lesion detected in the spinal cord of the patient, this can be substituted for one of the brain lesions (Tintore*, et al.*, 2000). Figure 1.4 shows examples of the types of lesions that are visible by MRI scans. In order to visualise lesions using Gd-enhancement BBB breakdown must occur, thus allowing the contrast agent to accumulate within the lesion (Kermode*, et al.*, 1990). It has been shown that BBB breakdown only occurs during the initial acute phase of lesion activity (McFarland*, et al.*, 1992).

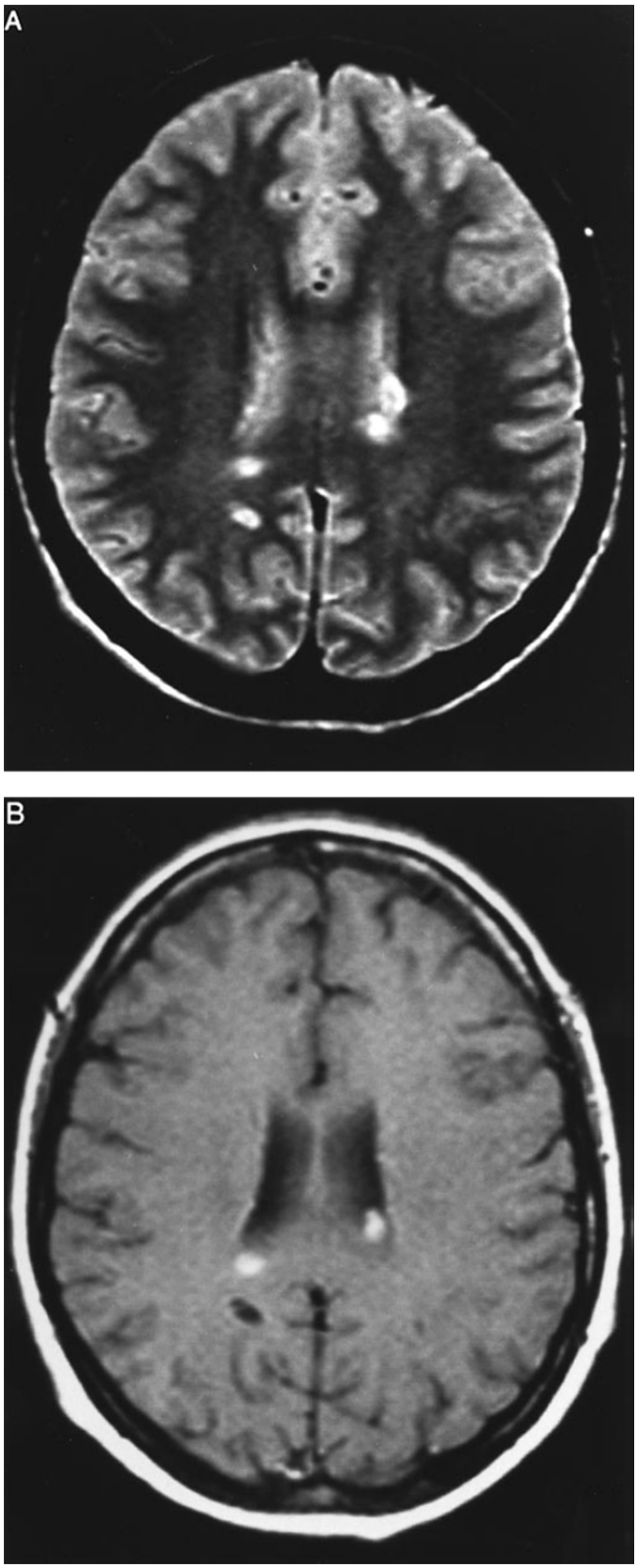


Figure 1.4: MRI brain scans of MS patients. A) T2 weighted image revealing the presence of MS lesions within the brain of an MS patient. B) T1 weighted image using Gd as a contrast agent the white areas reveal the presence of blood-brain-barrier breakdown due to the presence of MS lesions. Reprinted from (Barkhof*, et al.*, 1997) with kind permission of the journal.

McDonald *et al.* also saw the need to incorporate cerebrospinal fluid (CSF) analysis into the diagnostic criteria. It was noted by Andersson *et al.* 1994 and Link *et al.* 1997 that the presence of different oligoclonal Immunoglobulin G (IgG) bands in the CSF, when compared to the serum from the same patient, represented abnormalities within the CSF (Andersson*, et al.*, 1994; Link*, et al.*, 1977). This was the definition used by McDonald *et al.,* but CSF analysis was only to be taken into account if the imaging data was not fully conclusive (McDonald*, et al.*, 2001). The major problem with CSF analysis, which prevented it from being used alone, was the fact that at the time the analysis varied between laboratories and was hard to reproduce.

Visual evoked potential (VEP) can show the existence of a secondary lesion within the optical pathways in the CNS. If there is a lesion within the optical pathways then there will be a disruption to the EEG signal within the occipital lobe upon visual stimulus (Aminoff*, et al.*, 1994). This can only be used as diagnosis of MS so long as the original lesion identified by MRI is not within this area of the CNS (Gronseth*, et al.*, 2000).

1.5.4.2. McDonald criteria

Owing to the nature of the initial symptoms of MS the McDonald criteria had to take into account a wide range of scenarios. The authors set these out in a strict order from clinical symptoms which require no extra evidence, to cases which require far more stringent biomarker tests (McDonald*, et al.*, 2001). The diagnostic scheme is set out in Table 1.3.

The easiest diagnosis of MS requires two or more attacks that can be associated with two or more separate lesions. These attacks must be separated in time, and it is not valid to have two separate symptoms presenting at the same time. By the definitions given above (1.5.4.1) this means that it takes at

least 30 days to confirm a definite case of MS. While it would be unusual to have no supportive evidence from MRI, CSF or VEP analysis to confirm the diagnosis, they are not strictly needed if the first condition is met (McDonald*, et al.*, 2001). For example, if a patient suffers one attack of optical neuritis, followed by muscle weakening a few weeks later then this can provide evidence of two attacks disseminated in time, associated with two CNS lesions disseminated in space.

It is possible that a patient can suffer two or more attacks which only provide evidence of one lesion. For example, if a patient suffers from optical neuritis twice with a 30 day gap between the two attacks this provides evidence of a lesion within the visual pathways of the patient. However, it does not provide conclusive diagnosis of MS as there is no evidence of two separate lesions in time and space within the patients' CNS. Therefore, MRI must be used in order to identify whether there are any other lesions disseminated in space within the CNS that are clinically silent. If this is not evident, then there must be two lesions detected by MRI within the same region of the CNS and the analysis of IgG fractions within the CSF must be positive to confirm a diagnosis of MS. If there is still not enough evidence from the CSF tests then the patient must wait for a further attack to provide evidence of a lesion elsewhere in the CNS.

If there is only one attack, but clear clinical evidence of two lesions, it is still possible to diagnose MS. However, the dissemination of lesions through time becomes a critical issue in this case. These constraints reduce the chances of a misdiagnosis from such diseases as disseminated encephalomyelitis with affected speech patterns (Dale*, et al.*, 2000). In order to reduce this risk, the evidence for the two clinical lesions must be separated by at least 3 months (McDonald*, et al.*, 2001). For a more detailed description of the additional evidence required to make this diagnosis see Table 1.3.

In the case of CIS patients, showing only one attack and therefore one clinically objective lesion, there must be strong supporting evidence for a diagnosis of MS to be made. Once again, initially, there is no dissemination in time and space of lesion burden in the CNS. If the lesion present on the MRI scan is spatially resolved from the clinical symptoms then it is possible to diagnose MS immediately. If this is not possible, then there has to be supporting evidence from the CNS markers plus two or more lesions on the MRI scan. Other possible diagnosis scenarios are given in Table 1.3 (McDonald*, et al.*, 2001).

The McDonald criteria predominantly focused its attention on the initial diagnosis of MS. The guidelines did not provide a set of criteria for monitoring when patients make the transition from the RR phase into the SP phase. This transition between the phases is critical in terms of which treatment the patient receives (as discussed in 1.5.3). Therefore a set of biomarkers which could be followed serially within RR-MS patients would be an invaluable tool for clinicians and this has led to the exploration of the hypothesis that metabolomics can be used for the staging of MS.

A further problem that McDonald *et al.* faced when writing the criteria was the issue of PP-MS cases. Owing to the progressive nature of the disability there is little evidence for relapses and, thus, the dissemination of lesions in time and space is hard to prove. They concluded that a strict set of guidelines published by Thompson *et al.* was the only way to diagnose PP-MS (McDonald*, et al.*, 2001). These guidelines stated that the disability had to be progressing for at least 1 year before a diagnosis of MS could be made. They also noted that for a conclusive diagnosis, there must be clear evidence from CSF analysis showing that inflammatory events were occurring within the CNS (Thompson*, et al.*, 2000).

The final category that McDonald *et al.* included was a 'no better explanation' diagnosis. They advised extreme caution must be used for this diagnosis and only if all other autoimmune diseases had been ruled out (McDonald*, et al.*, 2001).

1.5.4.3. Revisions to the McDonald criteria

In 2005 another panel was set up to review the McDonald criteria and assess how successful the guidelines had been in the light of new studies using the criteria. One area the authors looked at was the growing body of evidence that as MRI scanners gained resolution, T2 lesions were as reliable a marker of MS as Gd enhanced lesions. However, these T2 lesions still require the breakdown of the BBB and therefore are still a late stage marker of disease. The greater sensitivity of T2 lesions arises from the fact that the T2 lesions persist longer than the Gd enhanced lesions and hence give a better indication of the time period between MRI scans. Therefore, T2 lesions could potentially be used to diagnose MS faster (Dalton*, et al.*, 2003). This review also recognised the fact that the McDonald criteria focused primarily on MS in the western world. There were significant number of misdiagnoses reported in Asia where there is a higher proportion of demyelinating diseases that overlap with MS (Polman*, et al.*, 2005). The criteria also failed to separate MS from other common demyelinating disorders such as neuromyelitis optica (NMO). Primarily at the time the guidelines were written there was debate on whether NMO was actually a separate disease or a specific type of MS. Therefore, the need to separate out this disease was not included within the criteria. However by 2005, a set of unique biomarkers where discovered in the CSF that enabled the diagnosis of NMO as a separate disease (Lennon*, et al.*, 2004).

The following revision to the McDonald criteria was proposed: if the symptoms present with two attacks, with only one clinically defined lesion, the diagnosis

time could be dropped from 3 months to 5 weeks using the revised imaging technique (Polman*, et al.*, 2005). Further to this revision, another panel was set up in 2010 to revise the diagnostic criteria for MS (Polman*, et al.*, 2011). This review attempted to speed up the diagnosis of MS by removing the 30 day limit for the new T2 lesion in order for it to be classified as disseminated in time. The relaxation of the 30 day limit was based on work by Tur *et al.* who reported that new T2 lesions appearing on an MRI scan before the 30 day limit does not reduce the specificity of the diagnosis of MS (Tur*, et al.*, 2008).

The inclusion of spinal cord imaging in the original report caused confusion as this was poorly defined in the original criteria. The panel in 2005 decided that, for a spinal cord lesion to replace a brain lesion, the lesion must be at least 3mm in size but less than two vertebral segments in length. They also stated that the spinal cord lesion could replace the infratentorial lesion, but not as either of the other lesions (as set out by Barkhof*, et al.*, 1997). It was noted that various studies had shown that abnormalities on a brain scan from a healthy individual can occur, especially in an aging individual. These lesions are far less common in the spinal cord (Bot*, et al.*, 2002; Kidd*, et al.*, 1993; Lycklama*, et al.*, 2003). Therefore, it was decided that more emphasis should be placed on the presence of spinal cord lesions in older patients (Polman*, et al.*, 2005). The authors also noted that lesions in the spinal cord must not be diffuse as these changes are not a good predictor of MS (Polman*, et al.*, 2005). In 2010 the panel noted that the dissemination in space requirement needed revision (Polman*, et al.*, 2011). This was based on a multicentre clinical trial known as Magnetic Imaging in MS, from which it was reported that the original MRI criteria set out by Barkof *et al.* and Tintoré *et al.* for the diagnosis of MS was too strict (Montalban*, et al.*, 2010; Rovira*, et al.*, 2009; Swanton*, et al.*, 2007). Therefore, the panel recommended that the guidelines set out by Swanton *et al.* should be used for showing lesion dissemination within space. These guidelines

stated that there only needed to be T2 lesions in two out of four CNS regions. These regions were the same as defined by Barkof *et al.* and Tintoré *et al.* with the addition of the spinal cord (Swanton*, et al.*, 2006; Swanton*, et al.*, 2007).

The last area that the panel in 2005 sought to improve was the diagnosis of PP-MS. Wolinsky *et al.* reported that CSF analysis was not required for a positive diagnosis of MS if MRI-detectable changes are present within the CNS (Wolinsky, 2003). The panel, therefore, recommended that the need for CSF analysis for the diagnosis of PP-MS was no longer required (Polman*, et al.*, 2005).

In 2010 at a meeting in Dublin , the panel noted that there is ~~a~~ great potential for biomarkers to be included in the diagnostic criteria for MS (Polman*, et al.*, 2011). This should enable a more rapid diagnosis of MS and, therefore, allow patients to take the appropriate treatments faster. Despite the various attempts to shorten the time to diagnose MS, in the majority of cases this can still take several months or years. Coles *et al.* have shown that the earlier you can start treatment with drugs such as Alemtuzumab, especially in the RR phase, the greater effect that therapy will have (Coles*, et al.*, 2011). Therefore, there is a desperate need for the identification of biomarkers in order to accelerate the process of diagnosing MS.

1.5.4.4. Current issues with MS diagnostics

There are still significant problems with the McDonald criteria, even with the two revisions, as a set of guidelines for the diagnosis of MS. The key areas that need to be improved are the length of time required to diagnose MS, and accurate staging of disease. It would be desirable to develop tests that categorise MS far more rapidly. This is especially true of separating RR-MS

from SP-MS patients as the treatment regimens for these two disease states are very different.

Clinical Presentation	Additional data required for MS Diagnosis 2001 criteria	Additional data required for MS Diagnosis 2005 revisions	Additional data required for MS Diagnosis 2010 revisions
Two or more attacks; objective evidence of 2 or more lesions	None[a]	None[a], however the authors of the report defined an attack as: an episode of neurological disturbance for which causative lesions are likely to be inflammatory and demyelinating in nature. There should be subjective report or objective observation that the event lasts for at least 24 hours	None, but the authors redefined an attack as: a patient reported or objectively observed event typical of an acute inflammatory demyelinating event in the CNS, current or historical, with a duration of at least 24 hours, in the absence of infection. They also allowed historical attack of a previous attack.
Two or more attacks; objective evidence of 1 lesion	Dissemination in space, demonstrated by MRI[b] ***or*** Two or more MRI detected lesions consistent with MS plus positive CSF[c] ***or*** Await further clinical attack implicating a different site within the CNS	No additional data required	No additional data required, however, the dissemination in space requirements were changed to more than one T2 lesion in at least 2 of the 4 MS-typical regions of the CNS
One attack; objective clinical evidence of 2 or more lesions	Dissemination in time, demonstrated by MRI[d] ***or*** Second clinical attack	No additional data required; however, lesion can be disseminated in time in two different ways: (A) Detection of Gd enhancement at least 3 months after the onset of the initial clinical event, if not at the site corresponding to initial event ***or*** (B) Detection of a new T2 lesion if it appears at any time compared with a reference scan done at 30 days after the onset of the initial clinical event	No additional data required, however, the dissemination in time requirements were changed to simultaneous presence of asymptomatic Gd-enhancing and nonenhancing lesions at any time; ***or*** A new T2 and/or Gd-enhancing lesion(s) on follow-up MRI, irrespective of its timing with reference to a baseline scan
One attack; objective clinical evidence of 1 lesion (CIS)	Dissemination in space, demonstrated by MRI[b] **or** Two or more MRI detected lesions consistent with MS plus positive CSF[c] ***and*** Dissemination in time, demonstrated by MRI[d] ***or*** Second clinical attack	No additional data required, however, using the definition of dissemination in time given above	No additional data required, however the updated definitions of dissemination in time and space should be used
Insidious neurological progression suggestive of MS	Positive CSF[c] ***and*** Dissemination in space, demonstrated by 1) Nine or more T2 lesions in brain ***or*** 2) 2 or more lesions in spinal cord, ***or*** 3) 4-8 brain plus 1 spinal cord lesion, or abnormal VEP[e] associated with 4-8 lesions, or with fewer than 4 brain lesions plus one spinal cord lesion demonstrated by MRI ***and*** Dissemination in time, demonstrated by MRI[d] ***or*** Continued progression for 1 year	One year of disease progression (retrospectively or prospectively determined) ***and*** Two of the following: (A) Positive brain MRI (nine T2 lesions or four or more T2 lesions with positive VEP[e]) ***or*** Positive spinal cord MRI (two focal lesions) ***or*** Positive CSF[c]	One year of disease progression (retrospectively determined) plus 2 of 3 of the following criteria[f]: (A) Evidence of dissemination in space in the brain based on one or more T2 lesions in the MS-typical CNS regions ***or*** (B) Evidence for dissemination in space in the spinal cord based on two or more T2 lesions in the cord ***or*** (C) Positive CSF[c]

Table 1.3: McDonald criteria for diagnosis of MS showing the revisions from both 2005 and 2010 (adapted from McDonald*, et al.*, 2001; Polman*, et al.*, 2005; Polman*, et al.*, 2011). If criteria indicated are fulfilled, the diagnosis is 'MS'; if the criteria are not completely met, the diagnosis is 'possible MS'; if the criteria are fully explored and not met, the diagnosis is 'not MS. [a] No additional tests are required; however, if tests [MRI, CSF] are undertaken and are negative, extreme caution should be taken before making a diagnosis of MS. Alternative diagnoses must be considered. There must be no better explanation of the clinical picture. [b] MRI demonstration of space dissemination must fulfill the criteria set out in Section 1.5.4.1 (derived from Barkhof*, et al.*, 1997; Tintore*, et al.*, 2000). [c] Positive CSF determined by oligoclonal bands detected by established methods different from any such bans in serum or by a raised IgG index (Andersson*, et al.*, 1994; Link*, et al.*, 1977). [d] MRI demonstration of time dissemination must fulfill the criteria listed in Section 1.5.4.2. [e] Abnormal VEP of the type seen in MS (delay with a well- preserved wave form) (Barret, 1994). [f] Gd-enhanced lesions are not required: symptomatic lesions are excluded from consideration in subjects with brain stem or spinal cord syndromes.

1.5.5. Animal models of MS

The main animal model used for studying MS is the experimental allergic encephalomyelitis (EAE) model. This condition was first observed by Louis Pasteur following a series of injections into humans of spinal cord homogenate from rabbits which resulted in paralytic episodes (as discussed by Baxter, 2007). In 1933 it was established that the injection of the spinal cord homogenate was the cause of the EAE symptoms (Rivers*, et al.*, 1933). EAE was induced in monkeys by injecting them with brain homogenate from rabbits multiple times. However, the induction of EAE took a long time and only occurred in a few animals (Rivers*, et al.*, 1933). It was not until the development of complete/incomplete Freund's adjuvant in 1942, which increased the antibody production (Freund*, et al.*, 1942), that a reliable animal model of EAE was developed (Freund*, et al.*, 1947; Kopeloff*, et al.*, 1947). It was noted that there were similarities between the animal models of EAE and human MS, including demyelination and the presence of CNS lesions (Wolf*, et al.*, 1947). Several attempts have been made to refine the EAE model in order for it to more closely resemble specific aspects of human diseases. For example, an EAE model was developed which resembled RR-MS (Brown*, et al.*, 1981; Zamvil*, et al.*, 1985). EAE was induced by the injection of T-cells which were specific to myelin basic protein in PL/J or (PLSJ)F_1 mice. This induced an acute phase of disability in all the animals, two thirds of these animals then went on to demonstrate a relapse-remitting pathology (Zamvil*, et al.*, 1985). Over the years the EAE models of MS have been used for a variety of reasons, including gaining a better understanding of how the demyelination occurs (Cammer*, et al.*, 1978). Recently, these models have been used to develop new therapies such as fingolmoid which has been tested in EAE models (Virley, 2005).

There are now multiple methods of inducing EAE in animals, however the majority of these methods cause an acute period of symptoms. The nature of the disease and extent of demyelination is affected by the means of induction (Baxter, 2007). One of the hypotheses in this thesis is that metabolomics can be used to differentiate between the different stages of MS in humans. Therefore, this thesis will use a chronic EAE (Cr-EAE) model that closely resembles human MS. It has been reported that such a model could be induced in Biozzi mice (Baker*, et al.*, 1990). This study reported that it was possible to induce Cr-EAE in mice with a high antibody titre following an injection of guinea pig spinal cord homogenate in complete Freunds adjuvant (CFA). It was also noted that the antibody low Biozzi mice were resistant to Cr-EAE (Baker*, et al.*, 1990). The relative ease of induction coupled with the low mortality rate of the mice during the disease time course makes this an ideal model for studying MS.

1.5.6. Previous biomarker studies in MS

The search for easily accessible biomarkers that can differentiate between the different clinical phenotypes of MS is an important goal for the development of new therapies in MS (Bielekova*, et al.*, 2004) and for monitoring the effects of neuroprotective treatment.

Identifying specific biomarkers using biofluids has previously been considered across a number of diseases both in animal models and humans. Urines from patients with neurological diseases, including MS, have been assayed for disease-specific markers, such as myelin basic protein-derived material indicating demyelination (Whitaker*, et al.*, 1994; Whitaker*, et al.*, 1995) or neopterine as a marker of CNS inflammation (Giovannoni*, et al.*, 1997; Ott*, et al.*, 1993b). However, these studies focussed on the detection of either a single or a small number of specific metabolites, and while differences have been identified at a group level, predictive value at an individual level has been low.

Therefore the need to develop a set of biomarkers which can diagnose MS at an earlier stage is crucial. It is also necessary to develop a set of markers which can distinguish between different stages of MS. This is needed in order to assist patients being put on the correct treatments at an earlier time point. As discussed previously, the only disease-modulating therapies in MS aim to treat RR-MS and have potentially lethal side effects. Getting MS patients onto the correct therapy for the disease stage will reduce the chance of the patient suffering from side effects when the therapy is no longer effective. The metabolomic profiles could also enable clinicians to monitor the effects of a specific drug on a patient-to-patient basis, thus personalising their treatment regimes. Therefore this thesis will attempt to identify a set of biomarkers within biofluids of MS patients which can be followed serially. This hypothesis will be explored in Chapter 3 of this thesis.

1.6. Alzheimer's disease

1.6.1. General

AD is a form of dementia first characterised by Alois Alzheimer in 1906 (Berchtold*, et al.*), and is characterised by neuronal loss, predominantly within the cerebral cortex. The exact causes for the disease remain unknown and there are several hypotheses for how neuronal loss occurs. However, several studies have reported that generalised neuroinflammation causes the neuronal damage (Akiyama*, et al.*, 2000; Rogers, 1995). There are several studies which link the underlying cause of this inflammation to the build-up of extra cellular proteins such as amyloid beta (Aβ) or the *tau* protein (Hardy*, et al.*, 1991; Mudher*, et al.*, 2002).

1.6.2. Prevalence of AD

AD is the most common form of cognitive impairment and accounts for 60-80% of all dementia cases. It is estimated that 33.9 million people suffer from AD worldwide (Barnes*, et al.*, 2011). However, it is estimated that by 2050 the number of AD cases will be around 106.2 million (Brookmeyer*, et al.*, 2007). The primary reason for this is the fact that the world's population is aging (Barnes*, et al.*, 2011; Brookmeyer*, et al.*, 2007). It has been reported that there is a marked increase in the incidences of AD cases within a population as the age increases (Launer*, et al.*, 1999). There is also an increased risk of females developing AD during their lifetime with a relative risk of 1.55 when compared to the male population (Launer*, et al.*, 1999). The reason for this increase in women is not fully understood but studies have reported that oestrogens and progesterone levels can have a neuroprotective effect within the CNS (Goodman*, et al.*, 1996). When the levels of these two hormones fall in

postmenopausal women this neuroprotective element is lost resulting in an increase in AD.

1.6.3. Clinical course of AD

There are 4 main stages of AD. However, AD can only be confirmed by autopsy (Dubois*, et al.*, 2007). There is a wide variation in the symptoms suffered on an individual basis. It is clear however, that the earlier treatment can be started the more effective it can be in slowing down the onset of full-blown dementia (Venneri*, et al.*, 2002). According to the NICE guidelines published in 2009 the mean life expectancy of a patient who is diagnosed with AD is 7 years . The four stages of AD are outlined below.

1.6.3.1. Stage I

The initial stage of AD is difficult to detect and is often put down to the normal aging process (Arnáiz*, et al.*, 2003). This is known as the prodromal phase of AD and is prior to the onset of dementia. The symptoms are classified as mild cognitive impairment (MCI) and not all patients with MCI will go on to develop AD (Arnáiz*, et al.*, 2003). In certain patients, it is also possible to have a long period which is asymptomatic apart from abnormalities on an MRI scan. These abnormalities are generally the reduction of brain volumes over time. This happens at a faster rate in AD patients than those who have MCI (Evans*, et al.*, 2010). This asymptomatic stage of disease is known as preclinical AD and results from the formation of the protein plaques within the CNS as discussed above in 1.6.1 (Figure 1.5). Treatment at this phase of disease is currently under investigation and it is hypothesised that if the formation of Aβ plaques can be disrupted the onset of AD will be delayed or prevented (Cherny*, et al.*, 2001).

1.6.3.2. Stage II

Following the pre-dementia stage, patients will start developing cognitive impairments which hamper their everyday living (Figure 1.5). The most common manifestation of this is memory impairment or learning difficulties (Förstl*, et al.*, 1999). Other dementia related symptoms include the reduction in the ability to organise and execute tasks. The patients' language skills are also affected with a general reduction in their vocabulary (Förstl*, et al.*, 1999). Patients can also suffer from several non-dementia symptoms, such as depression and loss of coordination (Burns*, et al.*, 1990; Kluger*, et al.*, 1997). Patients suffering from this phase of disease usually function with little outside care (Förstl*, et al.*, 1999). The neuronal damage starts during the pre-dementia phase, however, this phase of the disease shows a marked decrease in neuronal integrity (Perrin*, et al.*, 2009) as shown in Figure 1.5. Neurofibrillary tangles also start developing during this phase of disease (Craig-Schapiro*, et al.*, 2009; Perrin*, et al.*, 2009). Donepezil, a cholinesterase inhibitor (Inglis, 2002). has been shown to improve cognitive function within AD patients at an early stage, and following a meta-analysis study of several clinical trials it does slow down the onset of stage IV AD (Hansen*, et al.*, 2008). It should be noted that AD seems to selectively damage cholinergic neuron transmissions.

1.6.3.3. Stage III

Patients will then go on to develop the moderate form of AD which is classified by a general decline of multiple cognitive functions. The rate of neuronal damage becomes steadier, however, the build-up of extra cellular proteins such as Aβ levels off (Craig-Schapiro*, et al.*, 2009; Perrin*, et al.*, 2009) as shown in Figure 1.5. Commonly the patient will lose all recent memories and appear to be living in the past (Beatty*, et al.*, 1988). The difficulties in communication will also increase as the dementia worsens often resulting in paraphasia and difficulty in

finding words during speech (Förstl*, et al.*, 1999). Other symptoms include difficulty reading and writing and a loss of knowledge about their overall condition (Cummings*, et al.*, 1986; Förstl*, et al.*, 1999; Neils*, et al.*, 1989). The patients in this stage generally cannot support themselves in the general community. Treatment of this phase of AD is aimed at slowing down the neuronal damage in order to preserve function. Memantine, an NMDA acceptor agonist, has been shown to slow the neurocognitive decline in a double blind placebo trial of mid to late stage AD suffers (Reisberg*, et al.*, 2003). The authors showed that the placebo group declined faster according to several measures of AD, such as the clinicians assessment of the patients, during the time course when compared to the treated group (Reisberg*, et al.*, 2003). It is a non-competitive *N*-methyl-D-Aspartate receptor agonist (Danysz*, et al.*, 2000). It has been shown to prevent overstimulation of neurons from glutamate which has been shown to cause neuronal damage (Lipton*, et al.*, 1994).

1.6.3.4. Stage IV

Stage IV of AD is terminal however, the largest cause of death in AD patients is actually pneumonia, septicaemia or a myocardial infection (Förstl*, et al.*, 1999). The patient requires 24 hour care and is often bedridden. There is a wide range of symptoms a patient can suffer from such as problems with chewing and swallowing. The patients language will also be reduced to basic phrases and they can also become violent to outside offers of help (Förstl*, et al.*, 1999).

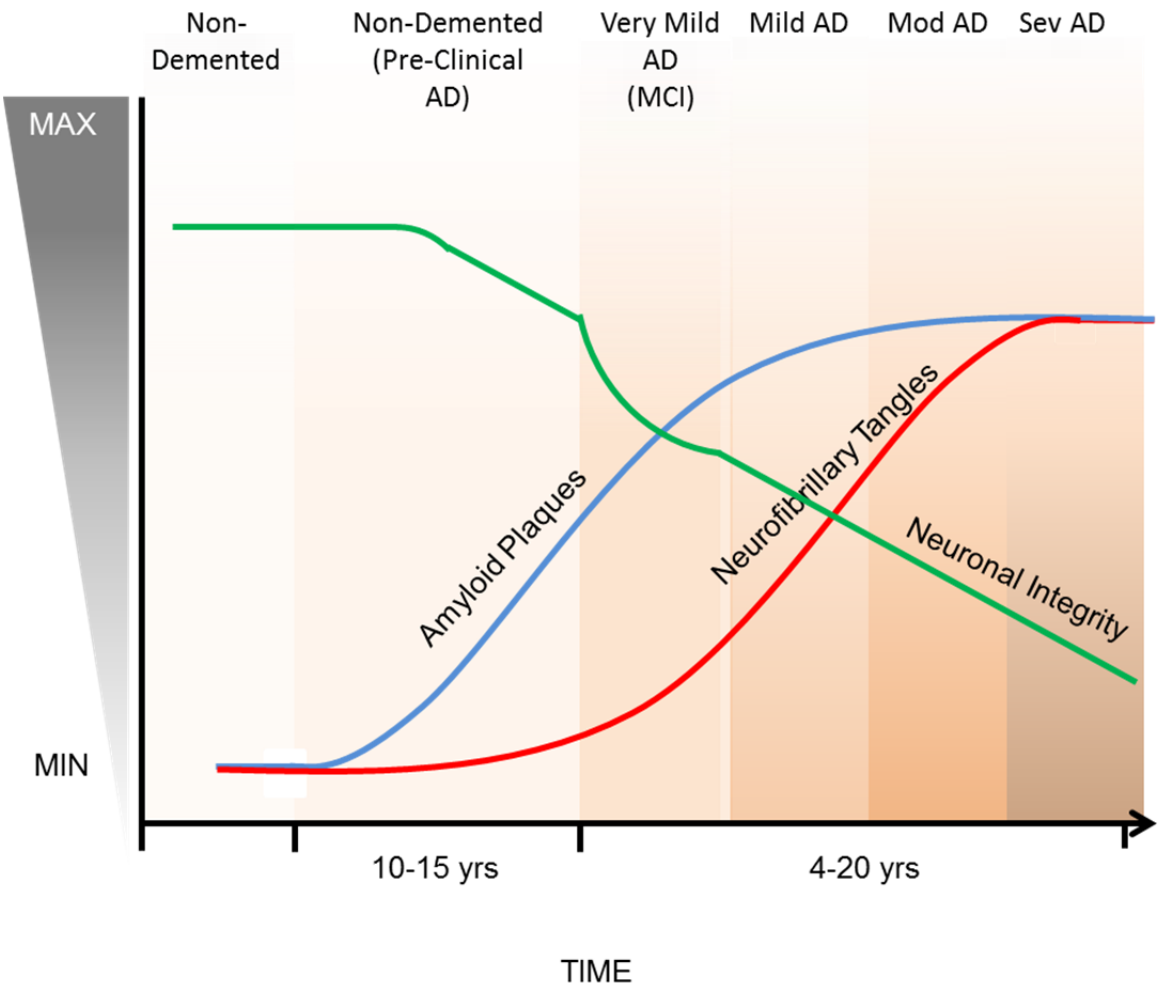


Figure 1.5: Clinical features of AD over time. Schematic showing the relative levels of common biomarkers during the disease time course and the various phases of disease (Figure adapted from Craig-Schapiro*, et al.*, 2009; and Perrin*, et al.*, 2009).

1.6.4. Current diagnostic criteria for AD

In order to diagnose AD, separation must be made from other forms of dementia. This is required because the mechanism of neurodegeneration in dementia and AD is likely to be different, such as the build-up of amyloid plaques (Van Broeck*, et al.*, 2007). Therefore separation of AD from other dementias is essential in order for the patient to be on the correct therapy. Early attempts at setting a standard for the diagnosis of AD concluded that the only way to get a definite diagnosis required a post mortem (Dubois*, et al.*, 2007). Therefore the authors described a set of criteria to define dementia and then a second set of criteria to diagnose 'probable' or 'possible' AD (McKhann*, et al.*, 1984).

They defined dementia as the 'decline of memory and cognitive functions in comparison with the patient's previous level of function'. This could be determined by a detailed analysis of the patient or by a set of neuropsychological tests. The level of dementia was determined using one of several tests such as the Mini-Mental test or the Blessed Dementia Scale (McKhann*, et al.*, 1984).

The clinical signs required for a diagnosis of 'probable' AD are in addition to the diagnosis of dementia defined above, and must include two of the following four conditions (McKhann*, et al.*, 1984):

1. 'Progressive worsening of memory and other cognitive functions'.
2. 'No disturbance in consciousness'.
3. 'Onset between ages 40 and 90, most often after age 65'.
4. 'Absence of systematic disorders or brain diseases that could account for the progression seen in point 1'.

In 1990, the Diagnostic and Statistical Methods of Mental Disorders, fourth edition (DSM-IV-TR) was published which required the presence of both a memory disorder and an impairment in the cognitive domain. These two conditions have to interrupt the social wellbeing of the patient (Association*, et al.*, 2000).

These two criteria have remained at the forefront of AD diagnosis, however, they are both late stage diagnosis of AD. In order for treatments to become more effective at slowing down the onset of dementia it would be desirable to have diagnostic tools which detected AD during the mild or even prodromal/preclinical stages. Positron emission tomography (PET) has been shown to be a useful tool in the diagnosis of AD. The reduction in glucose metabolism can be detected with fluorodeoxyglucose-PET (FDG-PET) as shown in Figure 1.6 C and D (Coleman, 2005). This reduction in glucose metabolism is caused by physical brain atrophy. As the cerebral volume decreases the need for energy reduces and hence glucose metabolism is reduced (Coleman, 2005). However there appears to be a great variation with the specificity and the sensitivity of this technique (Patwardhan*, et al.*, 2004). A more promising PET contrast agent appears to Pittsburgh compound B (PiB) as a radio ligand (Figure 1.6 A and B). PiB binds to amyloid deposits within the brain (Kemppainen*, et al.*, 2006; Klunk*, et al.*, 2004; Shoghi-Jadid*, et al.*, 2002) and therefore can be used to detect probable AD cases at a far earlier stage (Figure 1.6). PiB is generally considered to be a better PET imaging agent than FDG for diagnosing Alzheimer's due to the lack of amyloid plaques in a healthy brain thus creating a greater contrast between healthy and diseased brains (Klunk*, et al.*, 2004). The problem with the original PiB compound was that it used Carbon-11 as the source of positrons. Carbon-11 has a half-life of 20 mins and therefore the radio ligand has to be produced and used immediately (Pimlott*, et al.*, 2011). This has led to the development of a fluorinated version

of PiB known as 18F-AV-45 and has shown, in a clinical trial, to be an effective agent for the imaging of amyloid plaques within the CNS of AD patients (Choi*, et al.*, 2009). The advantage of using fluorine-18 over carbon-11 is the longer half-life of ^{18}F, 110 compared to 20 minutes. This gives the clinicians a little longer to administer the radiotracer and therefore if needed it can be transported short distances.

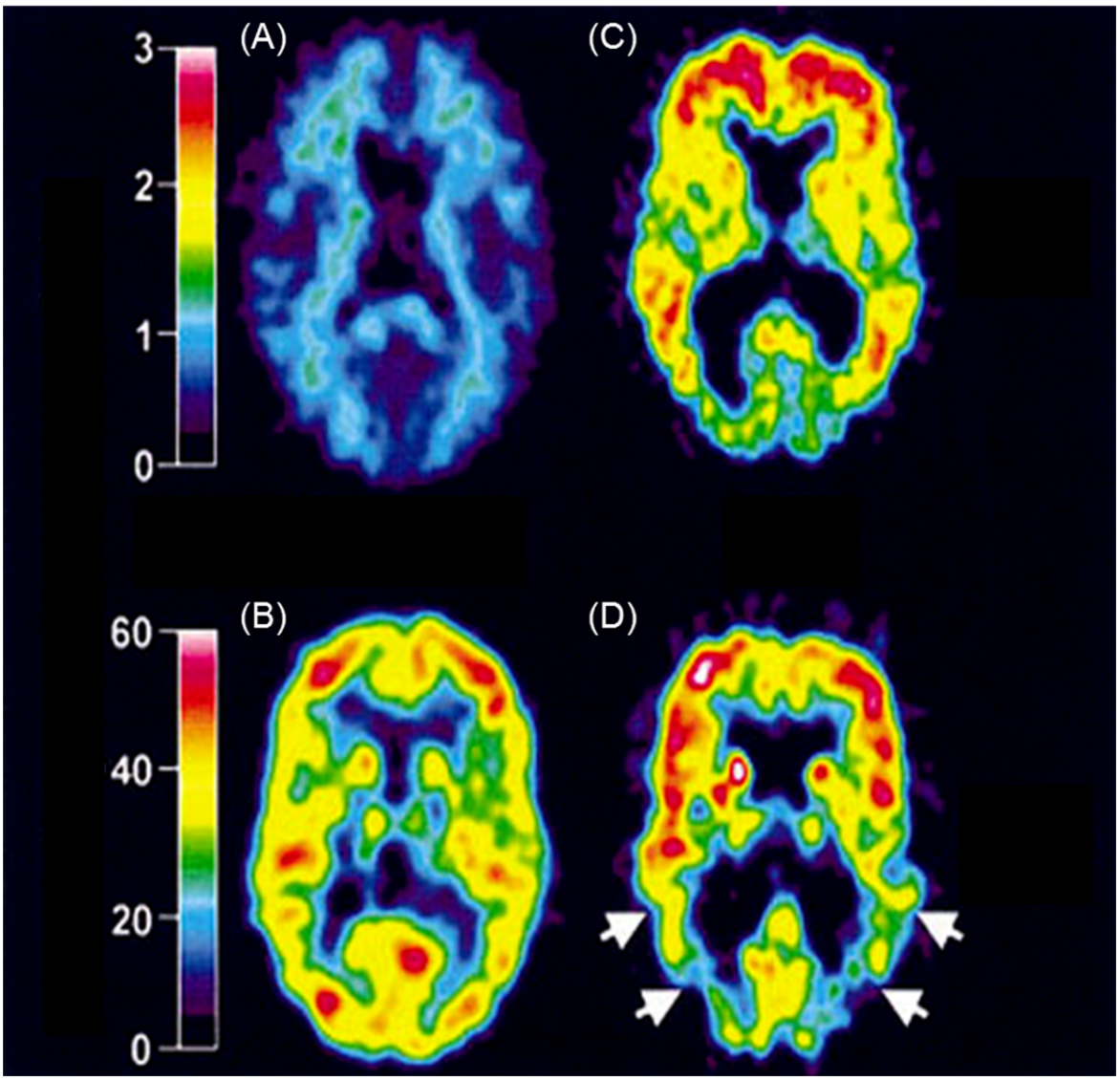


Figure 1.6: PET as a tool for AD diagnosis. (A) PET image of a healthy control brain using PiB as a radio ligand. (B) PET image of an AD patient's brain using PiB as a radio ligand. (C) PET image of a healthy control brain using FDG to image glucose metabolism. (D) PET image of an AD patient's brain using FDG to image glucose metabolism. (B) PET image of an AD patient's brain using PiB as a radio ligand. Arrow indicate area of reduced glucose metabolism. Reprinted from (Klunk*, et al.*, 2004) with kind permission of the journal.

1.6.5. Previous biomarker studies in AD

The primary focus of biomarker research into AD has been to try and predict which patients with MCI will go onto develop AD. It has been reported that the increased levels of *tau* protein and Aβ-42 within the CSF of MCI patients was a good predictor for the future development of AD (Hansson*, et al.*, 2006; Hulstaert*, et al.*, 1999). In order to measure these protein levels within the CSF a lumbar puncture is required in order to obtain the sample for analysis. Due to the nature of lumbar punctures it is difficult to get repeat measurements and therefore these would not be useful type II biomarkers. Therefore, in order to assist drug development it would be desirable to identify a set of biomarkers which could be obtained in a non-invasive fashion which discriminated between AD and other neurodegenerative diseases. N-acetyl aspartate (NAA) has been shown to be a biomarker of AD (Kantarci*, et al.*, 2000). NAA can be measured with the use of magnetic resonance spectroscopy within humans. This is a non-invasive technique, however, NAA is not specific to AD. It has been reported that a decrease in the levels of NAA in the CSF is a generic marker of neuronal damage (Griffin*, et al.*, 2002).

The idea that AD can be diagnosed using biomarkers such as PET imaging and protein levels in the CSF is now well established. The use of AD within this thesis will primarily be as a comparison between the MS patients and another form of neurodegeneration. A previous metabolomics study has attempted to do this, but with limited success ('t Hart*, et al.*, 2003). In this study it was reported that it was possible to distinguish between MS patients and other neurological disorders using urine obtained from these patients. However, 5 out of 19 patients with other neurological diseases were mis-diagnosed as having MS. The MS patient group was also not sub-typed into the different stages of MS ('t Hart*, et al.*, 2003). Therefore, one of the hypotheses of this thesis will be, that it

is possible to use metabolomics to separate out different forms of neurodegeneration using a combination of ^{1}H NMR and PLS-DA modelling. Other forms of modelling such as orthogonal modelling will also be used to try to reduce the amount of variability observed within the datasets. Other factors such as gender and disability score will also be modelled separately in order to examine whether these affect the models. This hypothesis will be explored in Chapter 4 of this thesis.

1.7. Human immunodeficiency virus associated dementia

1.7.1. General

Acquired immune deficiency syndrome (AIDS) was first described in 1981 when four patients were discovered to have multiple infections simultaneously, which was unexpected due to the number and nature of the infections (Gottlieb*, et al.*, 1981). All four patients were infected with symtopmatic *Pneumocystis carinii* pneumonia, which tends to only develop in severely immune-suppressed patients (Aliouat-Denis*, et al.*, 2008) and multiple viral infections. The patients also could not produce leukocytes in response to the addition of a soluble antigen (Gottlieb*, et al.*, 1981). This suggested that the immune systems of these patients were compromised and the underlying cause of this was HIV (Gottlieb*, et al.*, 1981). The link between the human immunodeficiency virus (HIV) and AIDS was not established until 1983 (Gallo*, et al.*, 1983). HIV is a type of lentivirus, which is a RNA retrovirus (Weiss, 1993). One of the targets of HIV is the CNS and the virus can normally be detected within the CSF of patients throughout the disease time course (McArthur*, et al.*, 1997; Pilcher*, et al.*, 2001). There is a significant number of HIV patients who will develop a dementia type pathology due to their infection (Shapshak*, et al.*, 2011). These symptoms can vary from mild neurocognitive disorders from asymptomatic neurodegeneration, which is diagnosed at post mortem to full-blown HIV associated dementia (HAD) (Shapshak*, et al.*, 2011).

1.7.2. Prevalence of HIV associated dementia

Historically, before the development of anti-retroviral treatments, the prevalence of dementia caused by HIV was estimated to be around 15-30% of HIV patients (Power*, et al.*, 2009). Originally, it was reported that the cause of HAD was a high viral load in the initial stages of disease (Childs*, et al.*, 1999). The

development of Highly Active Antiretroviral Therapy (HAART), which reduces the viral load within patients did lead to a significant drop in the number of dementia cases. The rate dropped to around 10% after HAART treatment (Marle*, et al.*, 2005). Therefore, high viral load can only account for a proportion of the HAD cases. There is a growing body of evidence indicating that the number of HAD cases is now increasing owing to patients with HIV living longer (Marle*, et al.*, 2005) because of HAART therapy. Studies have also shown that following the onset of AIDS, the patients who die fastest have a greater chance of developing HAD (McArthur*, et al.*, 1993).

1.7.3. Clinical course of HIV associated dementia

When a patient is infected with HIV there is a period of 4-8 weeks where the virus is active as it spreads around the body. The plasma viral load increases significantly and the levels of circulating $CD4^+$ lymphocytes in the plasma decrease (Marle*, et al.*, 2005). Following this period, both levels of viral load and $CD4^+$ lymphocytes in the plasma return to near baseline levels (Figure 1.7). This is typically an asymptomatic phase of HIV, however, some patients develop MCI during this disease phase. During this phase there is also a steady decline in the plasma $CD4^+$ lymphocytes levels as shown in Figure 1.7 (Power*, et al.*, 2009). Patients suffering from MCI at this phase present very similar symptoms to AD patients at this time point. These include such symptoms as: memory impairment, muscular weakness or loss of coordination and changes in the emotional state of the patient (Power*, et al.*, 2009). This period of disease typically lasts around 10 years (Figure 1.7).

With the onset of AIDS the symptoms relating to the HIV become apparent. This also corresponds to an acceleration of the drop in circulating $CD4^+$ lymphocytes and an increase in the plasma viral load (Figure 1.7). During this phase of disease patients can develop HAD. The onset of symptoms generally occurs

when the $CD4^+$ positive T cell count drops below 200 cells/μL of blood (Figure 1.7) (Simpson*, et al.*, 1994). The decline in cognitive function is varied and can range between a few weeks to several months (Power*, et al.*, 1994). The clinical symptoms of HAD are similar to that of the dementia phase of AD. There are three common areas where the symptoms can manifest. These are neurocognitive impairments such as forgetfulness and lack of concentration, emotional disturbances (apathy) and motor dysfunction including tremors and ataxia (Power*, et al.*, 2009). The treatment of HAD is mostly reliant on HAART which reduces the viral load. HAART, however, does not readily enter the CNS. Attempts have been made to generate CNS penetrating anti-retroviral drugs. These include, zidovudine, and stavudine but with limited success (Letendre*, et al.*, 2008; Nath*, et al.*, 2004). A clinical trial of Memantine, a drug which is used to treat AD (as described in Section 1.6.3), has been performed in HIV patients (Schifitto*, et al.*, 2007). However, this study reported that Memantine had little effect, suggesting the underlying causes of these two neurodegenerative processes are different.

1.7.4. Neuropathology and pathogenesis of HIV associated dementia

The exact causes and underlying mechanisms of HAD are not fully understood. However, it has been reported that similar plaques of Aβ as seen in AD are observed in HAD brains (Pulliam, 2009). HIV expresses several glycoproteins such as gp120 and TAT on the surface in order to assist infection of cells in the case of gp120 or regulation for the case of TAT (Freed*, et al.*, 2001; Freed*, et al.*, 1995). It has been reported that these glycoproteins can have a neurotoxic effect (Bansal*, et al.*, 2000; Nath*, et al.*, 2000). These neurotoxic effects cause inflammation within the CNS resulting in neuronal death.

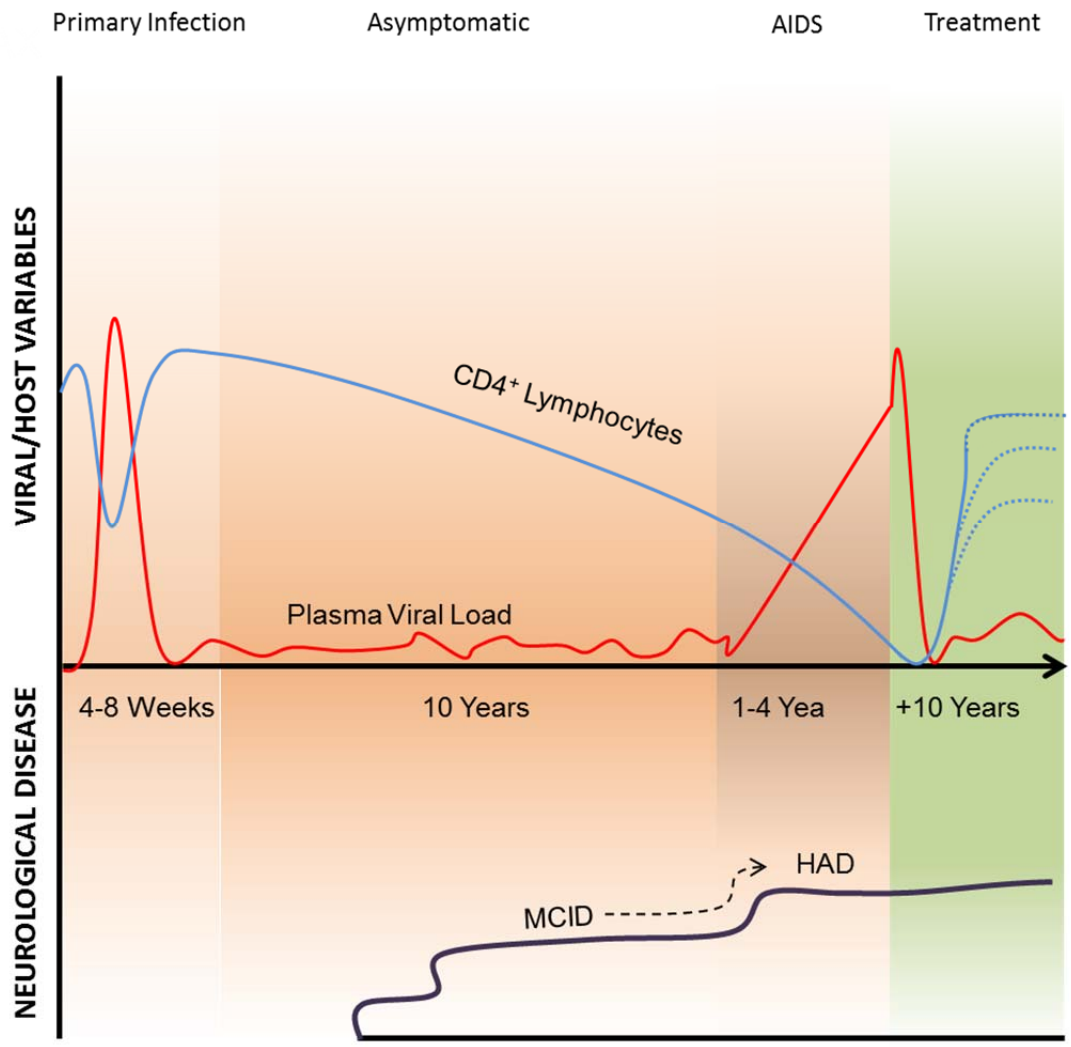


Figure 1.7: Clinical course of HIV associated dementia.(Adapted from Marle, *et al.*, 2005; and Power, *et al.*, 2009).

1.7.5. Diagnosis of HIV associated dementia

Typically the same neurocognitive tests used for AD are used for the diagnosis of HAD (see 1.6.4). In addition to this there are the HIV dementia scale and the international HIV dementia scale. However, their ability to diagnose specific dementia caused by the HIV from other neurodegenerative diseases remains unclear (Bottiggi*, et al.*, 2007; Power*, et al.*, 1995; Sacktor*, et al.*, 2005). There are a few radiological techniques which can be used for the identification of HIV associated dementia. It is possible to detect cerebral and basal ganglia atrophy T2 hyperintensities within the white matter (Simpson*, et al.*, 1994). These studies however, are not specific to HIV associated dementia despite there being a strong correlation between the amount of cerebral atrophy and the severity of the dementia (Aylward*, et al.*, 1993; Dal Pan*, et al.*, 1992). In a similar way to AD, FDG-PET has been shown as a useful tool for diagnosing late stage dementia.

Therefore the development of biomarkers which could distinguish patients who are developing HAD would have a beneficial effect. This is because the patients would be on the correct treatment at an earlier stage which could slow down the rate of neurodegeneration. Therefore Chapter 5 of this will explore the possibility of using ^{1}H NMR and PLS-DA modelling to distinguish between different neurocognitive states in a group of HIV patients.

1.8. Cancer metastases to the brain

1.8.1. General

Cancer is estimated to be the second most prevalent cause of death in the world, killing an estimated 7.6 million people in 2008 (Ferlay*, et al.*, 2011; Schouten*, et al.*, 2002). According to the World Health Organisation (2011), metastases account for the majority of cancer morbidity. Cancer metastasis refers to the process whereby a primary tumour spreads from its site of origin to a separate organ within the body and forms a new and distinct tumour (Hart*, et al.*, 1980). Metastatic tumours from peripheral origins are the most common form of tumour within the CNS (Arnold*, et al.*, 2001). The prognosis for the patient after diagnosis of CNS metastases is very poor, with the majority of treatments focused on palliative care (Patchell, 2003). From the onset of clinical signs, owing to the presence of brain metastases, death tends to occur within 3-6 months. Owing to the difficulties of surgery (discussed below) brain metastases frequently kill patients before the primary tumour does.

1.8.2. Prevalence of brain metastases

Between 20% and 40% of all patients who contract cancer will develop brain metastases during the course of their disease (Klos*, et al.*, 2004; Schellinger*, et al.*, 1999). The risk of developing brain metastases varies greatly depending on the primary tumour. A quarter of all brain metastases arise from patients initially suffering from lung cancer (Posner*, et al.*, 1978). Breast cancer and melanoma are the next most common causes (Klos*, et al.*, 2004).

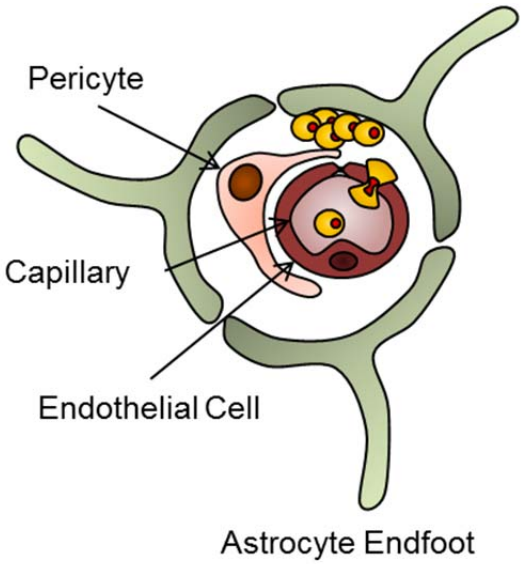
1.8.3. Formation of brain metastases

The mechanisms by which tumour cells metastasise remain unclear. Initially, it was thought that the dissemination of tumour cells from the primary tumour

occurred at a late stage in tumour development, and that, as a result, the metastatic cells would be genetically identical to the primary tumour cells (Klos*, et al.*, 2004). However, recently it has been noted that dissemination can occur at an early stage in primary tumour development (Podsypanina*, et al.*, 2008). Earlier dissemination can lead to metastatic cells that are not genetically identical to the primary cell line and, as a result, treatment developed for the primary tumour may be insufficient to treat the secondary tumour (as discussed in Klein, 2008).

Once the tumour cells have disseminated into the circulation they can arrest anywhere within the vasculature, with the potential to form a secondary tumour (Fidler, 2003). In order for a brain metastasis to form, the circulating cells must stop within the vasculature of the brain and then cross the BBB. However, not all circulating cells will be able to stop and form brain metastasis. It was noted in 1889 that the spread of breast cancer cells was not uniform across all organs within the body (Paget, 1889). The idea that certain cell lines metastasise to specific organs became known as the soil and seed hypothesis (Hart*, et al.*, 1980). The BBB is a layer of endothelial cells with tight junction proteins between the cells to ensure that the barrier is non-permeable to unwanted compounds and cells (Saunders*, et al.*, 2008). This is different from normal vasculature elsewhere in the body and confers on the brain a more tightly controlled environment than most other organs. Structurally, the barrier is supported by astrocytes, and the space between the endothelial cells and astrocytes is known as the perivascular space (Abbott*, et al.*, 2010). The mechanism by which cells cross the BBB remains unclear, however, it has been suggested that adhesion molecules may play a role in the arrest of circulating cells and their translocation across the endothelial layer (Biancone*, et al.*, 1996; Brodt*, et al.*, 1997; Kobayashi*, et al.*, 2000; Läubli*, et al.*, 2010a). Circulating inflammatory cells such as macrophages use a similar mechanism to cross the

BBB as part of the natural immune surveillance of the brain (Ubogu*, et al.*, 2006). Although evidence exists to support a role for adhesion molecules in metastasis to lung and liver (Brodt*, et al.*, 1997; Khatib*, et al.*, 1999; Läubli*, et al.*, 2010b; Ludwig*, et al.*, 2004; Vidal-Vanaclocha*, et al.*, 2000), there is as yet little experimental support for this in brain metastasis. However, other work within our group has shown that several adhesion molecules are upregulated early in metastasis pathogenesis in the brain (Serres*, et al.*, 2011; Soto*, et al.*, 2011). Following extravasation from the vasculature, the metastatic cells stop in the perivascular space where they can begin to replicate. It has been shown that metastases continue to grow within the perivascular niche for a fairly prolonged period (Carbonell*, et al.*, 2009), and it is only once they reach a certain size that they force their way into the brain parenchyma, as shown in Figure 1.8 (Fidler, 2003). Eventually, as the tumour grows the BBB will breakdown, however, this is late in tumour development.



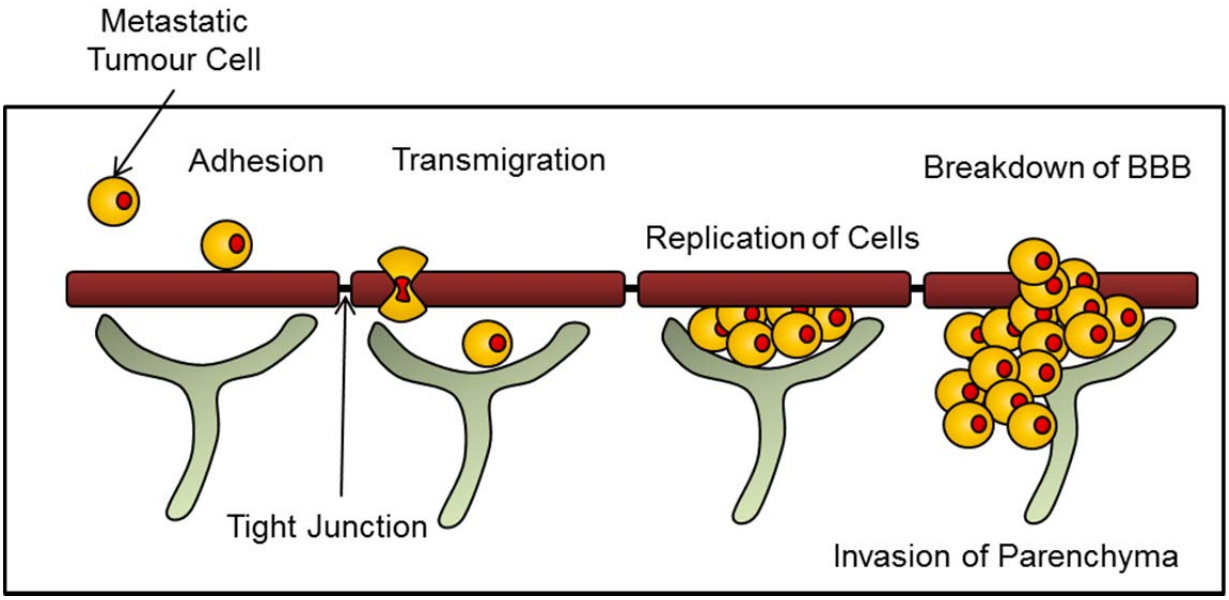


Figure 1.8: Formation of brain metastases.

1.8.4. Clinical symptoms of brain metastases

Patients with brain metastases may suffer from a wide range of neurological symptoms depending on the location of the metastasis within the CNS (Klos*, et al.*, 2004). One third of all patients with brain metastases, however, will never suffer from symptoms. These asymptomatic tumours are detected either during routine brain scans as part of any primary cancer follow up treatment or post-mortem (Klos*, et al.*, 2004). One of the most common symptoms is a headache, which arises from an increase in cerebral pressure caused by the presence of the brain tumour (Forsyth*, et al.*, 1993). Other common symptoms include cognitive impairment, seizures and focal weaknesses (Klos*, et al.*, 2004). These symptoms can arise from the presence of the tumour itself in a specific location. For example, if the metastatic lesion is located within the motor cortex of a patient then they will potentially suffer from limb weakness.

1.8.5. Treatment of brain metastases

There are few treatment options available to clinicians that will halt the growth of brain metastases. Left untreated the median survival time of a patient with brain metastases is 4 weeks (Klos*, et al.*, 2004). Corticosteroids have been used as a palliative drug to reduce the symptoms caused by brain metastases. These agents principally act by reducing the inflammatory response and reducing the edema caused by the presence of the metastasis within the CNS (Ruderman*, et al.*, 1965). However, corticosteriods do little to extend the life-expectancy of the patient with the median survival rate of 2 months (Chang*, et al.*, 1992; Markesbery*, et al.*, 1978; Ruderman*, et al.*, 1965). Other treatment options include whole brain radiotherapy, stereotaxic radiotherapy and surgery, which will be discussed below.

Whole brain radiotherapy (WBRT) is the most commonly used technique for treating brain metastases. Often this is the only option available to clinicians owing to the surgical inaccessibility of some deep brain tumours (Klos*, et al.*, 2004). WBRT can also be used to treat multiple metastases disseminated throughout the brain (Baschnagel*, et al.*, 2008). The treatment involves irradiating the patient's brain with a dose of radiation around 3000 Gy in 10 fractions over 2 weeks (Borgelt*, et al.*, 1980; Gelber*, et al.*, 1981; Leibel*, et al.*, 1987). However, this treatment only increases the median survival time for a patient suffering from brain metastases to between 3 and 6 months, depending on the primary tumour (Cairncross*, et al.*, 1980; Zimm*, et al.*, 1981). In addition to this, whole brain radiotherapy has the potential to cause lasting damage to the healthy brain owing to the levels of ionising radiation required during the treatment. These side effects can include cognitive impairment or leukoencephalopathy (Surma-aho*, et al.*, 2001).

In order to limit the dose of radiation to healthy brain tissue other techniques have been developed to locally administer radiation. These techniques include stereotaxic radiotherapy where the ionisation source is guided to the brain metastasis with use of a stereotaxic frame. This is not always a treatment option and is highly dependent upon the number and location of the tumours within the CNS.

Surgery is an option only if there are one or two tumours in accessible locations. WBRT is often used after surgery to remove any clinically undetected metastases. This combination of techniques has been shown in clinical trials to increase the lifespan of a patient by several months. Noordijk *et al.* 1994 reported that using the combination of surgery and whole brain radiotherapy increased median survival time from 6 months to 10 months. (Noordijk*, et al.*, 1994; Patchell*, et al.*, 1990; Vecht*, et al.*, 1993).

Even with all these treatment options the prognosis for brain metastasis still remains extremely poor. One of the main problems is the inability of current diagnostic techniques to detect brain metastases at an early stage, see below (1.8.6). The treatment options, even combined with chemotherapy, tend not to extend the life expectancy of the patient significantly (Robinet*, et al.*, 2001).

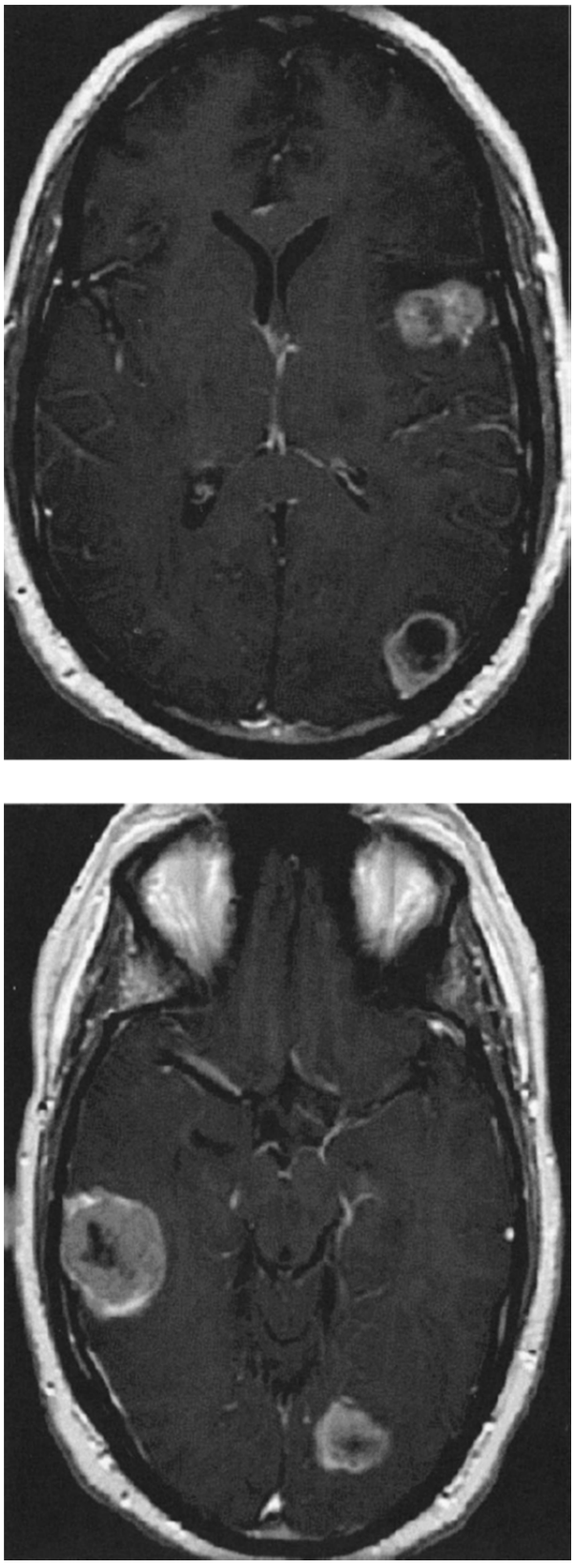


Figure 1.9: Diagnosis of brain metastases. Axial MRI T1 contrast weighted images revealing the presence of brain metathesis within the brain of a patient. Gd contrast shows the presence of BBB breakdown. A) and B) are both T1 weighted Gd enhanced MRI images showing the presence of brain metathesis within the CNS due to the breakdown in the BBB allowing the Gd to collected in the brain parenchyma. Reprinted from (Klos*, et al.*, 2004) with kind permission of the authors.

1.8.6. Current diagnostic tools for brain metastases

Brain metastases are currently diagnosed by identification of lesions on a brain scan. Two main techniques are used for this (as discussed by van den Bent, 2001): X-ray computed tomography scan (CT) or MRI scan (Figure 1.9). It has been reported that MRI reveals the presence of smaller brain metastases compared to CT (Schellinger*, et al.*, 1999). Another advantage of using MRI over CT is that, during a CT scan a patient is subjected to an effective dose of ionising radiation of around 1.5 mSv (Shrimpton*, et al.*, 2006). This is considered to be a non-harmful dose, however, it does limit the number of CT scans that can be performed in a year (Smith-Bindman*, et al.*, 2009). Positron electron tomography can also be used for the diagnosis of brain metastases, however, it has been reported that this technique is still not as sensitive as MRI (Kruger*, et al.*, 2010).

Currently, brain metastases are only detectable by MRI when they are 2-5 mm in diameter (Nomoto*, et al.*, 1994; Schaefer*, et al.*, 1996). These tumours are only detectable at this late stage as breakdown of the BBB is necessary for the Gd-based contrast agent to enter the tumour and provide contrast (Hasegawa*, et al.*, 2004). In order for more effective treatment of brain metastases, it is essential that methods are developed to detect this currently intractable disease at an earlier stage.

1.8.7. Previous biomarker studies for brain metastasis

Biomarkers are commonly used to predict the likelihood of a primary tumour becoming metastatic. This is mainly done using genetics to identify precisely which cancer a patient is suffering from and what genes are being expressed by that cancer. A study of brain metastasis arising from breast cancer identified several genes, such as cyclooxygenase 2 and epidermal growth factor

receptors, which assisted the cancer cells in crossing the BBB (Bos*, et al.*, 2009). Similar genetic markers have been found in metastasising, small cell lung cancers (Milas*, et al.*, 2003). However, these markers require a biopsy of the primary tumour and genetics do not explain all instances of metastases.

Other studies have attempted to identify markers of BBB disruption (Baschnagel*, et al.*, 2008). These are generally protein markers of disease, such as TNF-α and MMP-9, and were developed from studies in stroke patients. Use of such markers as a diagnostic tool encounters the same issue as diagnosing brain metastases with MRI. The breakdown of the BBB is a late stage event associated with tumour development.

Several cancer specific markers have been developed for the diagnosis of brain metastases. For example, it has been reported that elevated levels of neuron-specific enolase (NSE) in the serum reveals the presence of brain metastases in patients suffering from both small cell lung cancer and non-small cell lung cancer (Jacot*, et al.*, 2001; van de Pol*, et al.*, 1994). NSE has been studied in a multicentre clinical trial in order to assess its prognostic and diagnostic capabilities. Treatments for the lung cancers appeared to have little effect on the levels of NSE within the serum and therefore this is a type-0 biomarker for lung cancer (Jacot*, et al.*, 2001). Current screening programs for lung cancer do use serum NSE levels as a marker for lung cancer. As mentioned previously (1.2.1) the level of serum PSA is used as a biomarker for prostate cancer in the clinic (Oesterling, 1991). In a clinical trial, patients with a serum PSA level between 4 and 9.9 μg per litre had a 22% chance of having prostate cancer. If a patient has a PSA level above 10 μg per litre than the chance of them having prostate cancer increases to 67% (Catalona*, et al.*, 1991). However, these studies are specific to each cancer type and, therefore, generating a set of diagnostic markers that could be used to detect the presence of brain

metastasis from a range of primary tumours would be an invaluable tool within the clinic. Thus, the final hypothesis that will be tested in the work described in this thesis (Chapter 6), is that metabolomic analysis of biofluids can enable early detection of brain metastasis.

1.9. Overview of thesis

The different neuropathologies explored in this thesis all result in damage to the CNS. There are similarities and differences between the mechanisms which contribute to this neurodegeneration. There are four key features of pathology which are similar across all four diseases described in this thesis. These are: Microglia activation, T-Cell recruitment, axonal damage, and neuronal loss. Microglia have been shown to be present surrounding active chronic MS lesions (Trapp*, et al.*, 1999). This is also the case for brain metastasis, where it has been shown that there is considerable microglia activation surrounding the tumour cells (Zhang*, et al.*, 1995). In AD the presence of the Aβ has been shown to cause microglial activation (Barger*, et al.*, 1997). This Aβ microglial activation can also occur in patients with HAD, however the virus itself can also activate the microglia (Kaul*, et al.*, 2001). Microglia are the principal immune cells within the CNS (Benveniste, 1997), however the activation of these cells can result in neuronal damage due to the production of cytokines such as, TNF-α IL-1 and IL-6 (Minagar*, et al.*, 2002). These diseases also recruit T-cells as part of the inflammatory response (Balashov*, et al.*, 1999; Kaul*, et al.*, 2001; Togo*, et al.*, 2002; Weller*, et al.*, 1995), which in turn produce cytokines, leading to increased neurodegeneration (Kipnis*, et al.*, 2004). Therefore axonal damage and neuronal loss are common themes, which lead to impairment of brain function.

However, the underlying mechanisms which trigger this inflammatory response are fundamentally different in each disease. MS is primarily an immune modulated disease where the immune system degrades the myelin coat surrounding axons causing injury (Compston*, et al.*, 2002). The damage to the CNS from HAD arises from the initial infection of microglia. This is because microglia are the only cells within the CNS that can be infected with HIV (Kaul*,*

et al., 2001). In the case of AD the build-up of extra-cellular protein residues triggers the inflammatory process within the CNS (Barger*, et al.*, 1997). It has been reported that VCAM-1 is up-regulated in the presence of a brain metastasis (Serres*, et al.*, 2010). VCAM-1 plays a key role in the recruitment of leukocytes into the CNS (Polman*, et al.*, 2006), thus triggering an inflammatory response to the tumour. The different mechanisms of immune system activation in the CNS could lead to a difference in the metabolic profile of each disease. Therefore, this thesis will examine whether it is possible to distinguish between these diseases using metabolomics and identify any similar metabolomic pathways associated with neurodegeneration.

This thesis will comprise a methods chapter, four results chapters, and a final discussion and conclusions chapter. Chapter two of this thesis will describe all the general methods used throughout the thesis. Chapter three will describe the results of the biofluids analysis from both an animal model of MS and samples from human MS patients. Chapter four of this thesis will compare another neurodegenerative disease (AD) with MS. In chapter five of this thesis the result will describe the attempts at using CSF to categorise differing neurocognitive states of patients with HIV. This chapter will also attempt to include clinical data as a covariate in order to improve the models. The last results chapter will describe the results from an animal model of brain metastasis in order to facilitate an earlier diagnosis of this disease. The final chapter will discuss all the results in this thesis.

Chapter 2: Materials and Methods

2.1. Animals

Adult 6-10-week old Biozzi antibody high female (ABH) mice (Charles River, Kent, UK) were used for the Cr-EAE animal model of MS (10 animals per timepoint). All mice: BALB/c, SCID and C57Bl/6 (Harlan, UK) used for the cancer metastasis models were adult female animals aged between 6-7 weeks (6 animals per timepoint). All animals were acclimatised in the animal unit for 1 week prior to the onset of any experiments. All experiments were performed with UK Home Office approval (license numbers 30-2524 or 30-2620).

2.2. Human samples

The human MS samples were obtained from Dr. Jacqueline Palace (Clinical Neurology, John Radcliffe Hospital, Oxford). The samples were collected during patient visits to the MS clinic. The control samples were collected from an aged matched cohort of healthy individuals with no known neurological diseases.

2.3. Reagents

All reagents were obtained from Sigma Aldrich or Fischer Scientific unless otherwise stated. The spinal cord homogenate for the induction of Cr-EAE was obtained from UCB (Slough, UK).

2.4. Cancer cell lines

Cancer cell lines were kindly donated by Prof. Ruth Muschel (Gray Institute for Radiation Oncology and Biology) and grown using standard cell culture techniques by Dr. Sebastien Serres or Dr. James Larkin (Experimental Neuroimaging Group, Gray Institute for Radiation Oncology and Biology). The

cell lines used in this thesis were: 4T1-GFP mammary carcinoma cells, MDA231BR human breast adenocarcinoma cells and a murine melanoma cell line, B16F10-GFP.

2.5. *In vivo* protocols

2.5.1. Anaesthesia

Surgical anaesthesia was induced in all animals by use of isoflourane (1.5%-2%) in either pure oxygen or 70% nitrous oxide: 30% oxygen mix. Excess isoflourane was scavenged *via* a Fluovac system (International Market Supply).

2.5.2. Killing *via* overdose of an anaesthetic agent

Animals were either injected intraperitoneally with 100 μL of pentobarbitone or placed in a box with 5% isoflurane in a 70:30 N_2O:O_2 mixture. In the case of isoflourane, death was confirmed by cervical dislocation.

2.5.3. Sample Collection

Blood was collected *via* cardiac puncture using a heparin-coated syringe and placed immediately into a blood tube containing dipotassium ethylenediaminetetraacetic acid (EDTA) on ice. Blood samples were subsequently centrifuged (14000 rpm, 5min) at 4 ºC, after which the top layer of plasma was removed and stored at -80 ºC. Urine samples were either collected directly from the bladder after killing the animal or by placing a 96 well plate underneath the animal during the killing of the animal.

2.6. NMR spectroscopy

2.6.1. NMR phosphate buffer

For 100 mL of phosphate buffered deuterium oxide (D_2O), Na_2HPO_4 (115 mg, 0.81 mM) and NaH_2PO_4 (20 mg, 0.17 mM) were dissolved in D_2O (100 mL). To this solution NaCl (0.8 g 0.8%), 3-trimethylsilyl-1-[2,2,3,3-$^2H_4$] propionate (14.2 mg, 1 mM) and sodium azide (0.1 g, 0.1%) were added. This solution was then mixed and used immediately to prevent atmospheric absorption of H_2O.

2.6.2. Sample preparation

Plasma, serum and urine samples were defrosted overnight in a cold room prior to the NMR experiments. Plasma and serum samples were centrifuged (100000 g, 30 mins). The requisite volume of sample was pipetted into a sterile eppendorf and phosphate buffered D_2O added to make the total volume up to 600 μL. This solution was then transferred into a 5 mm borosilicate glass NMR tube which was sealed with a plastic cap. The outsides of the tubes were then disinfected with a 1% Virkon solution.

2.6.3. NMR experiments

^1H NMR spectra were acquired from each sample using a 16.4T (700 MHz) NMR system (Bruker Avance III equipped with a ^1H TCI cryoprobe). For all samples a 1D Nuclear Overhauser effect (NOESY) solvent presaturation sequence was performed. As stated previously, this was not to measure any nuclear Overhauser effects (Section 1.4.3). With the solvent presaturation occuring during the relaxation delay (TR) and mixing time (10ms), was used. For plasma samples alone, a Carr–Purcell–Meiboom–Gill (CPMG) sequence was also used with solvent presaturation and a T_2 filter (total duration 40 ms; 20 loops of 2 ms spin-echoes) for suppression of lipid resonances. The spectrum

was all internally referenced by the spectrometer using the D_2O signal from the solvent. Post-acquisition all spectra were referenced to the TSP peak at 0.00 ppm.

Two dimensional ^1H NMR spectra were acquired from a sample within each group to assist with metabolite identification. The 2D Correlation Spectroscopy (COSY) spectra were acquired on the same spectrometer as the 1D NMR spectra. The COSY spectra were acquired with 1.5 s solvent presaturation, a spectral width of 10 ppm (7002 Hz), and 16 or 32 transients per t_1 increment for 256 increments. These 2D spectra took 2 hours for the 16 transient spectra and 4 hours for the 32 transient spectra. All NMR experiments were acquired at 293K.

2.7. Statistical analysis

2.7.1. Bucket integration

The plasma spectra were sub-divided into 0.02 ppm integral regions and integrated, reducing each spectrum to 435 independent variables between 0.20-4.30 and 5.00-9.60 ppm. The urine spectra were sub-divided into 0.02 ppm integral regions and integrated, reducing each spectrum to 385 independent variables between 0.20-4.30 and 6.00-9.60 ppm. In all spectra, the region between 4.30 and 5.00 ppm was omitted owing to the water suppression. This region was omitted due to incomplete water suppression causing large modulations within the baseline of the spectra. In the case of the urine spectra the region between 5.00 and 6.00 ppm was also excluded to avoid the broad resonance arising from urea. These sections represent highly variable regions of the spectrum.

2.7.2. PLS modelling

Statistical pattern recognition was applied to the spectra to differentiate between samples obtained from different disease states. Prior to this modelling the data were Pareto scaled to reduce the effects of baseline noise (van den Berg*, et al.*, 2006). To do this, two statistical tests were used, PCA and PLS-DA. PCA, which is an unsupervised multivariate test, was used to identify any outliers within the dataset. PLS-DA is a class based system of modelling which attempts to identify separation between the pre-determined classes. In order to determine how predictive the models were, the q^2 value for each model was used as a guide to the validity of the PLS-DA model. The q^2 value is a measure of the accuracy of the model in predicting class membership (Salek*, et al.*, 2010). A q^2 value above 0.4 is considered statistically significant (Waterman*, et al.*, 2010) and, therefore, was taken to indicate reliable models for the separation between disease groups. A q^2 of 0.4 is generally accepted as a significant model in the case of biological samples (Umetrics F.A.Q.). However, with if the number of samples is low then the q^2 value must be correspondingly higher to ensure a predictive model. If the separation caused by the disease occurred within the second component, rather than the first, then an orthogonal PLS model (OPLS-DA) was produced in order to identify ^{1}H NMR regions specific to the disease separations rather than unrelated factors.

2.7.3. Reasons for spectral exclusions

If any of the data points lay outside the 95% confidence interval for the PCA test mentioned above (Section 2.7.2), the original spectra were examined. Spectra were also examined if they sat away from the main group of the model. All spectra beyond the 95% confidence interval indicated that the spectrometer had failed to lock onto the D_2O signal whilst running the spectra and thus poor water suppression was observed and therefore the spectra were excluded. Samples

were re-run if this failure to look was noticed at the time of spectra acquisition. Due to sample degradation, however, they were not re-run at a later date. In the serum and plasma samples the TSP signal was occasionally very broad. This caused a shift in the spectra and therefore, the spectra were removed from the analysis.

2.7.4. Model validation

One of the problems with multivariate analysis is the ability to over-model the data (Arnold, 1996). Therefore, in order to test the validity of the models they were subjected to two different model validation tests. These are known as the validation plot and a take-one-out analysis, and are described below (2.7.4.1 and 2.7.4.2).

2.7.4.1. Validation plots

The models were tested for their validity using the model validation plots available within SIMCA P+ (Umetrics, Sweden). The software assigns all of the samples to random classes and then generates a model from these classes. This process was repeated 100 times for each model and the resultant q^2 values were then plotted and compared to the observed q^2 value for that model (Figure 2.1). If the observed q^2 value is higher than 95% of the randomly generated q^2 values then the model is considered significant.

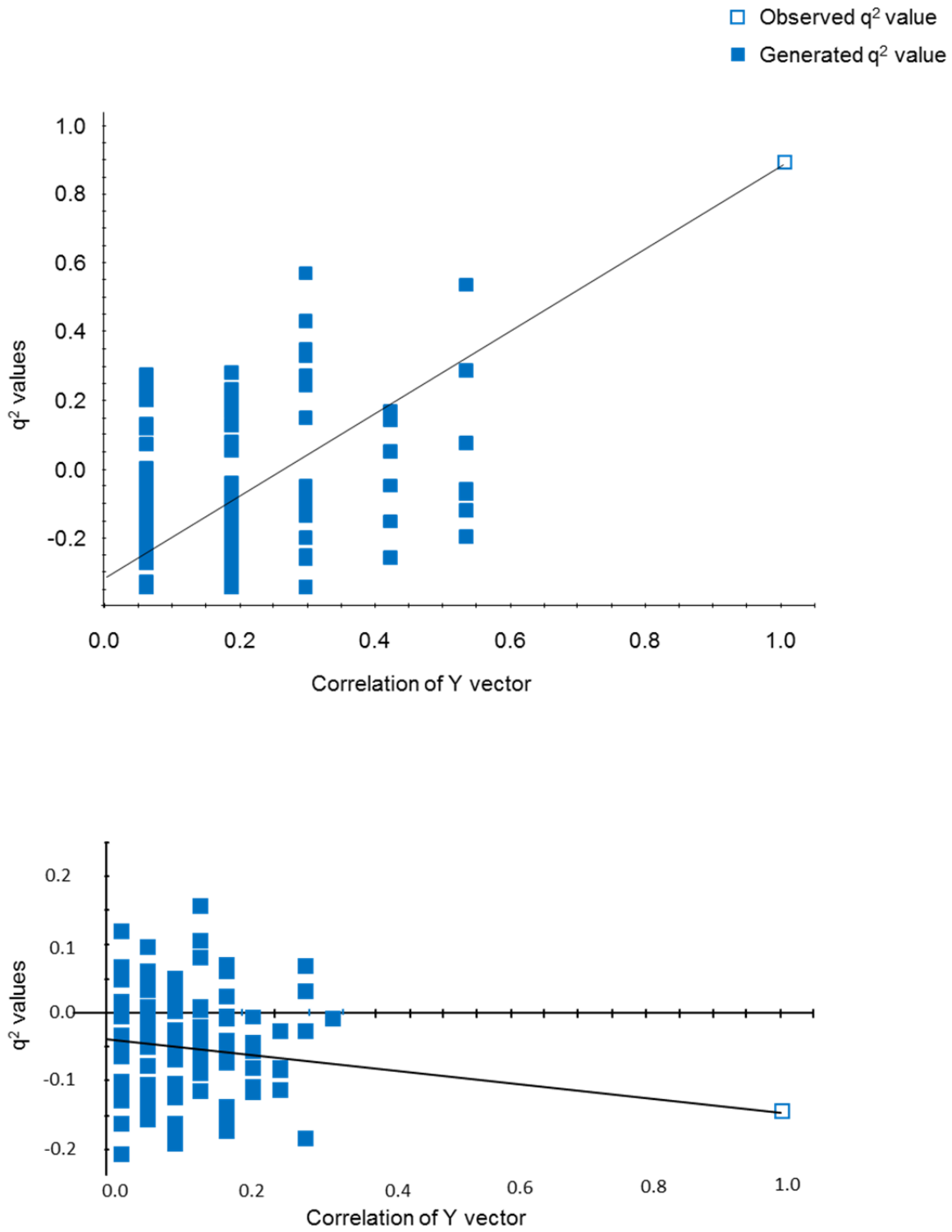


Figure 2.1: PLS model validation. (A) Validation plot from a statistically significant model. (B) Validation plot from a statistically non-significant model.

2.7.4.2. Take-one-out analysis

To further validate the PLS models, individual samples were systematically removed from the data set and the models were reformed without the removed samples. The samples were then specified as a prediction list within SIMCA. If the removed sample falls within the correct class it receives a score of one. A score of zero indicates it belongs to the other class within the model. An arbitrary cut off of 0.5 was used in order to determine class assignment (Brindle*, et al.*, 2002; Gavaghan*, et al.*, 2000).

2.7.5. Metabolite identification

S-plots were generated within SIMCA (for an example see Figure 2.2), this plot identifies regions within the NMR spectra that cause the separations in the PLS models. The regions with the greatest variance are displayed at the two extremes of the S-plot. From these regions the 1D NMR spectra were analysed and the metabolites which caused the separations between disease states were identified using a combination of 2D COSY spectroscopy and reference to literature values (Fan, 1996; Wishart*, et al.*, 2007; Wishart*, et al.*, 2009). Within the text of the results chapter $\delta_{x\text{-}y}$ is defined as the chemical shift of the centre of the region identified by the pattern recognition within SIMCA. The full literature assignments of the compounds identified in this thesis are listed in Table 2.1 and Figure 2.3 depicts how these assignments are derived. As observed in these examples hydrogens in the same chemical environment, such as the CH_3 group in lactate, have the same resonance within the NMR spectra. In the case of the CH_3 in the lactate this resonance is at 1.32 ppm. In addition to this each resonance has its own splitting pattern which is dependent on the number of hydrogens on the adjacent atoms. The formula for the number times the resonance is split is n+1 where n is the number of hydrogens on the adjacent atoms. For example, in lactate, the CH_3 group splits into a doublet due to the

single hydrogen on the next carbon. In certain circumstances hydrogens which appear to be in the same chemical environment, such as the two hydrogens next to the carboxylic acid group in β-hydroxybutyrate, show two resonances within the NMR spectra. This is due to the magnetic inequivalence of these hydrogens. This is caused by the presence of the chiral centre on the adjacent carbon and causes each hydrogen to have a separate resonance.

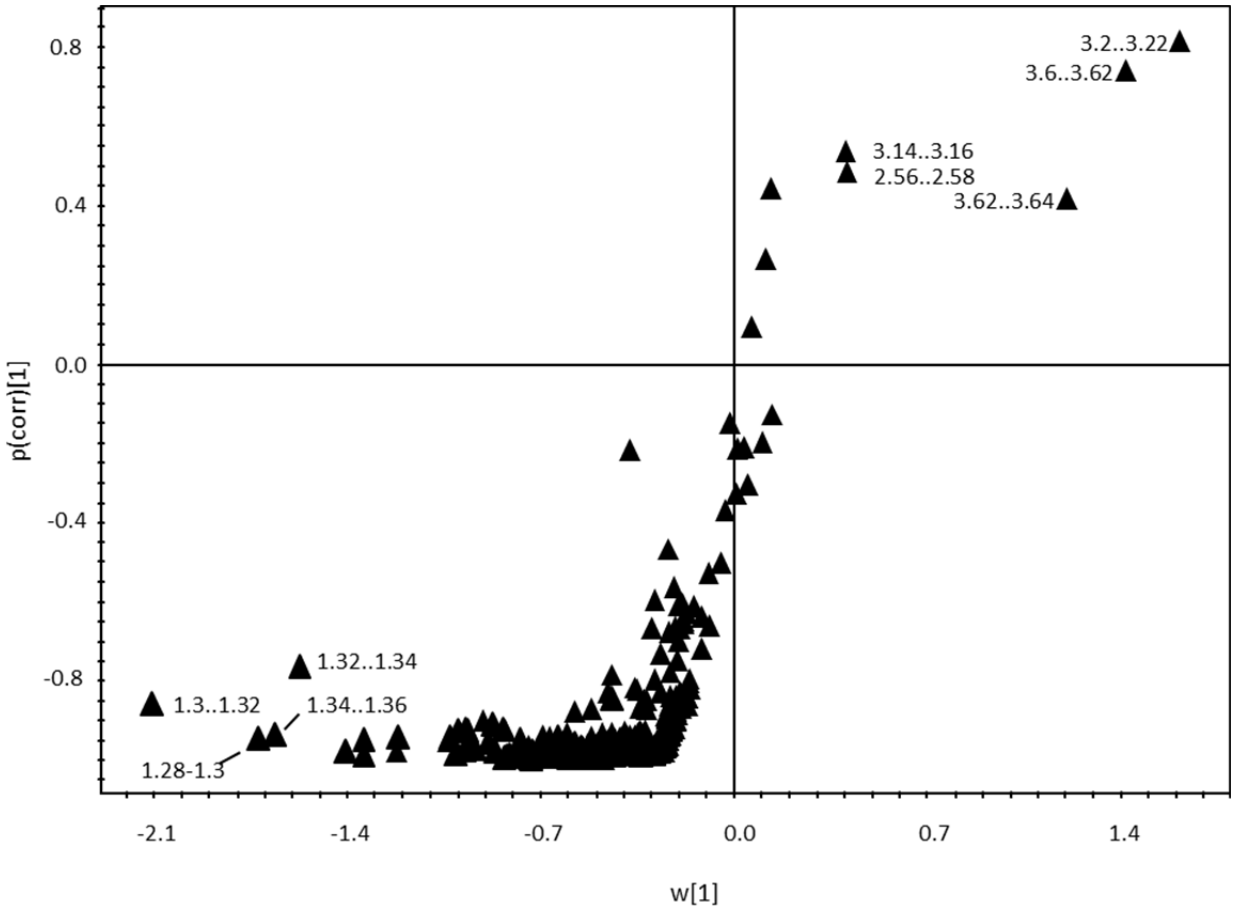


Figure 2.2: A sample S-Plot. Generated from the model which separated out plasma samples from Cr-EAE animals at day 38 from the naïve animals.

Metabolite	δ	M	A	δ	M	A	δ	M	A	δ	M	A	δ	M	A	δ	M	A	δ	M	A
Adenine	8.11	s	C(2)*H*	8.12	s	C(6)*H*															
Acetylglycine	2.05	s	OCC*H*$_3$	3.76	s	C*H*$_2$															
N-Acetyl species	2.03	br s	COC*H*$_3$																		
L-Alanine	1.46	d	C*H*$_3$	3.73	q	C*H*															
Butyric acid	0.88	t	C*H*$_3$	1.55	tq	C*H*$_2$CH$_3$	2.14	t	C*H*$_2$CH$_2$CH$_3$												
Choline	3.23	s	N(C*H*$_3$)$_3$	3.51	dd	NC*H*$_2$	4.06	ddd	NCH$_2$C*H*$_2$												
Citrate	2.5	d	CH$_A$H$_B$	2.65	d	CH$_A$*H*$_B$															
p-Cresol	2.47	s	C*H*$_3$	6.82	m	C(2,6)*H*	7.13	dd	C(3,5)*H*												
Creatine	3.04	s	NC*H*$_3$	3.94	s	C*H*$_2$															
Creatinine	3.05	s	NC*H*$_3$	4.10	s	C*H*$_2$															
Fatty acids	0.90	br	C*H*$_3$	1.30	br	C*H*$_2$CH$_3$	1.55	br	C*H*$_2$CH$_2$CH$_3$	2.05	br	CH$_2$CH=	2.25	br	CH$_2$COOH	5.35	br	CH$_2$C*H*=			
α-Glucose	3.42	dd	C(4)*H*	3.44	dd	C(6)H$_A$*H*$_B$	3.54	dd	C(2)*H*	3.73	dd	C(3)*H*	3.79	dd	C(6)H$_A$*H*$_B$	3.86	m	C(5)*H*	5.24	d	C(1)*H*
β-Glucose	3.26	dd	C(2)*H*	3.40	dd	C(4)*H*	3.47	dd	C(5)*H*	3.49	dd	C(3)*H*	3.86	d	C(6)*H*$_2$	4.63	d	C(1)*H*			
L–Glutamine	2.13	m	CH$_2$CHNH$_2$	2.45	m	OCC*H*$_2$	3.77	t	CH$_2$C*H*NH$_2$												
Glycine	3.54	s	C*H*$_2$																		
Hippuric acid	3.96	d	C*H*$_2$	7.54	t	C(3,5)*H*	7.62	tt	C(4)*H*	7.82	dd	C(2,6)*H*									
β-Hydroxybutyrate	1.19	d	C*H*$_3$	2.28	m	CH$_A$*H*$_B$	2.37	m	CH$_A$*H*$_B$	4.12	m	C*H*$_3$									
Lactate	1.32	d	C*H*$_3$	4.11	q	C*H*															
Maleic acid	6.04	s	C*H*=C*H*																		
myo-Inositol	3.27	t	C(2)*H*	3.52	dd	C(4,6)*H*	3.16	t	C(1,3)*H*	4.05	t	C(5)*H*									
Octenedioic acid	1.45	m	C(5)*H*	1.58	m	C(6)*H*	2.22	m	C(4,7)*H*	5.83	d	=C*H*COOH	6.72	td	C*H*=CHCO						
Oxalacetic acid	2.38	s	C*H*$_2$																		
Oxoglutaric acid	2.43	T	C*H*$_2$COOH	3.00	t	C*H*$_2$CO															
Phosphocholine	3.25	s	N(C*H*$_3$)$_3$	3.59	t	NC*H*$_2$	4.17	m	NCH$_2$C*H*$_2$												
Pyroglutamic acid	2.02	m	CH$_A$*H*$_B$	2.39	m	COCC*H*$_2$	2.50	m	CH$_A$*H*$_B$	4.17	dd	C*H*									
Sarcosine	2.73	s	C*H*$_3$	3.60	s	C*H*$_2$															
Taurine	3.25	t	CH$_2$C*H*$_2$NH$_2$	3.42	t	C*H*$_2$CH$_2$NH$_2$															
TMAO	3.26	s	ON(C*H*$_3$)$_3$																		
Trimethylamine	2.91	s	N(C*H*$_3$)$_3$																		
L-Tyrosine	3.05	dd	CH$_A$*H*$_B$	3.15	dd	CH$_A$*H*$_B$	3.91	dd	C*H*	6.88	d	C(3',5')*H*	7.18	d	C(2',6')*H*						
Ureidopropionic acid	2.38	t	NHCH$_2$ C*H*$_2$	3.31	t	NHC*H*$_2$ CH$_2$															
L-Valine	0.99	d	C*H*$_3$	1.04	d	C*H*$_3$	2.27	m	C*H*	3.60	d	C*H*									

Table 2.1: Full literature assignments for all compounds within this thesis. Assignments modified from the human metabolome database. Key: d - chemical shift, M - multiplicity, A Assignment of proton, s - singlet, d - doublet, t - triplet, q - quartet, dd - double doublet, ddd - double double doublet, dt - double triplet, tt - triple triplet, m - multiplet, br - broad resonance. Full assignments were obtained from the human metabolome database (Wishart*, et al.*, 2007; Wishart*, et al.*, 2009)

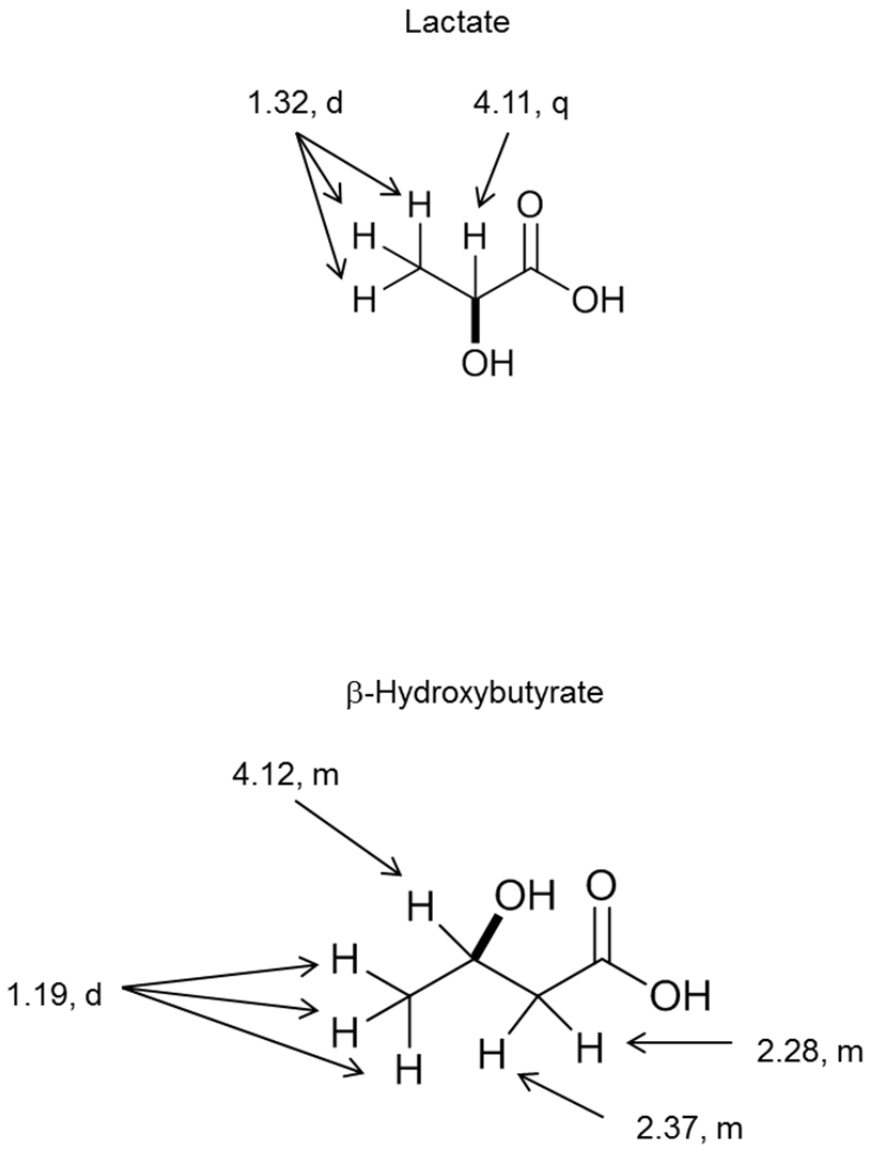


Figure 2.3: Demonstration of how NMR assignments are derived. (A) Full assignment of lactate (B) Full assignment of β-hydroxybutyrate .

.

2.7.6. Exclusion of regions within the spectra

The desired regions were set as dark regions within the ACD software. The spectra were then reintegrated into buckets as described in 2.7.1. The statistical pattern recognition (2.7.2) was then repeated in order to generate models which excluded the desired spectral regions. If these models returned a significant q^2 value then the model was further subjected to the same validation process given above (2.7.4) and metabolite identification (2.7.5).

2.7.7. Spiking experiments

In order to confirm the identities of the singlet resonances within the spectrum, the NMR sample were spiked with reference samples. The requisite chemical was dissolved in the buffered NMR solvent (2.6.1) to make a 100 mM solution. A ^{1}H NMR NOESY spectrum (8 scans, 2.6.3) was performed on the biofluids in order to obtain a baseline reference. A small concentration of the requisite chemical was then added into the NMR tube in order not to saturate the spectrum with the signal from that metabolite. A further ^{1}H NMR NOESY was then performed in order to observe which metabolite increased.

Chapter 3: Metabolomic changes in Multiple Sclerosis

3.1. Introduction

The identification of specific biomarkers in biofluids has previously been considered across a number of diseases both in animal models and humans. Urine samples from patients with neurological diseases, including MS, have been assayed for disease-specific markers, such as myelin basic protein-derived material, indicating demyelination (Whitaker*, et al.*, 1994; Whitaker*, et al.*, 1995), or neopterine as a marker of CNS inflammation (Giovannoni*, et al.*, 1997; Ott*, et al.*, 1993b). However, all of these studies focussed on the detection of either a single, or small number of, specific metabolites, and although differences have been identified at a group level, predictive value at an individual level has been low.

Drs. Sibson and Anthony have previously shown that it is possible to use such approaches to distinguish between groups of animals injected intracerebrally with replication-deficient recombinant adenoviruses expressing either TNF or IL-1β simply through analysis of their urine (Griffin*, et al.*, 2004a). These two adenoviruses induce markedly different lesions in the brain with TNF inducing a predominantly macrophage-mediated pathology and IL-1β a neutrophil-rich lesion. Using proton NMR spectroscopy of the urine samples, coupled with partial least squares discriminate analysis (PLS-DA), clear separation of the groups was evident. This finding suggests that the NMR/PLS-DA approach may be highly sensitive not just to the presence of pathology within the brain, but to differences and/or changes in pathological processes. Using a similar approach, 't Hart *et al.* identified characteristic metabolite patterns in the urines of MS patients and also in a marmoset model of MS ('t Hart*, et al.*, 2003). A number of

changes in the organic chemicals in the urine of EAE marmosets were found, although the specific metabolites contributing to the separation were not identified and only a very small group of animals was studied. That study reported 60% accuracy in distinguishing the metabolite profile of urine of MS patients from that of either healthy individuals or patients suffering from other neurological disorders, although again only a small cohort of patients was studied and no differentiation between disease states was made. Nevertheless, these data support the concept that biofluid NMR could be used to investigate pathological mechanisms in MS. Based on these previous studies, the goal of the current work was to determine whether the combined NMR/PLS-DA analysis of blood and/or urine samples could enable reliable differentiation between different disease states in both a clinically relevant animal model of MS and in MS patients.

3.1.1. Aims of Chapter

The aims of this chapter are:

1. To use PLS-DA modelling of NMR data to determine metabolite changes in urine and plasma samples from a clinically relevant animal model of MS.
2. To identify the metabolites that underlie the separations between disease stages.
3. To use PLS-DA modelling of NMR data to determine metabolite changes in urine and serum samples from different categories of MS patients.
4. To establish which metabolites underpin the separations between the different MS groups.

3.2. Materials and Methods

3.2.1. Animal Experimental Design

3.2.1.1. Induction of chronic experimental allergic encephalomyelitis (Cr-EAE)

Adult Biozzi ABH mice were fed a diet of jelly and high protein mash in the cage for a period of one week prior to Cr-EAE induction and throughout the disease time course. Spinal cord homogenate (500 μg) was suspended within an emulsion of sterile PBS and incomplete Freud's adjuvant supplemented with mycobacteria (*M.tuberculosis and M.butyricum)* (Difco Laboratories, Detroit, Michigan, USA). ABH mice were anesthetised as described in chapter 2. They were then injected subcutaneously (2 × 0.15 mL) into both abdominal flanks with the CFA emulsion. Animals were assessed daily for their weights and clinical scores. The clinical score was determined by assessing the animal for signs of disability which are shown in Table 3.1.

Clinical Score	Behaviour and Test
0	Healthy mice no signs of paralysis
0.5	Partial tail paralysis; assessed by running finger along tail to check for loss of tone at the tip of the tail.
1	Full tail paralysis; tail drops down through cage lid and complete loss of tail tone.
1.5	Partial hind limb paralysis; loss of righting reflex and feet will occasionally fall through the cage lid.
2	Incomplete hind limb paralysis; One leg completely paralysed and dragging behind in a paddle position.
2.5	Hind limb paralysis; One leg completely paralysed, the other leg showing signs of foot faulting.
3	Complete hind limb paralysis; both feet dragging in the paddle position.
4	Moribund; all limbs paralysed animals were sacrificed if they reached this clinical score.

Table 3.1: Table showing the clinical scoring system in Cr-EAE animals.

3.2.1.2. Killing of animals

Animals were placed in a sealed box and CO_2 was gradually added into the bottom in order to create a rising concentration of CO_2 until a 100 % atmosphere had been achieved. The animals were left in this atmosphere until breathing had ceased. Death was confirmed by gentle cervical dislocation in order not to damage the blood vessels in the neck. Blood samples were taken at days 10, 14, 17, 28 and 38 after Cr-EAE induction (n = 10, 8, 9, 8 and 5 respectively for the Cr-EAE cohort and n= 8, 9, 8, 9 and 8 for the CFA control cohort). Urine samples were collected from the animals at the same time points with the exception of day 17 as urine volume was inadequate (n = 8, 7, 0, 7 and 6 for the Cr-EAE cohort and n = 6, 10, 0, 8 and 10 for the CFA control cohort respectively). as described in Chapter 2 Section 2.5.3.

3.2.2. Human Experimental Design

Blood serum (n=58) and urine samples (n=84) were obtained from MS patients under Ethical approval (C03.054, Metabolic profiling of urine in MS, 08/H0604/155) with cohorts of RR-MS (urine n = 22; serum n = 19), PP-MS (urine n = 32; serum n = 13) and SP-MS (urine n = 30; serum n = 26) patients. Samples were collected as described in Chapter 2 Section 2.2.

Control samples were collected from age- and sex-matched volunteers (urine n = 28; serum n = 16).

3.2.3. NMR Spectroscopy and Data Analysis

The samples were prepared using the methods set out in Chapter 2 Section 2.6.2. The NMR spectroscopy and multivariate statistical analysis was also carried out as described in Chapter 2 Section 2.6.3 and 2.7. All models which returned a q^2 value of 0.05 or below were considered to be not significant and,

therefore, marked as ns. Any q^2 value above 0.05 was considered a model with a positive correlation and further testing was performed as described in Chapter 2 Section 2.7.4. All models which passed these validation tests are marked with a * in the following results tables.

3.2.4. Metabolite identification

The ^{1}H NMR spectral regions which caused the separation within the significant models were identified from the S-plot. The points on the S-plot at the outer extremes of the curve were used in order to identify the significant metabolites as these metabolites will have the greatest effect on the model. There was no correction applied for multiple comparisons if the metabolite in question had multiple significant buckets. This could bias the results in favour of metabolites which have multiple peaks within the spectra such as glucose. The metabolites were then identified using a combination of COSY spectroscopy (see Chapter 2 Section 2.7.5) and reference of the literature values (Fan, 1996; Wishart*, et al.*, 2007; Wishart*, et al.*, 2009). A sample COSY spectrum is given in Figure 3.1.

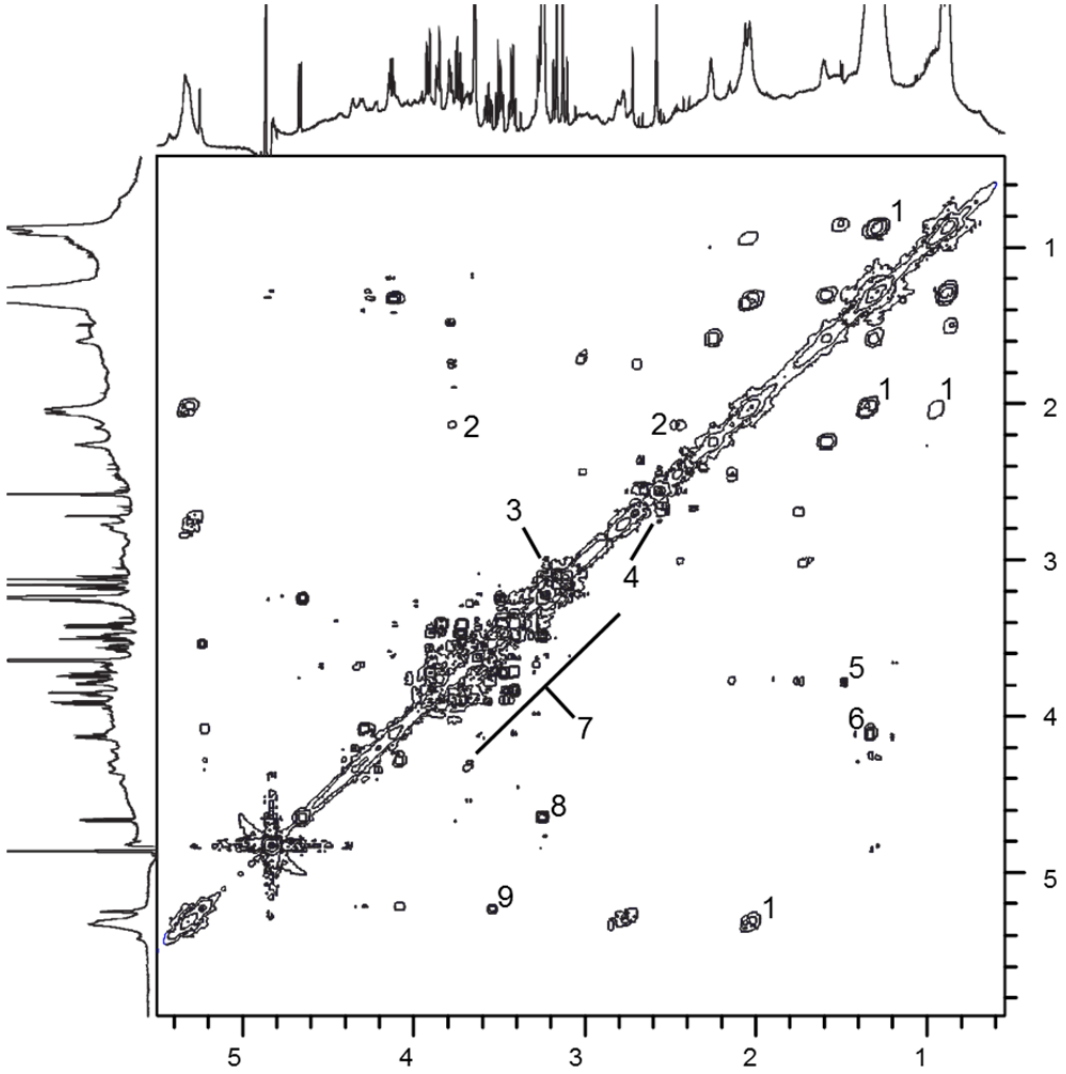


Figure 3.1: A sample plasma COSY spectra from a day 38 Cr-EAE animal showing highlighted correlations which assisted the metabolite identification. Key 1: Fatty Acids, 2: Glutamate, 3: Taurine, 4: Citrate, 5: Alanine, 6: Lactate, 7: Region containing glucose correlations, 8: β-glucose, 9: α-glucose.

3.2.5. Spiking experiments

In order to confirm the identities of any singlet resonance ^{1}H NMR resonances, spiking experiments were performed as described in Chapter 2 Section 2.7.7. All metabolites were made up to a final concentration of 100 mM in the phosphate buffer (Chapter 2 Section 2.6.1). The following volumes were then added into the NMR tubes to prevent the spectrum from becoming saturated from the signal from that metabolite: 1 μL of choline, 2 μL of N-acetyl aspartate, 2 μL of phosphocholine, 2 μL of trimethylamine (TMA), 2 μL trimethylamine-N-oxide (TMAO) and 5 μL of ureidopropionic acid.

3.3. Results

3.3.1. Cr-EAE: Animal Model

All Cr-EAE animals followed the typical disease course reported previously by (Baker*, et al.*, 1990); the animals exhibited significant weight loss and increased clinical score, which peaked at day 17, and was followed by full remission such that clinical score had returned to baseline values in all animals by day 26 (Figure 3.2). Subsequently, the animals entered a relapse phase, around day 32, with a second significant increase in clinical score and loss of weight. During peak disease Cr-EAE animals were hand-fed to reduce dehydration and weight loss. Injection of CFA alone (CFA group) did not cause any overt clinical signs or significant weight loss (Figure 3.2).

3.3.2. Initial Models

The first attempt at running the animal plasma and human serum models returned no significant models; although they visually showed the beginnings of a separation, the models did not pass the validation tests (Figure 3.3). On inspection of the spectra, it was found that the metabolite peaks were very broad owing to the presence of proteins within the samples despite the use of a CPMG sequence, which should fully suppress such broadening. It was decided, therefore, that all of the blood samples should be centrifuged (100,000 g) for 30 mins to remove any heavy proteins remaining in the samples. This separation in this model could not be attributed to batch effects, as all of the spectra were run on the same day in identical buffer.

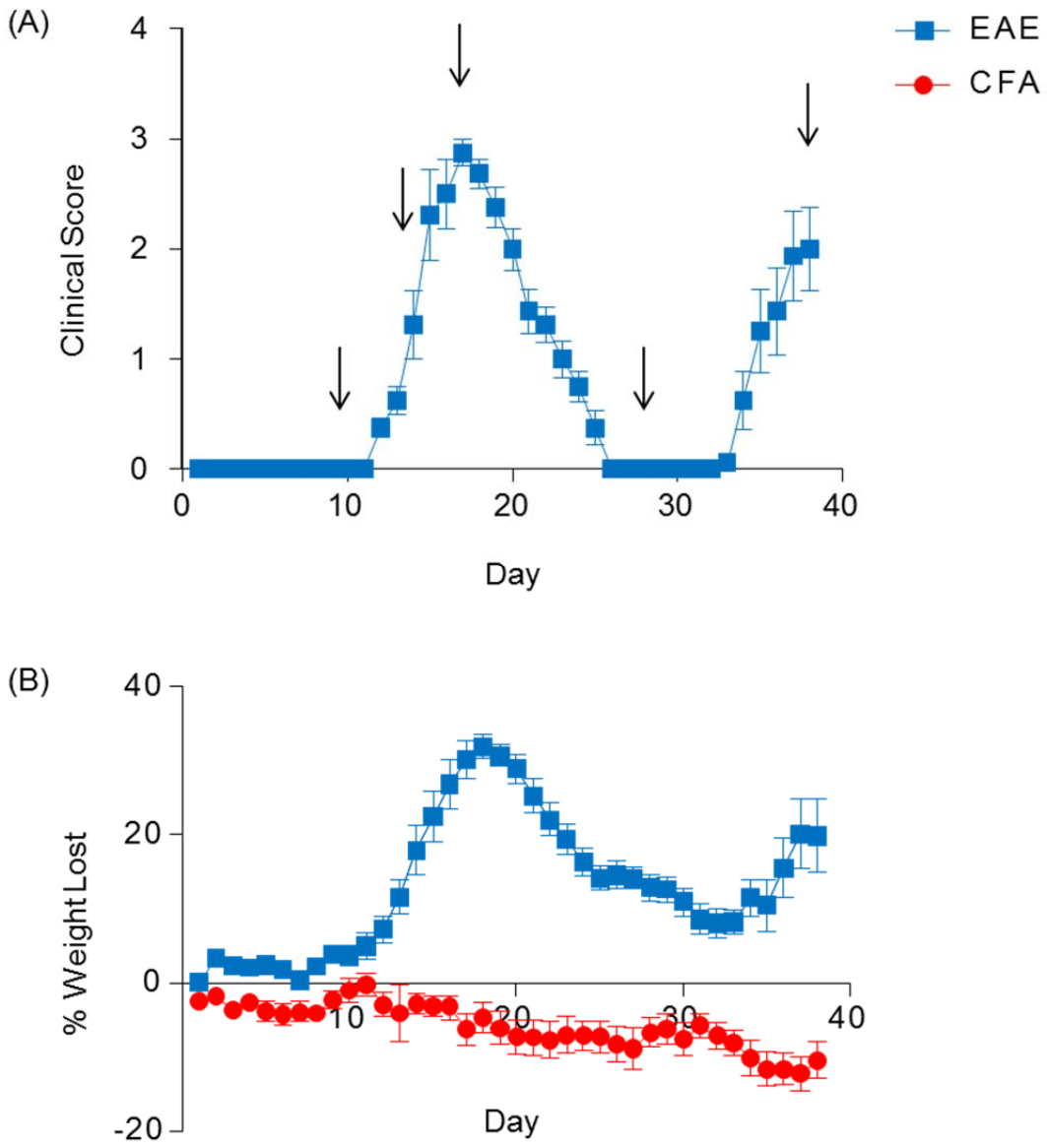


Figure 3.2: Cr-EAE animal model results. (A) A graph showing the clinical scores of the mice with Cr-EAE, CFA scores are not shown due to the fact that the score never deviated from 0. Arrows indicate when the samples were taken from each animal. (B) A graph showing the percentage weight loss of the both the EAE and CFA animals.

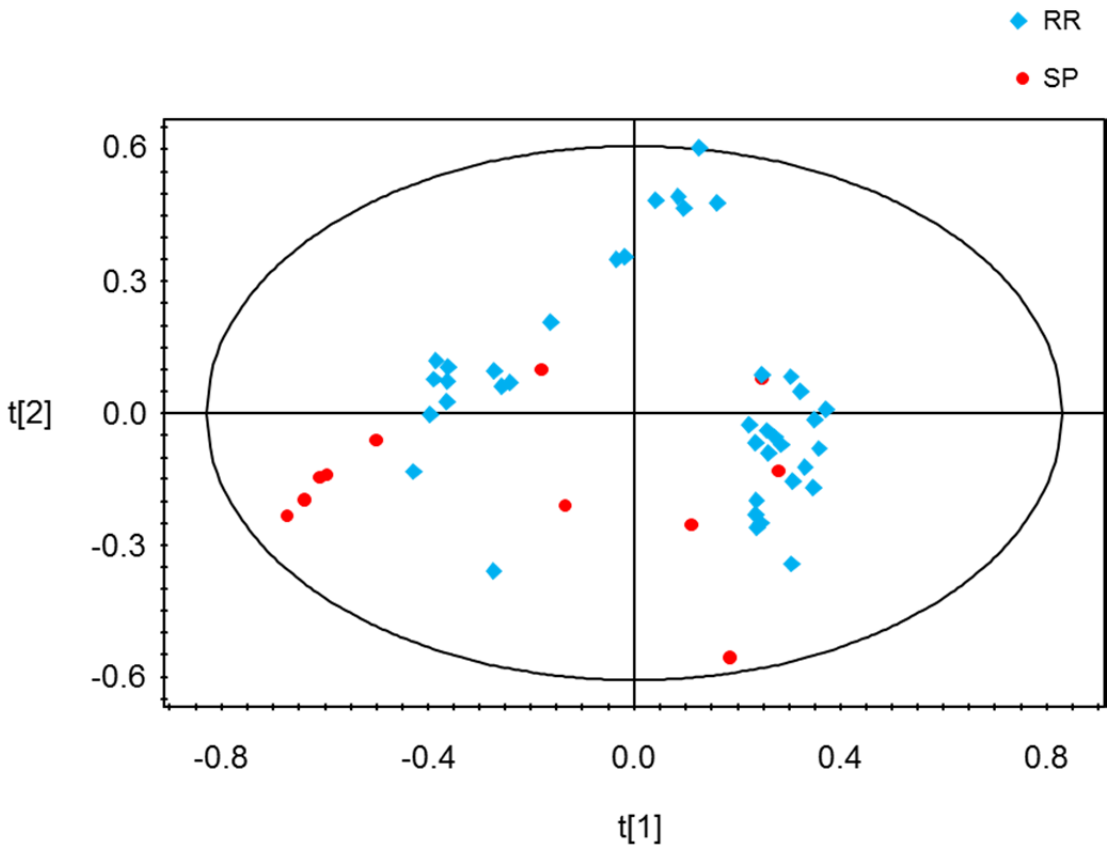


Figure 3.3: Initial PLS-DA plot of human serum samples comparing relapse remitting patients (blue diamonds) and Secondary Progressive patients (red circles).

3.3.3. Cr-EAE: Urine analysis

Spectra obtained by high resolution ^{1}H NMR spectroscopy were of sufficient resolution to allow identification of over 30 metabolites (Figure 3.4 A). PLS analysis of the urine spectra from the naïve animals at different time-points returned a model with a low q^2 (0.10), indicating that it was not predictive. Consequently, all naïve data were combined thereafter and analysis performed using a single control (naïve) group.

Visually, there appeared to be separation of the different disease groups, as illustrated in (Figure 3.4 B, C, and D). However, although many of the urine models returned a positive q^2 value indicating differences both within the Cr-EAE animals at different time-points and between the Cr-EAE and control (CFA or naïve) animals, only 12 models reached statistical significance against the defined criteria of $q^2 \geq 0.4$, (Table 3.2, A and B). At day 10 it was possible to separate both the Cr-EAE and the CFA animals from the naïve animals (q^2 = 0.55 and 0.53, respectively); (Table 3.2, A and B) although, whilst strongly positive, the separation between Cr-EAE and CFA animals at this time-point did not quite reach statistical significance (q^2 = 0.38). However, a significant separation was found between the Cr-EAE and CFA animals at day 14 with a q^2 value of 0.46 (Table 3.2, A). Cr-EAE animals at day 38 showed a positive separation from all other Cr-EAE time-points and also from the CFA and naïve controls (Table 3.2, A and B). No data were obtained from the animals at day 17 as the volume of urine collected was not adequate.

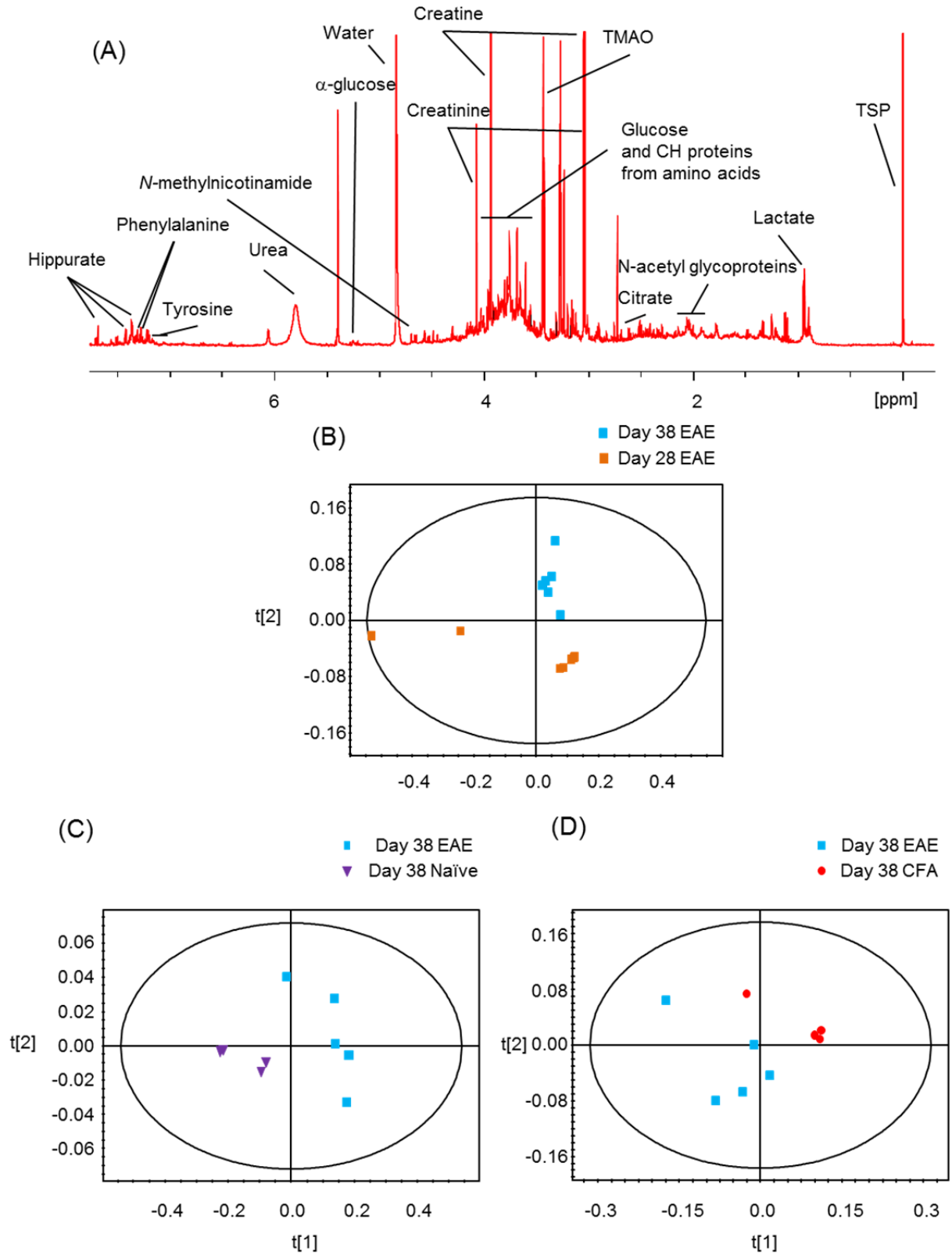


Figure 3.4: Cr-EAE animal PLS urine results. (A) ^{1}H NMR NOESY spectrum of a urine sample from a Day 38 animal. (B) PLS-DA plot of animal urine samples comparing EAE animals at Day 38 (light blue squares) and EAE animals at Day 28 (orange squares). (C) PLS-DA plot of animal urine samples comparing EAE animals at Day 38 (light blue squares) and naïve animals (purple triangles). (D) PLS-DA plot of animal urine samples comparing EAE animals at Day 38 (light blue squares) and CFA animals at Day 38 (red circles).

(A)

EAE v EAE EAE v CFA CFA v CFA

	Day 10	Day 14	Day 28	Day 38
Day 10	0.38	0.21	ns	0.79*
Day 14	0.47*	0.46*	ns	0.52*
Day 28	0.19	ns	ns	0.76*
Day 38	0.50*	ns	ns	0.52*

(B)

	EAE v Naïve	CFA v Naïve
Day 10	0.55*	0.53*
Day 14	ns	ns
Day 28	0.19	0.50*
Day 38	0.77*	0.66*

Table 3.2: q^2 values of the PLS models generated from the Cr-EAE animals. (A) Table showing the q^2 values of all the animal models. Values on the white background shows the EAE v EAE comparison, values on a light grey background shows the EAE v CFA comparisons and the values on the dark grey background shows the CFA v CFA comparisons. (B) Table to show the q^2 values of EAE animals at different time-points compared to a naïve group of animals.

CFA animals at day 10 showed a positive separation from both days 14 and 38 (q^2 = 0.47 and 0.5, respectively; Table 3.2 A), and at day 28 the CFA animals showed a separation from the naïve cohort (q^2 0.5;Table 3.2; B).

The loadings from the statistically significant models generated for the disease time course identified several key metabolites that were responsible for the separations between groups (see Chapter 2 Section 2.7.3 for full literature assignments). In particular, citrate (δ_{x-y} 2.50, 2.65), creatine (δ_{x-y} 3.03), taurine (δ_{x-y} 3.25, 3.40), an unassigned set of resonances (δ_{x-y} 3.13, two singlets in close proximity to each other), TMAO (δ_{x-y} 3.26), TMA (δ_{x-y} 2.89) and ureidopropionic acid (δ_{x-y} 2.37) all varied significantly over the disease time course. The identity of these last three metabolites was confirmed by spiking experiments (for full description see Section 3.3.7). Here δ_{x-y} is defined as the chemical shift of the centre of the region identified by the pattern recognition within SIMCA. With the exception of ureidopropionic acid, the same metabolites were also identified when comparing Cr-EAE animals with the two control groups (CFA and naïve). In addition, phosphocholine (δ_{x-y} 3.23), also confirmed by spiking was an important contributor to the model separating Cr-EAE and CFA animals at day 38. The direction of change in each metabolite varied over the disease time course. For example, at days 10 and 14, which are in the pre-clinical and early onset phases of disease, the levels of citrate were lower in Cr-EAE animals than in control animals, whilst during relapse at day 38 they were elevated compared to the CFA controls. In contrast, the levels of the TMAO resonance peaked in Cr-EAE animals during the remission phase just prior to relapse (day 28), but then remained elevated at day 38 (peak relapse) when compared to the pre-clinical and early symptomatic time-points (day 10 and day 14; Table 3.3).

A large number of samples had to be excluded from the models due to the poor quality of the spectra, this was probably due to the dilution of the urine samples which happened following the injection of saline to promote urine production. This will further be discussed in the discussion (Section 3.4.1). This makes the number of samples very low and therefore there should not be too much weight put on the urine results unless the q^2 value is higher than 0.4. In these results all the models at day 38, the q^2 values are above 0.5 and therefore, these models can be considered as significant.

(A)

Model		q^2	Metabolites			
			Positive Metabolites			
Day 38 v Day 28	EAE	0.76				
Day 38 v Day 14	EAE	0.52	TMAO	Citrate		
Day 38 v Day 10	EAE	0.79	Creatine	TMAO	Citrate	
Day 38 v Day 38	EAE v CFA	0.52	TMAO	Phosphocholine	Glucose	Citrate
Day 38 v Day 38	EAE v Naïve	0.77	TMAO	Glucose	Creatine	
Day 38 v Day 38	CFA v Naïve	0.53				
Day 14 v Day 14	EAE v CFA	0.46	Creatine	Creatinine	Glucose	
Day 10 v Day 10	EAE v Naïve	0.55	Creatine	Trimethylamine	TMAO	β-hydroxybutyrate
Day 10 v Day 10	CFA v Naïve	0.66				

(B)

Model		q^2	Metabolites		
			Negative Metabolites		
Day 38 v Day 28	EAE	0.76	Citrate	TMAO	
Day 38 v Day 14	EAE	0.52			
Day 38 v Day 10	EAE	0.79	Trimethylamine	β-hydroxybutyrate	Phenylalanine
Day 38 v Day 38	EAE v CFA	0.52	Creatine		
Day 38 v Day 38	EAE v Naïve	0.77			
Day 38 v Day 38	CFA v Naïve	0.53			
Day 14 v Day 14	EAE v CFA	0.46	Citrate		
Day 10 v Day 10	EAE v Naïve	0.55	Citrate		
Day 10 v Day 10	CFA v Naïve	0.66	Citrate		

Table 3.3: Metabolite changes in Cr-EAE urine models. Table showing both positive (A) and negative (B) metabolites that cause separation within the animal urine models.

3.3.4. Cr-EAE: Plasma analysis

Two different NMR sequences were used to obtain spectra from the plasma samples: (i) the NOESY pre-saturation sequence used for the urines; and (ii) a CPMG sequence with a T_2-dependent lipid suppression filter. For some samples phase modulation was evident in the CPMG spectra and, therefore, the NOESY pre-saturation spectra were used in all subsequent analysis. As for the urine, PLS analysis of the plasma spectra from the naïve animals at different time-points returned a model with a low q^2 (0.176), indicating that it was not predictive. Consequently, all naïve data were combined thereafter and analysis performed using a single control (naïve) group.

Although the spectra from all groups looked superficially similar upon initial overlay (Figure 3.5), it was possible to generate PLS plots which showed visual separations between the groups (Figure 3.6). From the spectral overlay the biggest difference in the spectra was in the lipid region. The CPMG spectra do not provide sufficient resolution to distinguish between different lipid species. If these species are to be probed further than another technique such as a diffusion edited pulse sequence or mass spec could be used. The multi-variant statistical analysis of the data sets showed predictive separations between the Cr-EAE groups at all time-points in the disease course and also when comparing Cr-EAE to both CFA and naïve animals (Table 3.4; A and B). It was also possible to generate predictive models based on the spectra from the plasma of the CFA animals across the time course, with the exception of day 14 *vs*. day 28 (Table 3.4; A). When the data from CFA animals were compared with the naïve cohort it was again possible to separate the animals at all time-points except day 28.

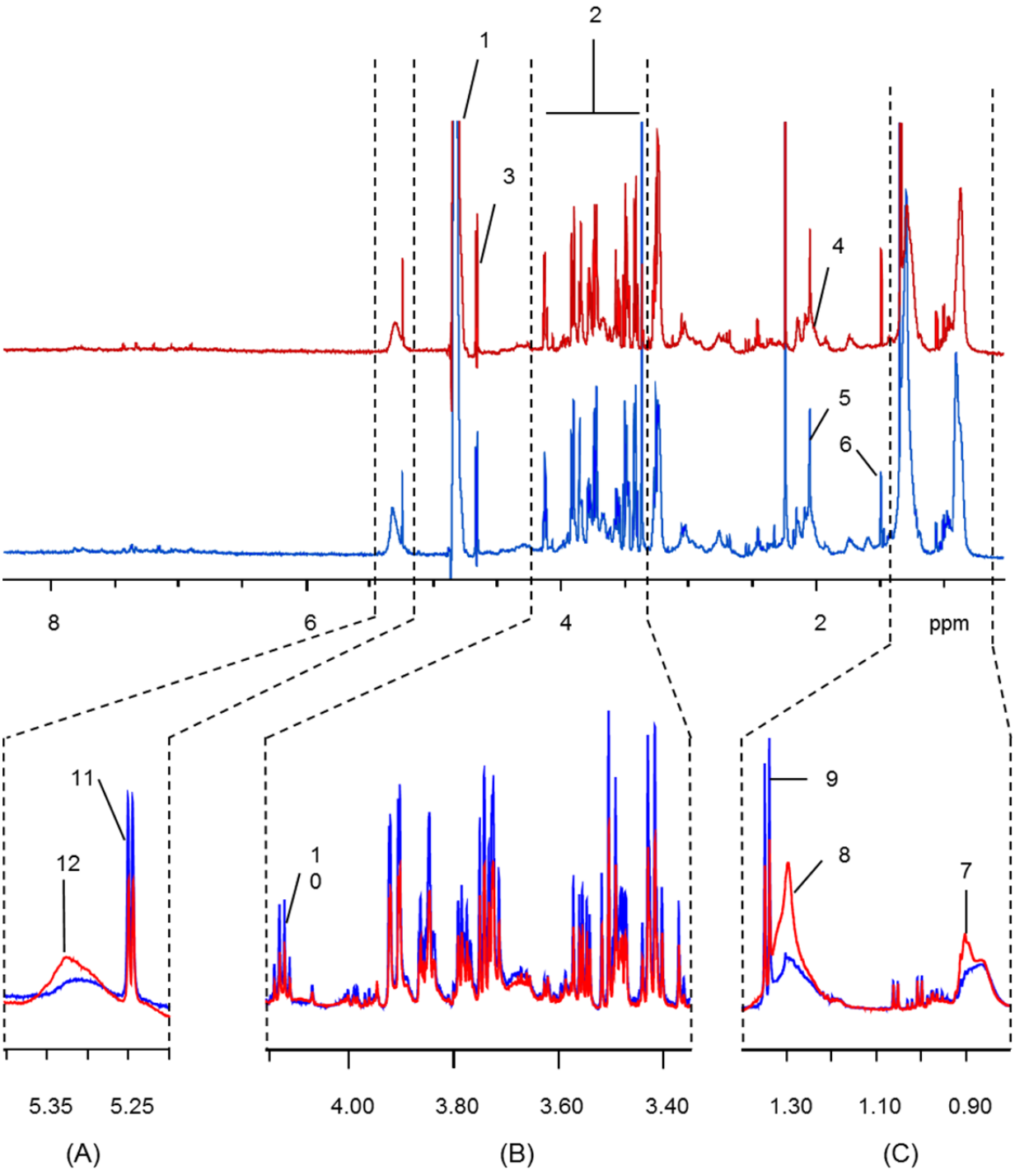


Figure 3.5: Overlaid ^{1}H NMR spectra (1D spectra recorded with solvent presaturation and CPMG background suppression) of serum from relapse remitting (blue) and secondary progressive (red) patients with key metabolites identified. Enlarged sections of spectra: (A) Anomeric region of a-glucose; (B) Sugar region; (C) Fatty acid region. Key: 1: Water, 2: Glucose resonances 3: b-Glucose anomeric protons 4: Fatty acids, 5: *N-acetyl aspartate*, 6: Alanine, 7: Fatty acid peak 8: Fatty acid peak, 9: Lactate, 10: a-Glucose anomeric protons, 11: Unsaturated fatty acids. Italics: singlets with putative assignment based on published data (Fan, 1996; Wishart*, et al.*, 2009).

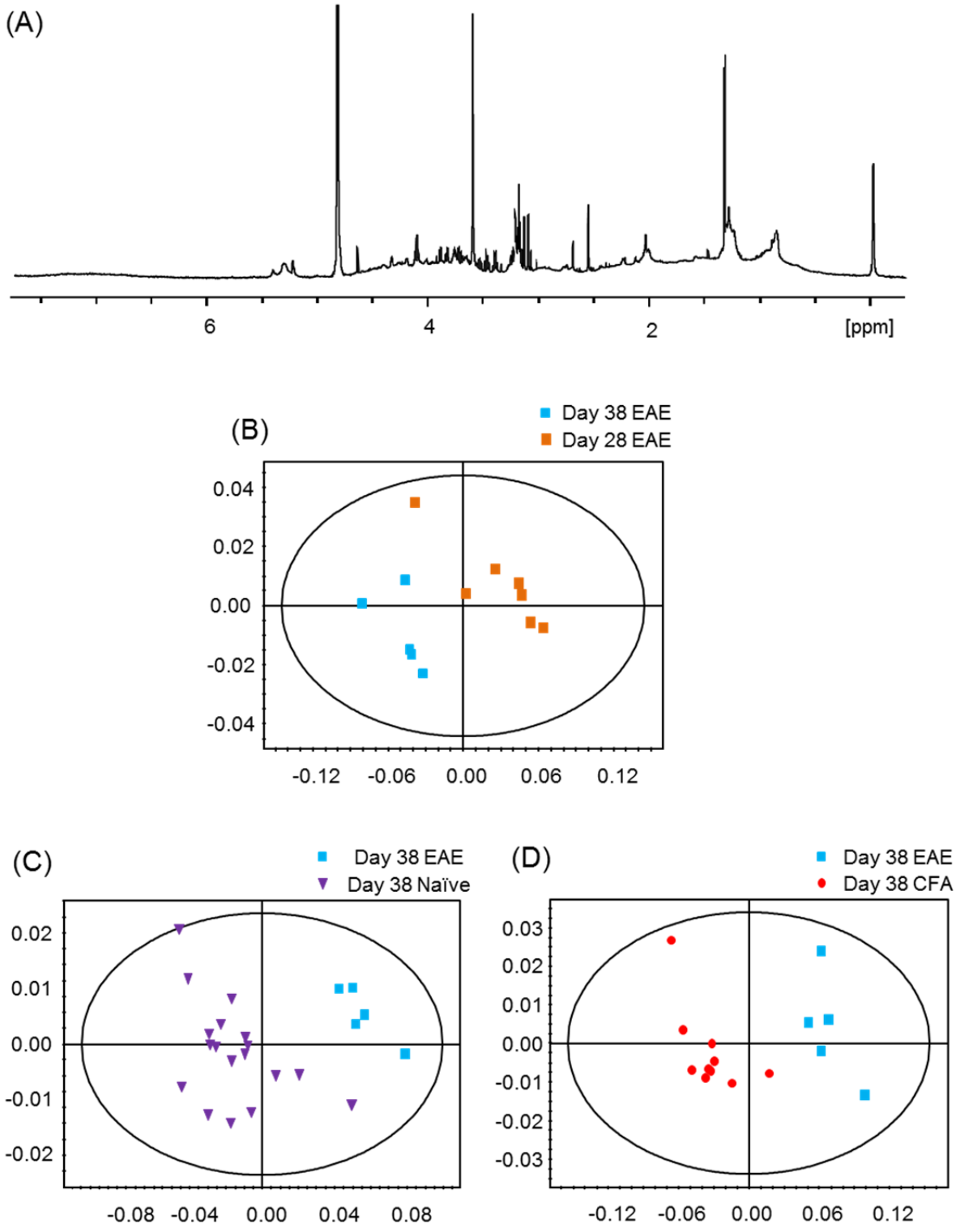


Figure 3.6: Plasma Cr-EAE animal PLS results. (A) ^{1}H NMR NOESY spectrum of an EAE animal at Day 38. B) PLS-DA plot of animal plasma samples comparing EAE animals at Day 38 (light blue squares) and EAE animals at Day 28 (orange squares). (C) PLS-DA plot of animal plasma samples comparing EAE animals at Day 38 (light blue squares) and naïve animals (purple triangles). (D) PLS-DA plot of animal plasma samples comparing EAE animals at Day 38 (light blue squares) and CFA animals at Day 38 (red circles).

(A)

EAE v EAE EAE v CFA CFA v CFA

	Day 10	Day 14	Day 17	Day 28	Day 38
Day 10	0.42*	0.58*	0.87*	0.93*	0.82*
Day 14	0.60*	0.50*	0.84*	0.90*	0.91*
Day 17	0.84*	0.92*	0.47*	0.88*	0.75*
Day 28	0.90*	044*	0.78*	0.50*	0.82*
Day 38	0.96*	0.92*	0.86*	0.67*	0.84*

(B)

	EAE v Naïve	CFA v Naïve
Day 10	0.77*	0.41*
Day 14	0.47*	0.51*
Day 17	0.82*	0.86*
Day 28	0.40*	0.32
Day 38	0.60*	0.62*

Table 3.4 q^2 values from the plasma Cr-EAE animals. (A) Table showing the q^2 values of all the animal models. Values on the white background shows the EAE v EAE comparison, values on a light grey background shows the EAE v CFA comparisons and the values on the dark grey background shows the CFA v CFA comparisons. (B) Table to show the q^2 values of EAE animals at different time-points compared to a naïve group of animals.

On examination of the loadings within the PLS models for the Cr-EAE time course several key metabolites were identified as generating the positive separations. The initial positive models showed variations in broad resonances likely to be fatty acids (δ_{x-y} 0.88, 1.58, 2.03) and glucose (δ_{x-y} 3.26, 5.25) as shown in Table 3.5. Following exclusion of these metabolites from the original spectra, it was possible to generate further positive models with significant q^2 values. Across all of the time-point comparisons the only models that were not statistically significant were the comparisons between Cr-EAE and CFA at days 17 and 28, i.e. during Cr-EAE remission (Table 3.5). Taurine (δ_{x-y} 3.25) and lactate (δ_{x-y} 1.32) were identified as metabolites that played a key role in generating the second round of positive models.

Key metabolites from the original models separating Cr-EAE animals from the control groups (CFA or naïve) were also identified. The metabolites that showed greatest variation in these models were: fatty acids (δ_{x-y} 0.88, 1.58, 2.03), citrate (δ_{x-y} 2.5, 2.65), lactate (δ_{x-y} 1.32, 4.11), glucose (δ_{x-y} 3.25) and phosphocholine (δ_{x-y} 3.23), as shown in Table 3.6 A. As above, removal of these metabolites from the original spectra generated further positive models with significant q^2 values. The metabolites that generated the positive q^2 values in the second round of models were: taurine (δ_{x-y} 3.25, 3.43) and valine (δ_{x-y} 0.99, 1.04) (Table 3.6 B).

All of the metabolites above showed both positive and negative changes compared to baseline over the disease time course (Table 3.6). In the case of taurine, a consistent pattern was found when comparing the Cr-EAE animals to both the CFA and the naïve animals, such that during peak disease, days 10 and 38, taurine increased in the Cr-EAE animal group compared with both control groups. Similarly, glucose and phosphocholine metabolites showed an increase relative to naïve animals during periods of active disease (e.g. days 14

and 38), whilst phosphocholine metabolites fell during remission (day 28). However, the relative concentration of glucose was lower at both days 10 and 28 in Cr-EAE animals than in CFA animals, but higher at day 38 (Figure 3.7).

In contrast to the increases observed above, the concentration of fatty acids in Cr-EAE animals was reduced during active disease, days 10, 14 and 38, relative to naïve animals, but elevated during remission (day 28). At these time-points the levels of fatty acids in the CFA animals were even lower than in the Cr-EAE animals, indicating a greater effect of CFA alone than Cr-EAE on these metabolites (Figure 3.7).

No differences in TMAO were evident between Cr-EAE and naïve animals. However, TMAO was lower over the early disease time course (days 10, 14 and 17) in Cr-EAE animals than CFA animals, and higher at day 38, again indicating differential effects of CFA and Cr-EAE (Figure 3.7).

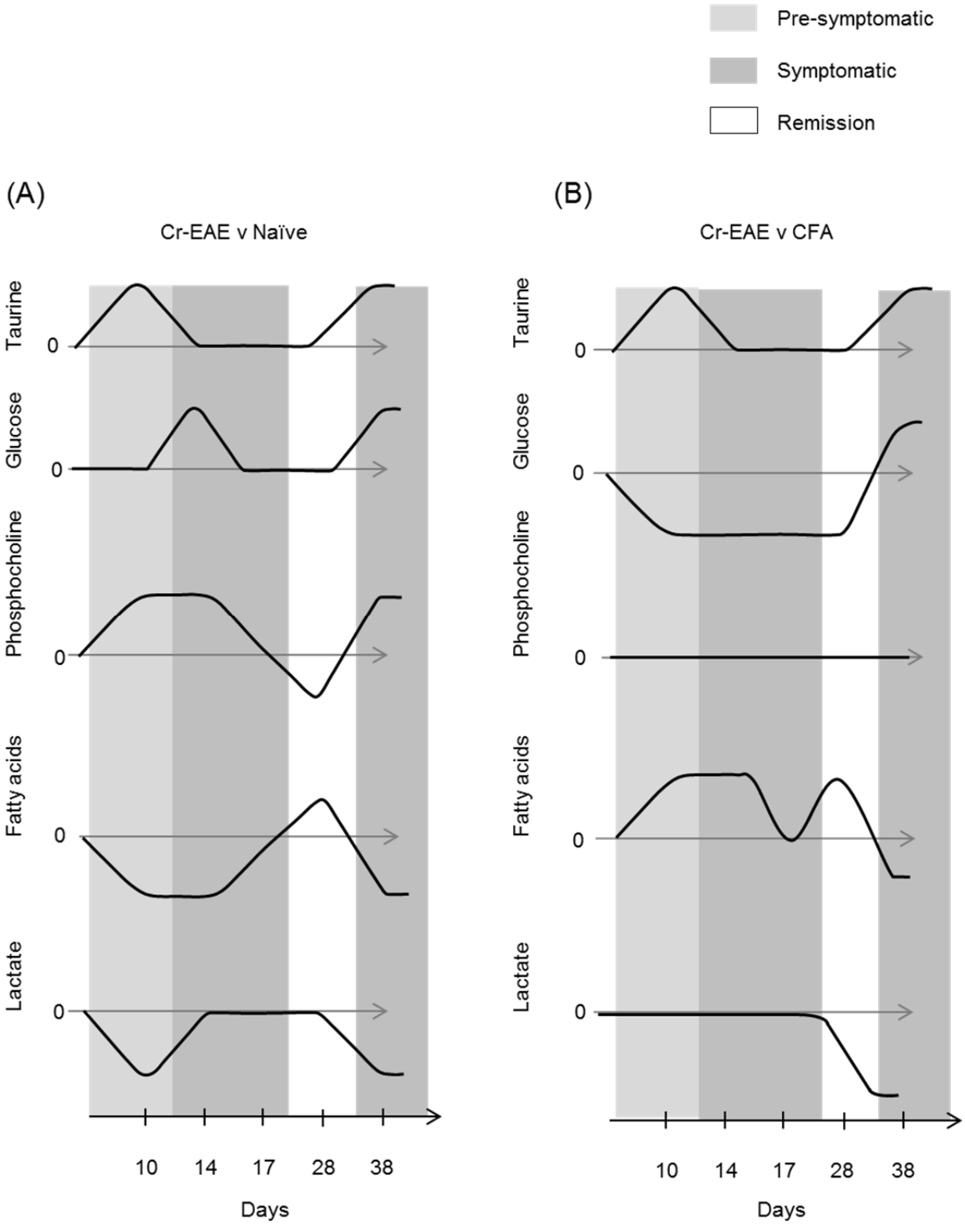


Figure 3.7: Schematic to show the metabolite changes over time in the animal models. (A) Schematic showing metabolite changes within the Cr-EAE animals with respect to naïve animals. (B) Schematic showing metabolite changes within the Cr-EAE animals with respect to CFA animals. Shaded bars represent period of active disease.

(A)

Model	q^2	Metabolites				
		Positive Metabolites		Negative Metabolites		
Day 14	0.58	Fatty acids	Lactate	TMAO	Taurine	Glucose
Day 17	0.84	Lactate		TMAO		
Day 28	0.88	Taurine	Fatty acids	Citrate	Glucose	Lactate
Day 38	0.82	Glucose		Fatty acids	Lactate	

(B)

Model	q^2	Metabolites				
		Positive Metabolites		Negative Metabolites		
Day 17	0.87	Fatty acids		TMAO		
Day 28	0.90	Alanine	Taurine	Citrate	Glucose	Lactate
Day 38	0.75	Glucose		Fatty acids		

(C)

Model	q^2	Metabolites				
		Positive Metabolites		Negative Metabolites		
Day 28	0.93			Glucose	Alanine	Fatty acids	Taurine
Day 38	0.91	Glucose		Fatty acids		

(D)

Model	q^2	Metabolites			
		Positive Metabolites		Negative Metabolites	
Day 38	0.82	Fatty acids	Taurine	Lactate	Glucose

Table 3.5: Plasma metabolites which varied during the Cr-EAE time course. (A) Table showing the positive and negative metabolites which cause the separation in the animal EAE plasma models when compared to animals at day 10. (B) Table showing the positive and negative metabolites which cause the separation in the animal EAE plasma models when compared to animals at day 14. (C) Table showing the positive and negative metabolites which cause the separation in the animal EAE plasma models when compared to animals at day 17. (D) Table showing the positive and negative metabolites which cause the separation in the animal EAE plasma models when compared to animals at day 21.

(A)

Model	q^2	Metabolites						
		Positive Metabolites				Negative Metabolites		
Day 10	0.71	Phosphocholine	Taurine			Fatty acids	Lactate	Valine
Day 14	0.42	Phosphocholine	Glucose			Fatty acids		
Day 17								
Day 28	0.44	Fatty acids				Phosphocholine		
Day 38	0.46	Citrate	Phosphocholine	Glucose	Taurine	Lactate	Fatty acids	Valine

(B)

Model	q^2	Metabolites				
		Positive Metabolites		Negative Metabolites		
Day 10	0.42	Fatty acids	Taurine	Glucose		
Day 14	0.50	Fatty acids		Glucose		
Day 17	0.47			Glucose		
Day 28	0.50	Fatty acids		Glucose		
Day 38	0.84	Glucose	Taurine	Fatty acids	Lactate	Valine

(C)

Model	q^2	Metabolites			
		Positive Metabolites		Negative Metabolites	
Day 10	0.62	Glucose		Unassigned broad resonance	
Day 14	0.51				
Day 17	0.86	Glucose		Unassigned broad resonance	Choline
Day 28	0.32			Unassigned broad resonance	
Day 38	0.47	Choline	Lactate	Unassigned broad resonance	

Table 3.6: Plasma metabolites which varied in the Cr-EAE compared to the control groups. (A) Table showing the positive and negative plasma metabolites which cause the separation between EAE and CFA animals at different time-points. (B) Table showing the positive and negative plasma metabolites which cause the separation between EAE and naïve animals at different time-points. (C) Table showing the positive and negative plasma metabolites which cause the separation between CFA and naïve animals at different time-points.

3.3.5. Human MS: Urine analysis

Initially, all of the MS patients were modelled against the control group. However, although positive (q^2 = 0.11), this model did not reach significance. When the different stages of disease were considered separately against controls, all of the PLS models again returned positive q^2 values indicating differences between each of these groups (RR-MS, PP-MS, SP-MS) and the healthy control groups. However, only the SP-MS *vs.* control model reached defined significance (q^2 = 0.51, take-one-out analysis $p < 0.05$; Figure 3.7 A). On examination of the loadings, citrate and TMAO were increased in the SP-MS group compared to the control group (Table 3.8 A). Relative levels of lactate and creatinine ($\delta_{x\text{-}y}$ 4.06) were reduced in the SP-MS group compared to control. When comparing RR-MS and PP-MS against the healthy control group the q^2 values were only 0.22 and 0.20, respectively, despite showing a visual separation of the groups. With respect to separations between the disease groups, comparison of the RR-MS and SP-MS groups showed a clear separation visually, but the q^2 value of 0.33 did not quite reach significance. No significant differences were found between the PP-MS group and either the SP-MS or RR-MS groups (Figure 3.7 A).

(A)

	RR	PP	SP	
Control	0.22	ns	0.33	RR
		0.20	ns	PP
			0.51*	SP

(B)

	RR	PP	SP	
Control	0.73*	ns	0.46*	RR
		0.64*	ns	PP
			0.70*	SP

Table 3.7: q^2 values from human MS samples. (A) Table to show the q^2 values of the human urine samples from all the models. (B) Table to show the q^2 values of the human serum samples from all the models.

(A)

Model	q^2	Metabolites	
		Positive Metabolites	Negative Metabolites
SP v Control	0.50	TMAO, Citrate	Creatinine, Lactate

(B)

Model	q^2	Metabolites					
		Positive Metabolites			Negative Metabolites		
RR v Control	0.70	Unknown Singlet	L-Glutamine	Alanine	Glucose	Phosphocholine	
SP v Control	0.57	Unknown Singlet			Glucose	Phosphocholine	Fatty Acids
PP v Control	0.64	Fatty acids	N-Acetyl species	Unknown Singlet	Glucose	Phosphocholine	
SP v RR	0.46	Fatty acids	Lactate		Alanine	Phosphocholine	

(C)

Model	q^2	Metabolites		
		Positive Metabolites	Negative Metabolites	
RR v Control	0.66		Lactate	
SP v Control	0.74		Lactate	
PP v Control	0.78	L-Glutamine	Unknown Singlet	
SP v RR	0.40	β-Hydroxybutyrate	N-acetyl species	Glucose

Table 3.8: Metabolite changes in the Human MS samples. (A) Table showing the first round of positive and negative metabolites that caused the separation in the Human urine model. (B) Table showing the first round of positive and negative metabolites that caused the separation in the Human serum models. (C) Table showing the second round of positive and negative metabolites that caused the separation in the human serum models.

3.3.6. Human MS: Serum analysis

The same two NMR sequences as used for the animal samples were run on the human serum samples. However, unlike the spectra obtained from the animal samples, no phase modulation was evident in the spectra obtained from the human samples (Figure 3.8). Since there were no differences between the two types of spectra, the CPMG spectra were used in all subsequent analysis.

Once again the whole cohort of MS patients was compared to the healthy control group. This model showed a significant separation between the two groups with a q^2 value of 0.40; take-one-out analysis $p < 0.05$. Subsequent to this, the different disease states were considered individually. All of the individual comparisons between the MS patient groups (RR-MS, PP-MS, SP-MS) and the healthy control group proved to be highly significant against the defined criteria of $q^2 > 0.4$ (q^2 = 0.73, 0.64, 0.70, respectively). On examination of the spectra from the control group three of the control samples contained an unknown contaminant (δ_{x-y} 3.66, 3.73). These buckets were excluded from the analysis and new models were generated, which all reached the defined significance (q^2 = 0.72, 0.67, 0.71, respectively). Interestingly, when comparing each of the individual stages of MS (RR-MS, PP-MS and SP-MS) against the controls, three metabolites, glucose (δ_{x-y} 3.25, 3.75, 3.91), phosphocholine (δ_{x-y} 3.23; confirmed by spiking) and an unidentified metabolite (singlet δ_{x-y} 3.37), were consistent across the groups (Table 3.8 B). The unidentified metabolite with a chemical shift δ_{x-y} = 3.37 could possibly be methanol or scylloinositol, but the corresponding peaks were not observed in the spectra. Glucose and phosphocholine were reduced in all MS patients relative to healthy controls, whilst the unknown singlet was higher in all MS groups. For the RR-MS group, the relative concentrations of L-glutamine (δ_{x-y} 2.15) and alanine (δ_{x-y} 1.47) were also higher than in healthy controls. When the loadings for the SP-MS *vs*.

control model were examined, no further metabolites were elevated in the SP-MS group compared to the control group, but fatty acids were reduced. In contrast, fatty acids were elevated in the PP-MS group compared to controls, as was a resonance assigned to N-acetyl species (δ_{x-y} 2.03).

Following the initial analysis, the metabolites responsible in each group for causing separations were removed from the spectra of that particular group and a second round of positive models was generated (Table 3.8; C). When comparing the RR-MS and healthy control groups, lactate was found to be reduced in the RR-MS patients. Lactate was also the only other metabolite that varied in the SP-MS *vs*. control model, and, similarly, was reduced in the SP-MS patients. When comparing the PP-MS and control groups, L-glutamine was found to be elevated in the PP-MS samples, whilst an unknown singlet (δ_{x-y} 2.65) was reduced.

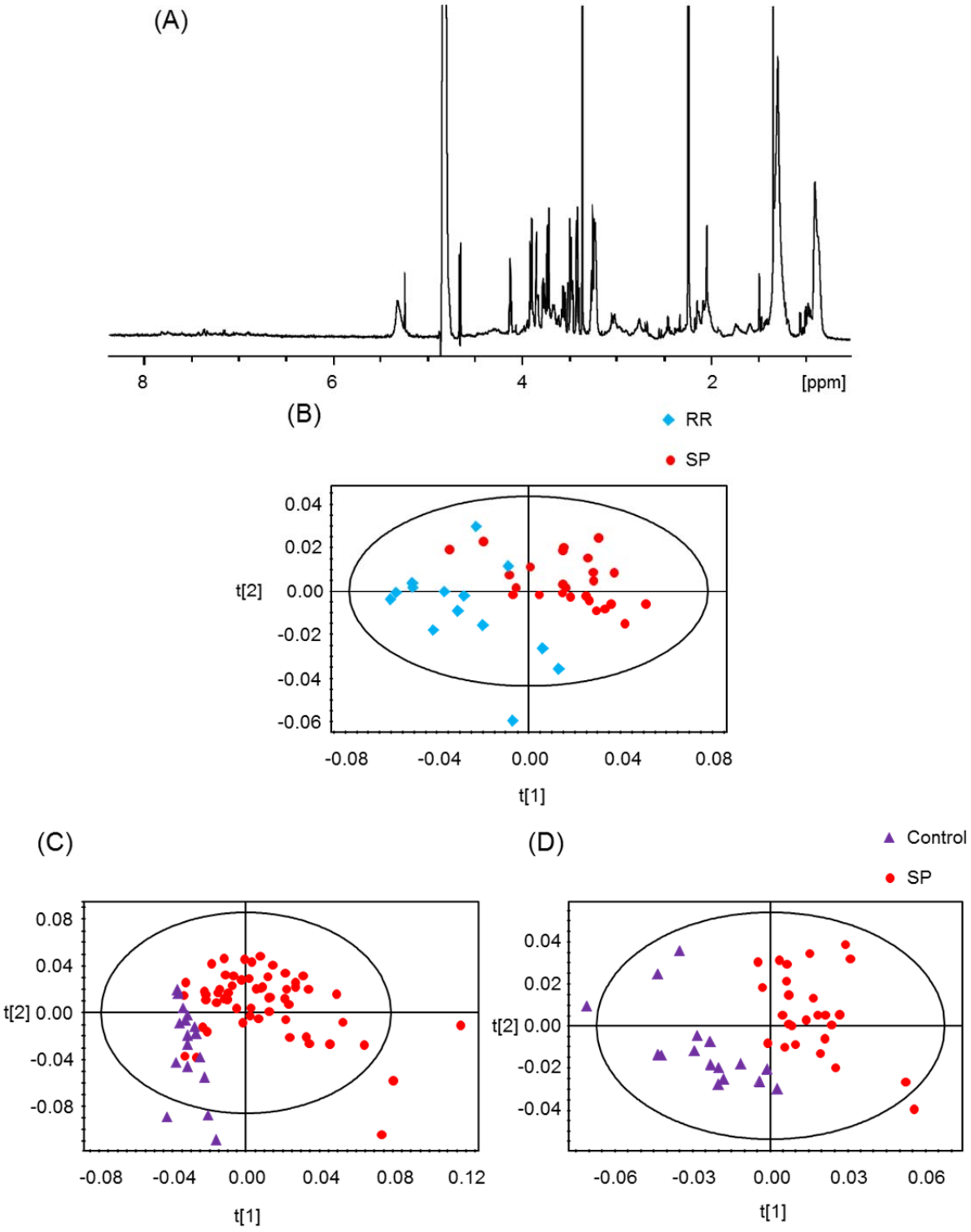


Figure 3.8: Human MS plasma results. (A) Sample 1H NMR NOESY with CPMG suppression spectrum of human serum. (B) PLS-DA plot of human serum samples comparing relapse remitting patients (light blue diamonds) and Secondary Progressive patients (red circles), R2X= 0.45; R2Y = 0.68. (C) PLS-DA plot of human urine samples comparing secondary progressive patients (purple triangles) and a control group (red circles), R2X = 0.63; R2Y = 0.62 (D) PLS-DA plot of human serum samples comparing secondary progressive patients (purple triangles) and a control group (red circles), R2X = 0.59; R2Y = 0.77.

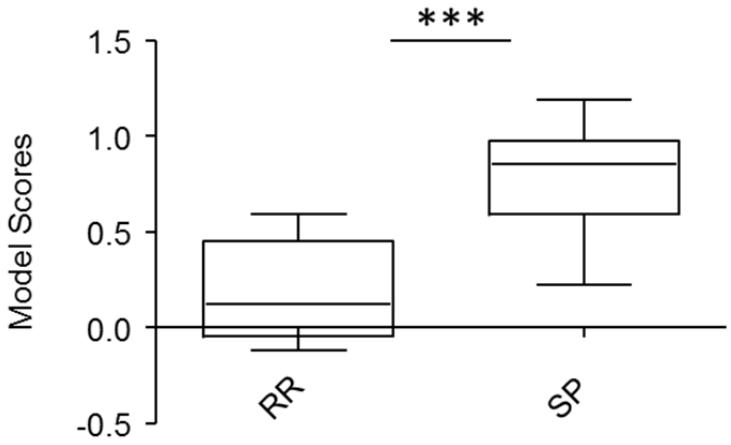


Figure 3.9: A sample box-and-whisker plot showing the take-one-out analysis of the RR v SP model. Stars indicate $p < 0.0001$ difference between the means of the two groups, box shows standard deviation, mid-line shows mean of two groups. Whiskers show the upper and lower limits of the data.

In the case of the RR-MS *vs*. SP-MS model, after the first round of analysis fatty acids (δ_{x-y} 0.88, 1.58 1.3) and lactate (δ_{x-y} 1.32) were found to be higher in the SP-MS group, whilst alanine (δ_{x-y} 3.73) and phosphocholine (δ_{x-y} 3.23) were found to be lower in the SP-MS group than the RR-MS group (Table 3.8 B). Removal of these regions from the spectra generated a further positive model (q^2 = 0.40), reflecting higher levels of β-hydroxybutyrate (δ_{x-y} 2.43) and lower levels of glucose, and a broad singlet like resonance which was tentatively assigned as N-acetyl species, (previously assigned as N-acetyl glycoproteins (Griffin*, et al.*, 2004a), in the SP-MS group (Table 3.8 C)).

3.3.7. Spiking experiments

From the metabolites mentioned above some were only putatively assigned because they were only based on a singlet resonance within the ^{1}H NMR spectrum. These metabolites were: choline, phosphocholine, N-acetyl aspartate, TMA, TMAO, and ureidopropionic acid. The ^{1}H NMR spectrum of all of these metabolites within the phosphate buffer is shown in Figure 3.10. Performing spiking experiments is vital in metabolomic studies as several factors, including ionic strength, pH, and solvent composition can shift the position of peaks in an NMR spectrum.

3.3.7.1. Pre-clinical urine spiking

Within the urine spectrum obtained from the urine of the Cr-EAE animals the metabolites which were identified on a singlet alone were: TMA, TMAO and ureidopropionic acid. Ureidopropionic acid is not a singlet resonance in the ^{1}H NMR spectrum (for NMR assignment see Chapter 2 Section 2.7.5), however, a spiking experiment was performed as the identification of this metabolite was not immediately clear from the COSY spectrum. The addition of these metabolites confirmed the identities of all these assigned peaks (Figure 3.11).

3.3.7.2. Clinical urine spiking

The metabolites which were assigned based on a singlet resonance in the clinical urine analysis were: phosphocholine TMA, and TMAO. Due to the superficial visual similarities between the urine spectra obtained from the pre-clinical studies and the clinical studies and the fact that the position of the reference peaks obtained in Section 3.3.7 did not shift when the spiked chemicals were added to the NMR solution. It was decided that the identity of the singlets could be identified by overlaying the spectra obtained in 3.3.7, this conformed the identity of the metabolites listed above.

3.3.7.3. Blood spiking experiments

The singlet metabolites identified by SIMCA in the plasma and serum samples were identified by spiking a ^{1}H NMR spectrum of human serum obtained from an RR patient. These experiments confirmed the identity of phosphocholine. The peak which has been assigned as N-acetyl species in this chapter could possibly have been N-acetyl aspartate, however, upon spiking the serum sample this was ruled out. The singlet at δ_{x-y} 2.03 was broader and shift slightly down field compared to the spiked N-acetyl aspartate peak. Since these peaks did not change when the chemicals were added to the biofluids the reference spectra was used throughout the rest of this thesis to confirm the identities of these metabolites in the future studies.

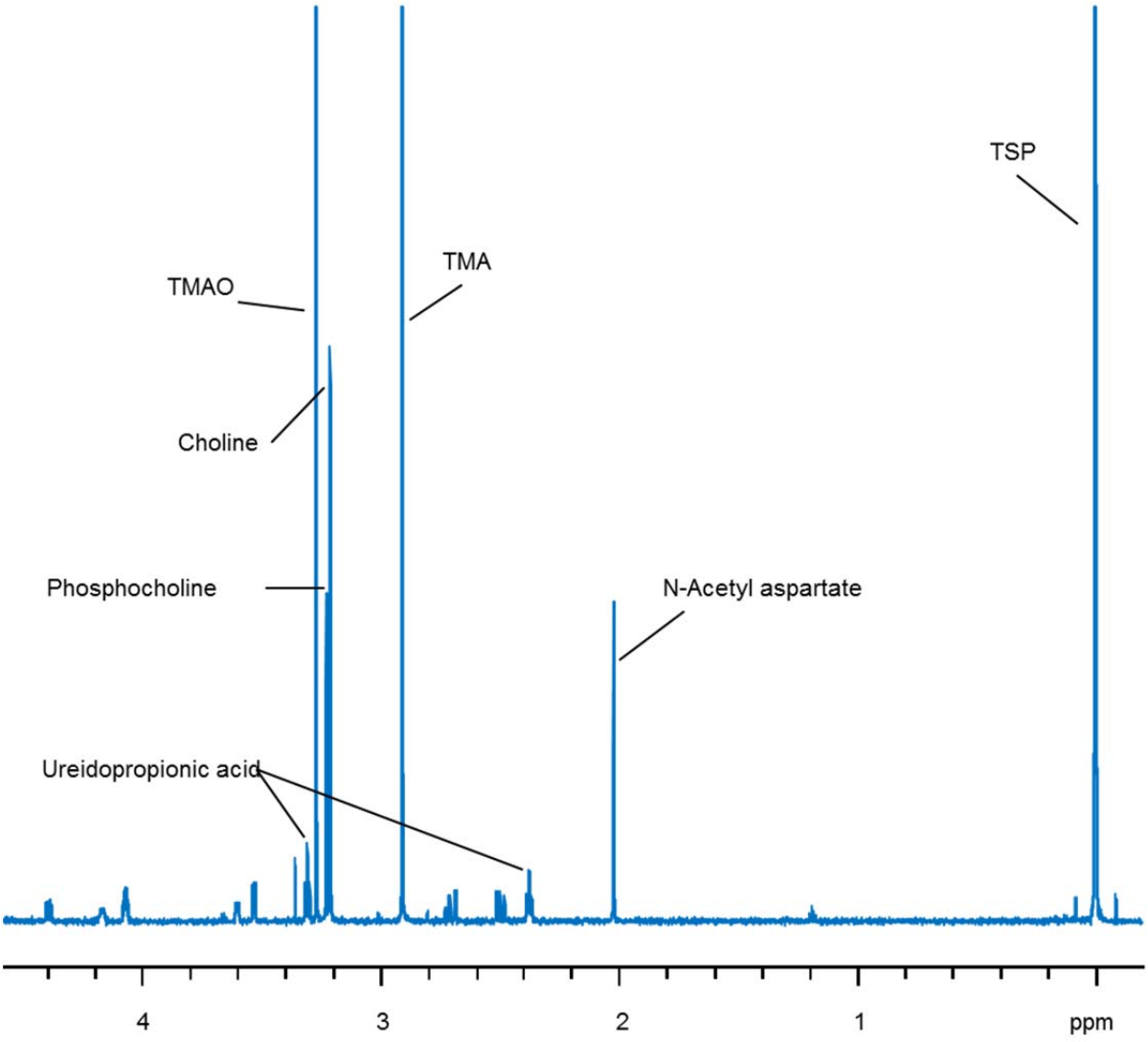


Figure 3.10: First spiking experiments. ^{1}H NMR spectrum, with no water suppression, of metabolites which were only putatively assigned within the chapter. This spectrum shows the NMR spectra of authentic samples of the metabolites which were to be added in the spiking experiments in order to establish the required concentration and peak positions within the NMR solvent system used in this thesis.

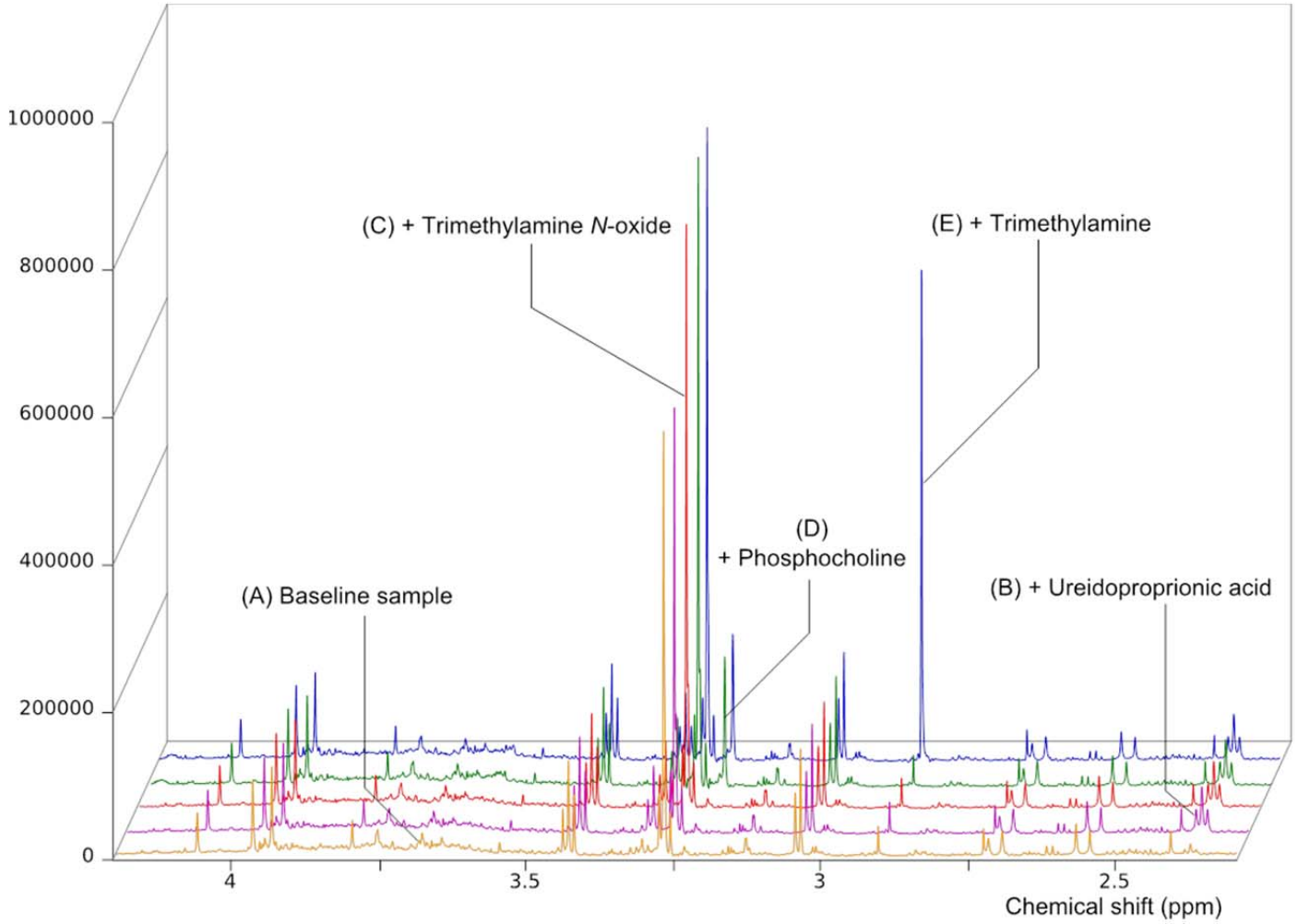


Figure 3.11: Urine NMR spiking experiments. 1H NMR spectrum of potential metabolites in order to confirm the identity of metabolites with a singlet resonance. (A, orange) Baseline 1H NMR NOESY of animal urine. (B, purple) Addition of ureidopropionic acid. (C, red) Addition of TMAO. (D, Green) Addition of phosphocholine. (E, blue) Addition of TMA (Figure created by Dr. James Larkin).

3.4. Discussion

This chapter has demonstrated that through the use of a principal components metabolomics analysis of NMR spectra acquired from urine and plasma samples, it is possible not only to differentiate Cr-EAE animals from control groups, but also to differentiate between different stages of the Cr-EAE disease time course. Subsequently, the same approach has been successfully applied to the analysis of spectra obtained from clinical MS urine and serum samples, and enabled reliable separation of relapsing remitting from secondary progressive MS patients. Models obtained from serum data also consistently separated each of the MS patient groups (RR-MS, SP-MS or PP-MS) from a healthy control group. For all positive models, animal and human, the majority of metabolites in the urine or plasma samples eliciting the separations have been identified. Overall, plasma or serum models were found to provide more robust results than models generated using data from urine samples.

3.4.1. Preclinical urine analysis

Previous work by Drs. Sibson and Anthony, using metabolomic analysis of urine samples, has shown that it is possible to differentiate between intracerebral lesions induced by injection of adenovirus causing overexpression of either Il-1β or TNF-α (Griffin*, et al.*, 2004a). It has also been shown that both MS (Sharief*, et al.*, 1991) and murine models of Cr-EAE (Baker*, et al.*, 1994) are associated with the expression of cytokines such as TNF-α and Il-1β. On this basis, it was hypothesised that it would be possible to follow disease progression in a chronic relapsing remitting model of MS by urine analysis. The results demonstrate that it is possible to generate discriminative ($q^2 > 0.40$) models in some, but not all cases. It has previously been shown that diet in healthy humans has a greater effect on urine metabolite composition than plasma from the same subject (Walsh*, et al.*, 2006). In this study, the diet of the animals is likely to have varied

over the disease time course, as they were given access to a mixed high-energy diet to prevent excessive weight loss. Thus variation in diet may account for the lack of significance in some models. At the same time, urine production varied considerably between animals, resulting in variable metabolite dilution. This dilution may be corrected by the normalisation of the spectra which was performed, and it is therefore hypothesised that the injection of 1 mL of saline diluted the urine too much to get reproducible spectra. However, it was important to determine whether models could be generated without restricting diet or controlling urine production in order to assess the potential for translation of this approach to the clinic.

Where $q^2 > 0.40$ values were generated in the urine-based models, separation between the pre-symptomatic, day 10 time-point and naïve animals was achieved for both Cr-EAE and CFA groups. CFA is key to the induction of EAE as it generates a Th1-type immunological response, and this might be expected to generate some metabolic changes *per se* ('t Hart*, et al.*, 2011). A small drop in weight also accompanied the CFA injection alone. Comparison of Cr-EAE and CFA animals at day 10 did not show significance in the urine analysis, and it is likely that the effects of the CFA injection are still dominant in the metabolite profile at this time-point.

CFA injections alone have previously been shown to cause lasting effects such as inducing arthritis-like pathology (Fan*, et al.*, 2005). However, by day 14 it was possible to generate a predictive model between the Cr-EAE animals and the CFA animals. At this time-point the Cr-EAE animals showed clear clinical signs, usually with complete tail paralysis. Thus, it would be anticipated that any metabolite markers caused by the induction of Cr-EAE would be substantially elevated at this time-point in accord with these behavioural findings. Importantly, at day 28, when the Cr-EAE animals had recovered from the initial

phase of disease and showed no overt clinical signs, it was no longer possible to separate the Cr-EAE animals from the CFA and naïve controls. Thus, the changes in the Cr-EAE urine metabolite profile appear to return to normal levels during this remission phase.

Perhaps the most important result was obtained at day 38 when the Cr-EAE animals entered the first relapse phase, and when the pathology is most relevant to human MS. While this phase is never as severe as the initial phase of disease in this experimental model, it is hypothesised that disability observed in the subsequent relapse contains a greater element of progressive neuronal damage with less oedema than in the first phase (Ahmed*, et al.*, 2001). Using the metabolomics approach it was possible to separate the Cr-EAE animals at this time-point from all other time-points in the disease and also from both of the control groups.

Two metabolites were key to the separations observed at all of the time-points when significant models were generated – citrate and TMA/TMAO. TMA and TMAO are considered as one metabolite change here due to the correlation between them in the models and the fact that TMA is readily metabolised to TMAO. Citrate was reduced relative to controls during the initial phase of disease (days 10 and 14), but elevated during relapse (day 38). In contrast TMA/TMAO was elevated both at day 10 and day 38 relative to controls. Similarly, glucose was elevated at both days 14 and 38. Other metabolites identified during the initial phase of disease were (i) creatine, which was elevated at both days 10 and 14 in the Cr-EAE animals, and (ii) ureidopropionic acid, which was elevated at day 10. Previous studies have shown that cachexia and dietary effects can be detected in rat urine using an NMR biomarker approach, with changes seen in both glucose and citrate (Connor*, et al.*, 2004). Moreover, a reduction in citrate concentration in urine samples has been shown

to be an early generic marker of non-specific toxicity and can be observed even prior to the onset of weight loss (Connor*, et al.*, 2004). The results at day 10 agree with those findings, and the reduction in citrate in both CFA and Cr-EAE animals suggests that despite no significant change in animal weight, an immunological response had been mounted. Given that Cr-EAE induces complete hind limb paralysis leading to cachexia during both the acute and relapse phases of the disease, it might be anticipated that citrate would also be low at days 14 and day 38 owing to the increased disability and weight loss. However, whilst citrate was indeed reduced at day 14, it was, in contrast, elevated relative to CFA controls during the relapse.

TMAO is commonly found within urine samples as it is a metabolic product of choline and has a protective effect as an osmolyte to counter the presence of increased urea concentration within the kidney (Baker*, et al.*, 1962; Neuhofer*, et al.*, 2006; Norris*, et al.*, 1945). Maschke *et al.* have shown that a reduced function of liver amine oxidase can lead to an increase in the concentration of the closely-related metabolite TMA in urine (Maschke*, et al.*, 1997). It is possible, therefore, that the increase in TMA/TMAO in the animals in this study, at days 10 and 38, relative to controls, may indicate a reduction in liver amine oxidase function immediately prior to and during the relapse phase of Cr-EAE.

In a previous metabolomics study of marmosets, comparing limited cohorts of EAE and naïve animals ('t Hart*, et al.*, 2003), a small number of metabolites were identified as separating the EAE animals from controls: N-acetyl aspartate (NAA), choline, *myo*-inositol and neopterine. Although these metabolites did not appear in the positive models generated here, when the corresponding spectral regions were modelled exclusively, positive separations were found between Cr-EAE and naïve animals at day 10 for NAA, choline and *myo*-inositol regions. In each case the levels of these buckets were elevated in the Cr-EAE animals,

as reported by 't Hart *et al*. Nevertheless, in the current models these were not the dominating metabolites underlying the separations. Neopterine was not identified in the current study since the majority of its proton resonances lie in the 4.3 to 5.0 ppm range, which was excluded owing to the water suppression used. Although neopterine has been described as a putative marker for MS (Giovannoni*, et al.*, 1997), it is more likely to be a generic marker of inflammation (Giovannoni*, et al.*, 1998; Murr*, et al.*, 2002). Though the earlier study by 't Hart *et al*. had similar aims to the current study, the choice of a relapsing model here has allowed investigation of both remission and relapse phases of the disease, which was not a feature of the model used in the earlier study. Moreover, the use of higher field strength in the current study than that of 't Hart *et al*. (700 MHz *vs.* 400 MHz, respectively) has enabled greater sensitivity and resonance separation, thus enabling a more comprehensive identification of discriminating metabolites. These metabolites include ureidopropionic acid and TMAO which have not been associated with MS in previous biomarker studies.

3.4.2. Preclinical blood analysis

The plasma models were able to separate all of the Cr-EAE time-points, with significant q^2 values, including separation between time-points when the disease was clinically silent, such as days 10 and 28. It was also possible to separate Cr-EAE from the two control groups, CFA alone and naïve animals, at all of the time-points. As for the urine analysis, it appeared that the effects of CFA alone complicated the models in the early phase of the disease. Interestingly, although it was also possible to separate the CFA and naïve groups across most of the time-points (day 10 and 38), these models were driven by fewer metabolites, including glucose, lactate and choline. Whilst glucose and lactate also varied in the Cr-EAE animals, these metabolites

changed in the opposite direction, relative to the naïve animals than in the CFA animals.

Several plasma metabolites varied over the disease time course when compared to the two control groups, for a schematic of these changes see Figure 3.7. The only metabolite that showed the same pattern when comparing the Cr-EAE with either the CFA or naïve samples was taurine. This metabolite was found to be elevated at both days 10 and 38 in the Cr-EAE animals. Levels of glucose followed a similar pattern in the plasma to that observed in the urine and, again, are probably an indicator of the reduced food intake and resulting cachexia in these animals. Similarly, the observed reductions in fatty acids during active disease likely reflect metabolic alterations as a consequence of reduced food intake. Increases in brain choline signals (at 3.2 ppm) detected by MRS have been reported in MS patients, and include contributions from phosphorylcholine and glycerophosphorylcholine owing to the lower spectral resolution at clinical field strengths. These increases in choline metabolites are thought to reflect heightened cell-membrane turnover associated with demyelination, remyelination and inflammation in MS patients (Narayana, 2005). Thus, the increases in the serum resonance assigned to phosphocholine during active disease observed in the Cr-EAE mice may reflect CNS myelin degradation.

3.4.3. Clinical studies

The preclinical studies strongly indicated that it might be possible to build models to monitor human MS. In accord with those findings, analysis of the MS urine samples produced clear visual separations between most of the groups and many of the models returned positive q^2 values, albeit not high enough to qualify as a predictive model. However, a significant separation, and thus a predictive model, was found between the SP-MS and control groups. Elevated

levels of TMAO and citrate in the urine of SP-MS cases were key to the separation of SP-MS from control groups, and this mirrored changes in these metabolites in the Cr-EAE urine data during the relapse phase. Interestingly, within the animal data, citrate was lower in Cr-EAE mice than in controls during acute active disease, but then rose during relapse. These observations suggest that the animal model may provide insight into the metabolic changes associated with secondary progressive MS. Studies have shown that metabolite composition in urine varies during the day in an individual (Saude*, et al.*, 2007). Urine obtained for the study was collected upon entry to the MS clinics and, thus, at different times in the day. In the light of the results, a more systematic approach is now justified in new and larger cohorts, and would be expected to generate more consistent data and predictive models. Others have shown that it is possible to use human urine to distinguish between healthy controls and people with neurological disease ('t Hart*, et al.*, 2003). That study reported an 80% success rate when separating the CNS disease group, including MS, from the healthy controls, and a 75% success rate in diagnosing MS specifically. However, out of the ten MS patients in the study, four were identified as either healthy or unclassifiable by the model, whilst seven non-MS patients or healthy controls were incorrectly classified as having MS. Moreover, no assignments were made as to the underlying metabolites.

Given the animal results, it was decided to investigate whether it would be possible to obtain more reliable models using serum from individuals with MS. Therefore serum was chosen rather than plasma owing to the fact that the mouse plasma samples showed strong resonances from calcium-bound EDTA, which is not present in the serum collection tubes. The pre-clinical samples were collected in EDTA plasma tubes. Due to the presence of the highly variable NMR signals observed in this study arising from EDTA, however, heparin plasma tubes should be used for any future studies. Predictive models

were generated that separated each of the individual stages of MS pathology from healthy controls. Key metabolites underlying these separations were identified, some of which were similar to the metabolites found to be varying in the animal model. In particular the reduction in fatty acids in SP-MS patients compared to healthy individuals was in accord with the reduction in fatty acids seen in the Cr-EAE mice during active disease compared to controls. Conversely, whilst glucose and phosphocholine were elevated during active disease in the Cr-EAE mice, they were reduced in all MS patients groups relative to controls. It has been reported that the cortisol response to corticotropin-releasing hormone in SP-MS is significantly lower than in normal control groups (Wei*, et al.*, 1997), and fatigue is a common phenomenon in MS. As cortisol antagonises the effects of insulin it is possible that adrenal hyporesponsiveness in MS, which is a cause of hypoglycaemia, may account for the reduced levels of circulating glucose observed in this study.

It is interesting to note that, whilst the only intra-MS separation to reach significance was SP-MS *vs.* RR-MS, there were differences in the metabolite profiles that caused the separations between each of the MS groups and the control group, indicating sensitivity to the different disease states. To my knowledge, no studies have been reported in which MS patients have been separated either from healthy controls or by sub-type of MS disease on the basis of NMR analysis of serum alone. Using a similar approach, Kuhle *et al.* recently reported an increase in the neurofilament heavy (NfH) chain within CSF during RR-MS and clinically isolated syndrome stages of disease, but not PP-MS and SP-MS (Kuhle*, et al.*, 2011). However, the concentration of NfH is also strongly correlated with age and this would need to be taken into account. Moreover, repeated CSF sampling via lumbar tap is more prohibitive than repeated urine, or even serum, sampling. The use of take-one-out analysis used in this chapter is not ideal for the number of samples used, especially in

the human studies. A better way would have been to use an independent dataset to validate the models. This was attempted but due to spectral alignment issues this was not successful and therefore, the take-one-out analysis was used as the 'best alternative'. This analysis was carried out in a blinded fashion with an independent researcher performing the analysis.

3.4.4. Chapter Summary

In conclusion, this study has shown that it is possible to use metabolomic profiling of urine, plasma and serum samples to investigate disease progression in both a clinically-relevant mouse model of MS and in MS itself. Several of the metabolites identified as causing a positive correlation in the animal models were also identified in the human models. These models could be used diagnostically to non-invasively separate disease states such as relapsing remitting and secondary progressive phases of MS. Moreover, this approach may provide new biomarkers for evaluating neuroprotective treatments. No simple relationship was found to exist between one individual metabolite and disease progression over time in either human MS or murine disease. This was expected, as no previous study has managed to identify a single predictive biomarker of MS in biofluids. The changes in metabolite concentration that underpin the predictive models reported here are difficult to interpret on the basis of our knowledge of MS biology. It has been speculated on why individual metabolites may be changing over time, but it is clear that further work will be required in larger cohorts to establish links between the clinical signs, pathology, and individual metabolites. However, the power of PLS-DA rests in its potential to generate predictive models of disease progression without either *a priori* etiological hypotheses or necessity to understand the pathology responsible for generating the models. This is due to the fact that PLS-DA modelling is an untargeted approach to identifying the metabolites that vary.

This enables all the ‘NMR visible’ metabolites to be studied together and the results are not biased by any preconceptions, which could happen in a targeted metabolic approach.

Chapter 4: Metabolomic changes in Alzheimer's Disease

4.1. Introduction

Chapter 3 of this thesis revealed that it is possible to distinguish between different stages of MS from a healthy control cohort. It also demonstrated that it was sensitive enough to distinguish between RR- and SP-MS. If metabolomics was ever to be adopted in clinics as a means of diagnosing MS it would need to distinguish between other neurological diseases. Previously, 't Hart *et al.* demonstrated that it was possible to distinguish between a number of brain diseases, such as stroke, Alzheimer's disease (AD) and Parkinson's from MS patients using a metabolomic analysis of their urine. However, the sample size was small, with only 10 MS patients and 19 patients with other brain diseases. From this, 5 of the patients with other brain diseases were classified as having MS and one of the MS patients was misclassified as having another brain disease ('t Hart*, et al.*, 2003). Therefore, a more focused study with a larger cohort of patients is needed in order to demonstrate the utility of metabolomics in distinguishing between other neurological diseases and MS. AD is a neurodegenerative disease that results in neuronal damage (see chapter 1 for a full introduction). AD is the most common form of dementia and is estimated to affect 33.9 million people worldwide (Barnes*, et al.*, 2011). It would be desirable to identify metabolites that could differentiate between MS and AD. In addition to this it would be interesting to identify metabolites which are common to both disorders (as discussed in Chapter 1 Section 1.9).

Chapter 3 has shown how the combination ^{1}H NMR of biofluids coupled with a multivariate statistical approach could be used as a diagnostic tool for MS. However, as shown by the model of PP v RR (Figure 4.1), not all the models

were significant, despite showing a strong visual separation. Therefore, it would be desirable to find a method in which the PLS-DA models of the MS patients could be developed in order to improve the diagnostic capabilities. As shown in the previous chapter, it is possible to incorporate clinical data into the PLS models. The Expanded Disability Status Scale (EDSS) scoring system was developed by Kurtzke *et al.* as a way of classifying the progression of MS (Kurtzke, 1983). The scale allows the quantification of MS on a scale from 0 (healthy) to 10 (death). Patients with scores 4.5 or below are considered to be fully mobile, while patients with scores above 5 are measured by the degree of impairment to their mobility (Figure 4.2). This chapter will use the EDSS scoring system as a Y variable in the MS models. This will determine the usefulness of the EDSS score as a means of categorising MS.

4.1.1. Aims of Chapter

Thus, the aims of this chapter are:

1. To explore whether the addition of clinical data into the MS models can generate more robust models.
2. To compare a different neurodegenerative disease (AD) with the MS models.
3. To identify metabolites that will distinguish AD from MS and conversely any metabolites which are common to both diseases.

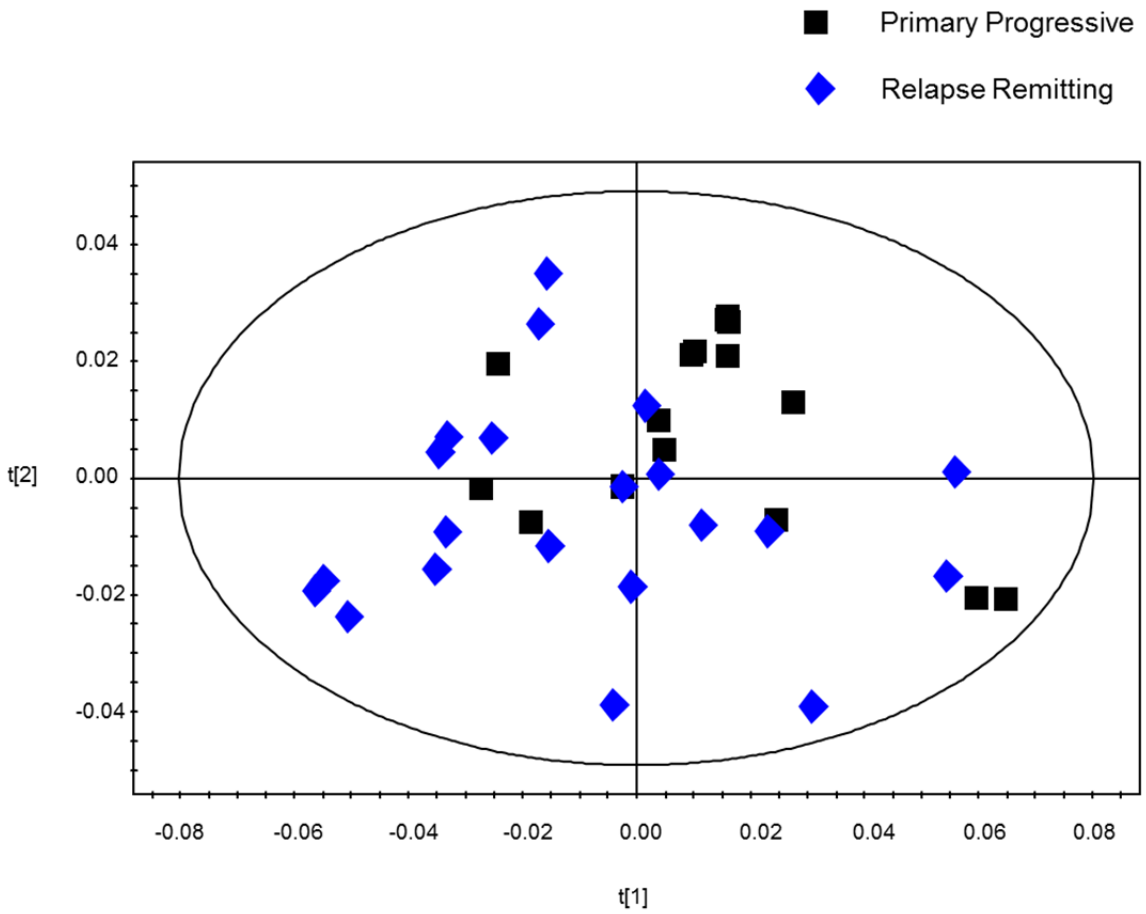


Figure 4.1: PLS-DA model between the PP-MS patients and RR-MS patients q^2 = -0.21.

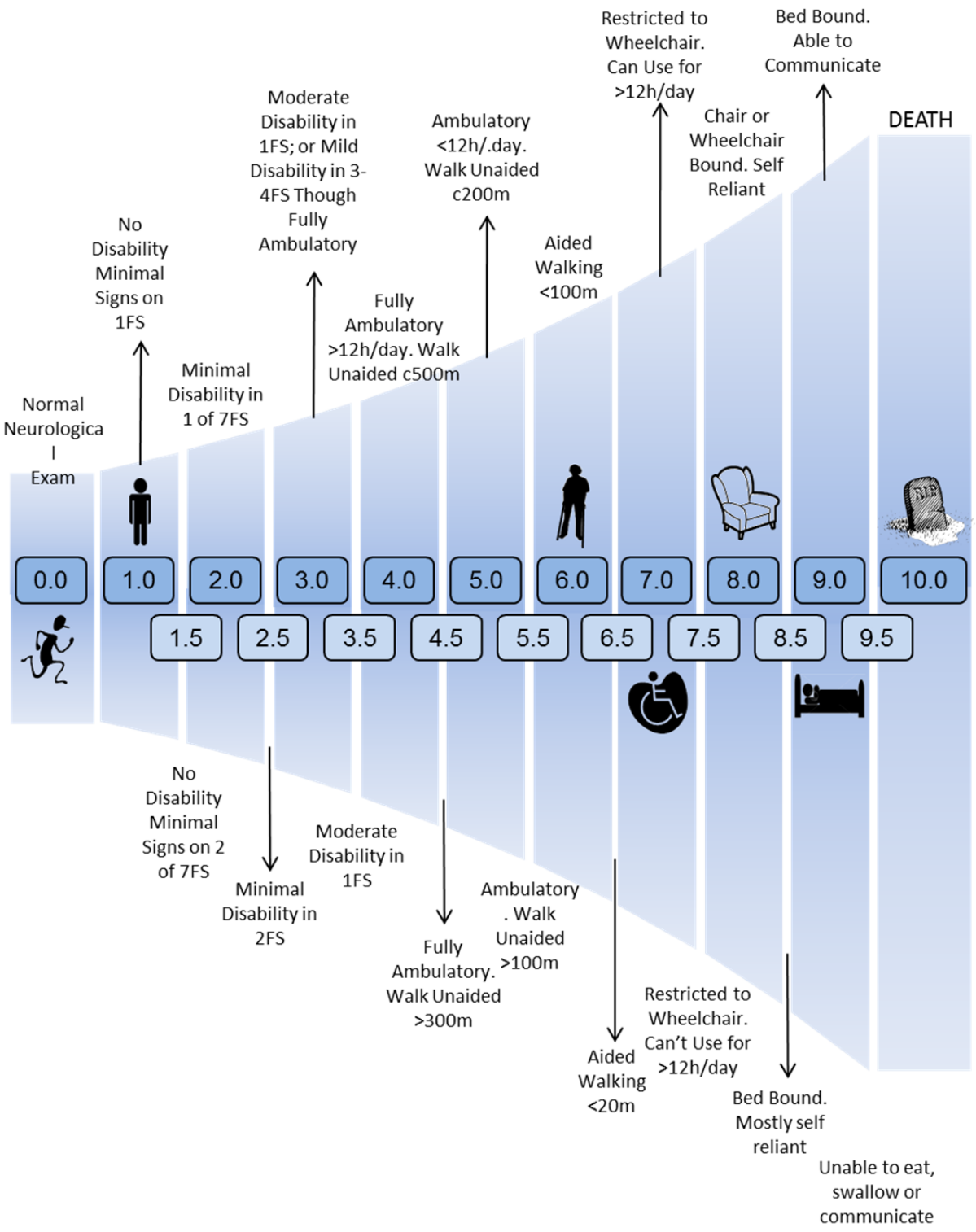


Figure 4.2: Table showing the EDSS scale for classify the progression of MS.

4.2. Methods

4.2.1. Sample collection

Further samples of serum were obtained from PP-MS (n = 16) patients. These samples were obtained from the MS clinic at the John Radcliffe Hospital. SP-MS (n = 30) patients were kindly donated by Raj Kapoor (National Hospital for Neurology, Queens Square, London). These samples also included the addition of EDSS score data of the patients from the time of sample acquisition. Urine (n = 49) and serum (n = 40) samples from Alzheimer's patients were acquired from the 'Oxford Project to Investigate Memory and Aging' (OPTIMA).

4.2.2. NMR sample preparation

The NMR samples were prepared as described in Chapter 2 Section 2.6.2 with the addition of the ultracentrifuge step for the serum samples as described in Chapter 3 Section 3.3.2.

4.2.3. NMR Spectroscopy

The NMR spectroscopy was performed as described in Chapter 2 Section 2.6.3.

4.2.4. Statistical analysis

The PLS-DA modelling was carried out as described in the methods chapter. The clinical data and lipid concentration data was modelled by defining them as a Y variable within the model. This led to the formation of PLS models using the same class based system as described in the Chapter 2 Section 2.7.2. The Y variables were scaled using unit variance scaling rather than Pareto variance scaling as used previously. he EDSS scores were also used to create groups within Simca P+. Arbitrarily, it was decided to place all the PP and SP cases of

MS with an EDSS score lower than 5 into one class and all PP and SP with an EDSS score equal or greater than 5 into a second class.

4.2.5. Metabolite identification

The metabolites causing the separations within the models were identified as described in Chapter 2 Section 2.7.5.

4.3. Results

4.3.1. Alzheimer's disease results

4.3.1.1. Urine results

The ^{1}H NMR spectra obtained from the urine was similar in appearance to the spectra obtained from the MS samples. However, comparison with the MS samples was not possible owing to the fact that only the SP versus controls model in the human urine was successful. There were also issues with the scaling of the spectra due to subtle variations in the TSP peak. This will discussed more in Chapter 6 Section 6.4.2. This meant the urine spectra obtained from the AD patients could not easily be compared to the original spectra from the MS study.

4.3.1.2. Plasma results

The ^{1}H NMR spectra of the serum obtained from the SP, PP and Alzheimer's patients was of similar resolution to the spectra acquired for the original MS study (Chapter 3 Section 3.3.6). Due to the scaling problems mentioned above (Section 4.3.1.1) it was not possible to compare the spectra obtained from the new SP, PP and AD patients to the original spectra from the MS study. However, it was possible to compare the new samples as they were run on the spectrometer using the same batch of D_2O and, therefore, the TSP peak was consistent.

The PLS-DA model of the new PP and SP serum generated a model which showed a significant separation, $q^2 = 0.50$ (Figure 4.3 A). Upon examinations of the loadings it was observed that this separation was caused by a single region within the spectrum ($\delta_{x\text{-}y}$ 3.37). This corresponded to a single NMR resonance which dominated the PP cases and not the SP cases. The peak was a broad

singlet at a much higher concentration to any other metabolite within the PP spectra. Therefore this peak was excluded from the spectra, as described in Chapter 2 Section 2.7.6 and the groups re-modelled. The resultant PLS-DA model did not show a statistically significant difference between the groups (q^2 = 0.23) (Figure 4.3 B).

This peak was then removed from all subsequent analysis of these samples. The PLS-DA models showed a visual separation between the AD patients and both the PP- and SP-MS patients (Figure 4.3 C and D). Further statistical testing revealed that these were significant separations (q^2 = 0.50 and 0.50 respectively). Upon examination of the loadings from this model it was possible to identify the metabolites which caused the separations in these two models. There were three metabolites which were constant at causing a significant separation between the models. These were, lactate (δ_{x-y} 1.35]), fatty acids (δ_{x-y} 0.87, 1.27, 2.05) and an unknown resonance (δ_{x-y} 3.24, multiplet). All these metabolites were elevated in the MS patients compared to the AD patients. In addition to this glucose was at higher level in the PP-MS patients compared to the AD patients. There were two metabolites which were at a lower level in the PP-MS patients: these were a p-cresol-like resonance (δ_{x-y} 2.25) and an unknown resonance (δ_{x-y} 4.05, triplet), as shown Table 4.1 A. When comparing the SP-MS patients with the AD patients, creatinine (δ_{x-y} 4.05) was also at a higher level in the MS patients. There were no metabolites at a lower level in the MS patients compared to the AD patients for the SP model (Table 4.1 B).

Removal of these metabolites generated two further significant models, q^2 = 0.50 (PP-MS v AD) and q^2 = 0.46 (SP-MS v AD). Interestingly, there were no further metabolites which were negative in the MS patients compared to the AD patients. Alanine (δ_{x-y} 1.49) and an unidentifiable broad multiplet (δ_{x-y} 2.08) were at a higher level in the PP-MS patients compared to the AD patients (Table 4.1

C). When comparing the SP-MS patients to the AD patients, glucose (δ_{x-y} 3.25, 3.77, 3.43, 3.85) was at a higher level in the SP-MS patients (Table 4.1 C).

It was also possible to separate out the AD patients from a control group (q^2 = 0.68). Fatty acids (δ_{x-y} 0.87, 2.05), glucose (δ_{x-y} 3.25, 3.91), and lactate were at a higher concentration in the AD patients compared to the controls. Three metabolites were found to be at a lower level in the AD patients compared to the controls. These were citrate, a p-cresol-like (δ_{x-y} 2.25) resonance and an unidentified singlet (δ_{x-y} 3.63). The p-cresol-like resonance is unlikely to be p-cresol in this case, the corresponding aromatic resonances were not observed in the spectra. This was partly due to the increase in the baseline noise in this region of the spectrum. p-Cresol is formed in the body by the breakdown of proteins. The reason it is unlikely to be p-cresol in man is that p-cresol is further metabolised *via* a secondary metabolism pathway which sulphates or glycosylates the p-cresol.

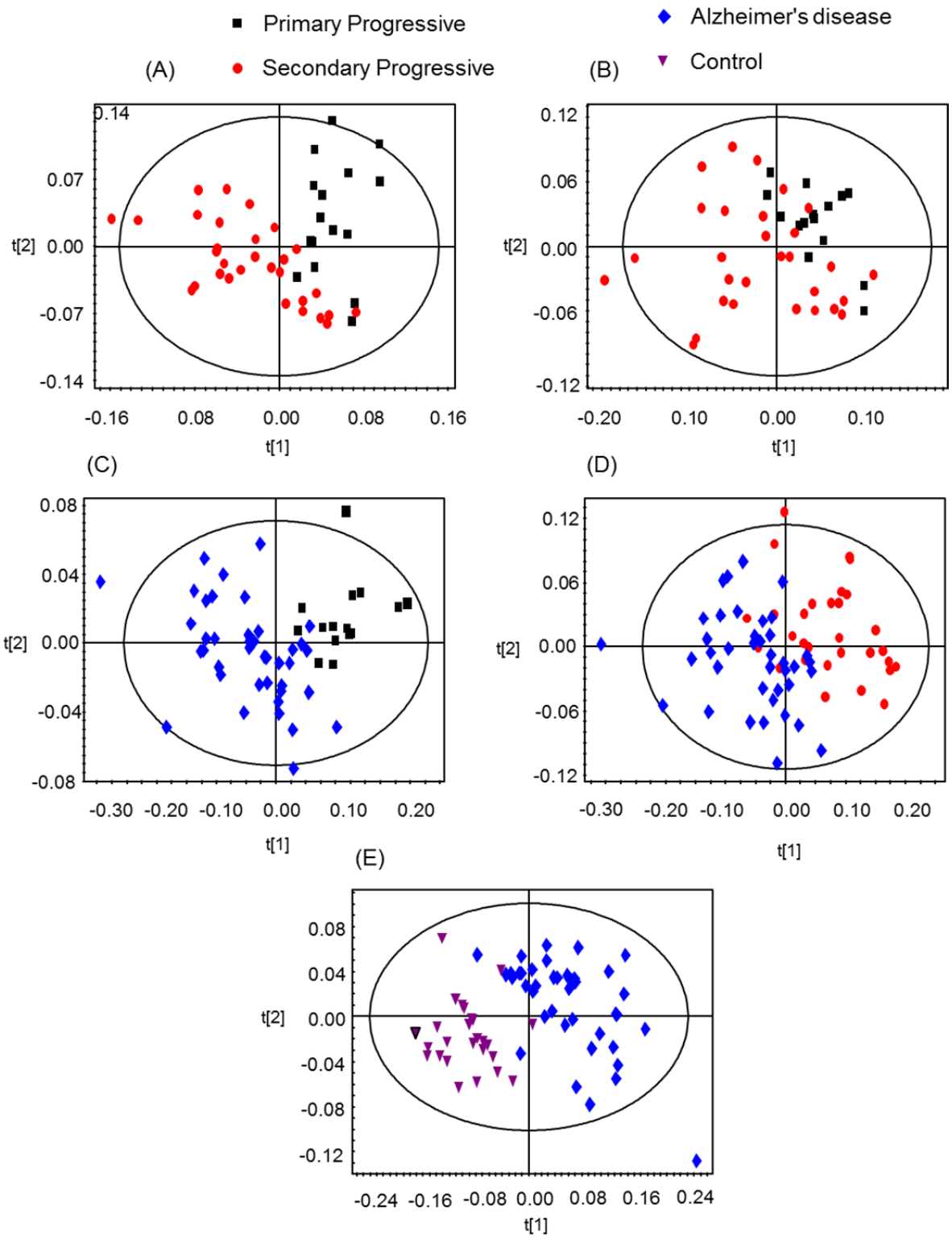


Figure 4.3: PLS-DA plots of PP v SP MS patients. (A) Initial plot showing a statistical significant separation (q^2 = 0.50) between the groups; PP-MS (black squares) and SP-MS (red circles) (B) Plot after the removal of the large singlet NMR resonance at d_{x-y} 3.37 with no statistical separation (q^2 = 0.23) between PP-MS (black squares) and SP-MS (red circles). (C) PLS plot showing the separation between the AD patients (blue diamonds) and the PP-MS patients (black squares). (D) PLS plot showing the separation between the AD patients (blue diamonds) and the SP-MS patients (red circles). (E) PLS plot showing the separation between the AD patients (blue diamonds) and a healthy control cohort (purple triangles).

(A)

Model	q^2	Positive Metabolites	
SP v Alzheimer's	0.50		
PP v Alzheimer's	0.50	Unknown triplet	p-cresol

(B)

Model	q^2	Negative Metabolites			
SP v Alzheimer's	0.50	Lactate	Fatty Acid	Unknown broad signal	Creatinine
PP v Alzheimer's	0.50	Lactate	Fatty Acid	Unknown broad signal	Glucose

(C)

Model	q2	Positive Metabolites	
SP v Alzheimer's	0.46	Glucose	
PP v Alzheimer's	0.50	Alanine	Unidentified broad multiplet

(D)

Model	q2	Positive Metabolites		
Alzheimer's v Control	0.68	Fatty Acids	Lactate	Glucose

(E)

Model	q2	Negative Metabolites		
Alzheimer's v Control	0.68	Unknown Singlet	*p-Cresol*	Citrate

Table 4.1: Table showing the metabolite differences between AD patients and PP- and SP-MS patients. (A) Positive metabolites with respect to the MS patients. (B) Negative metabolites with respect to the MS patients (C) Table showing second round positive metabolites from the MS patients compared to the AD patients. (D) Table showing the metabolites which generated the separation in PLS model between the AD patients and the controls.

4.3.2. Addition of clinical data

It was hypothesised that the inclusion of clinical data as Y variable within these models could improve the diagnostic power of these models. This would be especially beneficial when if this technique where ever to be used to study disease progression. Upon inclusion of the EDSS as Y variable into the PLS model, the two groups appeared to visually overlap even more and this was confirmed by a reduction in the q^2 value to a non-significant value (Figure 4.4 A). The range of EDSS scores from the combined cases of PP and SP gave a median at 5.5 and an average of 4.4 and therefore the arbitrary cut off for EDSS classification was set at 5. The PLS-DA model which combined the PP- and SP-MS patients together and used their EDSS scores as means of class separation did not furnish a statistically significant model (Figure 4.4 B).

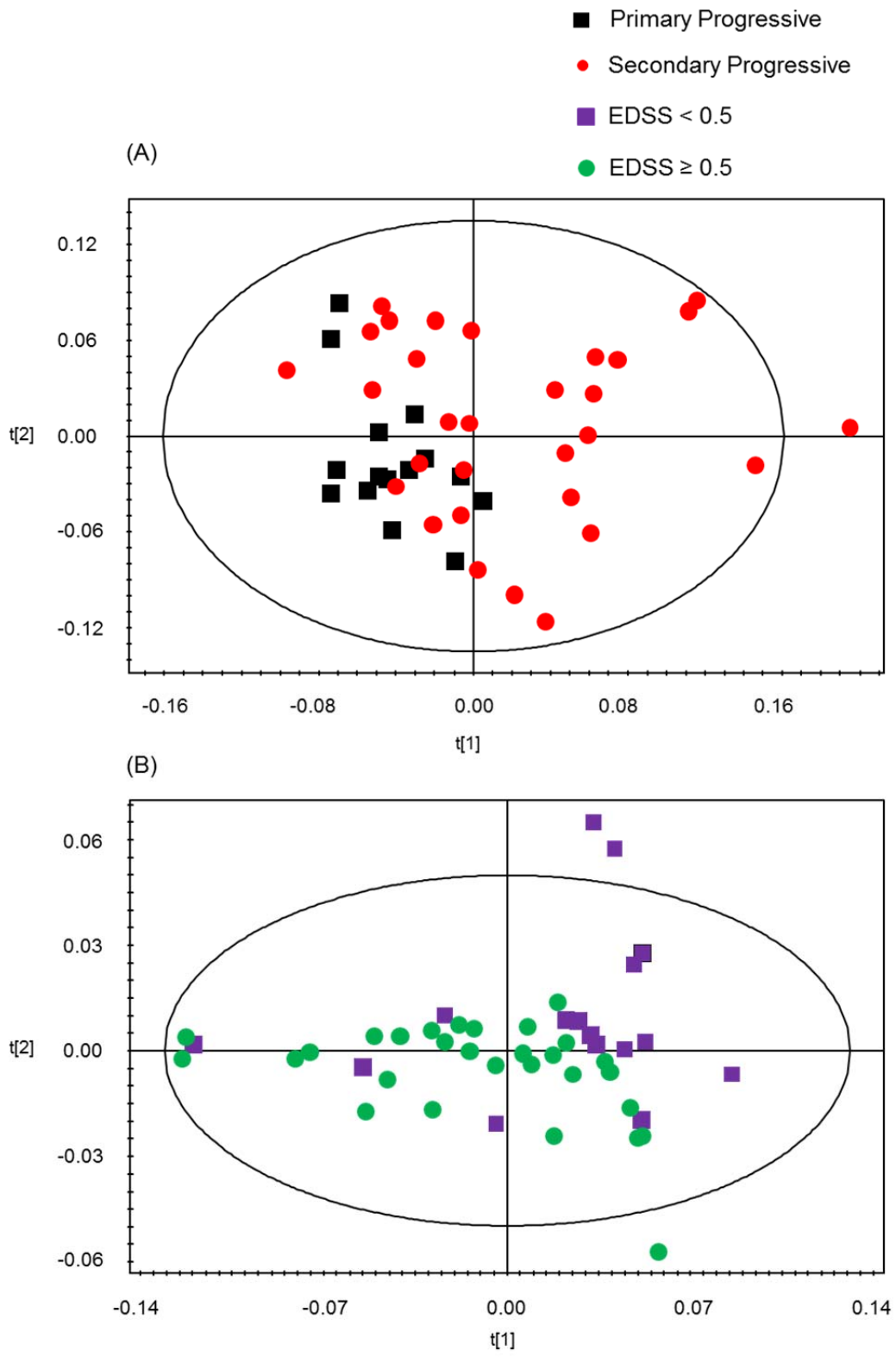


Figure 4.4: PLS models with the inclusion of EDSS data. (A) PLS model comparing PP patients (black squares) with SP patients (red circles) with the inclusion of EDSS data as a Y variable. (B) PLS-DA model of PP and SP MS cases grouped according to their EDSS score, patients with EDSS below 5 (purple squares), compared to patients with EDSS equal to or above 5 (green circles).

4.4. Discussion

This chapter has demonstrated that it is possible to use metabolomic analysis on serum samples to distinguish between two different neurodegenerative diseases. It has also demonstrated that it is possible to distinguish between AD patients and a healthy control group. In addition to this the addition of EDSS data as a Y-variable into the PLS models in an attempt to achieve a better separation in progressive form of MS (PP-MS and SP-MS) PLS. However, the addition of these data did not yield predictive models.

The ability of metabolomics to differentiate between neurological diseases demonstrated in this chapter the sensitivity of metabolomics as a technique for diagnosing brain disease. However, this quality also led to several problems in this chapter. One of the reasons for studying this dataset was to validate the models generated in Chapter 3 Section 3.3.6. This would have been in addition to the standard validation techniques described in Chapter 2 Section 2.7.4. The ability to place new samples into the existing models would be critical for this technique to gain traction in the clinic. Unfortunately, this was not possible to do with the samples acquired in this study. The NMR experiments were performed on the same magnet but at different times. This lead to variation in the NMR datasets which arose from the subtle variation in the TSP signal from different batches of phosphate buffered NMR solvent would have to be overcome. Inaccuracies were generated from having to weigh such a small amount (14.8 mg per 100 mL of buffer) of TSP. This generates small differences within the spectra run using different batches of solvent and thus generating false positive results. One solution to this problem would be to prepare a large batch of D_2O, however, D_2O is highly hygroscopic (Lipka*, et al.*, 1984) and therefore the amount of water suppression would need to increase, this may introduce more spectral variation. Another potential solution to this problem is to use an internal

standard within the biofluid such as glucose or creatinine. Variation of these metabolites in humans it would be necessary to measure these metabolites by an independent means and then to scale the spectra accordingly. In theory, this analysis should be spectrometer-independent and these issues should be resolvable by use of a peak alignment algorithm. However, subsequent analysis using such algorithms has so far proved unsuccessful with these samples.

The measurement of blood glucose in blood from humans is routinely performed as it is a vital technique in the management of diabetes (Karter*, et al.*, 2001). An assay has also been developed to measure the blood levels of creatinine (Jones*, et al.*, 1998), This assay is performed using a modified Jaffe reaction which uses the reaction of creatinine with picric acid in alkaline conditions, and which forms a red product which can be measured on a plate reader (Popper*, et al.*, 1937). The spectral region around the anomeric β-glucose (δ 5.22, doublet) resonance is normally undisturbed by other resonances within the spectrum. This is not always the case for the other resonances in both glucose and creatinine. This scaling of the spectra would overcome this problem encountered between the datasets and thus allow new sample to be added into the models in a similar fashion to the take-one-out analysis described in Chapter 2 Section 2.7.4.2.

4.4.1. MS and AD comparison

Metabolomics has been used to compare different neurological disorders from MS ('t Hart*, et al.*, 2003), however, as discussed previously (Section 4.1). This chapter focused on distinguishing between MS and one other neurodegenerative disease, AD. As discussed previously (Chapter 1 Section 1.9), there are similarities between these two diseases. This is especially true during the progressive degenerative stages of MS (PP-MS and SP-MS). Both diseases result in microglia activation, T-cell recruitment and neural loss

(Barger*, et al.*, 1997; Trapp*, et al.*, 1999). Interestingly, the metabolites which separate out both progressive forms of MS from AD are reasonably consistent. Lactate, fatty acids and an unknown broad resonance all appeared to be lower in the MS patients compared to the AD patients.

Lactate was consistently lower in both the PP-MS and SP-MS patients when comparing them to the controls. The role of lactate in the CNS will be discussed in more detail late (Chapter 7 Section 7.5). However, lactate has been shown that it is a source of emergency energy within the CNS (Quistorff*, et al.*, 2008). There are several mechanisms which can transport lactate across the BBB (Cremer*, et al.*, 1979; Poole*, et al.*, 1993). This drop in lactate in the plasma could indicate an increase in lactate metabolism within the CNS in the PP- and SP-MS patients.

When comparing the samples from the AD patients there was a decrease in the levels of serum citrate levels, this will be discussed in more detail later (Chapter 7 Section 7.5). This decrease may be due to the activation of microglia which is occurs around the Aβ plaques formed in the CNS of AD patients. In contrast to the MS patients, the levels of lactate in the serum were actually elevated in the AD patients when compared to the controls. This could indicate that there is a decrease in lactate metabolism within the CNS suggesting that there is considerable brain atrophy in this cohort.

4.4.2. Addition of EDSS scores

The results from the addition of the clinical data into the model suggests the metabolite changes in the PLS models does not correlate to the EDSS scores of the patients. This might suggest that metabolomics is not sensitive enough to distinguish between progressive stages of MS. However, it is more likely that the metabolite profiles of PP-MS and SP-MS are similar. These two stages do

seem to follow similar courses, as discussed in Chapter 1 Section 1.5.3 (Compston*, et al.*, 2002; Compston*, et al.*, 2008; Noseworthy*, et al.*, 2000).

4.4.3. Chapter Summary

This chapter has demonstrated that using a combination of ^{1}H NMR spectroscopy and PLS-DA modelling it is possible to distinguish between two different neurodegenerative disorders. The metabolites which generated the separations in the PLS models are constantly changed between the two stages of MS when compared to the samples from the AD patients. There was however one exception to this which was glucose. This study demonstrates that due to technological advances, such as increased magnet field strength, metabolomics can be used to distinguish between different neurological diseases with a greater accuracy than has previously been achieved.

Chapter 5: Metabolic changes in HIV-associated dementia

5.1. Introduction

HIV-associated dementia (HAD) currently affects 10% of all HIV patients who receive HAART, and the number of cases is predicted to increase because individuals with HIV are living longer under HAART therapy. (Marle*, et al.*, 2005). It would be desirable to predict which HIV patients are at risk of developing HAD at an early time-point. The exact reasons for patients developing HAD are unclear (as discussed in Chapter 1 Section 1.7.1), and therefore any biomarkers that could reveal the underlying pathology of the disease would be useful. Early diagnosis for HAD is essential for the effective treatment as the later stage of disease results in irreversible brain atrophy (Chiang*, et al.*, 2007). In this Chapter metabolomics is used to discover whether the analysis of CSF might identify potential biomarkers of HAD.

It has been shown that the addition of other 'omics' data can be used enhance the PLS-DA models. Use of a combination of metabolomics and transcriptomics identified early mechanistic markers of acute phenobarbital toxicity within rats. The addition of the transcriptomic data from rats dosed with phenobarbital daily allowed the authors to not only study metabolite markers but to link specific mRNA transcripts to these changes (Waterman*, et al.*, 2010). It is possible therefore to integrate other 'omic', or indeed any other non-binary data as a Y variable into the PLS models. The PLS modelling will then attempt to find variations within the X variables which correlate to the Y variables (Waterman*, et al.*, 2010). The advantage of this HAD cohort is that a clear patient history exist for each sample, and plenty of clinical data which could be used as Y variables, which, it is hypothesised, would improve any PLS models generated.

5.1.1. Aims of chapter

The aims of this chapter are:

1. To establish whether CSF can be used as an early marker of HAD.
2. To identify any metabolites which can be used for the diagnosis of HAD.
3. To investigate whether the addition of clinical data into these models results in improvement of the models.

5.2. Methods

5.2.1. Sample collection

The HIV cerebral spinal fluid (CSF) samples were obtained from Dr. Norman Haughey (Johns Hopkins University, USA). The CSF samples were split into 4 different categories depending on the patient's neurocognitive status. Initially, the analysis was performed blind with each group assigned a random identifier. The groups were: normal (n = 25), improved (n = 23), worsened (n = 26) and diminished (n = 25). The patients visited the clinic twice with a time interval of one year and gave a CSF sample on both occasions. There were, therefore, a total of 198 CSF samples. All the samples had an extensive clinical history provided with each sample, but this was not unblended until after the initial models had been generated.

5.2.2. Sample pre-treatment

The samples obtained from Johns Hopkins contained live HIV, and they had not been screened for other infections. To inactivate the HIV and Hepatitis C (HepC) virus the samples were placed in a heat block at 56 ˚C for 40 minutes (Song*, et al.*, 2010; Villalba*, et al.*, 2003), which has previously been shown to be effective for HIV and HepC.

5.2.3. NMR sample preparation

Following the pre-treatment (5.2.2), the NMR samples were prepared as described in chapter 2 using the 1D NOESY sequence. Due low concentration of metabolites in the of the CSF samples, 32 scans were required as opposed to 16 scans to generate spectra of good enough quality to process. This was also the case for the 2D COSY spectra. There was no need to add the ultracentrifuge step with the CSF samples owing to the low protein background

observed in the spectra. The samples were then processed as described in the methods chapter.

5.2.4. Statistical analysis

5.2.4.1. Multivariate analysis

The PLS-DA modelling was carried out as described in the methods chapter. The clinical data was incorporated into the study by defining them as a Y variable within the PLS models using SIMCA P+ 12.0 (Umetrics, Sweden). This led to the formation of PLS models using the same class-based system as described in the methods chapter. The Y variables were scaled using unit variance scaling rather than Pareto variance scaling as used previously.

5.2.4.2. Removal of baseline noise

For reasons explained in the results section below (5.3.2), the baseline noise was removed from the spectra leaving 66 buckets which contained ^{1}H NMR resonances. These buckets were: 1.32..1.34, 1.46..1.48, 1.90..1.92, 2.10..2.16, 2.36..2.70, 3.02..3.06, 3.22..3.64, 3.68..4.14, 5.22..5.24, (includes all 0.02ppm buckets between the two values). The baseline noise was removed by visual inspection of the spectra. The spectra were overlaid (Topspin 2.1, Bruker) and the regions containing peaks visible over the background noise were selected.

5.2.4.3. Clinical data analysis

All the clinical data sets used for the HIV study were analysed using a repeated measure analysis of variance (ANOVA) with a between-group factor of cognitive status and a within-subject factor of time. Mauchley test of sphericity was performed, but this was never significant and therefore all quoted *p*-values were the sphericity assumed value. A Bonferroni post-test was carried out to compare the intergroup comparisons where † is defined as a *p*-value < 0.05.

The clinical data was considered a good predictor of different disease states if $p < 0.05$. These tests were performed using SPSS v19.0 (IBM, USA) and graphs were drawn in Prism 5.01 (GraphPad inc., USA).

5.2.5. Metabolite identification

The metabolites causing the separations within the models were identified as described in Chapter 2 Section 2.7.5.

5.3. Results

5.3.1. Initial results

Spectra obtained by high resolution ^{1}H NMR spectroscopy were of sufficient resolution to allow the identification of over fifteen metabolites (Figure 5.1 A). Ethanol resonances (δ 1.19, triplet and 3.36, quartet) were observed in some of the spectra and therefore this was excluded prior to any analysis. Visually, the initial PLS-DA models of the CSF did not show any separation between the different groups at the same time point (Figure 5.1 B and C). In addition to this, none of these models returned a significant q^2 value. When looking at the longitudinal data there were visual separations observed in the plots between the first visit samples to the clinic and the second visit samples, within each group (Figure 5.1 D and E). However, despite the fact that all four models returned a positive q^2 value only two returned a significant model. The two models which showed a positive separation were between the patients whose cognitive state improved (q^2 = 0.56) and the patients whose cognitive status remained stably abnormal (q^2 = 0.73), these two models are shown in Figure 5.1 D and E.

Since there were only two positive models generated from this analysis attempts were made to improve these initial models and the results are described below.

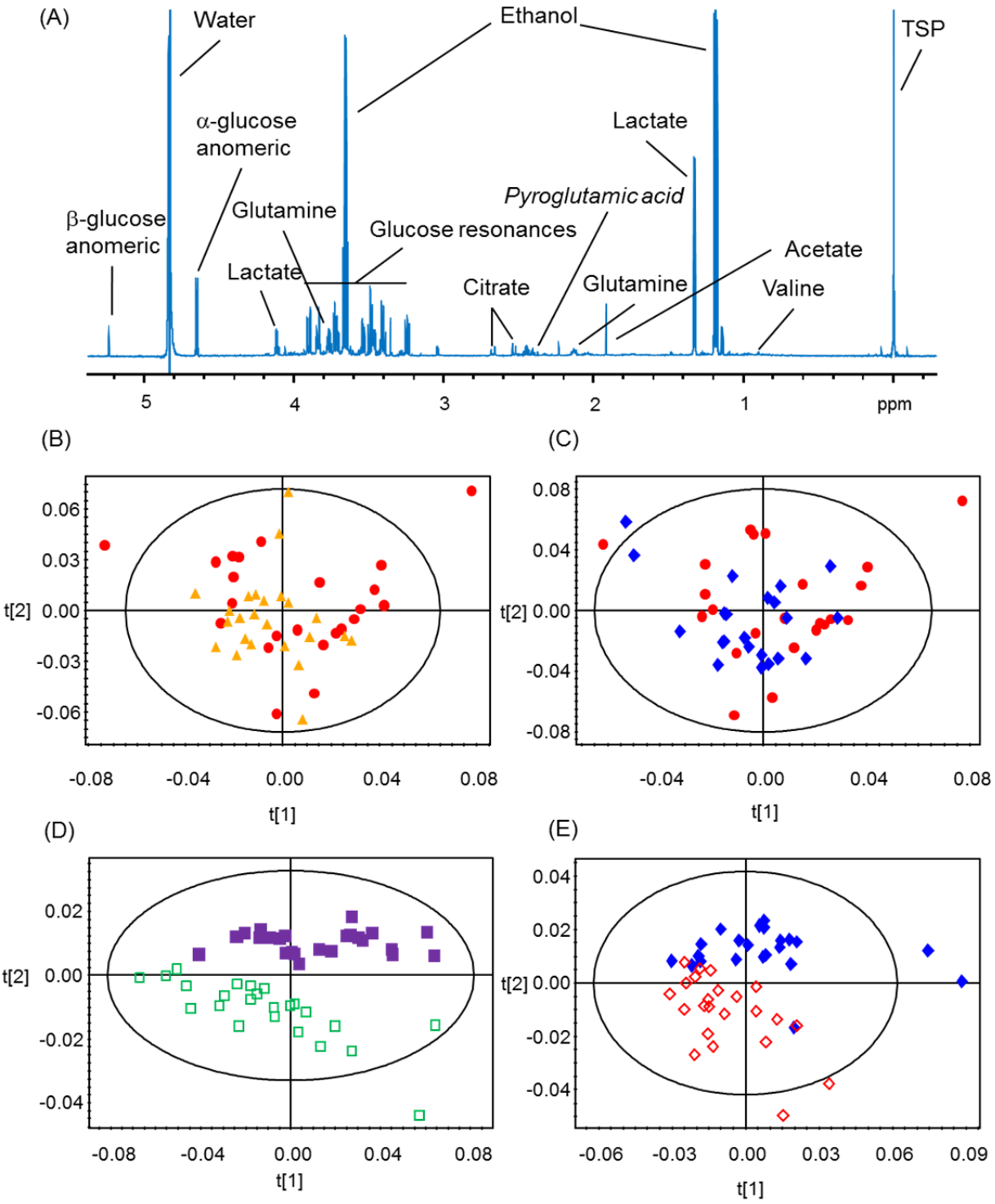


Figure 5.1: : Initial HIV PLS model results. (A) Sample ^{1}H NMR with NOESY presaturation sequence of CSF sample from a patient whose neurocognitive state improved. (B) PLS plot of human CSF from the first visit comparing patients whose cognitive state worsened (red circles) to patients whose cognitive state remained stably normal (orange triangles). (C) PLS plot of human CSF from the first visit comparing patients whose cognitive state worsened (red circles) to patients whose cognitive state improved (blue diamonds). (D) PLS plot of human CSF comparing the first visit of the patients whose cognitive state remained stably impaired (purple squares) to second visit of the same patients (green open squares). (E) PLS plot of human CSF comparing the first visit of the patients whose cognitive state improved (blue diamonds) to second visit of the same patients (red open diamonds).

5.3.2. Model improvements

The ^{1}H NMR spectra obtained from the CSF samples contained substantially fewer resonances than spectra obtained from urine or blood (Figure 5.2 A). The presence of the background noise could account for the poor predictability of the initial models. In order to eliminate this noise, new models were generated using the buckets which contained only resonances that were visible over the noise in the ^{1}H NMR spectrum. After the removal of the baseline noise, sixty-six buckets of information remained. These buckets are listed in the methods section above (5.2.4.2).

These sixty-six buckets of data did not furnish any significant models between the neurocognitive groups at the same time point. There was, however, a visual improvement in the models at the second visit especially when comparing the two groups that changed (improved and worsened) to the normal group Figure 5.3 A). Comparing the different neurocognitive groups between the two time-points revealed a visual separation between all the groups (Figure 5.3 B, C, D and E). All these models were now predictive with q^2 values equal to 0.61 (stably normal), 0.84 (stably abnormal), 0.47 (worsened) and 0.52 (improved). The separation between the classes occurred within the second component of the models and therefore in order to identify the metabolites all these models were actually OPLS-DA models (as described in Chapter 2 Section 2.7.2).

Upon examination of loadings of these OPLS models it was possible to identify several metabolites which caused the separation between the two visits. Lactic acid (δ_{x-y} 1.33), which was at a lower concentration at the first visit compared to the second visit, was the only consistent metabolite across all the comparisons of the neurocognitive status (Table 5.1). Citrate (δ_{x-y} 2.51, 2.65) and L-glutamic acid (δ_{x-y} 2.14, 2.47, 3.78) were inversely related, i.e. when the concentration of citrate was elevated the concentration of L-glutamic acid was lowered. Citrate

was at a higher concentration in the first visit of patients whose neurocognitive status remained stably normal or worsened compared to the second visit. However, in the stably abnormal and the improved groups citrate was at a higher concentration in the second visit (Table 5.1). A set of resonances which were tentatively assigned as pyroglutamic acid (δ_{x-y} 2.40) followed the same pattern as citrate. Glucose (δ_{x-y} 3.77) was at a higher concentration in the first visit of the improved and stably abnormal patients but unchanged in the worsened and stably normal patients. In addition to this two further metabolites varied in the stably abnormal group. These metabolites were a resonance that could tentatively be assigned as oxalacetic acid (δ_{x-y} 2.37), which was at a higher concentration in the first visit, and *myo*-inositol (δ_{x-y} 3.63), which was at a higher concentration in the second visit. These metabolites did not vary in any of the other models.

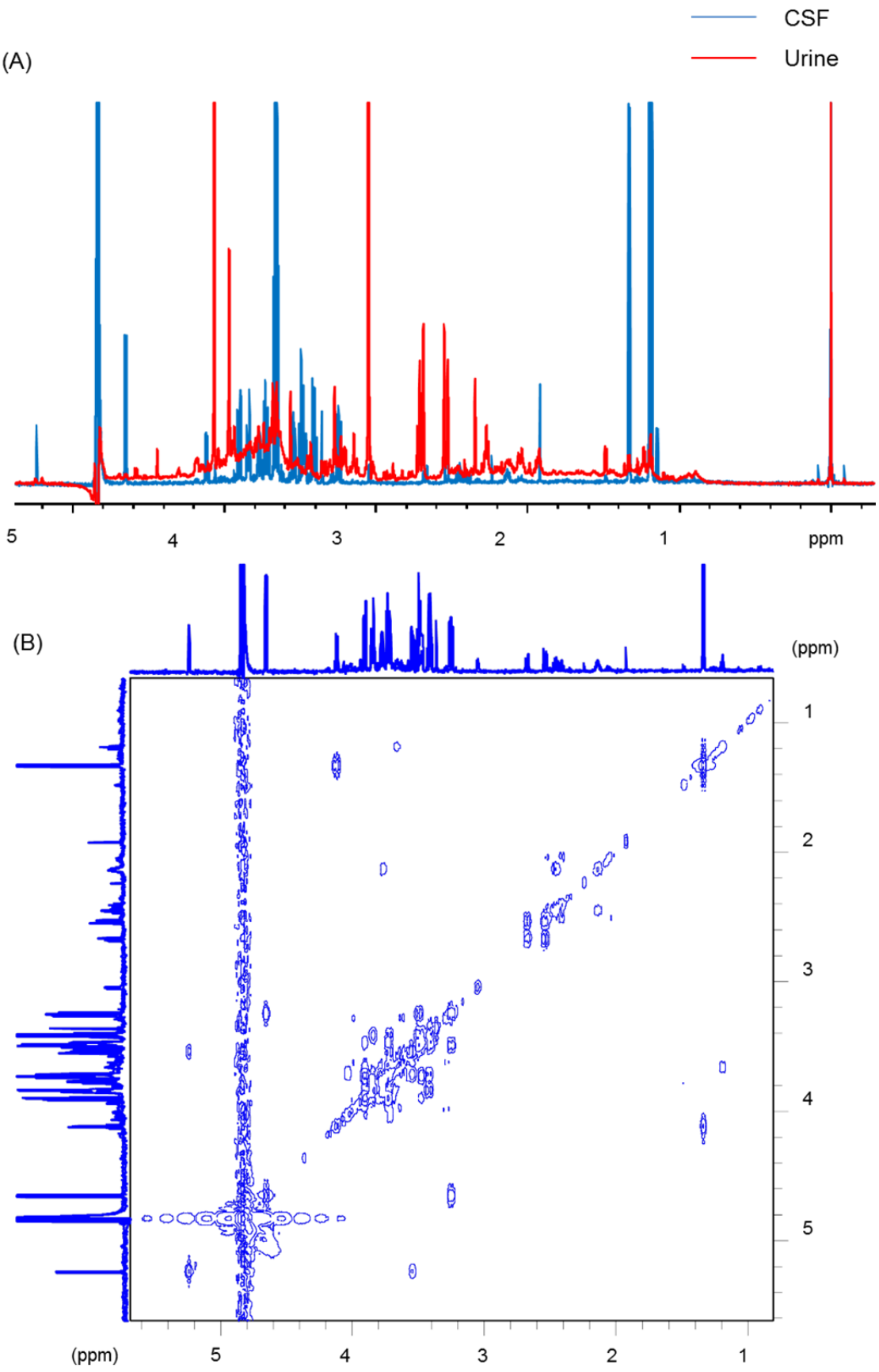


Figure 5.2: NMR spectra comparison. (A) Overlay of ^{1}H NMR NOESY obtained from CSF (blue spectrum) and human urine (red spectrum). (B) Sample of COSY spectra from a CSF sample.

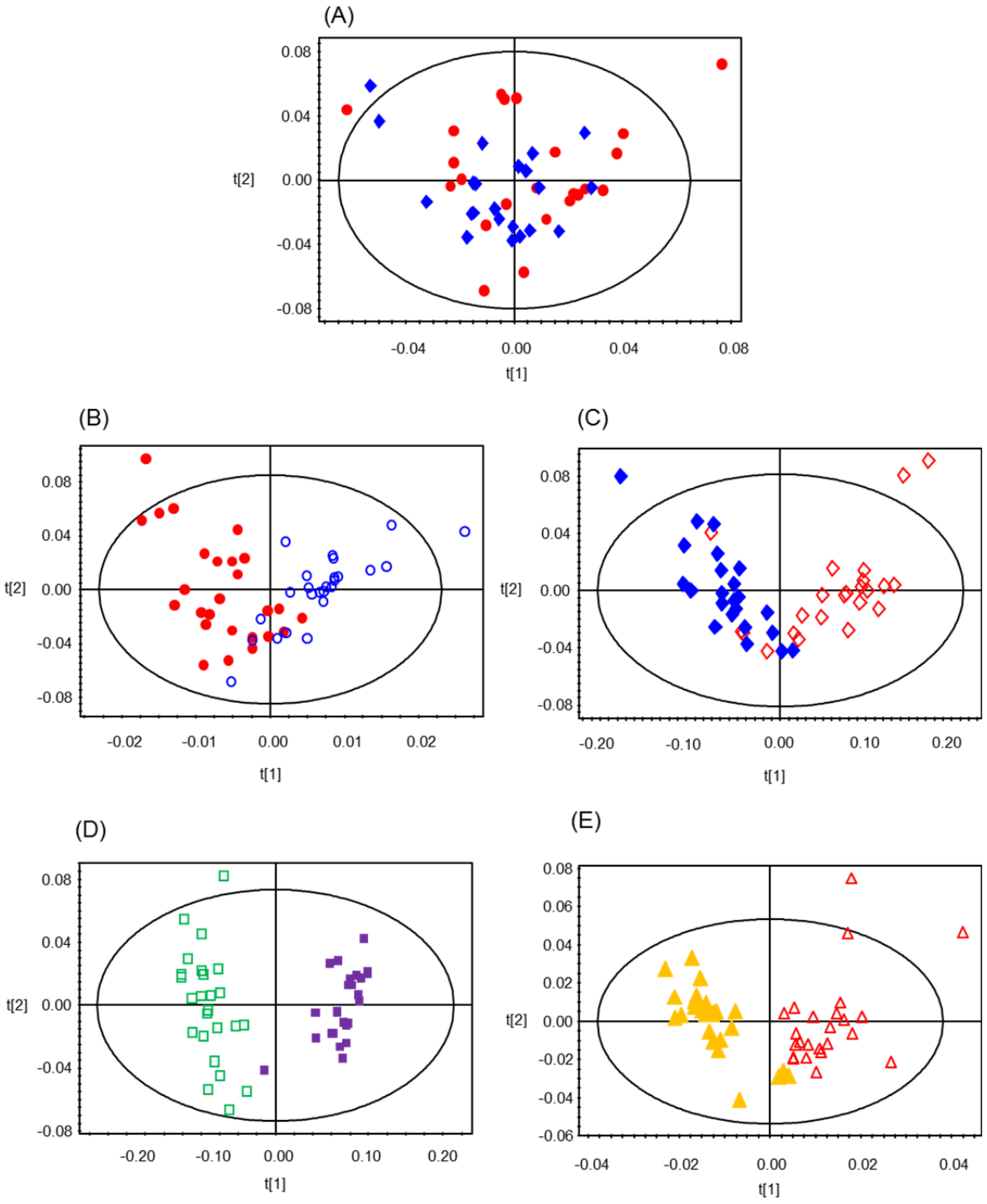


Figure 5.3: PLS plots of HIV samples with the baseline removed. (A) PLS plot of human CSF from the first visit comparing patients whose cognitive state worsened (red circles) to patients whose cognitive state improved (blue diamonds). (B) PLS plot of human CSF comparing the first visit of the patients whose cognitive state worsened (red circles) to second visit of the same patients (blue open circles). (C) PLS plot of human CSF comparing the first visit of the patients whose cognitive state improved (blue diamonds) to second visit of the same patients (red open diamonds). (D) PLS plot of human CSF comparing the first visit of the patients whose cognitive state remained stably impaired (purple squares) to second visit of the same patients (green open squares). (E) PLS plot of human CSF comparing the first visit of the patients whose cognitive state remained stably normal (orange triangles) to second visit of the same patients (red open triangles).

(A)

Model	q^2	Positive Metabolites		
Worsened	0.47	Citric Acid	*pyroglutamic acid*	
Improved	0.52	Glutamine	Glucose	
Stabaly Impaired	0.84	Glutamine	Glucose	*Oxalacetic acid*
Normal	0.61	Citric Acid	*Pyroglutamic acid*	

(B)

Model	q^2	Negative Metabolites			
Worsened	0.47	Glutamine	Lactic Acid		
Improved	0.52	Citric Acid	*Pyroglutamic acid*		Lactic Acid
Stabaly Impaired	0.84	Citric Acid	Lactic Acid	*Pyroglutamic acid*	*myo*-Inositol
Normal	0.61	Glutamine			Lactic Acid

Table 5.1: Metabolites causing separations between the PLS-DA models for the HIV samples. (A) Table showing the metabolites which generated the separation in the CSF models, which were increased in the patients' first visit. (B) Table showing the metabolites which generated the separation in the CSF models, which were reduced in the patients' first visit.

5.3.3. Clinical data

The clinical data provided with the HAD data-set was modelled as a Y-variable in order to examine the possibility that this would improve the models. Prior to this the clinical data was statistically assessed in order to determine which variables varied significantly across the different neurocognitive states. The repeated measures ANOVAs on the clinical data showed that three of the clinical data sets varied consistently either between the two visits or the different neurocognitive states. When comparing the number of $CD4^+$ T-cells/μL at the time of sample collection there was a significant main effect of neurocognitive state ($F_{3,60}$ = 4.506, p = 0.006). There was also a near-significant effect of time ($F_{1,20}$ 4.115, p = 0.055). There was no significant interaction between the main effects (p > 0.050). For graphical representation see Figure 5.4 A. The lowest recorder $CD4^+$ T-cells/μL showed a significant effect of both neurocognitive status ($F_{3,54}$ = 0.885, p = 0.047, see Figure 5.4 B) and time ($F_{1,18}$ = 5.700, p = 0.028, see Figure 5.4 B). Once again, there was no significant interaction between the main effects (p > 0.050). The only other data set which showed any significance was the recovery of the $CD4^+$ T-cells/μL. This was calculated by subtracting the lowest $CD4^+$ T-cells/μL level from the $CD4^+$ T-cells/μL recorded when the CSF samples were acquired. There was a significant main effect of neurocognitive status ($F_{3,51}$ = 3.214, p = 0.03, see Figure 5.4 C), however, there was no main effect of time. In addition to this there were two other data sets which neared significance. These were the CSF viral load (main effect of time, $F_{1,15}$ = 3.193, p = 0.094, see Figure 5.4 D), and the $CD8^+$ T-cells/μL levels (main effect of neurocognitive status, $F_{3,51}$ 2.113, p = 0.132, see Figure 5.4 E).

5.3.4. Incorporation of clinical data into models

The addition of the clinical data into the original PLS models as variables did not improve the separation between any of the time-points. This was the case when the data was added as a whole set of Y variables as well as when added individually for each model.

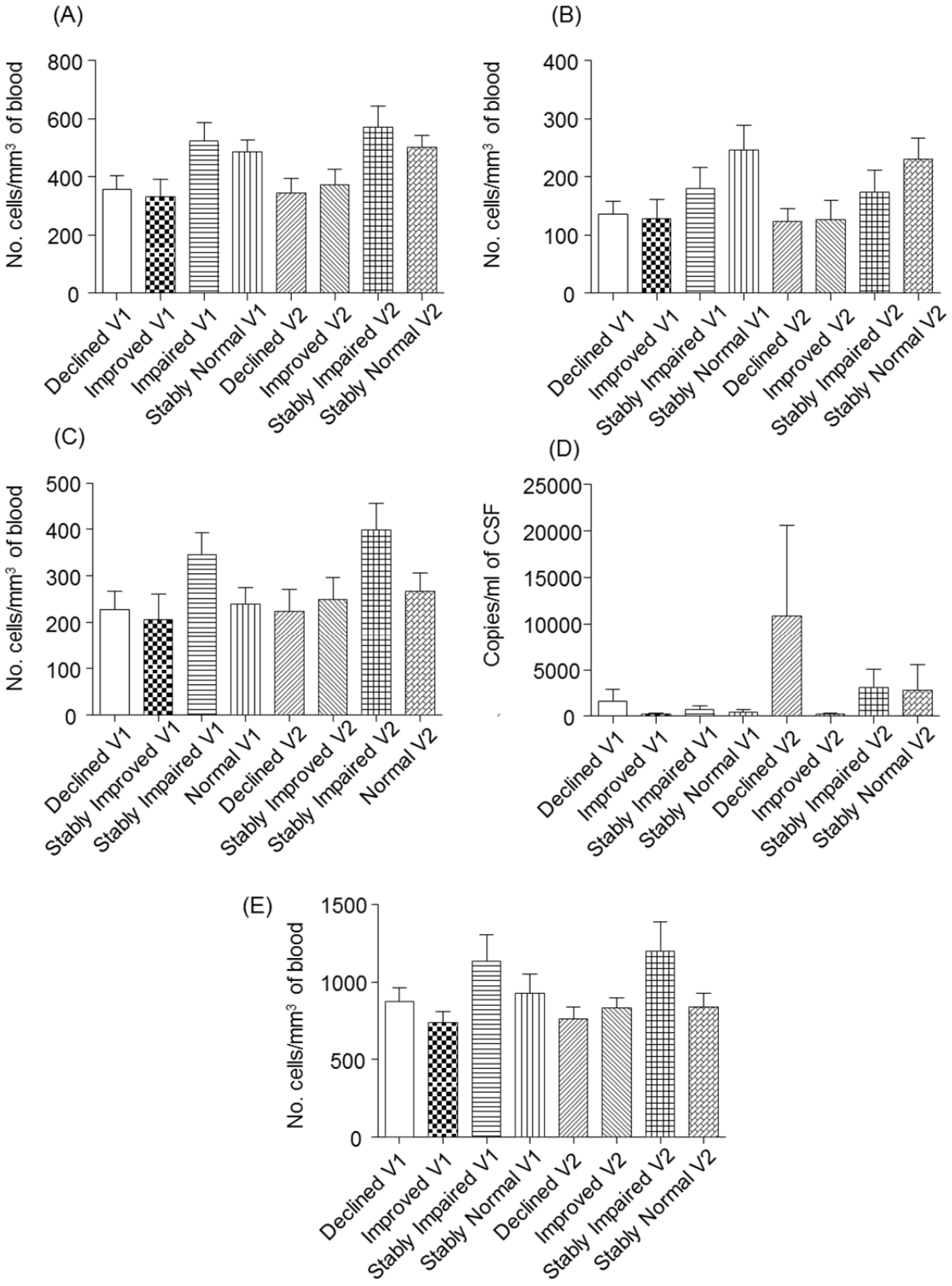


Figure 5.4: Clinical data results. (A) Average CD + T cell count between the different neurocognitive states and between visit one and visit two. (B) Nadir CD4. (C) Recovery CD4. (D) CSF viral load. (E) CD8 count.

5.4. Discussion

This chapter shows that it is possible to use metabolomics to monitor disease progression in HIV patients who have differing neurocognitive states. This is the first time that metabolomics has been used as a diagnostic tool in the field of HAD. This separation was only observed longitudinally and not between the groups at the same time point. AD studies have shown that it is only possible to detect significant changes in brain volume if one studies the patient longitudinally (Evans*, et al.*, 2010). As shown in the results section the number of detectable metabolites in CSF is lower than in plasma. Therefore, although there may well be metabolite changes occurring within these patients, the changes are not marked enough to separate out neurocognitive states at the same time-point. A study of the patients' plasma or urine may well reveal detectable metabolite changes within these patients at an early time-point. However, the results in this chapter do demonstrate the ability of metabolomics to monitor disease progression and identify several type 0 biomarkers of neurodegenerative diseases within the CSF of these patients.

The rationale for using CSF samples over any other biofluids in this chapter is that metabolites identified within the CSF could potentially be translated directly into clinical practice by use of magnetic resonance spectroscopy (MRS). Any pattern of biomarkers identified within the CNS could potentially be used in future MRS studies, thus developing a technique which can be used serially and non-invasively. This would also remove the need for the lumbar puncture which is required for obtaining the CSF samples. Although lumbar punctures are routine within the clinic there are several side effects which can range from simple headaches to disability (Chordas, 2001; Wang*, et al.*, 1997). Headaches is thought to be one of the commonest side-effects of a lumbar puncture, however, the reported incident rate in the literature varies from 0.5 to 60%

(Sand*, et al.*, 1987). The headaches arise from the damage to the dura membrane when the needle is inserted into the spinal column. This can lead to the leaking of the spinal fluid through the dura and thus the pressure increases (Lybecker*, et al.*, 1990).

5.4.1. Initial models

As mentioned above, the number of detectable metabolites in the CSF is far lower than in plasma or urine. The concentration of the metabolites within the CSF was also significantly lower than in the urine and hence required 32 scans, compared to 16 scans, to get spectra of comparable quality. 32 scans were deemed at the time of acquisition to produce spectra of sufficient quality and due to the potential risk associated with these samples the samples were sterilised immediately after acquisition. Therefore, it was not possible to re-run the samples with a higher number of scans at a later date. Despite the extra scans the signal to noise ratio of the CSF samples was 5 times worse than a comparable urine sample leading to a greater variation of the baseline from the samples. This led to significant level of background noise being fed into the analysis and thus the PLS-DA models did not reach significance. The removal of highly variable regions of the spectra is commonplace within the literature and, indeed, in this thesis. From urine spectra, the peaks caused by water and urea are routinely removed, as these can vary greatly sample to sample, for example, see Chapter 2 Section 2.7.1 and (Griffin*, et al.*, 2004a). The removal of baseline data has also been used within the literature to improve the separation in metabolite modelling (Xi*, et al.*, 2008). Therefore, removal of the variable baseline buckets from these spectra enabled more reliable models to be generated.

5.4.2. Metabolite identification

Lactate was the only metabolite that varied constantly across all the neurocognitive groups. Lactate metabolism within the CNS is not fully understood (Acosta*, et al.*, 2005), however, it has been suggested that it is an emergency energy source for the brain (Quistorff*, et al.*, 2008). It has also been reported that lactate levels rise within the CNS as a result of the aging process (Ross*, et al.*, 2010). In this study, prematurely aged mice showed an increased lactate resonance in the ^{1}H NMR spectrum acquired from the brain. This increase in lactate levels was attributed to an increase in the lactate dehydrogenase A/B gene expression ratio (Ross*, et al.*, 2010). In this Chapter lactate was also found to be at a higher level in the samples from the second visit. The primary role of glutamine in the CSF is to act as a buffer and remove excess nitrogen from the CNS (Shank*, et al.*, 1981). It has been reported that an increase in glutamine levels could indicate a general increase in amino acid metabolism due to the need for extra buffering effects and removal of nitrogen (Kelley*, et al.*, 1974). In patients whose neurocognitive status is declining there may well be brain atrophy leading to an increase in glutamine. Such a rise has been reported in AD patients (Stephen R, 2000). That this increase in glutamine is also observed in the stably normal patients could suggest that these patients are not normal but in a pre-symptomatic phase of disease. For the patients who remained stably abnormal and those who improved the glutamine levels were increased in the first visit when compared to the second visit suggesting the rate of brain atrophy was higher at the earlier time-point within the disease. It has been reported that HIV-associated dementia can be treated using HAART and this finding supports this theory (Dougherty*, et al.*, 2002).

5.4.3. Clinical data

Despite there being some significant differences between the clinical data from the patients, the addition of this data into the PLS models did not enhance any of the models. This indicates that any change in these clinical data sets does not have a detectable impact on the metabolism within the CNS. The reason for this could be traced back to the relatively small number of detectable metabolites within the CNS. Although this data-set does not improve the models there could be other data-sets available which could be successfully used as Y-variables. These will be discussed in Chapter 7 Section 7.6.2. However, this demonstrates the sensitivity of metabolomics as a diagnostic technique. The results demonstrate that it is possible to separate out patients with differing neurocognitive states, whereas the current diagnostic tests cannot.

5.4.4. Chapter summery

This chapter has shown that it is possible to follow the disease progression of HIV-associated dementia longitudinally. This could be developed as a potential tool for studying type 0 markers in MRS studies therefore removing the need for a spinal tap, as any markers identified in this study could potentially be developed as MRS markers for disease.

Chapter 6: Metabolic changes in brain cancer metastasis

6.1. Introduction

The last three results chapters have demonstrated how sensitive metabolomics is as a tool in the diagnosis of different neurological disorders which are associated with neurodegeneration and inflammation. This chapter will explore whether this sensitivity can be used as an early diagnostic tool in another neurodegenerative disease which is quite distinct from the other conditions, but presents similar challenges in terms of the need for early diagnosis. Brain metastasis affects 20-40% of all cancer patients (Klos*, et al.*, 2004; Schellinger*, et al.*, 1999). Currently the prognosis for patients with brain metastasis is very poor and life expectancy is a meagre 3-9 months. As discussed in Chapter 1 Section 1.8.6, this is assumed to largely reflect the late stage of the diagnosis (Robinet*, et al.*, 2001; Sperduto*, et al.*, 2008). It is hypothesised that if brain metastasis could be detected earlier, then treatments could be better directed and prognosis improved (Serres*, et al.*, 2010). From the results in the previous two chapters it has been shown that it is possible to differentiate MS patients from a healthy cohort and patients with another neurological disease (AD). The potential to diagnose disease at an earlier stage would be very welcome within the field of brain metastasis treatment. In addition to the likely benefits of earlier diagnosis, and, hence, treatment there are two further potential benefits to developing a set of biomarkers for the early diagnosis of brain metastases. Firstly, early diagnosis will prevent the harmful and unnecessary treatment of 'at risk' cancer patients that do have brain metastases (as discussed in Chapter 1, Section 1.8.5). Secondly, patients who do develop brain metastases could have their treatment monitored using a metabolomic approach. As stated in Chapter 1 Section 1.8 the aim of this chapter will be to use metabolomics to identify a

set of biomarkers that indicate the presence of brain metastases within the CNS at an earlier stage of disease than is currently possible clinically.

Breast cancer is one of the largest contributors to the incidence of brain metastasis (Klos*, et al.*, 2004). For this study, a model of breast cancer metastasis was chosen to study the effects of these metastases on the biofluid metabolomic profile of a mouse. The cell line chosen was the 4T1-GFP murine mammary carcinoma, which has been widely used as a model of metastasis both in the brain and systemically (Aslakson*, et al.*, 1992; Carbonell*, et al.*, 2009). It has been reported that if the primary tumour is implanted in the fat pad near the mammary gland, there will be spontaneous metastases to a range of organs including the brain (Pulaski*, et al.*, 2001). However, several variants of this model have been reported in the literature to the point where the site of injection of the 4T1 cells can alter the distribution of metastases throughout the body (Lelekakis*, et al.*, 1999). These models have been developed primarily because the development of systemic metastases from the mammary fat pad is not predictable and can take a substantial period of time to develop. Lelekakis *et al.* reported that tail vein injection of 4T1 cells primarily resulted in lung metastases. It has also been shown that it is possible to induce brain metastasis by an intracardiac injection, which eliminates the need for invasive surgery and the associated side-effects. It is thought that this approach may also confer a more relevant model of brain metastasis as the bolus of cells arriving in the brain is slightly dispersed as it leaves the heart (Carbonell*, et al.*, 2009). Finally, we have recently shown that it is possible to induce metastases within the CNS by direct injection of 4T1 cells into the brain (O'Brien*, et al.*, 2011). This approach creates a focal brain metastasis at a predetermined location, in the absence of any confounding systemic metastases.

Here, a focal model of brain metastasis is used to reveal the metabolite changes in plasma and urine caused by the presence of a single metastatic load in the brain. In the subsequent experiment, systemic induced models are used in order to determine how the presence of systemic metastases alters or confounds the detection of brain-specific metastases. The different injection routes (intracardiac and intravenous) yield different spatial distribution of metastases around the body. Thus, comparison of these three models (intracerebral, intracardiac and intravenous) enabled identification of markers of systemic metastases that are distinct from those associated with brain metastases alone. In order to confirm whether the identified biomarkers are transferable to other metastatic cancer types, two further metastatic cell lines are injected intracerebrally and the metabolites which cause these separations will be identified. This is then compared to the 4T1 models.

6.1.1. Aims of chapter

Thus, the aims of this chapter are:

1. To identify a set of metabolites in urine or plasma that enable detection of brain metastases induced by an intracerebral injection of 4T1-GFP cells (1×10^5).
2. To determine whether the set of biomarkers from the intracerebral model can be used to identify the presence of brain metastases when there are systemic metastases present.
3. To determine whether there are additional biomarkers that reflect the presence of systemic metastases.
4. To determine whether the biomarkers identified in the 4T1 model are translatable to other brain metastasis models.

6.2. Methods

6.2.1. Animal experimental design

A time course study of mice injected intracerebrally with 4T1-GFP mammary carcinoma cells was performed. Samples of plasma and urine were acquired at 4 different time points (days 5, 10, 21 and 35; n = 6 per time point). Two control groups of animal were also included within the study; (i) age-matched naïve animals (n = 6), and (ii) age-matched animals injected intracerebrally with sterile PBS and killed at day 5 (n = 6).

In a second study, 4T1-GFP cells were implanted either intravenously or intracardially, and urine and plasma samples acquired at day 10 (n = 6 per group). Again, a control set of age-matched animals injected via the appropriate route with sterile PBS was included in both groups (n = 6 per group). These were compared to animals injected intracerebrally, at day 5 with 4T1-GFP cells. Following an injection of 4T1-GFP cells intracerebrally the tumour grows rapidly within the brain. This is not the case when the cells are implanted elsewhere in the body as the number of initial cells which form the metastasis is far lower and they need to cross the BBB (as discussed in Chapter 1 Section 1.8.3). Therefore the animals injected intracardially or intravenously were compared to day 5 in animals injected intracerebrally in order that similar tumour masses were present within the CNS.

To verify the initial findings in additional models, two further cells lines were implanted intracerebrally, and urine and plasma samples were collected at days 5 and 10 (n = 6 per group). These cell lines were a human breast adenocarcinoma cells (MDA231BR) and a murine melanoma cell line (B16F10-GFP).

6.2.2. *In vivo* procedures

6.2.2.1. Intracerebral implantation of cells

The matched mouse strain for the given cell line was anaesthetised as described in Chapter 2 Section 2.5.1. The mouse was then placed on a stereotaxic frame (Kopf Instruments, US) and the skull was exposed in order for Bregma to be located. The brain of the animal was then exposed above the injection site *via* a burr hole drilled though the skull. A finely drawn glass microcannula with a tip diameter of *ca.* 75 μm was then inserted into the left striatum at the following stereotaxic coordinates relative to Bregma: + 0.5 mm anterior/posterior, − 1.5 mm medial/lateral, − 2.5 mm dorsal/ventral (d/v). The cannula was left in place for 2 minutes and then raised by + 0.5 mm d/v and left for a further 5 mins before removing the cannula altogether. The scalp wound was then closed with a non-absorbable Ethicon silk suture (Johnson & Johnson, UK). The animals were assessed daily and their weight and clinical scores were monitored. The clinical store system used was originally defined by Wolfensohn *et al.* and adapted to suit the model as described in the table below (Table 6.1) (Wolfensohn*, et al.*, 2003).

Parameter	Behaviour	Score
Appearance	Normal	0
	General lack of grooming	1
	Coat staring, ocular and nasal discharges	2
	Piloerection	3
Food and Water Intake	Normal	0
	Loss of 1 g of original body weight	1
	Greater than a 10 % loss in body weight	2
	Greater than a 20 % loss in body weight	3
Natural Behaviour	Normal	0
	Minor changes	1
	Less mobile and alert, isolated	2
	Vocalisation, self-mutilation, restless or still	3
Provoked Behaviour	Normal	0
	Minor depression or exaggerated response	1
	Moderate change in expected behaviour	2
	Reacts violently, or very weak and precomatose	3

Table 6.1: Table showing the clinical scoring system used for assessing the animals within the tumour cell models.

6.2.3. Intracardiac injection of tumour cells

Female BALB/c (6-7 weeks) were anaesthetised as described in Chapter 2. The hair covering the thoracic cavity on the side of the heart was removed using a combination of shaving and hair removal cream (Veet, Boots, UK). The shaved area was then coated with ultrasonic gel and the left ventricle of the heart was located with the aid of ultrasound imaging. A needle (25 FG) was then implanted into the left ventricle of the heart and 4T1 cells (1×10^5) in 100 μL sterile PBS were injected. The animals were allowed to recover in a heated box and, subsequently, were assessed daily and their weight and scores recorded. The animals were scored using the scoring system set out above (Table 6.1)

6.2.3.1. Intravenous implantation of tumour cells

The tail veins of female BALB/c mice (6-7 weeks) were heated using a UV lamp to make the vein more prominent and then cleaned using an alcohol swab. Subsequently, 4T1 cells in sterile PBS (10,000 cells 100 μL) were injected into this tail vein (23 FG needle). The animals were assessed daily and their weight and clinical scores were monitored using the score system set out above (Table 6.1).

6.2.4. Sample collection

Urine was collected prior to killing the animals as described in Chapter 2 Section 2.5.3

For blood sample collection, animals were placed in a box with 5% isoflurane in a 70:30 N_2O:O_2 mixture until they were terminally anaesthetised. The thoracic cavity was then opened to allow blood collection *via* cardiac puncture prior to the animals being perfusion-fixed as described in Chapter 2 under transcardiac perfusion.

The NMR samples were prepared as described in Chapter 2 with the addition of the ultracentrifuge step for the plasma samples as described in Chapter 3 Section 3.3.2. The samples were then processed as described in Chapter 2. For reasons explained below (6.3.3.1), it was necessary to apply absolute scaling to the spectra using the resonance arising from creatinine (δ 4.04). The relative concentration of creatinine within the sample was calculated by the addition of the two integral buckets δ_{x-y} 4.05 and 4.07. A normalisation factor was then calculated by dividing the area of the creatinine peak by the smallest calculated creatinine area. All buckets were then divided by this normalisation factor.

6.2.5. Statistical analysis and metabolite identification

The PLS-DA modelling was carried out as described in Chapter 2 Section 2.7.2. Subsequently, the metabolites causing the separations within the models were identified, again as described in Chapter 2 Section 2.7.5.

6.2.6. Histological analysis

6.2.6.1. Periodate Lysine Paraformaldehyde light fixative

PLP was prepared using the method first described by McLean *et al.* but the quantity of gluteraldehyde was halved to aid antibody retrieval. (McLean*, et al.*, 1974). For 1 L of PLP light fixative solution, lysine HCl (13.7g) was dissolved in 375 mL of d. H_2O. To this solution di-sodium hydrogen orthophosphate dihydrate (Sorrenson's salt [1.8 g dissolved in 100 mL of d.H_2O]) was added dropwise until the pH reached 7.4. Paraformaldehyde (20 g) was dissolved in hot d. H_2O (60 °C). In order to assist the process, NaOH was added dropwise into the solution until all the powder had dissolved. The paraformaldehyde solution was allowed to cool prior to the addition of the lysine solution. To this solution sodium periodate (2.14 g) was added and the pH adjusted to 7.2 with NaOH. The total volume of the solution was then made up to 1 L using

phosphate buffer (0.1 M). Immediately prior to use, gluteraldehyde (25% in H_2O, 1 mL) was added to the solution which turned a faint yellow colour.

6.2.6.2. Gelatinising Slides

Slides were washed in a 10% solution of Decon 90 in H_2O, rinsed with H_2O prior to drying overnight in a 37 °C incubator. Gelatine (2.5 g) was dissolved in 500 mL H_2O (60 °C), and the solution was allowed to cool to 40 °C prior to the addition of potassium sulphate (0.25 g). The solution was filtered and the slide dipped into the solution for 45 seconds before being placed in a 37 °C incubator to dry overnight.

6.2.6.3. Transcardiac perfusion

After an overdose of the required anaesthetic agent (see Chapter 2 Section 2.5.2) was administered, the thoracic cavity was exposed. The right atrium of the heart was then snipped prior to introduction of a cannula into the left ventricle of the heart. The animals were transcardially perfused with heparinised saline (5000 U/L) until the perfusate running from the right atrium was clear. The animals were then perfused with PLP (50 mL) prior to dissection of the required tissue section. All tissue sections were post-fixed in the same perfusate for 4 h.

6.2.6.4. Tissue preparation

After post fixation the samples were placed in a sucrose solution (30% in d. H_2O), in order to cryoprotect them, for 48 h. Tissue sections were subsequently dried and embedded in Tissue Tek (Bayer, UK), an optical coating compound, and frozen in an isopentane bath on dry ice at – 40 °C. Samples were stored at – 20 °C prior to being cut into sections (10 μm) on a cryostat (Lieca, UK) and

then placed on gelatinised slides. Sections were dried overnight and then stored at – 20 °C until needed for staining.

6.2.6.5. Immunohistochemistry

Slides were removed from the freezer and allowed to air dry prior to rehydration in PBS (3 × 5 mins). In order to quench the endogenous peroxide activity, the sections were placed into MeOH (300 mL) containing H_2O_2 (3 mL, 30% in H_2O) for 20 mins. The slides were then washed with PBS (3 × 5 mins) before being placed into Sequenza clips (Shanon, UK) under PBS to prevent dehydration. 130 μL of 10% of the requisite serum in H_2O was added to the slides to block any fc binding regions. The sections were washed with three times with PBS, after which the requisite primary antibody was added for the appropriate time (Table 6.2). Slides were then washed three times with PBS before the addition of the appropriate biotinylated secondary antibody (Vector labs, UK) for 1 h. (see Table 6.2). The slides were then washed three times with PBS, after which ABC solution (Vector labs, UK) was added to the slide. After 45 mins the slides were washed 3 times with PBS before being removed from the Sequenza clips and placed into a solution of diaminobenzidine hydrochloride (DAB) (0.5 μg/mL) made up in phosphate buffer (0.1 M) containing H_2O_2 (0.05%) until the optimal contrast was achieved.

Primary Antibody	Source	Concentration	Incubation Time	Secondary Antibody	Requisite Serum
Anti-GFP	Abcam	1:1000	1 h	Rabbit anti-Chicken IgY	Rabbit
Vimentin	Vector Laboratories	1:100	16 h	Goat anti-Rabbit	Goat

Table 6.2: Table to show the different antibodies used in this thesis.

6.2.6.6. Cresyl violet counterstain

After staining with DAB the slides were washed in phosphate buffer (0.1 M, pH 7.2, 2 × 5 min). The slides were then incubated for 5 mins in a solution of glacial acetic acid (200 μL) in H_2O (400 mL) before being placed directly into the Cresyl violet stain. This was prepared by dissolving Cresyl violet acetate (5 g, 15.6 mmol) in H_2O (1 L). The resultant mixture was stirred overnight and then filtered to remove any remaining solids. The pH of the solution was adjusted to 3.3 using glacial acetic acid. After the required level of Cresyl staining was reached (approximately 1 min), the slides were washed in d.H_2O to remove any stain left on the glass slide. The sections were then dehydrated by passing them through increasing concentrations of ethanol (70 %, 85%, 100%, 100%). The level of staining was assessed by inspection using a light microscope. The slides were then cleared in xylene (3 × 5 mins) and covered with a glass cover slip using DPX as a hard set mounting medium.

6.2.6.7. Haematoxylin counterstain

After staining with DAB, the slides were washed in phosphate buffered saline (0.1 M, pH 7.2, 2 × 5 min). The slides were then dipped in haematoxylin for up to 30 seconds until the required level of staining was achieved, as determined using a light microscope. The excess haematoxylin was then washed out using d.H_2O. The slides were subsequently washed in Scott's tap water for 5 mins prior to dehydration by placement into solutions of increasing concentration of ethanol (70 %, 85%, 100%, 100%), 3 mins in each solution. The slides were cleared in xylene (3 × 5 mins) and then covered with a glass cover slip using DPX as a hard set mounting medium.

6.3. Results

6.3.1. 4T1-GFP model

6.3.2. Intracerebral model

The implantation of 4T1-GFP cells initially induced a focal brain metastasis at the desired coordinates. This can be seen at days 5 and 10 (Figure 6.1, A and B). However by day 21 and 35 the metastatic cells appeared to disseminate from the initial injection site and grow along the blood vessels within the brain. The GFP tag on the cells allowed the metastatic regions to be identified using immunohistochemistry (Figure 6.1, C and D). Despite the presence of these tumours the mice did not show any statistically significant clinical signs as defined above (6.2.2.1). In addition to this, the average weights of the animals showed no statistically significant deviation from the sterile PBS-injected animals over the entire time course (Figure 6.1 E and F).

6.3.2.1. Urine analysis

The ^{1}H NMR spectroscopy furnished spectra which upon initial overlay, looked similar to the ^{1}H NMR spectra from the animal models in Chapter 3 Section 3.3.3 (Figure 6.2 A). Visually, there appeared to be separation of the different disease groups, as illustrated in (Figure 6.2 B, C and D). Statistically significant models were generated which could separate the cell-injected animals from both the PBS-injected and naïve animals with q^2 values of 0.49 and 0.70 respectively (Table 6.3 A). It was also possible to separate the animals at each of the points during the disease time course, q^2 values given in Table 6.3 B.

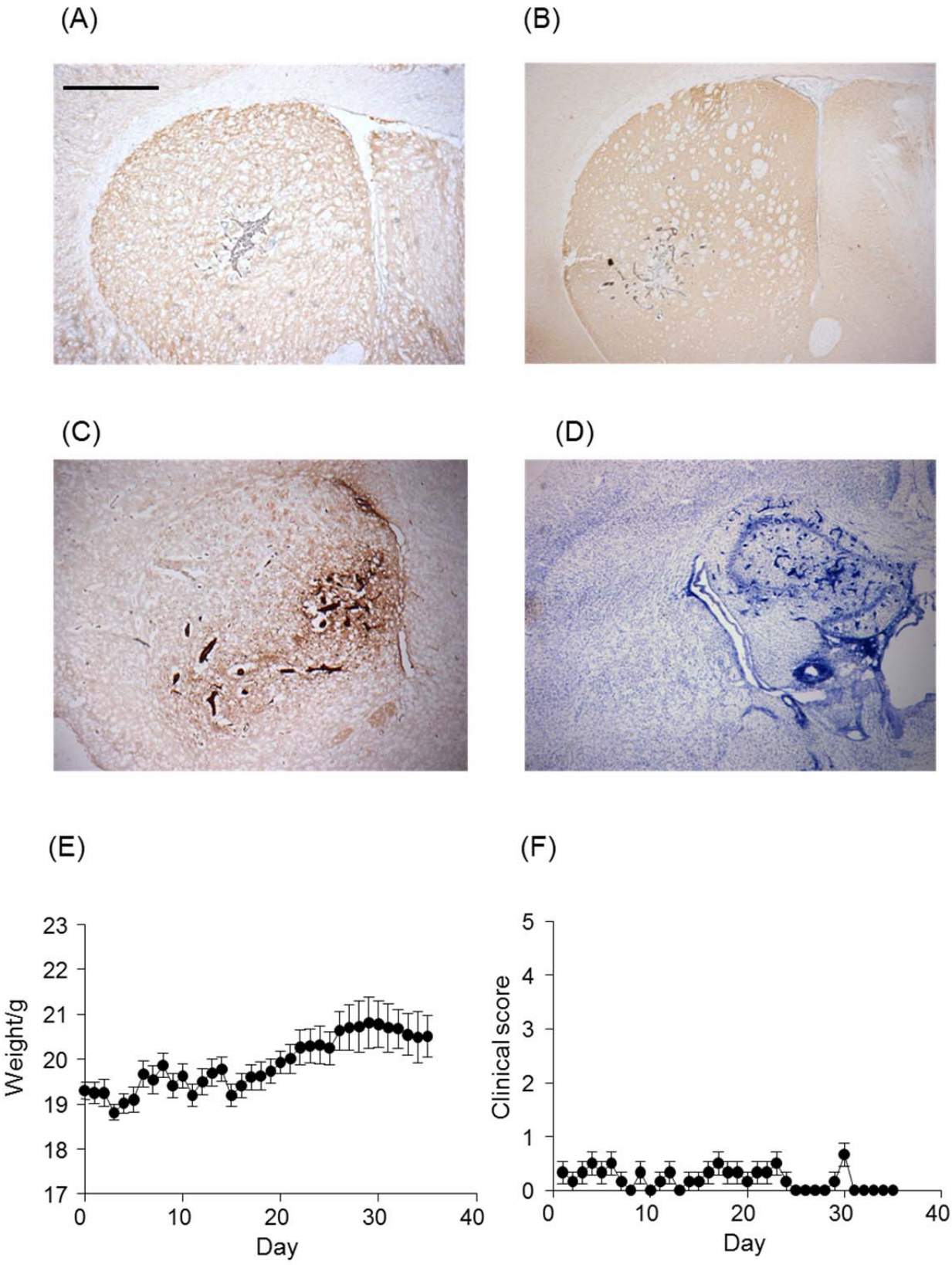


Figure 6.1: Immunohistochemical analysis of brain metastasis induced *via* the injection of 4T1-GFP cells. (A) Day 5. (B) Day 10. (C) Day 21. (D) Day 35. (E) Average clinical scores of BALB/c mice after the implantation of 4T1-GFP cells intracerebrally. (F) Average weights of BALB/c mice after the implantation of 4T1-GFP cells intracerebrally. Scale bar 500 mm .

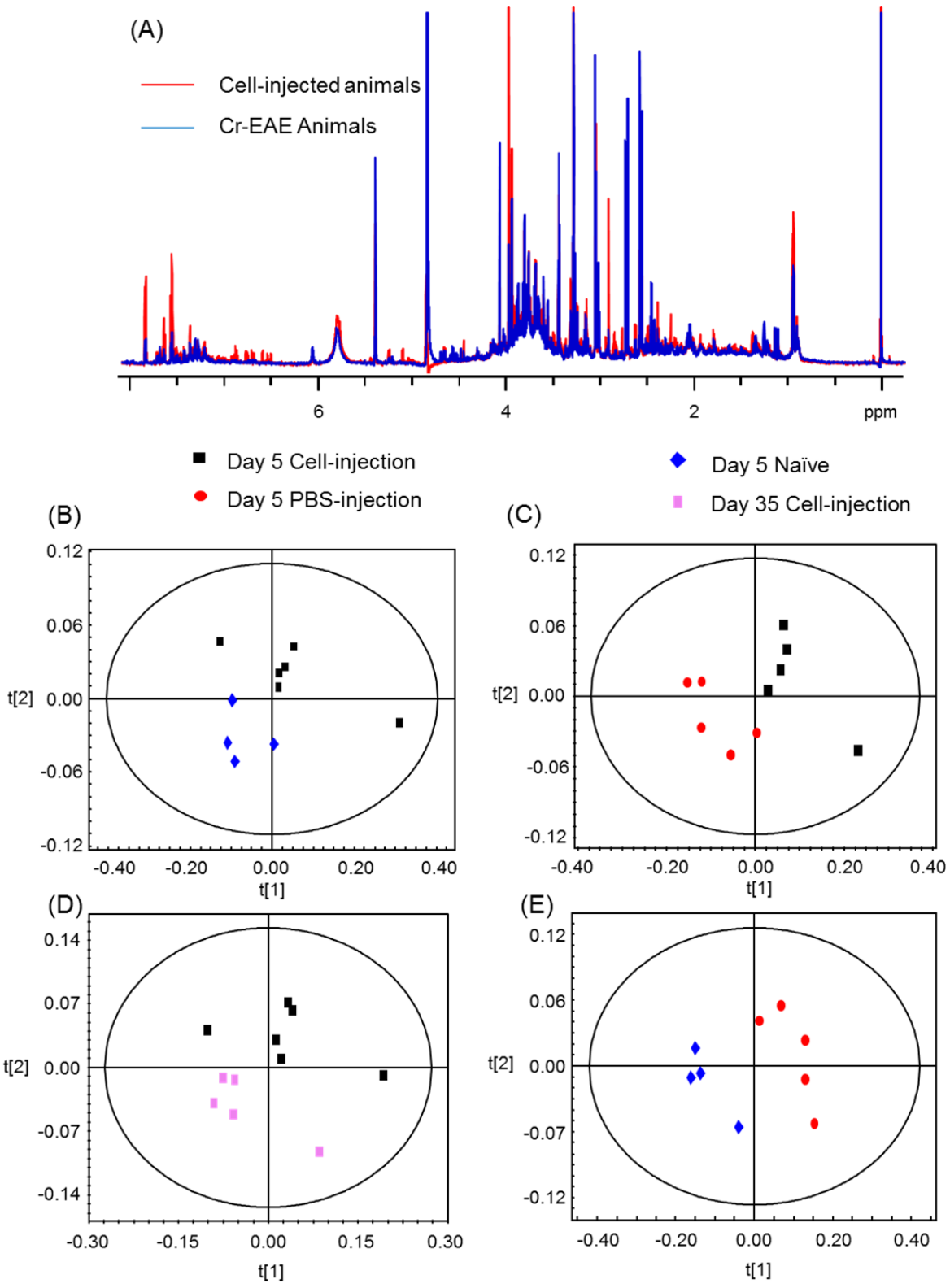


Figure 6.2: 4T1 intracerebral injection urine results. (A) Overlay of MS urine and brain metastasis NOESY spectra For full assignments please see Figure 3.4. (B) PLS-DA plot of animal urine samples comparing animals at day 5 injected with 4T1 cells and naïve animals , R2X = 0.87; R2Y 0.88. (C) PLS-DA plot of animal urine samples comparing animals at day 5 injected with 4T1 cells and PBS-injected animals , R2X = 0.82; R2Y 0.71. (D) PLS-DA plot of animal urine samples comparing animals at day 5 and day 35 injected with 4T1 cells, R2X = 0.89; R2Y 0.82. (E) PLS-DA plot of animal urine samples comparing animals at day 5 injected with PBS injected animals and naïve animals , R2X = 0.84; R2Y 0.95.

Urine

(A)

Cells	Day 10	Day 21	Day 35
Day 5	0.78*	0.48*	0.70*
Day 10		0.47*	0.90*
Day 21			0.66*
Day 35			

(B)

		PBS	Naïve
Cells	Day 5	0.70*	0.49*

Plasma

(C)

Cells	Day 10	Day 21	Day 35
Day 5	0.65*	0.56*	0.63*
Day 10		0.29	0.87*
Day 21			0.70*
Day 35			

(D)

		PBS	Naïve
Cells	Day 5	0.44	0.44

Table 6.3: 4T1 Intracerebral q^2 values. (A) Table showing the q^2 values when comparing the cell-injected animals to both control groups from the urine samples. (B) Table showing the q^2 values of the disease time course from the urine samples. (C) Table showing the q^2 values when comparing the cell-injected animals to both control groups from the plasma samples. (D) Table showing the q^2 values of the disease time course from the plasma samples.

When comparing the animals with tumour cells against the two control groups, the only consistent initial metabolite was taurine (δ_{x-y} 3.41), which was found to be at a relatively lower concentration in the diseased animals compared to the control groups. In addition to this, creatine (δ_{x-y} 3.03), ureidopropionic acid (δ_{x-y} 2.38, 3.30) and a TMAO (δ_{x-y} 3.25) resonance were lower in the cell-injected animals compared to the naïve animals. In contrast, hippuric acid (δ_{x-y} 3.97, 7.83, 7.55) and TMAO was found to be at a higher concentration in the cell-injected animals than the PBS-injected animals (Table 6.4).

Upon removal of these metabolites it was possible to generate further models with significant q^2 values. Once again only one metabolite varied consistently when comparing the tumour cell injected animals with the two control groups. In this case, citrate was found to be at a lower concentration in the diseased animals than in both control groups. In this second round, hippuric acid was shown to be higher in the cell-injected animals than in the naïve animals. When comparing the diseased animals with PBS-injected animals ureidopropionic acid and creatine were found to be higher in the diseased group. Two further metabolites were identified as being at a lower concentration in the cell-injected group than the PBS-injected group. These were oxoglutaric acid (δ_{x-y} 2.45) and an unknown resonance (δ_{x-y} 3.13 which had a complex multiplet structure) (Table 6.4). The other resonances, of taurine and oxoglutarate, were not detected by SIMCA, however, they were observed to be varying in a similar manner within the spectra. One possible reason for them not to be observed in varying within the models could be the influences from other resonances in that spectral area.

When the PBS-injected animals were compared to the naïve animals, a model with a significant q^2 value was generated (Table 6.4). TMAO, creatine, hippuric acid, and ureidopropionic acid were all found to be at a relatively lower

concentration in the PBS-injected animals than the naïve animals. Upon removal of these metabolites it was again possible to generate a second model with a significant q^2 value. Taurine and adenine (δ_{x-y} 8.13) were found to be at a relatively lower concentration and citrate, sarcosine (δ_{x-y} 3.61), and a trimethylamine peak were found to be at a higher concentration in the PBS-injected animals compared to the naïve group (Table 6.4 A).

Upon examinations of the loadings several metabolites were identified as varying throughout the disease time course. In particular a TMAO peak was constantly found to be at a higher level at day 5 when compared to all other time points (days 10, 21 and 35) and taurine was found to be consistently at a lower concentration at day 5 in the same comparisons. Other metabolites which showed variation were hippuric acid, glucose, citrate, creatine, oxoglutaric acid, and a trimethylamine peak (Table 6.4). When these metabolites were excluded from the original models, adenine, ureidopropionic acid, a p-cresol-like peak, an unknown multiplet (δ_{x-y} 3.11), and two unknown singlets (δ_{x-y} 3.79 and 2.41) were identified as causing further significant separations within the model (Table 6.4 B).

(A)

Model	q^2	Metabolites					
		Positive Metabolites		Negative Metabolites			
Cell Injected v PBS	0.70	TMAO	Hippuric acid	Taurine			
Cell Injected v Naïve	0.49			TMAO	Taurine	Creatine	Ureidpropionic acid
PBS v Naïve	0.88			TMAO	Hippuric acid	Creatine	Ureidpropionic acid

(B)

Model	q^2	Metabolites					
		Positive Metabolites			Negative Metabolites		
Cell Injected v PBS	0.68	Ureidpropionic acid	Creatine		Citrate	Oxoglutaric acid	Unknown resonance
Cell Injected v Naïve	0.73	Hippuric Acid			Citrate		
PBS v Naïve	0.55	Citrate	Trimethylamine	Sarcosine	Taurine	Adenine	

(C)

Model	q^2	Metabolites					
		Positive Metabolites			Negative Metabolites		
Day 5 v Day 10	0.78	Hippuric Acid	TMAO		Citrate	Glucose	Taurine
Day 5 v Day 21	0.48	Citrate	TMAO	Hippuric acid	Taurine		
Day5 v Day 35	0.70	Trimethylamine	TMAO		Taurine	Citrate	Creatine
Day 10 v Day 21	0.47	Citrate	Taurine		Creatinine	Glucose	
Day 10 v Day 35	0.90	Trimethylamine	Glucose		Creatinine	Hippuric acid	Oxoglutaric acid
Day 21 v Day 35	0.66	Trimethylamine			Citrate	Hippuric acid	Creatine

(D)

Model	q^2	Metabolites			
		Positive Metabolites	Negative Metabolites		
Day 5 v Day 10	0.78		Ureidopropionic acid	Unknown singlet	
Day 5 v Day 21	0.48	Adenine	Ureidopropionic acid	Unknown singlet δ2.23	
Day5 v Day 35	0.70	Ureidopropionic acid	Unknown resonance	Unknown singlet	2-Oxyglutaric acid
Day 10 v Day 21	0.47	Adenine		2-Oxyglutaric acid	TMAO
Day 10 v Day 35	0.90		Citrate		
Day 21 v Day 35	0.66	Taurine	Glucose	Unknown resonance	

Table 6.4: Significant metabolites in the 4T1 animal models. (A) Metabolites which generated the separation in the first round of the PLS models between the disease animals with both control groups (naïve and PBS). (B) Metabolites which generated the separation in the second round of the PLS models between the disease animals with both control groups (naïve and PBS). (C) Metabolites which generated the separation within the first round PLS models which changed when comparing the disease animals over the disease time course. (D) Metabolites which generated the separation within the second round PLS models which changed when comparing the disease animals over the disease time course.

6.3.2.2. Plasma analysis

Visually, there appeared to be a separation between the cell-injected animals and both control groups (PBS-injected and naïve) (Figure 6.3). Despite this, the models generated were not statistically significant, with q^2 values of -0.21 and 0.31, respectively. The presence of EDTA (δ 3.11, 3.17, 3.63) from the plasma collection appeared to be highly variable within the spectra. Therefore, it was decided to omit these buckets from the spectra as described in Chapter 2 Section 2.7.6. Plasma was again collected in EDTA tubes, as these samples were collected before EDTA was realised to be a problem. In future studies heparinised plasma tubes should be used. Again, there was a visual separation in the models between the cell-injected animals and both control groups as illustrated in Figure 6.3 C and D. These models were statistically significant, with q^2 values of 0.44 for both models. Unlike the urine result, it was not possible to separate the PBS-injected animals from the naïve animals. It was, however, possible to generate significant models between each of the time points throughout the disease, with the exception of the comparison between day 10 and day 21 (illustrated in Figure 6.3 E and F). The q^2 values for all of these models are given in Table 6.5; A.

From the significant models it was possible to identify the metabolites that caused the separations between the groups. When comparing the cell-injected animals with both of the control groups, 3 metabolites varied consistently. These were a phosphocholine resonance, an unknown resonance (δ_{x-y} 7.38, triplet; 7.42, quartet) and glucose (δ_{x-y} 3.25). The phosphocholine resonance was at a higher concentration in the cell-injected animals compared to the control groups (Table 6.5; B), whilst the other two metabolites were at a lower concentration. When comparing the cell-injected animals with naïve animals, fatty acids (δ_{x-y} 0.87, 1.26) were also found to be increased in the cell-injected

animals (Table 6.5; B). In addition to this, an unknown resonance (δ_{x-y} 1.19, triplet) was found to be at a lower level in the cell-injected animals (Table 6.5; B). Only one further metabolite varied when the cell-injected animals were compared to the PBS-injected animals. This was an acetylglycine-like resonance (δ_{x-y} 2.05), which was lower in the cell-injected animals (Table 6.5; B).

It was possible to identify metabolites which were at a higher level at day 5 in the cell-injected animals when compared to the other time points, but they did not vary as consistently, with increases at some time points only (Table 6.5; C). These metabolites were fatty acids (day 5 v days 21, 35), lactate (day 5 v days 21, 35), a phosphocholine resonance (day 5 v days 10, 21), and a p-cresol-like resonance (day 5 v day 10). There were also 3 metabolites that were occasionally at a lower level at day 5 compared to the rest of the disease time course (Table 6.5 C). These were an acetylglycine-like resonance and two unknown resonances (δ_{x-y} 4.21, multiplet, days 10, 21; the unknown triplet at δ_{x-y} 1.19 mentioned above, days 21, 35). Interestingly, levels of glucose appeared to increase from day 5 to days 10 and 21, but by day 35 had dropped again to levels below those at day 5. An acetylglycine-like resonance also appeared to drop at day 35 compared to days 10 and 21 (Table 6.5 C), whilst a phosphocholine resonance increased at day 35. In addition to these metabolites, when comparing day 10 animals with day 35 animals, fatty acids were at a higher concentration and the unknown resonance (δ_{x-y} 1.21, triplet) at a lower concentration in the day 10 group (Table 6.5 C).

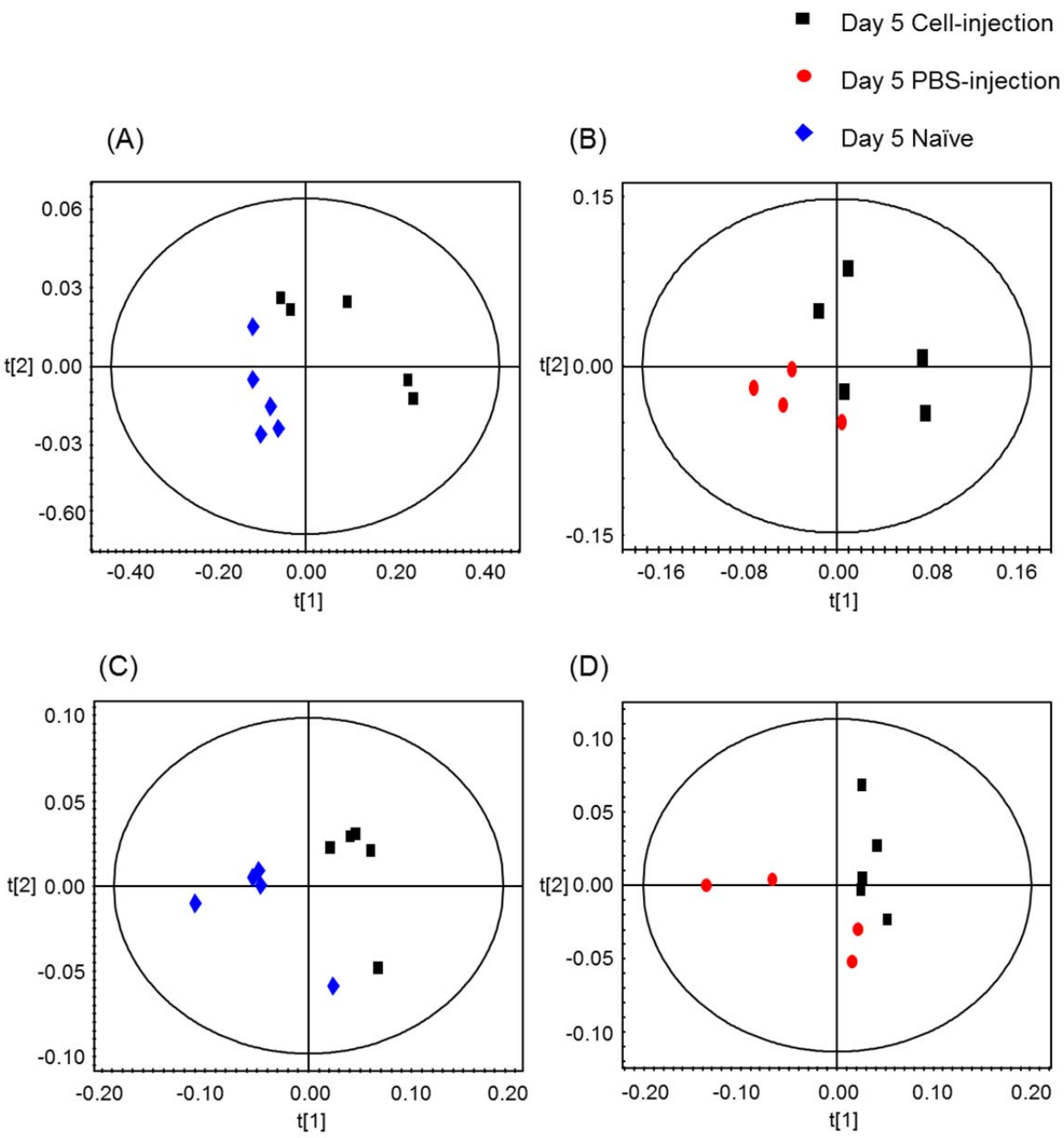


Figure 6.3: 4T1 intracerebral injection plasma results. (A) PLS-DA plot of animal plasma samples comparing animals at day 5 injected with 4T1 cells and naïve animals. (B) PLS-DA plot of animal plasma samples comparing animals at day 5 injected with 4T1 cells and PBS-injected animals. (C) PLS-DA plot of animal plasma samples comparing animals at day 5 injected with 4T1 cells and naïve animals after the removal of EDTA from the spectra. (D) PLS-DA plot of animal urine samples comparing animals at day 5 injected with 4T1 cells and PBS-injected animals after the removal of EDTA from the spectra.

(A)

Model	q^2	Metabolites						
		Positive Metabolites		Negative Metabolites				
Cell-injected v PBS	0.44	Phosphocholine		Glucose	Unknown	aromatic	Acetylglycine	
Cell-injected v Naïve	0.44	Fatty acids	Phosphocholine	Glucose	Unknown	aromatic	Unknown triplet linked to 3.66	

(B)

Model	q^2	Metabolites			
		Positive Metabolites			
Day 5 v Day 10	0.78	Phosphocholine	p-cresol		
Day 5 v Day 21	0.48	Phosphocholine	Fatty acids	Lactate	
Day 5 v Day 35	0.70	TMAO	Fatty acids	Glucose	Lactate
Day 10 v Day 21	0.47				
Day 10 v Day 35	0.90	TMAO	Acetylglycine	Fatty acids	Glucose
Day 21 v Day 35	0.66	TMAO	Acetylglycine		Glucose

(C)

Model	q^2	Metabolites				
		Negative Metabolites				
Day 5 v Day 10	0.78	TMAO	Unknown multiplet	Glucose	Acetylglycine	
Day 5 v Day 21	0.48	TMAO	Acetylglycine	Unknown multiplet	Unknown triplet	Glucose
Day 5 v Day 35	0.70	Unknown triplet				
Day 10 v Day 21	0.47					
Day 10 v Day 35	0.90	Phosphocholine	Unknown triplet			
Day 21 v Day 35	0.66	Phosphocholine				

Table 6.5: Intracerebral injection of 4T1-GFP plasma results. (A) q^2 values of models generated from the plasma samples taken from animals which have been injected intracerebrally with 4T1 cells over different time points. (B) Table of metabolites which caused the separation of the intracerebral injected disease group from both the control groups (naïve and PBS-injected). (C) List of metabolites which varied over time during the disease timecourse following an intracerebral injection of 4T1-GFP cells. Direction of metabolite change with respect to model highlighted.

6.3.3. Comparison of different tumour induction routes

The intracardiac and intravenous implantation of 4T1-GFP tumour cells into BALB/c mice resulted in no significant weight loss or overt clinical symptoms during the 10-day time period (data not shown).

6.3.3.1. Urine analysis

The initial PLS models formed from the urine taken at day 10 (intracardiac and intravenous implantation) or day 5 (intracerebral implantation) showed a visual and statistically significant separation between all of the animal groups. Surprisingly, this included a separation between animals injected with PBS intravenously and the naïve group of animals with a q^2 value of 0.79 (Figure 6.4 A). However, the urine samples from the naïve group were acquired during the initial study with the intracerebral model and, hence, the NMR experiments were performed at an earlier time point. It was determined that there were subtle differences between the spectra acquired on different days that caused an artificial separation between these two groups. In order to eliminate such differences between datasets the spectra were normalised to creatinine as described in chapter 2.

The need to absolutely scale the spectra to creatinine arose from the differences observed between the animals injected with PBS into the tail vein and the naïve animals. This variation arose because the spectra were run on different days using fresh buffer each day. Owing to errors from the weighing scales, variations arose in the amount of TSP that was added to the buffer each day, giving rise to variations in the spectral peak for TSP. Thus, it was decided to scale the spectra to an internal standard. Metabolomic studies regularly use creatinine as an internal reference for the scaling of metabolites (Fauler*, et al.*, 1997; Prévot*, et al.*, 2002). This is due to the fact that creatinine levels have

been shown to remain constant in animals as creatinine is the breakdown of phosphocreatine from muscles (Craig*, et al.*, 2006). The kidneys then filter this creatine out of the blood supply by glomerular filtration and partial tubular excretion (Wishart*, et al.*, 2009). However, it has been reported that, 4T1 cells can metastasise to the kidneys (Tao*, et al.*, 2008) where a rise in creatinine levels is a late stage event in kidney failure (Herget-Rosenthal*, et al.*, 2004). The animals used in the current study were culled on day 10 and therefore the kidney function would not be compromised by the metastatic burden.

Upon normalisation to creatinine it was possible to generate models which separated the intracardiac injected animals from both control groups (PBS-injected and naive) with q^2 values of 0.43 and 0.59, respectively. This was also the case for the intravenously injected animals with q^2 values of 0.46 and 0.4, respectively. It was not possible, however, to generate a model to separate the PBS-injected animals from the naïve group in both the intracardiac and intravenous groups. With regards to the different routes of tumour induction, statistically significant models were generated that separated each of the different injection routes from each other. The q^2 values for these models were: 0.78 for the intracranial animals compared to the intracardiac animals, 0.89 for the intracranial animals compared to the intravenous animals and 0.84 for the intracardiac animals compared to the intravenous animals (Figure 6.4 B, C and D).

In the intracardiac model, taurine and a TMAO resonance were observed to be at a lower level in the cell-injected animals than both control groups. When comparing the cell-injected animals to the naïve group, hippuric acid, glucose, and a sarcosine-like resonance (δ_{x-y} 3.59) were found to be at a higher concentration in the tumour-bearing animals (Table 6.6 A). In contrast, creatine and an unknown singlet resonance (δ_{x-y} 2.23) were found to be lower in the cell-

injected group than in the naïve animals. When comparing the cell-injected and PBS-injected animals, butyric acid (δ_{x-y} = 1.61, 2.29), two unidentified regions (δ_{x-y} 3.75, doublet and δ_{x-y} 1.87, double doublet) and a maleic acid-like resonance (δ_{x-y} 6.05) were found to be at a higher concentration in the tumour-bearing animals (Table 6.6; A). In addition to the metabolites mentioned above, citrate and an unknown singlet (δ_{x-y} 3.79) were also found to be at a lower concentration in the cell-injected animals (Table 6.6; A).

When comparing the intravenously injected animals with both control groups, five metabolites varied consistently; citrate and hippuric acid were at a higher concentration in the cell-injected animals, whilst taurine, creatine, and a TMAO resonance were at a lower concentration (Table 6.6 B). No further metabolites were at a higher level in the cell-injected animals compared to the naïve cohort. However, glucose was found to be at a lower concentration in the cell-injected animals compared to the naïve animals. When comparing the cell-injected animals with the PBS-injected group, a further unidentified resonance (δ_{x-y} 8.13, doublet) was found to be at a higher concentration. In addition to this, a trimethylamine resonance was at a lower concentration in the cell-injected animals (Table 6.6 B).

When comparing the different routes of tumour induction it was possible to identify metabolites causing the separations between the groups. When comparing the intracardiac and intracerebral models octenedioic acid (δ_{x-y} 2.32, 2.25), a maleic acid-like resonance and an unknown resonance (δ_{x-y} 3.75, doublet) were all at a higher concentration in the intracardiac animals. In addition to this, taurine, creatine, glucose and citrate were all at a lower concentration in the intracardiac animals. When comparing the intravenous animals with the intracranial animals, citrate, maleic acid, butyric acid and guanine-like resonances were all found at a higher concentration in the

intravenous animals. Taurine, creatine and glucose were found to be at a lower concentration in the intravenous animals. From the final comparison between the intravenous animals and the intracardiac animals, glucose, a TMAO resonance, a glycine-like resonance (δ_{x-y} 3.57) and two unknown resonances (δ_{x-y} 3.75, 0.93 both doublets) were all lower in the intravenous animals. Citrate was the only metabolite at a higher concentration in the intravenous animals.

6.3.3.2. Plasma analysis

From the plasma data it was possible to generate several significant models. However, a similar problem was found in the plasma results as seen for the urine results in section 6.3.3.1; it was possible to generate a statistically significant model between the intravenous PBS model and the naïve cohort with a q^2 value of 0.55. This was because only one naïve cohort of BALB/c animals was run, with the initial intracerebral models as discussed above. Since no metabolite was considered to be stable between all the groups, it was not possible to normalise the plasma spectra as was done for the urine data. Consequently, it was not possible to use the plasma data to differentiate between the different injection routes.

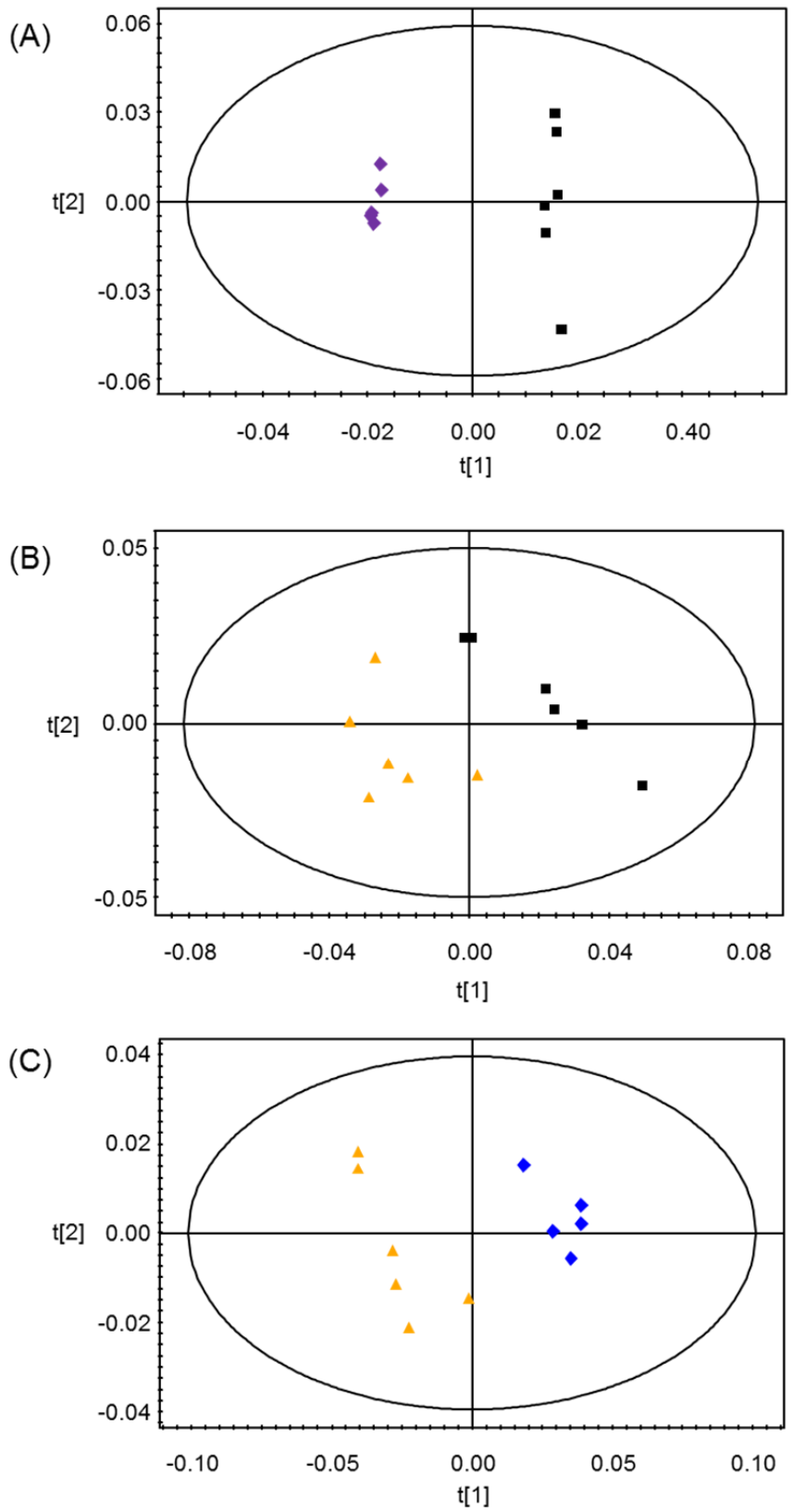


Figure 6.4: PLS plots of differing tumour burdens within the CNS. (A) PLS plot showing the artificial separation between intravenous injected PBS and a naïve group of animals. (B) PLS plot showing the separation between intracerebral injected animals and intracardiac injected animals (C) PLS plot showing the separation between intracerebral injected animals and intravenous injected animals (D) PLS plot showing the separation between intravenous injected animals and intracardiac injected animals.

(A)

Model	q^2	Metabolites							
		Positive Metabolites				Negative Metabolites			
Cell Injected v PBS	0.45	Unknown Doublet	*Maleic acid*	Butyric acid	Unknown double doublet	Taurine	TMAO	Citrate	Unknown singlet
Cell Injected v Naïve	0.59	Hippuric acid	Glucose	*Sarcosine*		Taurine	TMAO	Creatine	*p-cresol*

(B)

Model	q^2	Metabolites						
		Positive Metabolites		Negative Metabolites				
Cell Injected v PBS	0.46	Hippuric acid	Unknown Double	Taurine	TMAO	Creatine	Trimethylamine	
Cell Injected v Naïve	0.40			Taurine	TMAO	Creatine	Glucose	

(C)

Model	q^2	Metabolites								
		Positive Metabolites					Negative Metabolites			
Intracardiac v Intracranial	0.78	Unknown doublet	*Octenedioic acid*	Maleic acid	Unknown double doublet		Taurine	Creatine	Glucose	Citrate
Intravenous v Intracranial	0.89	Citrate	Maleic acid	*Butyric acid*	*Guanine*		Taurine	Creatine	Glucose	
Intracardiac v Intravenous	0.84	Unknown doublet	TMAO	Glycine	Unknown doublet	Glucose	Citrate			

Table 6.6: Urine metabolites responsible for the separation in the different routes of injection models. (A) Table showing the metabolites which caused the separation in the PLS models between the animals injected into the heart with 4T1-GFP cells and both control groups (PBS injected and naïve). (B) Table showing the metabolites which caused the separation in the PLS models between the animals injected into the tail vein with 4T1-GFP cells and both control groups (PBS injected and naïve). (C) Table showing the metabolites which caused the separation in the PLS models between the animals with different tumour burdens in the CNS. Direction of metabolite changes are with respect to the highlighted group.

6.3.4. Additional intracerebral models

Intracerebral injection of MDA231BR cells into SCID mice or B16F10 cells into C57Bl/6 mice resulted in the formation of a focal brain metastasis (Figure 6.5 A and B). The MDA231BR cells formed a metastasis similar to the metastasis formed by the 4T1-GFP cells (Figure 6.5 A and B), in that these tumours appeared to be growing along the blood vessels by day 10. In contrast, the B16F10-GFP cells appeared to grow in a tight cluster of cells and not along the vascular bed (Figure 6.5 C and D). At day 10, when the animals were killed, no overt clinical signs or significant changes in weight were evident in either group (data not shown).

6.3.4.1. Urine analysis

The urine obtained from the SCID mice injected with MDA231BR furnished models that showed a visual separation compared to both the control groups (PBS injected and naïve). However, none of the models reached the defined level of significance (Figure 6.6 B and C).

From the urine taken from the C57Bl/6 mice it was possible to generate OPLS-DA models that separated the cell-injected animals from both of the control groups (naïve and PBS-injected) with q^2 of 0.48 and 0.93, respectively. It was not possible to generate a model to separate the PBS-injected animals from the naïve animals in this case (Figure 6.6 C and D). Creatine was the only metabolite that varied consistently when comparing both control groups, and was lower in the cell-injected animals. In addition to this, citrate and hippuric acid were lower in the cell-injected animals compared to the naïve animals. No metabolites were elevated in the cell-injected animals compared to naïves, however, taurine and an unknown resonance ($\delta_{x\text{-}y}$ 3.13, singlet) were both lower in the cell-injected group compared to the PBS-injected group. Only one

metabolite was higher in the cell-injected animals compared to the PBS-injected animals, an unknown resonance (δ_{x-y} 3.33, multiplet). Upon removal of these metabolites from the models it was possible to generate a further significant OPLS-DA model when comparing the cell-injected animals to the naïve group (q^2 = 0.92). The metabolites underlying this model were taurine (δ_{x-y} 3.25 3.43), TMAO (δ_{x-y} 3.25) and glucose (δ_{x-y} 3.77, 3.83), all of which were lower in the cell-injected animals. It was not possible to generate a second significant model between the cell-injected and PBS-injected groups (q^2 = 0.3) as shown in Table 6.7. Interestingly, creatine, citrate, taurine, and TMAO all vary constantly in the intracerebral injected animals compared to the control groups, irrespective of cell type. However, hippuric acid is elevated in the 4T1-GFP model but lower in the B16F10 models. Upon examination of the loadings of the animals injected with 4T1-GFP cells compared to the naïve animals, glucose was also at a lower level in the cell injected animals compared to the naïve group (Table 6.7). However, it did not quite reach the defined significance and hence is not reported above. This suggests that there is a decrease in glucose in the plasma of all animals following an intracerebral injection of tumour cells.

6.3.4.2. Plasma analysis

Once again, the ^{1}H NMR spectra of the plasma samples from the naïve SCID animals were acquired at a different time from the intracerebral injection. Therefore, it was not possible to use this dataset to generate models owing to the lack of an appropriate metabolite to normalise against. This was not the case for the plasma from the C57Bl/6 animals injected with B16F10-GFP cells. However, despite a visual separation within the PLS plots, it was not possible to generate a significant model to separate the cell-injected animals from either the naïve group or the PBS-injected group (q^2 = 0.23 and -0.21, respectively).

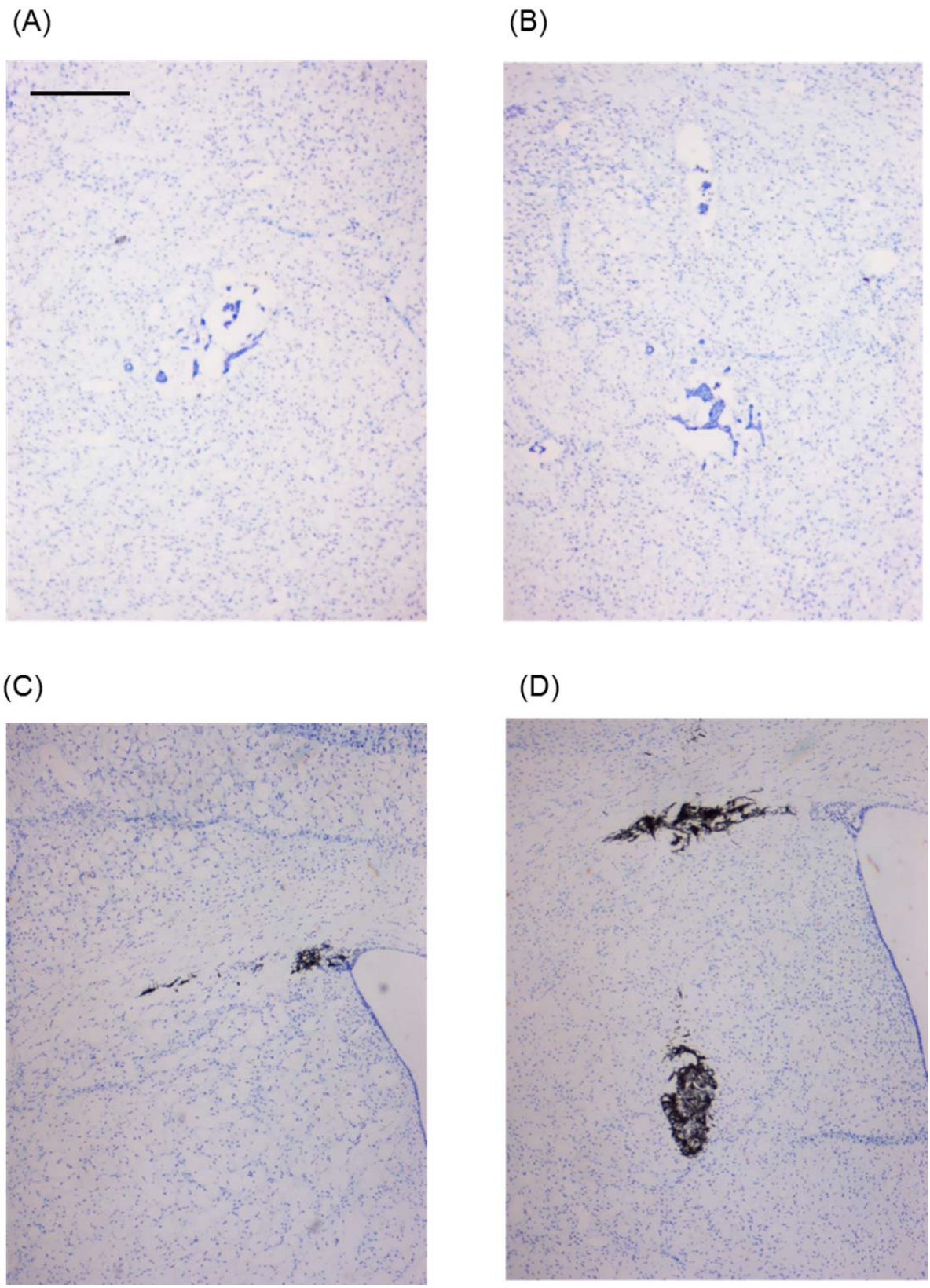


Figure 6.5: Additional intracerebral models results. (A and B) Immunohistochemistry of brains of SCID mice which have been injected with MDA231BR cells at day 10. (C and D) Immunohistochemistry of brains of C57 Black 6 mice which have been injected with B16F10-GFP cells at day 10. Scale bar 250 mm.

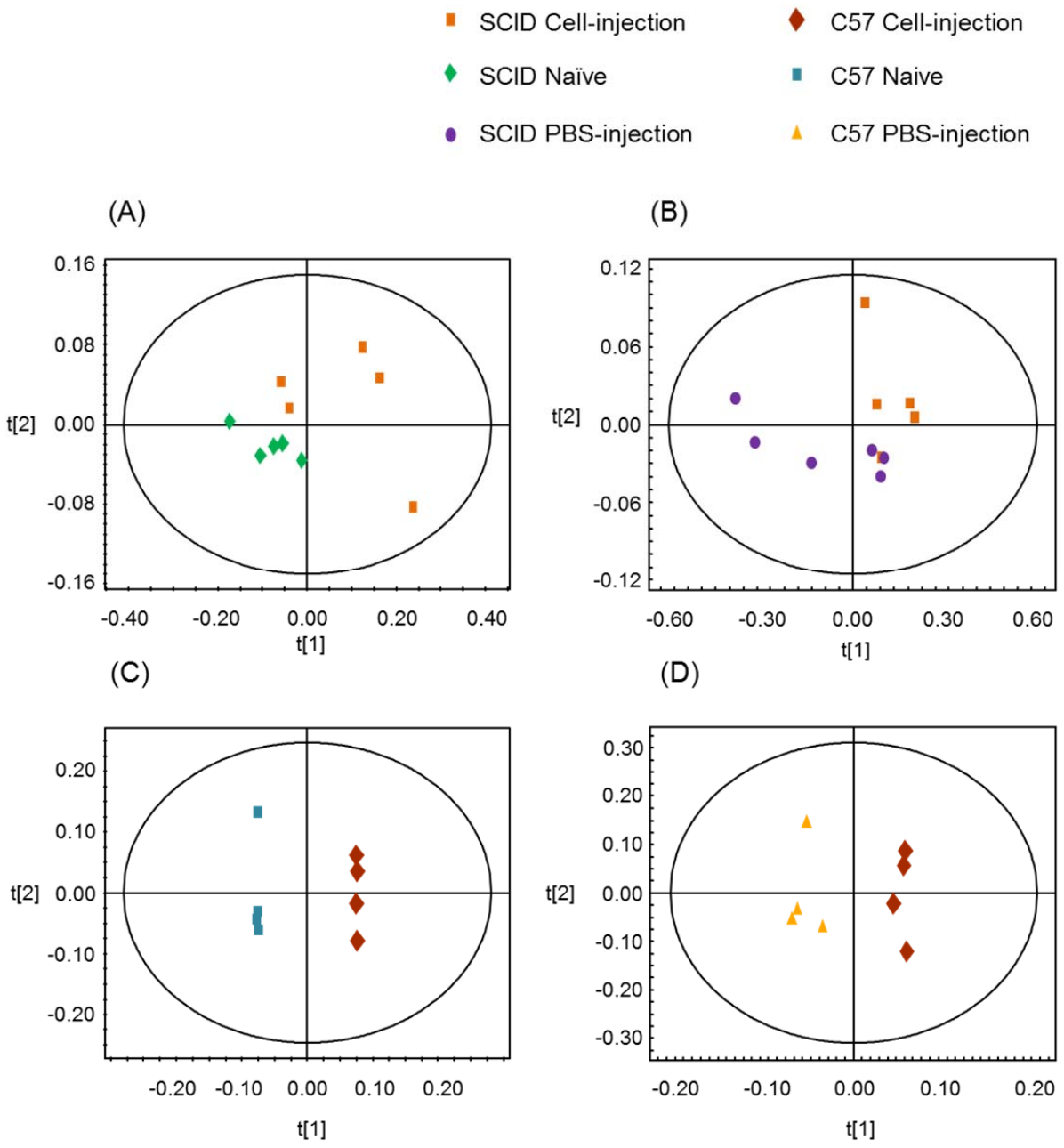


Figure 6.6: PLS plots of additional intracerebral models. (A) PLS-plots of SCID mice showing the separation between cell-injected animals and naïve animals. (B) PLS-plots of SCID mice showing the separation between cell-injected animals and PBS animals. (C) PLS-plots of C57Bl/6 mice showing the separation between cell-injected animals and naïve animals. (D) PLS-plots of C57Bl/6 mice showing the separation between cell-injected animals and PBS animals.

(A)

Model	q^2	Metabolites				
		Positive Metabolites	Negative Metabolites			
Cell-injected v PBS	0.48	Unknown resonance d_{x-y} 3.33	Creatine	Unknown resonance d_{x-y} 3.13	Taurine	
Cell-injected v Naïve	0.93		Creatine	Citrate	Hippuric acid	

(B)

Model	q^2	Positive Metabolites		
Cell-injected v Naïve	0.92	Taurine	TMAO	Glucose

Table 6.7: Additional intracerebral models metabolite identification. (A) Metabolites which generated the separation in the first round of PLS models between the C57Bl/6 animals injected with B16F10 cells intracerebrally. (B) Metabolites which generated the separation in the second round of the PLS models between the C57Bl/6 animals injected with B16F10 cells intracerebrally. Direction of metabolite changes are with respect to the highlighted group.

6.4. Discussion

In this chapter it has been demonstrated that it is possible to detect the presence of 4T1-GFP tumour cells implanted intracerebrally as early as 5 days after injection using a combination of ^{1}H NMR and metabolomics analysis of urine and plasma samples. Using the same approach it was also possible to separate animals injected intracerebrally with B16F10-GFP cells from control animals at day 10. Subsequently, the same technique was used to follow tumour development over the disease timecourse and significant differences were found between time points. Finally, this study showed that this biofluid metabolomics approach enables differentiation between animals that have different distributions of metastases throughout the body.

6.4.1. Intracerebral injections

6.4.1.1. Urine analysis

It has been widely reported that cancer cells have a very different metabolite profile compared to healthy tissue (Warburg*, et al.*, 1927). This has led to the development of such techniques as PET imaging for cancer diagnosis, as the PET agent, fluorodeoxyglucose (FDG), which is based on glucose, is more readily taken up by tumour cells than normal tissue (Pauwels*, et al.*, 2000). This has also led to a number of NMR studies in order to measure these metabolic changes. It has previously been shown that, using similar techniques to those used in this chapter, it is possible to detect prostate cancer from seminal fluid (Kline*, et al.*, 2006). That study showed that the citrate level in seminal fluid was a better predictor of prostate cancer than prostate specific antigen (PSA), which is the current gold standard for prostate diagnosis. It has also been shown that it is possible to use *in vivo* NMR to differentiate between different types of tumours within the CNS. For example, studies have demonstrated that patients

with glial tumours and meningiomas have low N-acetyl aspartate levels around the tumours that later can be further distinguished by a reduction in creatine (Alger*, et al.*, 1990; Gill*, et al.*, 1990; Ott*, et al.*, 1993a; Usenius*, et al.*, 1994). Other studies have also reported that variation in choline resonances is an effective marker of tumour malignancy (Usenius*, et al.*, 1996) However, in order to perform this study the tumours need to be visible by MRI or a biopsy sample must be obtained (Griffin*, et al.*, 2007). From those studies and the work done in the previous chapters, it was hypothesised that the presence of brain metastases within the CNS could be detected using metabolomics analysis of urine samples. The aim of this work was to develop a diagnostic test that would enable earlier detection of brain metastases than is currently possible using present diagnostic techniques. The results demonstrate that it is possible to separate animals injected intracerebrally with tumour cells from both the control groups (PBS-injected and naïve animals) as early as 5 days after tumour induction. Previous work within Dr Nicola Sibson's group has shown that following the implantation of 4T1-GFP cells into BALB/c mice it is not possible to visualise the tumours using Gd-DTPA-enhanced MRI until at least day 35 (O'Brien*, et al.*, 2011). Therefore, this study shows that it is possible to detect the presence of metastatic tumours in the brain at an earlier time-point than current techniques.

Metabolomic analysis has been shown to be a highly sensitive technique and can detect small permutations in metabolism. For example it is possible to detect metabolic changes in the urine of a rat after 19 days of exposure to cadmium (35.7 μg/g) in their diet (Griffin*, et al.*, 2001). It is likely, therefore, that the separation found between the PBS-injected animals and the naïve animals at day 5 was caused by the surgery required to inject the PBS intracerebrally. At this early time point, the scalp wound is still recovering and resulting metabolite changes are likely. Nevertheless, the significant separation between cell-

injected and PBS-injected animals, indicates that the effects of the 4T1-GFP tumours in the brain overrides any metabolic changes caused by the surgery alone.

Several metabolites were found to be lower in the 4T1-injected animals than in the naïve animals, including taurine, citrate, creatine, ureidopropionic acid and TMAO, some of which were also decreased in the PBS-injected animals compared to naïves (taurine, creatine, TMAO and ureidopropionic acid). In the case of taurine, however, the decrease was greater in the 4T1-injected animals giving rise to a positive separation between the 4T1- and PBS-injected groups. This finding suggests that the effects of brain metastases on taurine levels in the urine are over and above those induced by surgery and vehicle injection alone. Taurine is an organic acid and found in relatively high concentrations in several organs including the brain (Barbeau*, et al.*, 1974). The role of taurine in the body is not fully understood. Studies have demonstrated that it has a possible role in neurotransmission (Davison*, et al.*, 1971) owing to its close association with gamma-aminobutyric acid in the CNS. However, other studies have reported that the taurine effects the stability of cell membranes (Barbeau*, et al.*, 1974).

Taurine also plays a key role in osmoregulation within the CNS. A study, used *in vivo* brain dialysis in a rat, reported that there is an increase in extracellular taurine in response to the addition of a hypertonic solution (Solís*, et al.*, 1988). Using MRS, it has been shown that taurine is elevated in colon tumours. That study showed the triplet resonance at δ = 3.43, which was assigned to taurine, increased by a factor of 4 (Moreno*, et al.*, 1993). This increase in taurine was attributed to increased metabolism within the tumour cells, since increases in taurine have been found in metabolically active tissues (as disscused in Wright*, et al.*, 1986). The decrease in urine taurine levels found in the current study in

the cell-injected animals compared to the control groups may indicate uptake of taurine by the metastatic cells. Interestingly, over the time course of the intracerebral 4T1 model the levels of taurine rose from these acutely reduced levels at day 5 to higher levels by day 10, before dropping again between days 21 and 35. These findings suggest a dynamic and changing response to the development of metastases in the brain. This changing response may reflect the more diffuse nature of the metastases along the vascular tree at days 21 and 35 compared to the earlier time points. These changes could also be in response to other effect within the body such as the cytokine or the glucocorticoid response to the presence of the tumour lesion within the CNS. This has been shown to be commonly detected in metabolomic studies (Connor*, et al.*, 2004). Future studies could be performed where these effects are induced in the animals and compared to the metabolites identified in this study in order to tease out the specific changes in metabolites which relate to the presence of brain tumours and which metabolite changes relate to the systemic immune response to the presence of a tumour.

TMAO, creatine and ureidopropionic acid were all constantly lower in the cell-injected and PBS-injected animals when compared to the naïve animals. This suggests that these metabolites are lowered as a result of the surgery required to implant the cells intracerebrally. Interestingly, all three metabolites were at a higher level in the cell-injected animals than in the PBS-injected animals. This finding suggests that the changes to these metabolites may reflect the surgery *per se* rather than the presence of the tumour. Contrary to this, citrate was lower in the cell-injected animals than both control groups, this is similar to results found at an early time point in the Cr-EAE animals (Chapter 3 Section 3.3.3). The possible reasons for this are discussed later (Chapter 7 Section 7.5).

In contrast to the reductions described above, hippuric acid was found to be elevated in animals injected with cells at day 5 compared to both control groups. Moreover, hippuric acid appeared to be reduced (rather than elevated) in the PBS-injected animals compared to the naïve group, indicating differential effects of surgery/vehicle injection and the presence of brain metastases. Interestingly, in the time course study, hippuric acid was found to be at a higher level at days 5 and 35 compared to days10 and 21. Hippuric acid is present in the urine of most mammals and is produced from the reaction between benzoic acid and glycine (Quick*, et al.*, 1933). The authors of that study reported that the rate of hippuric acid production in the urine of rabbits remained constant even after a large dose of benzoic acid, and that the rate-liming step was the production of glycine within the liver. The authors then showed that when there was liver damage, hippuric acid levels within the urine dropped and, thus, reductions in urinary hippuric acid levels could be used as a marker of compromised liver function (Quick*, et al.*, 1933). However, in the current study elevated levels of hippuric acid were found in the tumour-bearing animals. Hippuric acid has been shown to increase in the urine of patients who have been exposed to the solvent toluene (Hasegawa*, et al.*, 1983). Toluene is oxidised in the methyl position to benzoic acid (Williams, 1959) which is then converted into hippuric acid, as mentioned above. Physiologically, increased levels of benzoic acid, in the absence of toxins such as toluene, have been shown to be derived from an increase in global phenylalanine metabolism (Wishart*, et al.*, 2009). Thus, the elevation in hippuric acid observed in the current study, may reflect increased phenylalanine metabolism in the tumour bearing mice due to an increase in dopamine production in response to the tumour.

6.4.1.2. Plasma analysis

The results from the plasma did not generate such robust models as from the urine. The removal of the EDTA peaks from the spectra did improve the models, however, at day 5 the q^2 values of the models comparing the cell-injected animals to both control groups only just reached the defined significance. It was not possible to distinguish between the PBS-injected animals and the naïve animals. The reason for this could be attributed to the plasma being more of a snapshot of the metabolism (Griffin*, et al.*, 2004a) and therefore, smaller changes are less likely to be detected (as discussed in Chapter 7 Section 7.2). Interestingly there were several metabolites which were consistent between the cell-injected animals and both the control groups. These included phosphocholine, glucose, and an unknown set of aromatic resonances. Phosphocholine was elevated in the cell injected animals. A similar pattern was observed in the Cr-EAE animals; just prior to and during active disease (days 10, 14 and 35) phosphocholine was elevated in the diseased animals (Chapter 3 Section 3.3.4). This similarity will be discussed later (Chapter 7 Section 7.5). Plasma glucose is reduced in the cell-injected animals supporting the hypothesis that glucose metabolism in the tumour cells is increased in the cell injected animals. Glucose also varies throughout the time course and is lower on day 5 compared to days 10 and 21. This suggests that the tumours maybe less metabolically active at these time points as observed in the urine from these animals (Section 6.4.1.1). By day 35 however, the glucose levels were lower even than at day 5.

6.4.2. Variation in distribution of tumour burden

The ability to detect intracerebrally implanted 4T1-GFP cells at an early time point led to the hypothesis that it could be possible to generate a set of metabolites which could detect the presence of brain metastases in the

presence of systemic metastasis. Currently, it is possible to determine the presence of systemic metastasis by use of a biopsy (Shields*, et al.*, 2001) or looking for specific blood markers (Weigelt*, et al.*, 2005). The problem in the clinic is trying to identify which patients are developing brain metastasis as prognoses and treatment for brain metastasis is very poor (as discussed in Chapter 1 Section 1.8.1). As discussed in 6.1 it is possible to vary the tumour burden to the CNS and systemic sites depending on the site of injection. The results described in this chapter (Section 6.3.3.1) demonstrate that it is possible to differentiate between mice with different burdens of metastases in systemic organs and the brain using metabolomic analysis of the urine.

At day 10 following either an intravenous or intracardiac injection of PBS it was not possible to distinguish between these animals and the naïve cohort. Therefore, to simplify the cross group comparisons only the separations from the naïve will be discussed here. A number of metabolites varied consistently across the groups, notably hippuric acid was elevated in cell injected animals in all groups. In contrast, taurine, creatine, and TMAO were all at a lower level in the cell injected animals. In the case of taurine, creatine and TMAO, all of these metabolites were found to be even lower in the intravenous group than the intracerebral group, suggesting an additional contribution of systemic disease to the changes in these markers. It is possible that all of these metabolites simply reflect the presence of 4T1-GFP metastases within the body. However, further individual comparisons between the groups for each metabolite specifically may reveal more subtle differences between the groups. For example, if comparison of hippuric acid between the intravenous and intracerebral/intracardiac models were to reveal a greater effect in the latter models, then this biomarker may reflect the presence of brain metastases specifically.

Interestingly, one metabolite appeared to respond differently in the animals with high brain tumour burden (intracerebral and intracardiac) compared to those with a lower brain metastasis burden (intravenous); citrate was increased in the intravenous group, but reduced in the intracerebral group. At the same time, although a change in citrate was not found in the first two rounds of models for the intracardiac animals vs. naïve, it was found to be lower in the intracardiac group than the intracerebral group. This finding implies that citrate is also decreased in the intracardiac group. In accord with the above findings, citrate was found to be lower in the intracardiac group compared to the intravenous group. These observations suggest that the reduction in citrate may be a specific biomarker of the presence of tumours within the CNS. Comparison of citrate specifically between the intracardiac and naïve group could further validate this finding. Reduction in citrate levels in semen (Kline*, et al.*, 2006) and the prostrate (Kurhanewicz*, et al.*, 2000) have been observed in patients with prostate cancer. However, the mechanism that underpins the variation in citrate within the prostrate is unlikely to be the same as with tumours within the CNS. Production of citrate in the prostrate is unique, occurring in the epithelial cells of the prostate gland, and is an endpoint in metabolism (Costello*, et al.*, 1991). In normal tissue, citrate is an intermediary in the Krebs cycle (Krebs*, et al.*, 1938) which provides a source of energy for cells (Thauer, 1988). A recent study of human stroke patients has shown a reduction in citrate levels in their urine following a stroke. This was identified using a combination of ^{1}H NMR and PLS-DA modelling (Jung*, et al.*, 2011). The authors of this report reasoned that, owing to the limiting oxygen supply following an infarction, less pyruvate will enter the Krebs cycle resulting in reduced citrate levels (Jung*, et al.*, 2011). It has been shown that large solid tumours within the CNS can become hypoxic (Rajendran*, et al.*, 2004). However, the tumours in this study, especially at day 5, are not a solid mass and are, therefore, unlikely to be hypoxic. Normoxic brain tumours, on the other hand, are highly metabolically active, which is

demonstrated by the increased turnover of FDG that is exploited as a diagnostic tool in PET imaging (Stokkel*, et al.*, 1998). Therefore, the reduction in citrate in the urine suggests that the highly metabolically active tumours within the CNS may be taking citrate from the blood supply to use as energy. However, it would seem unlikely that a small CNS tumour could do this. Therefore, the reduction in citrate may reflect a systemic metabolism in response to this CNS tumour. The role of citrate in CNS disorders will further be discussed in the general discussion (Section 7.5).

This hypothesis is supported by the citrate levels across the different models. Citrate levels are consistently higher in the animals with a lower CNS tumour burden, and indeed elevated, rather than reduced, in the animals with predominantly systemic tumour burden. Interestingly, citrate levels were higher in the intracerebrally injected animals compared to the intracardiac injected animals. This observation would also support the above theory, since there is expected to be a higher tumour burden within the CNS in the animals which were injected via the heart than those injected intracerebrally. When the intergroup models were examined, glucose was also found to be at a lower level in the animals with a high CNS tumour burden. This mirrors the findings for citrate, again suggesting that the tumours are highly metabolically active and are utilising more glucose when the tumour load is greater in the CNS compared to the animals with a low CNS tumour burden. Although it did not come out in the second round of modelling, further examining of the loadings did show that the levels of glucose were slightly reduced in the day 5 animals compared to the naïve group, thus supporting the idea that the higher the tumour burden within the CNS the greater the glucose metabolism.

6.4.3. Different tumour cell lines

Intracerebral injection of the MDA231BR cells into SCID animals did not generate models that reached the defined significance, however, a visual separation was evident between the groups. A possible explanation for the lack of significance in the model, could be the slow growth rate of these cells relative to the 4T1 cells, which has been observed in previous studies using this cell line (Serres*, et al.*, 2011). In that study the animals were injected with MDA231BR via the heart and imaged at day 21 to investigate the area of VCAM-1 up-regulation surrounding the tumour. The area of VCAM-1 upregulation was found to be slightly smaller than in animals injected intracardially with 4T1 cells and imaged at day 10 (548 ± 117 μm^2 compared to 680 ± 187 μm^2) (Serres*, et al.*, 2011). This was the reason the later time point of day 10 was chosen for this model in the current study, rather than day 5 as for the 4T1 and B16F10 models. Nevertheless, this time point appears to still be too early for metabolomics to distinguish reliably between the cell-injected animals and the control groups, although the visual separation of the groups suggests that this may not be far off.

Urine from animals injected intracerebrally with B16F10-GFP cells did furnish statistically significant models that could separate the cell-injected animals from both of the control groups (PBS injected and naive). When comparing the cell-injected animals with the naïve animals, several metabolites were common to both the BALB/c cohort and C57Bl/6 animals; taurine, TMAO, creatine and citrate. These metabolites were all at a lower level in the cell-injected animals than naïve mice. Similarly, taurine and creatine were found to be reduced in B16F10-GFP-injected mice compared to the PBS-injected animals. As discussed above (Section 6.4.1 and 6.4.1.2), the reduction in taurine may be a marker of increased metabolism within the CNS tumour. Interestingly, hippuric

acid appears to go in the opposite direction in these models compared to the 4T1-BALB/c models. The other three common metabolites could potentially be used as biomarkers of generic brain metastasis, which is not dependent upon cancer type. However, TMAO and creatine were found to be at a lower level in the animals with a low tumour burden within the CNS. Therefore, a reduction in citrate appears to be the only metabolite change that is consistent across all animal groups studied with a high tumour burden in the CNS. This would enhance the diagnostic potential of metabolomics over current biomarkers available, as it would not be cancer specific (as discussed in Chapter 1 Section 1.8.6).

6.4.4. Chapter Summery

In this chapter it has been shown that through metabolomics analysis of urine, it is possible to diagnose the presence of metastatic tumour cells with the CNS. This technique enables detection of metastatic tumours at an earlier time point than is currently possible by conventional diagnostic techniques, such as Gd-enhanced MRI. The findings in this chapter have also demonstrated that it is possible to distinguish between animals with differing tumour burdens within the CNS and systemic organs using metabolomics. Finally, it has been possible to identify a small number of metabolites that were common between the different models used and which may prove to be specific to brain metastasis. This chapter suggests that a clinical trial of this technique could lead to a novel set of biomarkers for the early diagnosis of brain metastasis.

Chapter 7: General Discussion

7.1. Principal findings of this thesis

1. This thesis sought to discover whether MS could be diagnosed and its stages identified using metabolomics. It was possible to separate RR, SP and PP MS from healthy controls. It was also possible to separate RR-MS from SP-MS.
2. This thesis also explored, using the same technique, whether it was possible distinguish other neurological diseases from each other. Here, it has been shown that MS can be separated out from other neurological diseases such as AD.
3. A further model of neurodegeneration was studied using a combination of ^{1}H NMR spectroscopy and PLS-DA modelling. This demonstrated that CSF can be used to monitor the neurocognitive status within HIV patients.
4. The early diagnostic capabilities of metabolomics were explored by examining different models of brain metastasis. Using metabolomics it is possible to detect the presence of brain metastasis at an earlier stage of disease than is currently possible with other diagnostic methods.

This thesis has demonstrated that with advances in analytical technology, such as higher field strength magnets, it is now possible to distinguish between the two key stages of MS. This technique, ^{1}H NMR coupled to PLS-DA modelling, was also used to investigate the changes in the metabolic profiles of other neurological diseases such as, AD, brain metastasis, and HAD. Metabolomics has proven to be a useful tool in providing earlier or more accurate diagnosis in both animal models and human brain diseases. There are some clear differences in the biomarkers identified in each chapter for each condition. However, there are also some metabolites that appear in the models more consistently, and therefore, I will now discuss these metabolites in more detail

bellow. If these metabolite changes are unrelated, the diagnostic capabilities of these models are not devalued as examining the patient's clinical history would enable the patient to receive the correct diagnosis. For example, a diagnosis of brain metastasis would only be possible if the patient had a primary tumour. I will also discuss any future directions this work could be taken in and the possible problems that need to be addressed in the study design.

7.2. Biofluids used in this thesis

The biofluids used in this thesis included urine, blood (plasma or serum) and CSF. Different biofluids generated more robust models depending on the particular study. From the animal results in this thesis it is interesting to note that for the studies on the Cr-EAE animals, more robust PLS-DA models were generated from the plasma of the animals. However, this was not the case for the cancer metastasis models. Here, although the plasma did generate some statistically significant models, the urine was able to generate more robust models at an earlier time-point. It has been reported that urine provides an average of the metabolite composition over time (Giovannoni*, et al.*, 1998), whereas plasma provides a snapshot of the metabolism at the time of sample acquisition (Griffin*, et al.*, 2004a). Therefore, small changes in the metabolite composition may be enhanced in the urine of the animals.

In the case of the Cr-EAE animals, there was a confounding problem was dehydration owing to the nature of the disease in which animals become less mobile and take less daily water. Prior to killing these animals 1 mL of saline was administered sub-cutaneously in order to promote urine production but prolonged dehydration is likely to have had an appreciative effect on metabolism. Studies have shown that variations in diet and hydration levels effect the urine composition far more than the plasma composition (Walsh*, et al.*, 2006). Therefore, for future studies including any studies aimed at finding

type-2 biomarkers for clinical trials, the animals should be allowed to urinate naturally. In order to address this dehydration problem the animals could be hand fed for a longer time period then was performed in this study. However, the extra handling required to do this would increase the stress on the mice. This was not done in the current study as during peak disease it was considered ethically unsound to house the animals in special metabolic cages. Therefore any potential type-2 biomarkers for the peak disease will have to be identified in blood from the animals. This may in fact be the most appropriate biofluid as the serum obtained from the MS patients also generated more robust PLS-DA models, formally indicating that urine is not always the best option irrespective of the problems induced by dehydration in the animals. It was for this reason that only serum was explored when comparing MS to AD.

The rationale for using CSF in the HAD study was very different. In this case, any set of metabolites identified in the CSF could potentially be used without the need for extracting the CSF sample, using magnetic resonance spectroscopy (MRS). Studies have demonstrated that it is possible to use MRS to follow metabolite changes in the CNS (Barker*, et al.*, 1994; Bonavita*, et al.*, 1999; Bonvento*, et al.*, 2002). Barker *et al.* reported that, using MRS, it was possible to measure the reduction of N-acetyl aspartate and an increase in lactate in the CNS of stroke patients. Therefore, it would be interesting to attempt some MRS of patients suffering from HAD to see if the same spectral regions identified in Chapter 5 can be detected using MRS. The problem with MRS when comparing it to NMR is the reduction in spectral resolution. This is a technological problem with two elements. Firstly, human MRI machines, which are needed for MRS, have a lower magnetic field strength, typically 1.5-7 T than NMR machines, which can reach field strengths of 20 T or more. Secondly, it is possible to get the RF coil which records the spectrum significantly closer to the sample in high resolution NMR compared to MRS. This considerably increases the signal to

noise ratio of the acquired spectrum and thus the resolution is improved (Atalar*, et al.*, 1996). These two problems will always be an issue with human MRI. Even though it has been reported that high magnetic field strengths have little effect on the body (Formica*, et al.*, 2004), the gradients used in the sequences for imaging or voxel selection can induce electrical currents within the nerves of patients (Schaefer*, et al.*, 2000). This same phenomenon, where electrical currents can be induced in the nerves, can occur if the patient moves in the magnetic field (Schaefer*, et al.*, 2000). This movement includes moving the patient in and out of the magnetic field prior to a scan. This induction of electrical currents in the nerves results in a painful sensation for the patient (Budinger*, et al.*, 1991; Den Boer*, et al.*, 2002) and is more of a problem in higher field magnets (Irnich*, et al.*, 1995). However, the technological advances associated with MRI are far from over, and developments such as the introduction of cryoprobes will assist in improving the resolution of MRS (Ratering*, et al.*, 2008). Therefore, the demonstration that it is possible to differentiate between different neurocognitive states using CSF could lead to a simple MRS diagnostic procedure for HAD and, fundamentally, NMR on biofluids enables high throughput screening (HTS).

There are different merits to each biofluid used in this thesis and the selection of what biofluid to study should depend on what information is required from the individual study. However, there are some general points which is worth considering when planning an experiment. Urine is by far the easiest biofluid to sample as it just requires the patient to urinate in a pot. However, the time before the sample is frozen should be carefully considered to prevent degradation of the sample. Blood sampling is not particularly tricky and therefore, this biofluid can be obtained with relative ease. Plasma is preferable to serum due to the fact that serum samples can vary depending on the clotting time of the sample. CSF is the hardest biofluid to obtain as it requires a lumbar

puncture which can have side effects (as described in section 5.4). However, CSF has one major advantage to the other biofluids. This advantage is that the CSF metabolite composition is a more accurate picture of the metabolism with the CNS of the patient as other factors such as gut metabolism does not directly affect the CSF as it does with plasma and urine.

7.3. Biomarker technology

The idea that HTS could enable faster and cheaper methods in developing drugs and diagnostic tools has been reported in the literature for around sixty years (as discussed by Persidis, 1998). Initially, in the 1950s, the primary focus of this research centred on developing anti-tumour agents. The National Cancer Institute in America began collecting tumour cell lines in order to trial new cancer therapies using HTS (as discussed by Gura, 1997). In 1978, a high throughput screen was developed for detecting abnormal secretions in milk from cows. This is one of the earliest examples of HTS being used to detect abnormalities in mammals (Kitchen*, et al.*, 1978). Since then there has been a marked expansion in the number of papers demonstrating HTS as a means of diagnosing different diseases, including screens for DNA mutations, metabolic changes and protein abnormalities (Ellis*, et al.*, 2006; Schweitzer*, et al.*, 2002; Shortreed*, et al.*, 2000). These high throughput screens are beginning to find their way into clinical practice, but clinicians appear to be reluctant to adopt them. Given the results in this thesis and those of others it is hard to explain why this approach has not generated traction within the clinic. An explanation for this may lie in the poor understanding of the models generated and a lack of agreement between disciplines. The generation of standard operating procedures and the determination of approaches that will enable biofluid from different centres to be compared, would greatly improve the situation.

A recent HTS study of 1415 blood samples from patients with liposomal storage disease, which effects 1 in 7000 births (Meikle*, et al.*, 1999), has been carried out. The screen examined abnormalities in the proteins within the blood and managed to predict with a 99% accuracy which liposomal disease the patient had (Fuller*, et al.*, 2011). This screen could be hugely beneficial in identifying these disorders in newborn children. The authors of this report highlight the main problem with HTS, which is the availability of the technology to perform the analytical tests. This is relevant to the technology used in this thesis, as discussed previously (Chapter 1 Section 1.3.2) the cost of running a ^{1}H NMR spectrum on a biofluid is relatively low, around £0.60 a sample (Griffin*, et al.*, 2004b). However, the initial cost of the machine is relatively high, which and can now be several millions of pounds. Therefore, the use of 'omics' techniques for disease diagnostics in clinics has not been widely adopted (Botros*, et al.*, 2008). However, if this is compared to the disappointing results achieved by expensive GWAS studies, the cost of HTS by NMR looks much more attractive.

This leads to the question: is high resolution ^{1}H NMR the ideal tool to use if metabolomics is ever to be used in the clinic in the field of disease diagnostics? The obvious competitor would be mass spectrometry. As discussed in Chapter 1 Section 1.3.2.1 of this thesis, mass spectrometry is already widely used in the field of metabolomics. Mass spectrometers are generally less expensive than high field strength NMR magnets, although the initial cost can still be high (Dettmer*, et al.*, 2007), estimated to be between £250,000 and £450,000 (Vogeser*, et al.*, 2008). There are, however, several drawbacks to the use of mass spectrometry. The primary problem is the amount of sample preparation required for mass spectrometry samples: normally there is a separation process, such as HPLC or gas chromatography, prior to the measurement of the mass spectrum (Bedair*, et al.*, 2008; Dunn*, et al.*, 2005). The samples often need to be lyophilised or treated with chemicals in order to ensure they fly in the

mass spectrometer (Lindon*, et al.*, 2007; Want*, et al.*, 2005). A further issue is the estimated running cost of mass spectrometry. The cost of running a single analysis on a mass spectrometer is also estimated to be slightly higher than NMR, around £2 to £6, depending on the type of mass spectrometry performed (Vogeser*, et al.*, 2008).

Due to the advances in automation, a high field strength NMR machine can run an estimated 300 samples per day (Holmes*, et al.*, 2002). Therefore, the initial investment in the cost of an NMR machine would be useful if metabolomics could be used to get patients onto the correct treatment at an earlier time point. With the development of type-2 biomarkers, this technique could also speed up and therefore save money in any future drug trials, as discussed in Chapter 1 Section 1.2.1 (Frank*, et al.*, 2003; Lesko*, et al.*, 2001). The use of mass spectrometry could be a useful tool to confirm the findings within this thesis, however, due to the increased cost in both monetary terms and time associated with mass spectrometry, NMR would appear to be the most effective tool for future HTS of metabolic changes.

7.4. Limitations of metabolomics

The use of ^{1}H NMR coupled with PLS-DA modelling to probe the metabolic state has been sown to be a highly sensitive technique. Indeed, as discussed previously (Chapter 1 Section 1.4.4), it is possible to distinguish differences between related rodent species (Griffin*, et al.*, 2000). While the sensitivity of this method has its advantages, it can also produce major confounding factors. One key problem could be the difference between the metabolic profile of males and females. A study has demonstrated that using both urine and plasma it is possible to distinguish between sexes using metabolomics (Kochhar*, et al.*, 2006). The authors reported that there were several metabolites which underpinned these differences, such as lipoproteins, choline, taurine, lactate,

and glycine. This study also revealed that the metabolomic profile of humans varied with age (Kochhar*, et al.*, 2006). The MS samples described in Chapter 3 contained both male and female MS patients and a spread of ages. These patients were modelled separately according to their sex, but there was no significant improvement to the models (data not shown). With these issues in mind the control cohort for this population was carefully sex- and age-matched in order not to bias the control groups. As demonstrated in Chapter 3 of this thesis, despite the confounds of age and sex within the MS population it was possible to distinguish between patients who had RR-MS and SP-MS, and also to differentiate three subtypes of MS from a healthy control group. This indicates that the metabolite changes arising from the disease override any metabolite change as a result of sex or age. In fact all the patients in Chapter 3 were on different drug trials. A proportion of the RR patients were taking part in a double blind phase III placebo controlled trial for cladrabine and therefore, there was no information on which patients were receiving the drug or the placebo. Even with this confound, which arises from the breakdown of different drugs in the body (Bollard*, et al.*, 2005), the metabolite changes caused by the different disease states were greater than any drug induced effect.

Another potential problem in the human models is the ethnicity of the sample population. MS is predominantly a disease which affects the Western world (Noseworthy*, et al.*, 2000), although there are some incidences in Asia and Latin America (Chong*, et al.*, 2009; Románb, 2006), and therefore this present a difficulty with using metabolomics as tool for disease diagnostics. There are several reports of inter-racial differences in the metabolomic profile of humans suffering from the same disease (Hashim AbdAlla*, et al.*, 2011; Sugimoto*, et al.*, 2010). In a study of patients with cholangiocarcinoma, Hashim *et al.* reported a significant reduction in the levels of bile phosphatidylcholine in patients from Egypt when compared to patients from the UK (Hashim AbdAlla*, et al.*, 2011).

This confound was observed in Chapter 6 Section 6.3.4 of this thesis, when attempts were made at comparing the animals which were injected intracerebrally with different cancer cell lines to the original 4T1-GFP models. This potential confound needs to be kept in mind for any future large scale human studies, however as mentioned above the metabolite changes arising from the disease appear to be stronger than the problems of gender, age and drug regime. However, these models are relatively simple to generate and could be modified for different ethnicities.

7.5. Biology of neurodegenerative diseases

One metabolite which seemed to vary constantly was citrate. In the Cr-EAE animals the levels of citrate in the urine were lower at day 10 compared to the naïve animals. Citrate also appeared to be at a lower concentration in the urines obtained from the cancer models. Studies have also demonstrated that following a brain injury, levels of citrate are lower in urine taken from stroke patients (Jung*, et al.*, 2011). The lowering of the citrate in the Cr-EAE animals could be attributable to muscle wasting and general loss of weight (Connor*, et al.*, 2004) demonstrated by these animals during the disease timecourse (Chapter 3 Section 3.3.1). However, this muscle wasting was not observed in any of the models of brain metastasis (Chapter 6 Section 6.3.2, 6.3.3, and 6.3.4) as the weights of the animals actually slightly increased over the disease time course. Jung *et al.* did not report whether the patients in their report suffered from a significant weight loss or muscle wasting. They put the decrease in citrate down to the reduction of pyruvate entering the Krebs cycle due to the increase in anaerobic glycosylation. As discussed in Chapter 1 Section 1.9, one of the common aspects to the neurodegeneration seen in all the brain diseases described in this thesis is the activation of microglia. It has

been demonstrated by use of PK11195 that microglia become activated following a stroke (Gerhard*, et al.*, 2005).

This suggests that perhaps the reduction in citrate found in the urine may be a marker of the microglia activation. A study has reported that the excessive production of nitric oxide, results in the up-regulation of the iron regulatory protein (IRP) in the microglia (Chénais*, et al.*, 2002). The increase in nitric oxide production in microglia is frequently associated with neurological disease (González-Scarano*, et al.*, 1999; Hirsch, 2000; Knott*, et al.*, 2000; Liberatore*, et al.*, 1999; Nakajima*, et al.*, 1998). IRP-1 is an aconitase and therefore converts citrate into isocitrate within the cytosol of cells (Chénais*, et al.*, 2002), which is a key step in the Krebs cycle (Krebs*, et al.*, 1938). Thus if IRP-1 is activated by nitric oxide in sufficient quantities and there is not an increase in pyruvate entering the Krebs cycle, it would be expected a decrease in citrate levels globally in the body to maintain the increase in isocitrate production caused by the up-regulation of IRP-1. Thus microglia activation could explain the observed decrease in citrate levels in the urine. However, nitric oxide has also been shown to inhibit the aconitase activity of IRP-1 and so this may not fully explain the citrate acid reduction.

It has also been reported that neurons lack the enzymes (pyruvate carboxylase and malic enzyme) required for the conversion of pyruvate or lactate into a source of carbon atoms (Bukato*, et al.*, 1995; Frenkel, 1972; Kurz*, et al.*, 1993; Qu*, et al.*, 2000), which is required for the Krebs cycle (Krebs*, et al.*, 1938). These carbon atoms are vital for replenishing the brain's supply of neurotransmitters such as glutamate and GABA (Cohen, 1997). Glutamate has been shown to be released from activated microglia following an increase in the cytokine TNF-α (Barger*, et al.*, 2001; Takeuchi*, et al.*, 2006). Therefore, the neurons must recruit the intermediates for the Krebs cycle to maintain brain

function. Thus, citrate would be drawn out of the circulation to replenish the glutamate supply, and therefore the level of citrate will be reduced in the urine. Interestingly there is one exception to this which is that citrate is at a higher level in the day 38 Cr-EAE animals compared to the CFA animals at the same time point. It would be expected that the microglia are very active during this phase of disease as the animals are in a relapse phase. However, there is also significant cachexia which could account for this difference in the citrate levels at this time point (Connor*, et al.*, 2004).

Interestingly, there appeared to be a consistent pattern in the levels phosphocholine in the animal models. Phosphocholine levels were elevated just prior or during the acute phases of disease in the Cr-EAE animals (days 10, 14 and 38). This elevation of phosphocholine in was also observed in the plasma of the brain metastasis. In the Cr-EAE this increase in phosphocholine may be as result of the demyelination process occurring in the lesions (discussed in Chapter 3 Section 3.4.3). Phosphocholine levels have been shown to increase in the blood of patients with a range of different tumours (Ackerstaff*, et al.*, 2003). This elevation in phosphocholine is reportedly due to the disruption between the choline uptake required for the synthesis of the cell membranes (Kwee, 2008). Both of these mechanisms involve disruptions to the cell membrane and therefore perhaps an elevation of phosphocholine in the blood is indicative of this cell membrane disruption.

TMAO levels are closely linked to the choline levels within the body. Choline is metabolised within the gut flora to TMA (Rak*, et al.*, 2011), this is then subsequently metabolised further to TMAO as described previously (3.3.3). Therefore an increase in phosphocholine or choline coupled to a reduction of TMAO could suggest a disruption in this metabolism pathway.

All of the above discussion has considered the presence of the brain injury as causing a direct effect on the metabolism. However, it could also be possible that the metabolite variation within these diseases arises from the systemic response to the brain lesions. It has been demonstrated that following a brain injury nuclear factor-κB, which regulates the expression of a wide array of immune and inflammatory genes, is activated in the liver and other organs (Campbell*, et al.*, 2008). While these systemic responses appear to coordinate immunological responses to brain injury, the diversity of the genes that are observed to have been upregulated suggests that the peripheral response to brain injury might have much wider effects on other processes including metabolic changes. This has not been investigated. Thus the source of the metabolite changes detected in this thesis, which would, at first glance seem to stem from local changes in the brain, could be, generated by other organs in response to brain pathology.

7.6. Future Directions

7.6.1. Multiple Sclerosis

The results in this thesis demonstrate that it is possible to differentiate between MS patients from control groups, and it is also possible to distinguish between RR and SP patients using metabolomics. All the samples obtained in this study came from the John Radcliffe Hospital. In order to fully validate these models as type-0 biomarkers for MS, and therefore their use as a diagnostic tool, a multicentre trial would need to be established. If such a trial were to be performed, then the variation in the NMR datasets run at different time must be considered Another issue encountered during the study of the MS serum was the small shift and line broadening observed in the TSP resonance. This variation in the TSP resonance was attributed to the TSP binding to the serum proteins (Kriat*, et al.*, 1992). The anomeric β-glucose signal which could be

used for the scaling of the spectra (as discussed in Chapter 4 Section 4.4) could also be used to re-reference the spectra. Therefore, any future studies carried out in this area could be scaled and referenced to a known concentration of an internal metabolite standard. This would overcome the problems encountered in my studies.

The biomarkers described in this thesis are type-0 biomarkers, however, they could potentially be used as type-II biomarkers during a clinical trial. This would be especially relevant to any new drugs which attempt to delay the transition of patients from RR-MS to SP-MS. This could lead to the reduction in cost of any future drug trials in MS as the end-point of the trial would be better defined and more measurable (as discussed in Chapter 1 Section 1.2.1). Further prospective work is required to follow metabolite changes in a cohort of patients over time.

Chapter 4 of this thesis demonstrated that it was possible to distinguish between two different types of neurodegeneration, MS and AD. It would be beneficial to explore whether it is possible to separate out MS patients from those with other neurological disorders with a greater degree of accuracy than has been achieved in the past ('t Hart*, et al.*, 2003). It would be useful to explore the use of metabolomics to identify a neurological disorders which are associated with immune mediated disease to the CNS. These diseases could include neuromyelitis optica and Devic's disease both of which involve demyelination within the CNS caused by the immune system. It would be especially beneficial to separate patients with CIS who will go on to develop MS and those who will not. This is vital, as the sooner treatment is started with MS, the greater the potential effect in modifying the disease course (Kuhle*, et al.*, 2011).

7.6.2. HIV-associated dementia

The metabolites identified in Chapter 5 of this thesis which caused the separation between the different neurocognitive states were predominantly energy related metabolites (discussed in Chapter 5 Section 5.4.2). Studies have shown that by investigating multiple biofluids within a patient it is possible to discover more about the disease pathology. At present it is unclear whether these metabolites varied in a consistent or inconsistent pattern within other biofluids in the body. Studies investigating these issues would allow a better understanding of why the metabolites are changing within the CNS.

The HIV samples were acquired for a large multicentre research project and as such other groups are focusing on investigating the genetic, proteomic and lipidomic variations within these samples. Studies have shown that using a combination of metabolic data and genetic data it is possible to discover which genes were responsible for variation in the metabolites (Waterman*, et al.*, 2010). In this study the authors demonstrated that it was possible to detect the effects of acute phenobarbital poisoning in rats using PLS modelling. Waterman *et al.* reported that there was a link between an increase in succinate, identified using both ^{1}H NMR and mass spectrometry, with an increase in expression of the enzyme 5-aminovulinate (Waterman*, et al.*, 2010). This enzyme catalyses the reaction between succinyl coenzyme A and glycine which is an important step in the production of haem (Ades, 1990). This increase in haem production is consistent with acute exposure to phenobarbital due to an increase in P450 enzyme activity (Kakizaki*, et al.*, 2003). The authors also identified a link between the plasma levels of lipids and an increase in the hepatic lipoprotein lipase. This enzyme is not normally expressed in the liver of an adult rat, however, it can be expressed following exposure to a toxin such as fenofibrate (Staels*, et al.*, 1992). Therefore, combining the other ‘omic’ data from other

studies could provide a powerful tool in identifying the underlying disease mechanisms of HAD which are causing the changes in the metabolite composition in the CSF.

7.6.3. Cancer Metastasis

The results from Chapter 6 of this thesis demonstrate that using a combination of ^{1}H NMR spectroscopy and PLS-DA modelling it is possible to distinguish between different models of brain metastasis. However, it was not possible to separate out the SCID animals injected with MDA231BR intracerebrally from both the control groups. There was, however, a significant visual separation between these models in the PLS plots (Chapter 6 Section 6.3.4.1). As discussed previously (Chapter 6 Section 6.3.4), these cells are slower growing than the 4T1-GFP cells (Serres*, et al.*, 2010). Therefore, any future work should study this model in more detail, including later time points, in order to determine at which point it is possible to separate out the cell injected animals from the control groups.

The results from Chapter 6 strongly support the need for a trial within human metastatic patients. The results demonstrate that urine appears to generate more robust models for early cancer diagnosis, however, studies have demonstrated that the urine composition of humans varies during the day (Giovannoni*, et al.*, 1998; Saude*, et al.*, 2007). It has been shown that neopterin can vary as much as 50% during a 24 hour period (Auzéby*, et al.*, 1988). Therefore, when obtaining the samples, care must be that the urine is collected uniformly. To this end, it would be advisable to collect the urine mid-stream first thing in the morning. This would hopefully eliminate any dietary variations in the sample population. In order for this to become a diagnostic test NMR spectroscopy would need to be performed on multiple days. This would result in the need to scale the spectra to an internal standard within the spectra (as

discussed above 7.6.1). Glucose would not be suitable here as the expression of glucose in urine is not high in patients with normal kidney functions (Shaykhutdinov*, et al.*, 2009). Therefore, a simple creatinine test should be performed on the urine of these patients in order to provide a known internal standard. It would also be useful to acquire a matching set of serum samples from these patients in order to confirm any results found from the urine study.

7.7. Summary

In conclusion, this thesis demonstrates that metabolomics can be used to diagnose and differentiate between RR v SP MS. The results describe the type 0 biomarkers which underpin these changes. The results also describe a set of metabolites which can be monitored in a clinically relevant model of MS. These metabolites could potentially be used to identify type 2 biomarkers for future clinical trials. The results also show that it is possible to distinguish between different neurodegenerative diseases using a combination of ^{1}H NMR and PLS-DA modelling on different biofluids samples. Finally, this thesis has demonstrated that it is possible to detect the presence of brain metastasis at an earlier stage of disease than is possible using current diagnostic tools.

Bibliography

't Hart BA, Vogels JTWE, Spijksma G, Brok HPM, Polman C, van der Greef J. H-1-NMR spectroscopy combined with pattern recognition analysis reveals characteristic chemical patterns in urines of MS patients and non-human primates with MS-like disease. Journal of the Neurological Sciences. 2003; **212**(1-2): 21-30.

't Hart BA, Gran B, Weissert R. EAE: imperfect but useful models of multiple sclerosis. Trends in Molecular Medicine. 2011; In Press, Corrected Proof.

Abbott NJ, Patabendige AAK, Dolman DEM, Yusof SR, Begley DJ. Structure and function of the blood-brain barrier. Neurobiology of disease. 2010; **37**(1): 13-25.

Ackerstaff E, Glunde K, Bhujwalla ZM. Choline phospholipid metabolism: A target in cancer cells? Journal of cellular biochemistry. 2003; **90**(3): 525-33.

Acosta ML, Fletcher EL, Azizoglu S, Foster LE, Farber DB, Kalloniatis M. Early markers of retinal degeneration in rd/rd mice. Mol Vis. 2005; **11**: 717-28.

Ades IZ. Heme production in animal tissues: the regulation of biogenesis of delta-aminolevulinate synthase. The International journal of biochemistry. 1990; **22**(6): 565.

Ahmed Z, Gveric D, Pryce G, Baker D, Leonard JP, Cuzner ML. Myelin/Axonal Pathology in Interleukin-12 Induced Serial Relapses of Experimental Allergic Encephalomyelitis in the Lewis Rat. Am J Pathol. 2001; **158**(6): 2127-38.

Akiyama H, Barger S, Barnum S, Bradt B, Bauer J, Cole GM, *et al.* Inflammation and Alzheimer's disease. Neurobiology of Aging. 2000; **21**(3): 383-421.

Alger JR, Frank JA, Bizzi A, Fulham MJ, DeSouza BX, Duhaney MO, *et al.* Metabolism of human gliomas: assessment with H-1 MR spectroscopy and F-18 fluorodeoxyglucose PET. Radiology. 1990; **177**(3): 633-41.

Aliouat-Denis C-M, Chabé M, Demanche C, Aliouat EM, Viscogliosi E, Guillot J, *et al.* Pneumocystis species, co-evolution and pathogenic power. Infection, Genetics and Evolution. 2008; **8**(5): 708-26.

Aminoff MJ, Goodin DS. Visual evoked potentials. Journal of Clinical Neurophysiology. 1994; **11**(5): 493.

Andersson M, Alvarez-Cermeno J, Bernardi G, Cogato I, Fredman P, Frederiksen J, *et al.* Cerebrospinal fluid in the diagnosis of multiple sclerosis: a consensus report. Journal of Neurology, Neurosurgery & Psychiatry. 1994; **57**(8): 897.

Aran ´ bar N, Ott KH, Roongta V, Mueller L. Metabolomic analysis using optimized NMR and statistical methods. Analytical Biochemistry. 2006; **355**(1): 62-70.

Arnáiz E, Almkvist O. Neuropsychological features of mild cognitive impairment and preclinical Alzheimer's disease. Acta Neurologica Scandinavica. 2003; **107**: 34-41.

Arnold MA. New developments and clinical impact of noninvasive monitoring. New York, NY: John Wiley & Sons; 1996. p. 631–47.

Arnold SM, Patchell RA. Diagnosis and management of brain metastases. Hematology/oncology clinics of North America. 2001; **15**(6).

Aslakson C, Miller F. Selective events in the metastatic process defined by analysis of the sequential dissemination of subpopulations of a mouse mammary tumor. Cancer Res. 1992; **52**(6): 1399 - 405.

Association AP, DSM-IV. APATFo. Diagnostic and statistical manual of mental disorders: DSM-IV-TR: American Psychiatric Publishing, Inc.; 2000.

Atalar E, Bottomley PA, Ocali O, Correia LCL, Kelemen MD, Lima JAC*, et al.* High resolution intravascular MRI and MRS by using a catheter receiver coil. Magnetic resonance in medicine. 1996; **36**(4): 596-605.

Atkinson AJ. Principles of clinical pharmacology: Academic Pr; 2007.

Auzéby A, Bogdan A, Krosi Z, Touitou Y. Time-dependence of urinary neopterin, a marker of cellular immune activity. Clinical chemistry. 1988; **34**(9): 1866.

Aylward EH, Henderer J, McArthur JC, Brettschneider P, Harris G, Barta P*, et al.* Reduced basal ganglia volume in HIV 1 associated dementia. Neurology. 1993; **43**(10): 2099.

Baker D, O'Neill JK, Gschmeissner SE, Wilcox CE, Butter C, Turk JL. Induction of chronic relapsing experimental allergic encephalomyelitis in Biozzi mice. J Neuroimmunol. 1990; **28**(3): 261-70.

Baker D, Butler D, Scallon BJ, O'Neill JK, Turk JL, Feldmann M. Control of established experimental allergic encephalomyelitis by inhibition of tumor necrosis factor (TNF) activity within the central nervous system using monoclonal antibodies and TNF receptor-immunoglobulin fusion proteins. European Journal of Immunology. 1994; **24**(9): 2040-8.

Baker JR, Chaykin S. The Biosynthesis of Trimethylamine-N-Oxide. Journal of Biological Chemistry. 1962; **237**(4): 1309-13.

Balashov KE, Rottman JB, Weiner HL, Hancock WW. CCR5+ and CXCR3+ T cells are increased in multiple sclerosis and their ligands MIP-1α and IP-10 are expressed in demyelinating brain lesions. Proceedings of the National Academy of Sciences. 1999; **96**(12): 6873.

Bales JR, Higham DP, Howe I, Nicholson JK, Sadler PJ. Use of high-resolution proton nuclear magnetic resonance spectroscopy for rapid multi-component analysis of urine. Clinical chemistry. 1984; **30**(3): 426.

Bansal AK, Mactutus CF, Nath A, Maragos W, Hauser KF, Booze RM. Neurotoxicity of HIV-1 proteins gp120 and Tat in the rat striatum. Brain research. 2000; **879**(1-2): 42-9.

Barbeau A, Donaldson J. Zinc, Taurine, and Epilepsy. Arch Neurol. 1974; **30**(1): 52-8.

Barger SW, Harmon AD. Microglial activation by Alzheimer amyloid precursor protein and modulation by apolipoprotein E. Nature. 1997; **388**(6645): 878-81.

Barger SW, Basile AS. Activation of microglia by secreted amyloid precursor protein evokes release of glutamate by cystine exchange and attenuates synaptic function. Journal of Neurochemistry. 2001; **76**(3): 846-54.

Barker PB, Gillard JH, van Zijl PC, Soher BJ, Hanley DF, Agildere AM, *et al.* Acute stroke: evaluation with serial proton MR spectroscopic imaging. Radiology. 1994; **192**(3): 723-32.

Barkhof F, Filippi M, Miller DH, Scheltens P, Campi A, Polman CH, *et al.* Comparison of MRI criteria at first presentation to predict conversion to clinically definite multiple sclerosis. Brain. 1997; **120**(11): 2059.

Barnes DE, Yaffe K. The projected effect of risk factor reduction on Alzheimer's disease prevalence. The Lancet Neurology. 2011; **10**(9): 819-28.

Baschnagel A, Wolters PL, Camphausen K. Neuropsychological testing and biomarkers in the management of brain metastases. Radiation Oncology. 2008; **3**(1): 26.

Baxter AG. The origin and application of experimental autoimmune encephalomyelitis. Nature Reviews Immunology. 2007; **7**(11): 904-12.

Beatty WW, Salmon DP, Butters N, Heindel WC, Granholm EL. Retrograde amnesia in patients with Alzheimer's disease or Huntington's disease. Neurobiology of Aging. 1988; **9**: 181-6.

Bedair M, Sumner LW. Current and emerging mass-spectrometry technologies for metabolomics. TrAC Trends in Analytical Chemistry. 2008; **27**(3): 238-50.

Benveniste EN. Role of macrophages/microglia in multiple sclerosis and experimental allergic encephalomyelitis. Journal of Molecular Medicine. 1997; **75**(3): 165-73.

Berchtold NC, Cotman CW. Evolution in the Conceptualization of Dementia and Alzheimer's Disease: Greco-Roman Period to the 1960s. Neurobiology of Aging. **19**(3): 173-89.

Beutler E, Sipe J, Romine J, Koziol J, McMillan R, Zyroff J. The treatment of chronic progressive multiple sclerosis with cladribine. Proceedings of the National Academy of Sciences. 1996; **93**(4): 1716.

Biancone L, Araki M, Araki K, Vassalli P, Stamenkovic I. Redirection of tumor metastasis by expression of E-selectin in vivo. The Journal of experimental medicine. 1996; **183**(2): 581.

Bielekova B, Martin R. Development of biomarkers in multiple sclerosis. Brain. 2004; **127**(7): 1463-78.

Blasco H, Corcia P, Moreau C, Veau S, Fournier C, Vourc'h P, *et al.* ^{1}H-NMR-Based Metabolomic Profiling of CSF in Early Amyotrophic Lateral Sclerosis. PLoS ONE. 2010; **5**(10): e13223.

Bleakney W, Gould AJ. The relative abundance of hydrogen isotopes. Physical Review. 1933; **44**(4): 265.

Bloch F, Hansen W, Packard M. Nuclear induction. Physical Review. 1946; **70**(7-8): 460-74.

Bloch F. Method and Means for Chemical Analysis. Google Patents; 1955.

Blount BC, Milgram KE, Silva MJ, Malek NA, Reidy JA, Needham LL*, et al.* Quantitative Detection of Eight Phthalate Metabolites in Human Urine Using HPLC−APCI-MS/MS. Analytical chemistry. 2000; **72**(17): 4127-34.

Blow N. Metabolomics: Biochemistry's new look. Nature. 2008; **455**(7213): 697-700.

Bobholz JA, Rao SM. Cognitive dysfunction in multiple sclerosis: a review of recent developments. Current Opinion in Neurology. 2003; **16**(3): 283.

Bollard ME, Stanley EG, Lindon JC, Nicholson JK, Holmes E. NMR-based metabonomic approaches for evaluating physiological influences on biofluid composition. NMR in Biomedicine. 2005; **18**(3): 143-62.

Bonavita S, Di Salle F, Tedeschi G. Proton MRS in neurological disorders. European Journal of Radiology. 1999; **30**(2): 125-31.

Bonetta L. Protein-protein interactions: Interactome under construction. Nature. 2010; **468**(7325): 851-4.

Bonvento G, Sibson N, Pellerin L. Does glutamate image your thoughts? Trends in neurosciences. 2002; **25**(7): 359-64.

Borgelt B, Gelber R, Kramer S, Brady LW, Chang CH, Davis LW*, et al.* The palliation of brain metastases: final results of the first two studies by the Radiation Therapy Oncology Group. International Journal of Radiation Oncology* Biology* Physics. 1980; **6**(1): 1-9.

Bos PD, Xiang HFZ, Nadal C, Shu W, Gomis RR, Nguyen DX*, et al.* Genes that mediate breast cancer metastasis to the brain. Nature. 2009; **459**(7249): 1005-9.

Bot JCJ, Barkhof F. Differentiation of multiple sclerosis from other inflammatory disorders and cerebrovascular disease: value of spinal mr imaging1. Radiology. 2002; **223**(1): 46.

Botros L, Sakkas D, Seli E. Metabolomics and its application for non-invasive embryo assessment in IVF. Molecular Human Reproduction. 2008; **14**(12): 679-90.

Bottiggi KA, Chang JJ, Schmitt FA, Avison MJ, Mootoor Y, Nath A*, et al.* The HIV Dementia Scale: predictive power in mild dementia and HAART. Journal of the Neurological Sciences. 2007; **260**(1-2): 11-5.

Brindle JT, Antti H, Holmes E, Tranter G, Nicholson JK, Bethell HWL*, et al.* Rapid and noninvasive diagnosis of the presence and severity of coronary heart disease using 1 H-NMR-based metabonomics. Nature Medicine. 2002; **8**(12): 1439-45.

Brinkmann V, Billich A, Baumruker T, Heining P, Schmouder R, Francis G*, et al.* Fingolimod (FTY720): discovery and development of an oral drug to treat multiple sclerosis. Nature Reviews Drug Discovery. 2010; **9**(11): 883-97.

Brodt P, Fallavollita L, Bresalier RS, Meterissian S, Norton CR, Wolitzky BA. Liver endothelial E selectin mediates carcinoma cell adhesion and promotes liver metastasis. International Journal of Cancer. 1997; **71**(4): 612-9.

Brønnum-Hansen H, Koch-Henriksen N, Stenager E. Trends in survival and cause of death in Danish patients with multiple sclerosis. Brain. 2004; **127**(4): 844-50.

Brookmeyer R, Johnson E, Ziegler-Graham K, Arrighi HM. Forecasting the global burden of Alzheimer's disease. Alzheimer's and Dementia. 2007; **3**(3): 186-91.

Brown A, McFarlin D. Relapsing experimental allergic encephalomyelitis in the SJL/J mouse. Laboratory investigation; a journal of technical methods and pathology. 1981; **45**(3): 278.

Brown SC, Kruppa G, Dasseux J-L. Metabolomics applications of FT-ICR mass spectrometry. Mass Spectrometry Reviews. 2005; **24**(2): 223-31.

Brownell AL, Jenkins BG, Elmaleh DR, Deacon TW, Spealman RD, Isacson O. Combined PET/MRS brain studies show dynamic and long-term physiological changes in a primate model of Parkinson disease. Nature Medicine. 1998; **4**(11): 1308-12.

Budinger TF, Fischer H, Hentschel D, Reinfelder HE, Schmitt F. Physiological effects of fast oscillating magnetic field gradients. Journal of computer assisted tomography. 1991; **15**(6): 909.

Bukato G, Kochan Z, Świerczyński J. Different regulatory properties of the cytosolic and mitochondrial forms of malic enzyme isolated from human brain. The International Journal of Biochemistry & Cell Biology. 1995; **27**(10): 1003-8.

Bundy D, Cooper E. *Trichuris* and Trichuriasis in Humans. Advances in Parasitology. 1989; **28**: 107-73.

Burns A, Jacoby R, Levy R. Psychiatric phenomena in Alzheimer's disease. III: Disorders of mood. The British Journal of Psychiatry. 1990; **157**(1): 81.

Burt MG, Gibney J, Ho KKY. Characterization of the metabolic phenotypes of Cushing's syndrome and growth hormone deficiency: a study of body composition and energy metabolism. Clinical endocrinology. 2006; **64**(4): 436-43.

Cairncross JG, Kim JH, Posner JB. Radation therapy for brain metastases. Annals of neurology. 1980; **7**(6): 529-41.

Cammer W, Bloom BR, Norton WT, Gordon S. Degradation of basic protein in myelin by neutral proteases secreted by stimulated macrophages: a possible mechanism of inflammatory demyelination. Proceedings of the National Academy of Sciences. 1978; **75**(3): 1554.

Campbell SJ, Anthony DC, Oakley F, Carlsen H, Elsharkawy AM, Blomhoff R*, et al.* Hepatic Nuclear Factor [kappa] B Regulates Neutrophil Recruitment to the Injured Brain. Journal of Neuropathology & Experimental Neurology. 2008; **67**(3): 223.

Carbonell WS, Ansorge O, Sibson N, Muschel R. The Vascular Basement Membrane as "Soil" in Brain Metastasis. PLoS ONE. 2009; **4**(6): e5857.

Carswell SR. Pathological anatomy: illustrations of the elementary forms of disease: Longman, Orme, Brown, Green and Longman; 1838.

Catalona WJ, Smith DS, Ratliff TL, Dodds KM, Coplen DE, Yuan JJJ, *et al.* Measurement of Prostate-Specific Antigen in Serum as a Screening Test for Prostate Cancer. New England Journal of Medicine. 1991; **324**(17): 1156-61.

Chang DB, Yang PC, Luh KT, Kuo S, Hong RL, Lee LN. Late survival of non-small cell lung cancer patients with brain metastases. Influence of treatment. Chest. 1992; **101**(5): 1293.

Charcot JM. Histologie de la sclerose en plaques; 1868.

Chard DT, Dalton CM, Swanton J, Fisniku LK, Miszkiel KA, Thompson AJ, *et al.* MRI only conversion to multiple sclerosis following a clinically isolated syndrome. Journal of Neurology, Neurosurgery & Psychiatry. 2011; **82**(2): 176-9.

Chénais B, Morjani H, Drapier J-C. Impact of endogenous nitric oxide on microglial cell energy metabolism and labile iron pool. Journal of Neurochemistry. 2002; **81**(3): 615-23.

Cheng LL, Newell K, Mallory AE, Hyman BT, Gonzalez RG. Quantification of neurons in Alzheimer and control brains with< i> ex vivo</i> high resolution magic angle spinning proton magnetic resonance spectroscopy and stereology. Magnetic resonance imaging. 2002; **20**(7): 527-33.

Cherny RA, Atwood CS, Xilinas ME, Gray DN, Jones WD, McLean CA, *et al.* Treatment with a Copper-Zinc Chelator Markedly and Rapidly Inhibits β-Amyloid Accumulation in Alzheimer's Disease Transgenic Mice. Neuron. 2001; **30**(3): 665-76.

Chiang MC, Dutton RA, Hayashi KM, Lopez OL, Aizenstein HJ, Toga AW, *et al.* 3D pattern of brain atrophy in HIV/AIDS visualized using tensor-based morphometry. Neuroimage. 2007; **34**(1): 44-60.

Childs E, Lyles R, Selnes O, Chen B, Miller E, Cohen B, *et al.* Plasma viral load and CD4 lymphocytes predict HIV-associated dementia and sensory neuropathy. Neurology. 1999; **52**(3): 607.

Choi SR, Golding G, Zhuang Z, Zhang W, Lim N, Hefti F, *et al.* Preclinical properties of 18F-AV-45: a PET agent for A plaques in the brain. Journal of Nuclear Medicine. 2009; **50**(11): 1887.

Chong H, Kira J, Tsai C, Ong B, Li P, Kermode A, *et al.* Proposed modifications to the McDonald criteria for use in Asia. Multiple Sclerosis. 2009; **15**(7): 887-8.

Chordas C. Post-dural puncture headache and other complications after lumbar puncture. Journal of Pediatric Oncology Nursing. 2001; **18**(6): 244-59.

Cohen DM. Inhibition of Glutamine Synthetase Induces Critical Energy Threshold for Neuronal Survival. Annals of the New York Academy of Sciences. 1997; **826**(1): 456-60.

Coleman RE. Positron emission tomography diagnosis of Alzheimer's disease. Neuroimaging Clinics of North America. 2005; **15**(4): 837-46.

Coles AJ, Fox E, Vladic A, Gazda SK, Brinar V, Selmaj KW, *et al.* Alemtuzumab versus interferon beta-1a in early relapsing-remitting multiple sclerosis: post-hoc and

subset analyses of clinical efficacy outcomes. The Lancet Neurology. 2011; **10**(4): 338-48.

Comi G, Filippi M, Wolinsky JS. European/Canadian multicenter, double blind, randomized, placebo controlled study of the effects of glatiramer acetate on magnetic resonance imaging–measured disease activity and burden in patients with relapsing multiple sclerosis. Annals of neurology. 2001; **49**(3): 290-7.

Compston A. The 150th anniversary of the first depiction of the lesions of multiple sclerosis. Journal of Neurology, Neurosurgery & Psychiatry. 1988; **51**(10): 1249.

Compston A, Coles A. Multiple sclerosis. The Lancet. 2002; **359**(9313): 1221-31.

Compston A, Coles A. Multiple sclerosis. The Lancet. 2008; **372**(9648): 1502-17.

Confavreux C, Vukusic S, Moreau T, Adeleine P. Relapses and progression of disability in multiple sclerosis. New England Journal of Medicine. 2000; **343**(20): 1430-8.

Confavreux C, Vukusic S, Adeleine P. Early clinical predictors and progression of irreversible disability in multiple sclerosis: an amnesic process. Brain. 2003; **126**(4): 770.

Connor S, Wu W, Sweatman B, Manini J, Haselden J, Crowther D*, et al.* Effects of feeding and body weight loss on the 1H-NMR-based urine metabolic profiles of male Wistar Han rats: implications for biomarker discovery. Biomarkers. 2004; **9**(2): 156-79.

Coplen S, Antman E, Berlin J, Hewitt P, Chalmers T. Efficacy and safety of quinidine therapy for maintenance of sinus rhythm after cardioversion. A meta-analysis of randomized control trials [published erratum appears in Circulation 1991 Feb;83(2):714]. Circulation. 1990; **82**(4): 1106-16.

Corder EH, Friedman GD, Vogelman JH, Orentreich N. Seasonal variation in vitamin D, vitamin D-binding protein, and dehydroepiandrosterone: risk of prostate cancer in black and white men. Cancer Epidemiology Biomarkers & Prevention. 1995; **4**(6): 655.

Costello LC, Franklin RB. Concepts of citrate production and secretion by prostate 1. Metabolic relationships. The Prostate. 1991; **18**(1): 25-46.

Craig-Schapiro R, Fagan AM, Holtzman DM. Biomarkers of Alzheimer's disease. Neurobiology of disease. 2009; **35**(2): 128-40.

Craig A, Cloarec O, Holmes E, Nicholson JK, Lindon JC. Scaling and normalization effects in NMR spectroscopic metabonomic data sets. Analytical chemistry. 2006; **78**(7): 2262-7.

Cremer JE, Cunningham VJ, Pardridge WM, Braun LD, Oldendorf WH. Kinetic Of Blood-Brain-Barrier Transport Of Pyruvate, Lactate and Glucose in Suckling, Weaning and Adult Rats. Journal of Neurochemistry. 1979; **33**(2): 439-45.

Cruveilhier J. Anatomie pathologique du corps humain: description, avec figures lithographiées et coloriées, des diverses altérations morbides dont le corps humain est susceptible. EST-INT: JB Baillière; 1842.

Cummings JL, Houlihan JP, Hill MA. The pattern of reading deterioration in dementia of the Alzheimer type: Observations and implications* 1. Brain and Language. 1986; **29**(2): 315-23.

Dal Pan G, McArthur J, Aylward E, Selnes O, Nance-Sproson T, Kumar A*, et al.* Patterns of cerebral atrophy in HIV–1–infected individuals. Neurology. 1992; **42**(11): 2125.

Dale R, De Sousa C, Chong W, Cox T, Harding B, Neville B. Acute disseminated encephalomyelitis, multiphasic disseminated encephalomyelitis and multiple sclerosis in children. Brain. 2000; **123**(12): 2407.

Dalton CM, Brex PA, Miszkiel KA, Fernando K, MacManus DG, Plant GT*, et al.* New T2 lesions enable an earlier diagnosis of multiple sclerosis in clinically isolated syndromes. Annals of neurology. 2003; **53**(5): 673-6.

Danysz W, Parsons C, MÖbius H-J, StÖffler A, Quack G. Neuroprotective and symptomatological action of memantine relevant for alzheimer's disease — a unified glutamatergic hypothesis on the mechanism of action. Neurotoxicity Research. 2000; **2**(2): 85-97.

Davison A, Kaczmarek L. Taurine—a Possible Neurotransmitter? 1971.

Den Boer JA, Bourland JD, Nyenhuis JA, Ham CLG, Engels JML, Hebrank FX*, et al.* Comparison of the threshold for peripheral nerve stimulation during gradient switching in whole body MR systems. Journal of Magnetic Resonance Imaging. 2002; **15**(5): 520-5.

Dettmer K, Aronov PA, Hammock BD. Mass spectrometry-based metabolomics. Mass Spectrometry Reviews. 2007; **26**(1): 51.

Dougherty RH, Skolasky R, McArthur JC. Progression of HIV-associated dementia treated with HAART. AIDS READER-NEW YORK-. 2002; **12**(2): 69-74.

Dubois B, Feldman HH, Jacova C, DeKosky ST, Barberger-Gateau P, Cummings J*, et al.* Research criteria for the diagnosis of Alzheimer's disease: revising the NINCDS-ADRDA criteria. The Lancet Neurology. 2007; **6**(8): 734-46.

Dunn WB, Ellis DI. Metabolomics: Current analytical platforms and methodologies. TrAC Trends in Analytical Chemistry. 2005; **24**(4): 285-94.

Dyment DA, Ebers GC, Dessa Sadovnick A. Genetics of multiple sclerosis. The Lancet Neurology. 2004; **3**(2): 104-10.

Edan G, Miller D, Clanet M, Confavreux C, Lyon-Caen O, Lubetzki C*, et al.* Therapeutic effect of mitoxantrone combined with methylprednisolone in multiple sclerosis: a randomised multicentre study of active disease using MRI and clinical criteria. Journal of Neurology, Neurosurgery & Psychiatry. 1997; **62**(2): 112.

Ellis DI, Goodacre R. Metabolic fingerprinting in disease diagnosis: biomedical applications of infrared and Raman spectroscopy. Analyst. 2006; **131**(8): 875-85.

Evans MC, Barnes J, Nielsen C, Kim LG, Clegg SL, Blair M*, et al.* Volume changes in Alzheimer's disease and mild cognitive impairment: cognitive associations. European radiology. 2010; **20**(3): 674-82.

Fan AY, Lao L, Zhang RX, Zhou AN, Wang LB, Moudgil KD*, et al.* Effects of an acetone extract of Boswellia carterii Birdw. (Burseraceae) gum resin on adjuvant-induced arthritis in lewis rats. Journal of Ethnopharmacology. 2005; **101**(1-3): 104-9.

Fan WMT. Metabolite profiling by one- and two-dimensional NMR analysis of complex mixtures. Progress in Nuclear Magnetic Resonance Spectroscopy. 1996; **28**: 161-219.

Fauler G, Leis H, Huber E, Schellauf C, Kerbl R, Urban C*, et al.* Determination of Homovanillic Acid and Vanillylmandelic Acid in Neuroblastoma Screening by Stable Isotope Dilution GC MS. Journal of mass spectrometry. 1997; **32**(5): 507-14.

Ferlay J, Shin H, Bray F, Forman D, Mathers C, Parkin D. GLOBOCAN 2008 v1. 2, Cancer Incidence and Mortality Worldwide: IARC CancerBase No. 10 [Internet]. Lyon, France: International Agency for Research on Cancer; 2010 [cited 2011 Jul 20]. Phlebologie. 2011; **5**.

Fidler IJ. The pathogenesis of cancer metastasis: the'seed and soil'hypothesis revisited. Nature Reviews Cancer. 2003; **3**(6): 453-8.

Filippini G, Brusaferri F, Sibley W, Citterio A, Ciucci G, Midgard R*, et al.* Corticosteroids or ACTH for acute exacerbations in multiple sclerosis. Cochrane database of systematic reviews (Online). 2000; (4): CD001331.

Fischl MA, Richman DD, Grieco MH, Gottlieb MS, Volberding PA, Laskin OL*, et al.* The Efficacy of Azidothymidine (AZT) in the Treatment of Patients with AIDS and AIDS-Related Complex. New England Journal of Medicine. 1987; **317**(4): 185-91.

Fleming JO, Cook TD. Multiple sclerosis and the hygiene hypothesis. Neurology. 2006; **67**(11): 2085-6.

Fleming TR, DeMets DL. Surrogate End Points in Clinical Trials: Are We Being Misled? Annals of Internal Medicine. 1996; **125**(7): 605-13.

Formica D, Silvestri S. Biological effects of exposure to magnetic resonance imaging: an overview. BioMedical Engineering OnLine. 2004; **3**(1): 11.

Förstl H, Kurz A. Clinical features of Alzheimer's disease. European Archives of Psychiatry and Clinical Neuroscience. 1999; **249**(6): 288-90.

Forsyth PA, Posner JB. Headaches in patients with brain tumors: a study of 111 patients. Neurology. 1993; **43**(9): 1678.

Frank R, Hargreaves R. Clinical biomarkers in drug discovery and development. Nature Reviews Drug Discovery. 2003; **2**(7): 566-80.

Freed E, Martin M. HIVs and their replication. Fields virology. 2001; **2**: 1971–2041.

Freed EO, Martin MA. The role of human immunodeficiency virus type 1 envelope glycoproteins in virus infection. Journal of Biological Chemistry. 1995; **270**(41): 23883.

Frenkel R. Isolation and some properties of a cytosol and a mitochondrial malic enzyme from bovine brain* 1. Archives of biochemistry and biophysics. 1972; **152**(1): 136-43.

Freund J, McDermott K. Sensitization to horse serum by means of adjuvants. Experimental Biology and Medicine. 1942; **49**(4): 548.

Freund J, Stern E, Pisani T. Isoallergic encephalomyelitis and radiculitis in guinea pigs after one injection of brain and Mycobacteria in water-in-oil emulsion. Journal of immunology (Baltimore, Md: 1950). 1947; **57**(2): 179.

Fuller M, Tucker JN, Lang DL, Dean CJ, Fietz MJ, Meikle PJ*, et al.* Screening patients referred to a metabolic clinic for lysosomal storage disorders. Journal of Medical Genetics. 2011; **48**(6): 422-5.

Gallo RC, Sarin PS, Gelmann E, Robert-Guroff M, Richardson E, Kalyanaraman V*, et al.* Isolation of human T-cell leukemia virus in acquired immune deficiency syndrome (AIDS). Science. 1983; **220**(4599): 865.

Gavaghan CL, Holmes E, Lenz E, Wilson ID, Nicholson JK. An NMR-based metabonomic approach to investigate the biochemical consequences of genetic strain differences: application to the C57BL10J and Alpk: ApfCD mouse. FEBS letters. 2000; **484**(3): 169-74.

Gelber RD, Larson M, Borgelt BB, Kramer S. Equivalence of radiation schedules for the palliative treatment of brain metastases in patients with favorable prognosis. Cancer. 1981; **48**(8): 1749-53.

Gerhard A, Schwarz J, Myers R, Wise R, Banati RB. Evolution of microglial activation in patients after ischemic stroke: a [11C](R)-PK11195 PET study. Neuroimage. 2005; **24**(2): 591-5.

Gill SS, Thomas DGT, Bruggen NV, Gadian DG, Peden CJ, Bell JD*, et al.* Proton MR Spectroscopy of Intracranial Tumours: In Vivo and In Vitro Studies. Journal of computer assisted tomography. 1990; **14**(4): 497-504.

Giovannoni G, Lai M, Kidd D, Thorpe JW, Miller DH, Thompson AJ*, et al.* Daily urinary neopterin excretion as an immunological marker of disease activity in multiple sclerosis. Brain. 1997; **120 (Pt 1)**: 1-13.

Giovannoni G, Thompson EJ. Urinary markers of disease activity in multiple sclerosis. Multiple Sclerosis. 1998; **4**(3): 247-53.

Giovannoni G, Comi G, Cook S, Rammohan K, Rieckmann P, Sørensen PS*, et al.* A placebo-controlled trial of oral cladribine for relapsing multiple sclerosis. New England Journal of Medicine. 2010; **362**(5): 416-26.

González-Scarano F, Baltuch G. MICROGLIA AS MEDIATORS OF INFLAMMATORY AND DEGENERATIVE DISEASES. Annual Review of Neuroscience. 1999; **22**(1): 219-40.

Goodin D, Arnason B, Coyle P, Frohman E, Paty D. The use of mitoxantrone (Novantrone) for the treatment of multiple sclerosis. Neurology. 2003; **61**(10): 1332.

Goodman Y, Bruce AJ, Cheng B, Mattson MP. Estrogens Attenuate and Corticosterone Exacerbates Excitotoxicity, Oxidative Injury, and Amyloid β-Peptide Toxicity in Hippocampal Neurons. Journal of Neurochemistry. 1996; **66**(5): 1836-44.

Gottlieb MS, Schroff R, Schanker HM, Weisman JD, Fan PT, Wolf RA*, et al.* Pneumocystis carinii pneumonia and mucosal candidiasis in previously healthy homosexual men. New England Journal of Medicine. 1981; **305**(24): 1425-31.

Griffin JL, Walker LA, Garrod S, Holmes E, Shore RF, Nicholson JK. NMR spectroscopy based metabonomic studies on the comparative biochemistry of the kidney and urine of the bank vole (Clethrionomys glareolus), wood mouse (Apodemus sylvaticus), white toothed shrew (Crocidura suaveolens) and the laboratory rat. Comparative Biochemistry and Physiology Part B: Biochemistry and Molecular Biology. 2000; **127**(3): 357-67.

Griffin JL, Walker LA, Shore RF, Nicholson JK. Metabolic Profiling of Chronic Cadmium Exposure in the Rat. Chemical Research in Toxicology. 2001; **14**(10): 1428-34.

Griffin JL, Bollard M, Nicholson JK, Bhakoo K. Spectral profiles of cultured neuronal and glial cells derived from HRMAS 1H NMR spectroscopy. NMR in Biomedicine. 2002; **15**(6): 375-84.

Griffin JL, Anthony DC, Campbell SJ, Gauldie J, Pitossi F, Styles P*, et al.* Study of cytokine induced neuropathology by high resolution proton NMR spectroscopy of rat urine. FEBS Letters. 2004a; **568**(1-3): 49-54.

Griffin JL, Shockcor JP. Metabolic profiles of cancer cells. Nat Rev Cancer. 2004b; **4**(7): 551-61.

Griffin JL, Kauppinen RA. A metabolomics perspective of human brain tumours. FEBS Journal. 2007; **274**(5): 1132-9.

Gronseth GS, Ashman EJ. Practice parameter: The usefulness of evoked potentials in identifying clinically silent lesions in patients with suspected multiple sclerosis (an evidence-based review). Neurology. 2000; **54**(9): 1720.

Gura T. Systems for Identifying New Drugs are Often Faulty. Science. 1997; **278**(5340): 1041-2.

Hansen RA, Gartlehner G, Webb AP, Morgan LC, Moore CG, Jonas DE. Efficacy and safety of donepezil, galantamine, and rivastigmine for the treatment of Alzheimer's disease: a systematic review and meta-analysis. Clinical interventions in aging. 2008; **3**(2): 211.

Hansson O, Zetterberg H, Buchhave P, Londos E, Blennow K, Minthon L. Association between CSF biomarkers and incipient Alzheimer's disease in patients with mild cognitive impairment: a follow-up study. The Lancet Neurology. 2006; **5**(3): 228-34.

Hanwell HEC, Banwell B. Assessment of evidence for a protective role of vitamin D in multiple sclerosis. Biochimica et Biophysica Acta (BBA) - Molecular Basis of Disease. 2011; **1812**(2): 202-12.

Hardy J, Allsop D. Amyloid deposition as the central event in the aetiology of Alzheimer's disease. Trends in pharmacological sciences. 1991; **12**(0): 383-8.

Hart IR, Fidler IJ. Role of organ selectivity in the determination of metastatic patterns of B16 melanoma. Cancer Research. 1980; **40**(7): 2281.

Hasegawa K, Shiojima S, Koizmui A, Ikeda M. Hippuric acid and o-cresol in the urine of workers exposed to toluene. International archives of occupational and environmental health. 1983; **52**(3): 197-208.

Hasegawa Y, Suzuki K, Yamamoto M, Ando M, Shima K, Sako C*, et al.* Magnetic resonance imaging and computed tomography in the diagnoses of brain metastases of lung cancer. Lung Cancer. 2004; **46**(3): 357-60.

Hashim AbdAlla MS, Taylor-Robinson SD, Sharif AW, Williams HRT, Crossey MME, Badra GA*, et al.* Differences in phosphatidylcholine and bile acids in bile from Egyptian and UK patients with and without cholangiocarcinoma. HPB. 2011; **13**(6): 385-90.

Hauser SL, Waubant E, Arnold DL, Vollmer T, Antel J, Fox RJ*, et al.* B-cell depletion with rituximab in relapsing–remitting multiple sclerosis. New England Journal of Medicine. 2008; **358**(7): 676-88.

Hayes CE. Vitamin D: a natural inhibitor of multiple sclerosis. Proceedings of the Nutrition Society. 2000; **59**(04): 531-5.

Hemminki K, Li X, Sundquist J, Hillert J, Sundquist K. Risk for multiple sclerosis in relatives and spouses of patients diagnosed with autoimmune and related conditions. neurogenetics. 2009; **10**(1): 5-11.

Herget-Rosenthal S, Marggraf G, Husing J, Goring F, Pietruck F, Janssen O*, et al.* Early detection of acute renal failure by serum cystatin C. Kidney international. 2004; **66**(3): 1115-22.

Hiestand PC, Rausch M, Meier DP, Foster CA. Ascomycete derivative to MS therapeutic: S1P receptor modulator FTY720. Natural Compounds as Drugs. 2008: 361-81.

Hirsch EC. Glial cells and Parkinson's disease. Journal of Neurology. 2000; **247**(0): II58-II62.

Hoang T, Bluml S, Dubowitz D, Moats R, Kopyov O, Jacques D*, et al.* Quantitative proton-decoupled 31P MRS and 1H MRS in the evaluation of Huntington's and Parkinson's diseases. Neurology. 1998; **50**(4): 1033-40.

Holick MF. Vitamin D: the underappreciated D-lightful hormone that is important for skeletal and cellular health. Current Opinion in Endocrinology, Diabetes and Obesity. 2002; **9**(1): 87.

Holmes E, Foxall PJD, Nicholson JK, Neild GH, Brown SM, Beddell CR*, et al.* Automatic Data Reduction and Pattern Recognition Methods for Analysis of 1H Nuclear Magnetic Resonance Spectra of Human Urine from Normal and Pathological States. Analytical Biochemistry. 1994; **220**(2): 284-96.

Holmes E, Antti H. Chemometric contributions to the evolution of metabonomics: mathematical solutions to characterising and interpreting complex biological NMR spectra. Analyst. 2002; **127**(12): 1549-57.

Holmøy T, Hestvik ALK. Multiple sclerosis: immunopathogenesis and controversies in defining the cause. Current opinion in infectious diseases. 2008; **21**(3): 271.

Hore P. Solvent suppression in Fourier transform nuclear magnetic resonance. Journal of Magnetic Resonance (1969). 1983; **55**(2): 283-300.

Houzen H, Niino M, Hata D, Nakano F, Kikuchi S, Fukazawa T, *et al.* Increasing prevalence and incidence of multiple sclerosis in northern Japan. Multiple Sclerosis. 2008; **14**(7): 887-92.

Hoyte LC, Brooks KJ, Nagel S, Akhtar A, Chen R, Mardiguian S, *et al.* Molecular magnetic resonance imaging of acute vascular cell adhesion molecule-1 expression in a mouse model of cerebral ischemia. J Cereb Blood Flow Metab. 2010; **30**(6): 1178-87.

Hulstaert F, Blennow K, Ivanoiu A, Schoonderwaldt HC, Riemenschneider M, De Deyn PP, *et al.* Improved discrimination of AD patients using beta-amyloid(1-42) and tau levels in CSF. Neurology. 1999; **52**(8): 1555-62.

Hutas G. Ocrelizumab, a humanized monoclonal antibody against CD20 for inflammatory disorders and B-cell malignancies. Current opinion in investigational drugs (London, England: 2000). 2008; **9**(11): 1206.

Ilyin SE, Belkowski SM, Plata-Salaman CR. Biomarker discovery and validation: technologies and integrative approaches. Trends in Biotechnology. 2004; **22**(8): 411-6.

Inglis F. The tolerability and safety of cholinesterase inhibitors in the treatment of dementia. International journal of clinical practice Supplement. 2002; (127): 45.

Irnich W, Schmitt F. Magnetostimulation in MRI. Magnetic resonance in medicine. 1995; **33**(5): 619-23.

Jacot W, Quantin X, Boher J, Andre F, Moreau L, Gainet M, *et al.* Brain metastases at the time of presentation of non-small cell lung cancer: a multi-centric AERIO analysis of prognostic factors. British journal of cancer. 2001; **84**(7): 903.

Janardhan V, Bakshi R. Quality of life in patients with multiple sclerosis: The impact of fatigue and depression. Journal of the Neurological Sciences. 2002; **205**(1): 51-8.

Janssens ACJW, van Duijn CM. Genome-based prediction of common diseases: advances and prospects. Human Molecular Genetics. 2008; **17**(R2): R166-R73.

Jenkins B, Rosas H, Chen YCI, Makabe T, Myers R, MacDonald M, *et al.* 1H NMR spectroscopy studies of Huntington's disease. Neurology. 1998; **50**(5): 1357-65.

Jones CA, McQuillan GM, Kusek JW, Eberhardt MS, Herman WH, Coresh J, *et al.* Serum creatinine levels in the US population: Third National Health and Nutrition Examination Survey. American Journal of Kidney Diseases. 1998; **32**(6): 992-9.

Jones JL, Coles AJ. New treatment strategies in multiple sclerosis. Experimental Neurology. 2010; **225**(1): 34-9.

Jung JY, Lee H-S, Kang D-G, Kim NS, Cha MH, Bang O-S, *et al.* 1H-NMR-Based Metabolomics Study of Cerebral Infarction. Stroke. 2011; **42**(5): 1282-8.

Kakizaki S, Yamamoto Y, Ueda A, Moore R, Sueyoshi T, Negishi M. Phenobarbital induction of drug/steroid-metabolizing enzymes and nuclear receptor CAR. Biochimica et Biophysica Acta (BBA)-General Subjects. 2003; **1619**(3): 239-42.

Kantarci K, Jack C, Xu Y, Campeau N, O'Brien P, Smith G, *et al.* Regional metabolic patterns in mild cognitive impairment and Alzheimer's disease. Neurology. 2000; **55**(2): 210.

Kantarci O, Siva A, Eraksoy M, Karabudak R, Sütla N, A ao lu J, *et al.* Survival and predictors of disability in Turkish MS patients. Neurology. 1998; **51**(3): 765.

Kappos L, Antel J, Comi G, Montalban X, O'Connor P, Polman CH, *et al.* Oral fingolimod (FTY720) for relapsing multiple sclerosis. New England Journal of Medicine. 2006; **355**(11): 1124-40.

Karter AJ, Ackerson LM, Darbinian JA, D'Agostino RB. Self-monitoring of blood glucose levels and glycemic control: the Northern California Kaiser Permanente Diabetes registry** 1. The American journal of medicine. 2001; **111**(1): 1-9.

Kasper LH, Shoemaker J. Multiple sclerosis immunology: the healthy immune system vs the MS immune system. Neurology. 2010; **74**(1, Supplement 1): S2.

Kaul M, Garden GA, Lipton SA. Pathways to neuronal injury and apoptosis in HIV-associated dementia. Nature Genetics. 2001; **2**: 988-94.

Kelley MA, Kazemi H. Role of ammonia as a buffer in the central nervous system. Respiration Physiology. 1974; **22**(3): 345-59.

Kemppainen N, Aalto S, Wilson I, Någren K, Helin S, Brück A, *et al.* Voxel-based analysis of PET amyloid ligand [11C] PIB uptake in Alzheimer disease. Neurology. 2006; **67**(9): 1575.

Kermode A, Thompson A, Tofts P, MacManus D, Kendall B, Kingsley D, *et al.* Breakdown of the blood-brain barrier precedes symptoms and other MRI signs of new lesions in multiple sclerosis. Brain. 1990; **113**(5): 1477.

Khatib AM, Kontogiannea M, Fallavollita L, Jamison B, Meterissian S, Brodt P. Rapid induction of cytokine and E-selectin expression in the liver in response to metastatic tumor cells. Cancer Research. 1999; **59**(6): 1356.

Kidd D, Thorpe J, Thompson A, Kendall B, Moseley I, MacManus D, *et al.* Spinal cord MRI using multi array coils and fast spin echo. Neurology. 1993; **43**(12): 2632.

Kidd P. Th1/Th2 balance: the hypothesis, its limitations, and implications for health and disease. Alternative medicine review. 2003; **8**(3): 223-46.

Kipnis J, Cardon M, Avidan H, Lewitus GM, Mordechay S, Rolls A, *et al.* Dopamine, through the extracellular signal-regulated kinase pathway, downregulates CD4+ CD25+ regulatory T-cell activity: implications for neurodegeneration. The Journal of neuroscience. 2004; **24**(27): 6133.

Kitchen B, Middleton G, Salmon M. Bovine milk N-acetyl-β-D-glucosaminidase and its significance in the detection of abnormal udder secretions. Journal of Dairy Research. 1978; **45**(01): 15-20.

Klein CA. The Metastasis Cascade. Science. 2008; **321**(5897): 1785-7.

Kline EE, Treat EG, Averna TA, Davis MS, Smith AY, Sillerud LO. Citrate Concentrations in Human Seminal Fluid and Expressed Prostatic Fluid Determined via

1H Nuclear Magnetic Resonance Spectroscopy Outperform Prostate Specific Antigen in Prostate Cancer Detection. The Journal of Urology. 2006; **176**(5): 2274-9.

Klos KJ, O'Neill BP. Brain metastases. The Neurologist. 2004; **10**(1): 31.

Kluger A, Gianutsos JG, Golomb J, Ferris SH, George AE, Franssen E*, et al.* Patterns of Motor Impairment in Normal Aging, Mild Cognitive Decline, and Early Alzheimer'Disease. The Journals of Gerontology Series B: Psychological Sciences and Social Sciences. 1997; **52**(1): P28.

Klunk WE, Engler H, Nordberg A, Wang Y, Blomqvist G, Holt DP*, et al.* Imaging brain amyloid in Alzheimer's disease with Pittsburgh Compound-B. Annals of neurology. 2004; **55**(3): 306-19.

Knott C, Stern G, Wilkin GP. Inflammatory Regulators in Parkinson's Disease: iNOS, Lipocortin-1, and Cyclooxygenases-1 and -2. Molecular and Cellular Neuroscience. 2000; **16**(6): 724-39.

Kobayashi K, Matsumoto S, Morishima T, Kawabe T, Okamoto T. Cimetidine inhibits cancer cell adhesion to endothelial cells and prevents metastasis by blocking E-selectin expression. Cancer Research. 2000; **60**(14): 3978.

Kochhar S, Jacobs DM, Ramadan Z, Berruex F, Fuerholz A, Fay LB. Probing gender-specific metabolism differences in humans by nuclear magnetic resonance-based metabonomics. Analytical Biochemistry. 2006; **352**(2): 274-81.

Kopeloff LM, Kopeloff N. Neurologic manifestations in laboratory animals produced by organ (adjuvant) emulsions. Journal of immunology (Baltimore, Md: 1950). 1947; **57**(3): 229.

Krebs HA, Salvin E, Johnson WA. The formation of citric and -ketoglutaric acids in the mammalian body. Biochemical Journal. 1938; **32**(1): 113.

Kriat M, Confort Gouny S, Vion Dury J, Sciaky M, Viout P, Cozzone PJ. Quantitation of metabolites in human blood serum by proton magnetic resonance spectroscopy. A comparative study of the use of formate and TSP as concentration standards. NMR in Biomedicine. 1992; **5**(4): 179-84.

Krökki O, Bloigu R, Reunanen M, Remes A. Increasing incidence of multiple sclerosis in women in Northern Finland. Multiple Sclerosis Journal. 2011; **17**(2): 133-8.

Kruger S, Mottaghy F, Buck A, Maschke S, Kley H, Frechen D*, et al.* Brain metastasis in lung cancer. Comparison of cerebral MRI and 18F-FDG-PET/CT for diagnosis in the initial staging. Nuklearmedizin. 2010; **50**.

Kuhle J, Leppert D, Petzold A, Regeniter A, Schindler C, Mehling M*, et al.* Neurofilament heavy chain in CSF correlates with relapses and disability in multiple sclerosis. Neurology. 2011; **76**(14): 1206-13.

Kumar A, Bala L, Kalita J, Misra UK, Singh RL, Khetrapal CL*, et al.* Metabolomic analysis of serum by (1) H NMR spectroscopy in amyotrophic lateral sclerosis. Clinica Chimica Acta. 2010; **411**(7–8): 563-7.

Kurhanewicz J, Vigneron DB, Nelson SJ. Three-dimensional magnetic resonance spectroscopic imaging of brain and prostate cancer. Neoplasia (New York, NY). 2000; **2**(1–2): 166.

Kurtzke JF. Rating neurologic impairment in multiple sclerosis: an expanded disability status scale (EDSS). Neurology. 1983; **33**(11): 1444.

Kurz GM, Wiesinger H, Hamprecht B. Purification of cytosolic malic enzyme from bovine brain, generation of monoclonal antibodies, and immunocytochemical localization of the enzyme in glial cells of neural primary cultures. Journal of Neurochemistry. 1993; **60**(4): 1467-74.

Kwee S. Cancer Localization in the Prostate with F-18 Fluorocholine Position Emission Tomography: DTIC Document; 2008.

Läubli H, Borsig L. Selectins promote tumor metastasis. 2010a: Elsevier; 2010a. p. 169-77.

Läubli H, Borsig L. Selectins as mediators of lung metastasis. Cancer Microenvironment. 2010b; **3**(1): 97-105.

Launer L, Andersen K, Dewey ME, Letenneur L, Ott A, Amaducci LA*, et al.* Rates and risk factors for dementia and Alzheimer's disease. Neurology. 1999; **52**(1): 78.

Leibel SA, Sheline GE. Radiation therapy for neoplasms of the brain. Journal of Neurosurgery. 1987; **66**(1): 1-22.

Lelekakis M, Moseley JM, Martin TJ, Hards D, Williams E, Ho P*, et al.* A novel orthotopic model of breast cancer metastasis to bone. Clinical and Experimental Metastasis. 1999; **17**(2): 163-70.

Lennon VA, Wingerchuk DM, Kryzer TJ, Pittock SJ, Lucchinetti CF, Fujihara K*, et al.* A serum autoantibody marker of neuromyelitis optica: distinction from multiple sclerosis. The Lancet. 2004; **364**(9451): 2106-12.

Lesko LJ, Atkinson Jr A. Use of biomarkers and surrogate endpoints in drug development and regulatory decision making: criteria, validation, strategies 1. Annual review of pharmacology and toxicology. 2001; **41**(1): 347-66.

Letendre S, Marquie-Beck J, Capparelli E, Best B, Clifford D, Collier AC*, et al.* Validation of the CNS penetration-effectiveness rank for quantifying antiretroviral penetration into the central nervous system. Archives of neurology. 2008; **65**(1): 65.

Liberatore GT, Jackson-Lewis V, Vukosavic S, Mandir AS, Vila M, McAuliffe WG*, et al.* Inducible nitric oxide synthase stimulates dopaminergic neurodegeneration in the MPTP model of Parkinson disease. Nature Medicine. 1999; **5**(12): 1403-9.

Lindon J, Holmes E, Nicholson J. Metabonomics in pharmaceutical R & D. FEBS Journal. 2007; **274**(5): 1140-51.

Link H, Tibbling G. Principles of albumin and IgG analyses in neurological disorders. III. Evaluation of IgG synthesis within the central nervous system in multiple sclerosis. Scandinavian Journal of Clinical & Laboratory Investigation. 1977; **37**(5): 397-401.

Lipka G, Chowdhry BZ, Sturtevant JM. A comparison of the phase transition properties of 1, 2-diacylphosphatidylcholines and 1, 2-diacylphosphatidylethanolamines in water and deuterium oxide. The Journal of Physical Chemistry. 1984; **88**(22): 5401-6.

Lips P, Duong T, Oleksik A, Black D, Cummings S, Cox D*, et al.* A global study of vitamin D status and parathyroid function in postmenopausal women with osteoporosis: baseline data from the multiple outcomes of raloxifene evaluation clinical trial. Journal of Clinical Endocrinology & Metabolism. 2001; **86**(3): 1212.

Lipton SA, Rosenberg PA. Excitatory Amino Acids as a Final Common Pathway for Neurologic Disorders. New England Journal of Medicine. 1994; **330**(9): 613-22.

Lublin F, Reingold S. for the National Multiple Sclerosis Society (USA) Advisory Committee on Clinical Trials of New Agents in Multiple Sclerosis. Defining the clinical course of multiple sclerosis: results of an international survey. Neurology. 1996; **46**(4): 907-11.

Lublin FD, Reingold SC. Guidelines for clinical trials of new therapeutic agents in multiple sclerosis. Neurology. 1997; **48**(3): 572.

Lucetti C, Del Dotto P, Gambaccini G, Bernardini S, Bianchi M, Tosetti M*, et al.* Proton magnetic resonance spectroscopy (1 H-MRS) of motor cortex and basal ganglia in de novo Parkinson's disease patients. Neurological sciences. 2001; **22**(1): 69-70.

Ludwig RJ, Boehme B, Podda M, Henschler R, Jager E, Tandi C*, et al.* Endothelial P-selectin as a target of heparin action in experimental melanoma lung metastasis. Cancer Research. 2004; **64**(8): 2743.

Lybecker H, Møller JT, May O, Nielsen HK. Incidence and Prediction of Postdural Puncture Headache A Prospective Study of 1021 Spinal Anesthesias. Anesthesia & Analgesia. 1990; **70**(4): 389-94.

Lycklama G, Thompson A, Filippi M, Miller D, Polman C, Fazekas F*, et al.* Spinal-cord MRI in multiple sclerosis. The Lancet Neurology. 2003; **2**(9): 555-62.

Lynch MJ, Masters J, Pryor JP, Lindon JC, Spraul M, Foxall PJD*, et al.* Ultra high field NMR spectroscopic studies on human seminal fluid, seminal vesicle and prostatic secretions. J Pharmaceut Biomed. 1994; **12**(1): 5-19.

Markesbery WR, Brooks WH, Gupta GD, Young AB. Treatment for patients with cerebral metastases. Archives of neurology. 1978; **35**(11): 754.

Marle G, Power C. Human immunodeficiency virus type 1 genetic diversity in the nervous system: Evolutionary epiphenomenon or disease determinant? Journal of neurovirology. 2005; **11**(2): 107-28.

Maschke S, Wahl A, Azaroual N, Boulet O, Crunelle V, Imbenotte M*, et al.* 1H-NMR analysis of trimethylamine in urine for the diagnosis of fish-odour syndrome. Clinica Chimica Acta. 1997; **263**(2): 139-46.

Mauch E, Kornhuber H, Krapf H, Fetzer U, Laufen H. Treatment of multiple sclerosis with mitoxantrone. European Archives of Psychiatry and Clinical Neuroscience. 1992; **242**(2): 96-102.

Max M, Menaker M. Regulation of melatonin production by light, darkness, and temperature in the trout pineal. Journal of Comparative Physiology A: Neuroethology, Sensory, Neural, and Behavioral Physiology. 1992; **170**(4): 479-89.

McArthur J, Hoover D, Bacellar H, Miller E, Cohen B, Becker J*, et al.* Dementia in AIDS patients. Neurology. 1993; **43**(11): 2245.

McArthur JC, McClernon DR, Cronin MF, Nance Sproson TE, Saah AJ, St Clair M*, et al.* Relationship between human immunodeficiency virus—associated dementia and viral load in cerebrospinal fluid and brain. Annals of neurology. 1997; **42**(5): 689-98.

McDonald W, Compston A, Edan G, Goodkin D, Hartung H, Lublin F, *et al.* Recommended diagnostic criteria for multiple sclerosis: guidelines from the International Panel on the diagnosis of multiple sclerosis. Annals of neurology. 2001; **50**(1): 121-7.

McFarland HF, Frank JA, Albert PS, Smith ME, Martin R, Harris JO*, et al.* Using gadolinium enhanced magnetic resonance imaging lesions to monitor disease activity in multiple sclerosis. Annals of neurology. 1992; **32**(6): 758-66.

McFarland HF. Correlation between MR and Clinical Findings of Disease Activity in Multiple Sclerosis. AJNR Am J Neuroradiol. 1999; **20**(10): 1777-8.

Mckay RT. How the 1D NOESY suppresses solvent signal in metabonomics NMR spectroscopy: An examination of the pulse sequence components and evolution. Concepts in Magnetic Resonance Part A. 2011; **38**(5): 197-220.

McKhann G, Drachman D, Folstein M. Clinical diagnosis of Alzheimer's disease: Report of the NINCDS-ADRDA work group under the auspices of Department of Health and Human Services Task Force on Alzheimer's disease. Neurology. 1984; **34**(7): 939-44.

McLean I, Nakane PK. Periodate-lysine-paraformaldehyde fixative a new fixative for immunoelectron microscopy. Journal of Histochemistry & Cytochemistry. 1974; **22**(12): 1077.

Meikle PJ, Hopwood JJ, Clague AE, Carey WF. Prevalence of Lysosomal Storage Disorders. JAMA: The Journal of the American Medical Association. 1999; **281**(3): 249-54.

Milas L, Mason K, Ang K. Epidermal growth factor receptor and its inhibition in radiotherapy: in vivo findings. International journal of radiation biology. 2003; **79**(7): 539-45.

Minagar A, Shapshak P, Fujimura R, Ownby R, Heyes M, Eisdorfer C. The role of macrophage/microglia and astrocytes in the pathogenesis of three neurologic disorders: HIV-associated dementia, Alzheimer disease, and multiple sclerosis. Journal of the Neurological Sciences. 2002; **202**(1-2): 13-23.

Montalban X, Tintoré M, Swanton J, Barkhof F, Fazekas F, Filippi M*, et al.* MRI criteria for MS in patients with clinically isolated syndromes. Neurology. 2010; **74**(5): 427-34.

Moreno A, Rey M, Montane JM, Alonso J, Arús C. 1H NMR spectroscopy of colon tumors and normal mucosal biopsies; elevated taurine levels and reduced

polyethyleneglycol absorption in tumors may have diagnostic significance. NMR in Biomedicine. 1993; **6**(2): 111-8.

Mudher A, Lovestone S. Alzheimer's disease – do tauists and baptists finally shake hands? Trends in neurosciences. 2002; **25**(1): 22-6.

Murr C, Widner B, Wirleitner B, Fuchs D. Neopterin as a marker for immune system activation. Current drug metabolism. 2002; **3**(2): 175-87.

Nakajima K, Kohsaka S. Functional roles of microglia in the central nervous system. Human cell: official journal of Human Cell Research Society. 1998; **11**(3): 141.

Narayana PA. Magnetic resonance spectroscopy in the monitoring of multiple sclerosis. Journal of Neuroimaging. 2005; **15**: 46S-57S.

Nath A, Haughey NJ, Jones M, Anderson C, Bell JE, Geiger JD. Synergistic neurotoxicity by human immunodeficiency virus proteins Tat and gp120: protection by memantine. Annals of neurology. 2000; **47**(2): 186-94.

Nath A, Berger J. HIV dementia. Current Treatment Options in Neurology. 2004; **6**(2): 139-51.

Neils J, Boller F, Gerdeman B, Cole M. Descriptive writing abilities in Alzheimer's disease. Journal of Clinical and Experimental neuropsychology. 1989.

Neuhofer W, Beck F-X. Survival in Hostile Environments: Strategies of Renal Medullary Cells. Physiology. 2006; **21**(3): 171-80.

Nicholson JK, Wilson ID. High resolution proton magnetic resonance spectroscopy of biological fluids. Progress in Nuclear Magnetic Resonance Spectroscopy. 1989; **21**(4-5): 449-501.

Nicholson JK, Lindon JC. Systems biology: Metabonomics. Nature. 2008; **455**(7216): 1054-6.

Nomoto Y, Miyamoto T, Yamaguchi Y. Brain metastasis of small cell lung carcinoma: comparison of Gd-DTPA enhanced magnetic resonance imaging and enhanced computerized tomography. Japanese Journal of Clinical Oncology. 1994; **24**(5): 258.

Noordijk EM, Vecht CJ, Haaxma-Reiche H, Padberg GW, Voormolen JHC, Hoekstra FH, *et al.* The choice of treatment of single brain metastasis should be based on extracranial tumor activity and age. International Journal of Radiation Oncology* Biology* Physics. 1994; **29**(4): 711-7.

Normand J, Legendre M, Kahn J, Bourdarias J, Mathivat A. Comparative efficacy of short-acting and long-acting quinidine for maintenance of sinus rhythm after electrical conversion of atrial fibrillation. British Heart Journal. 1976; **38**(4): 381.

Norris ER, Benoit GJ. Studies on Trimethylamine Oxide. Journal of Biological Chemistry. 1945; **158**(2): 443-8.

Noseworthy J, Hopkins M, Vandervoort M, Karlik S, Lee D, Penman M, *et al.* An open trial evaluation of mitoxantrone in the treatment of progressive MS. Neurology. 1993; **43**(7): 1401.

Noseworthy JH, Lucchinetti C, Rodriguez M, Weinshenker BG. Multiple Sclerosis. New England Journal of Medicine. 2000; **343**(13): 938-52.

Nowell PC, Hungerford DA. National Academy of Sciences. Abstracts of Papers Presented at the Autumn Meeting, 14-16 November 1960, Philadelphia, Pennsylvania. Science. 1960; **132**(3438): 1488-501.

Noyes HP. The Physical Description of Elementary Particles. American Scientist. 1957; **45**(5): 431-48.

O'Brien E, Serres S, Bristow C, Anthony DC, Sibson N. Astrocyte Activation in Brain Metastasis. XXVth Interantional symposium on cerebral blood flow, metabolism and function. 2011.

Oesterling JE. Prostate specific antigen: a critical assessment of the most useful tumor marker for adenocarcinoma of the prostate. The Journal of urology. 1991; **145**(5): 907.

Oliver SG, Winson MK, Kell DB, Baganz F. Systematic functional analysis of the yeast genome. TRENDS in Biotechnology. 1998; **16**(9): 373-8.

Oshinsky RJ, Elfont RM, Lublin FD. Incidence and clinical characteristics of the progressive relapsing form of MS. Neurology. 1998; **50**(4): A209-A.

Ott D, Hennig J, Ernst T. Human brain tumors: assessment with in vivo proton MR spectroscopy. Radiology. 1993a; **186**(3): 745-52.

Ott M, Demisch L, Engelhardt W, Fischer PA. Interleukin-2, soluble interleukin-2-receptor, neopterin, L-tryptophan and beta 2-microglobulin levels in CSF and serum of patients with relapsing-remitting or chronic-progressive multiple sclerosis. J Neurol. 1993b; **241**(2): 108-14.

Paget S. The distribution of secondary growths in cancer of the breast. Lancet. 1889; **1**(2): 99-101.

Pan Z, Raftery D. Comparing and combining NMR spectroscopy and mass spectrometry in metabolomics. Analytical and Bioanalytical Chemistry. 2007; **387**(2): 525-7.

Patchell RA, Tibbs PA, Walsh JW, Dempsey RJ, Maruyama Y, Kryscio RJ*, et al.* A randomized trial of surgery in the treatment of single metastases to the brain. New England Journal of Medicine. 1990; **322**(8): 494-500.

Patchell RA. The management of brain metastases. Cancer Treatment Reviews. 2003; **29**(6): 533-40.

Patwardhan MB, McCrory DC, Matchar DB, Samsa GP, Rutschmann OT. Alzheimer Disease: Operating Characteristics of PET—A Meta-Analysis1. Radiology. 2004; **231**(1): 73.

Paty D, Li D. Interferon beta 1b is effective in relapsing remitting multiple sclerosis. Neurology. 1993; **43**(4): 662.

Pauwels EKJ, Sturm EJC, Bombardieri E, Cleton FJ, Stokkel MPM. Positron-emission tomography with [^{18}F]fluorodeoxyglucose. Journal of Cancer Research and Clinical Oncology. 2000; **126**(10): 549-59.

Pearson K. LIII. On lines and planes of closest fit to systems of points in space. Philosophical Magazine Series 6. 1901; **2**(11): 559-72.

Pedersen TR, Olsson AG, Færgeman O, Kjekshus J, Wedel H, Berg K, *et al.* Lipoprotein Changes and Reduction in the Incidence of Major Coronary Heart Disease Events in the Scandinavian Simvastatin Survival Study (4S). Circulation. 1998; **97**(15): 1453-60.

Perrin RJ, Fagan AM, Holtzman DM. Multimodal techniques for diagnosis and prognosis of Alzheimer's disease. Nature. 2009; **461**(7266): 916-22.

Persidis A. High-throughput screening. Nature Biotechnology. 1998; **16**(5): 488.

Pfefferbaum A, Adalsteinsson E, Spielman D, Sullivan EV, Lim KO. In vivo brain concentrations of N-acetyl compounds, creatine, and choline in Alzheimer disease. Archives of general psychiatry. 1999; **56**(2): 185.

Pilcher CD, Shugars DC, Fiscus SA, Miller WC, Menezes P, Giner J, *et al.* HIV in body fluids during primary HIV infection: implications for pathogenesis, treatment and public health. Aids. 2001; **15**(7): 837.

Pimlott SL, Sutherland A. Molecular tracers for the PET and SPECT imaging of disease. Chemical Society Reviews. 2011; **40**(1): 149-62.

Podsypanina K, Du Y-CN, Jechlinger M, Beverly LJ, Hambardzumyan D, Varmus H. Seeding and Propagation of Untransformed Mouse Mammary Cells in the Lung. Science. 2008; **321**(5897): 1841-4.

Polman CH, Reingold SC, Edan G, Filippi M, Hartung H-P, Kappos L, *et al.* Diagnostic criteria for multiple sclerosis: 2005 revisions to the "McDonald Criteria". Annals of neurology. 2005; **58**(6): 840-6.

Polman CH, O'Connor PW, Havrdova E, Hutchinson M, Kappos L, Miller DH, *et al.* A randomized, placebo-controlled trial of natalizumab for relapsing multiple sclerosis. New England Journal of Medicine. 2006; **354**(9): 899-910.

Polman CH, Reingold SC, Banwell B, Clanet M, Cohen JA, Filippi M, *et al.* Diagnostic criteria for multiple sclerosis: 2010 Revisions to the McDonald criteria. Annals of neurology. 2011; **69**(2): 292-302.

Ponsonby AL, Lucas R, Mei IAF. UVR, vitamin D and three autoimmune diseases—multiple sclerosis, type 1 diabetes, rheumatoid arthritis. Photochemistry and photobiology. 2005; **81**(6): 1267-75.

Poole RC, Halestrap AP. Transport of lactate and other monocarboxylates across mammalian plasma membranes. American Journal of Physiology - Cell Physiology. 1993; **264**(4): C761-C82.

Popper H, Mandel E, Mayer H. Zur Kreatininbestimmung im Blute. Biochem Z. 1937; **291**: 354.

Poser CM, Paty DW, Scheinberg L, McDonald WI, Davis FA, Ebers GC, *et al.* New diagnostic criteria for multiple sclerosis: guidelines for research protocols. Annals of neurology. 1983; **13**(3): 227-31.

Posner J, Chernik N. Intracranial metastases from systemic cancer. Advances in neurology. 1978; **19**: 579.

Power C, McArthur JC, Johnson RT, Griffin DE, Glass JD, Perryman S, *et al.* Demented and nondemented patients with AIDS differ in brain-derived human immunodeficiency virus type 1 envelope sequences. J Virol. 1994; **68**(7): 4643.

Power C, Selnes OA, Grim JA, McArthur JC. HIV Dementia Scale: a rapid screening test. Journal of acquired immune deficiency syndromes and human retrovirology: official publication of the International Retrovirology Association. 1995; **8**(3): 273.

Power C, Boissé L, Rourke S, Gill MJ. NeuroAIDS: an evolving epidemic. The Canadian Journal of Neurological Sciences. 2009; **36**(3): 285-95.

Prabakaran S, Swatton J, Ryan M, Huffaker S, Huang JTJ, Griffin J, *et al.* Mitochondrial dysfunction in schizophrenia: evidence for compromised brain metabolism and oxidative stress. Molecular psychiatry. 2004; **9**(7): 684-97.

Preti G. Metabolomics comes of age. The Scientist. 2005; **19**(8).

Prévot A, Martini S, Guignard J. Glomerular filtration markers in pediatrics]. Revue medicale de la Suisse romande. 2002; **122**(12): 625.

Pugliatti M, Sotgiu S, Rosati G. The worldwide prevalence of multiple sclerosis. Clinical Neurology and Neurosurgery. 2002; **104**(3): 182-91.

Pulaski BA, Ostrand-Rosenberg S. Mouse 4T1 Breast Tumor Model. Current Protocols in Immunology: John Wiley & Sons, Inc.; 2001.

Pulliam L. HIV regulation of amyloid beta production. Journal of Neuroimmune Pharmacology. 2009; **4**(2): 213-7.

Purcell EM, Torrey H, Pound R. Resonance absorption by nuclear magnetic moments in a solid. Physical Review. 1946; **69**(1-2): 37-8.

Qu H, Håberg A, Haraldseth O, Unsgård G, Sonnewald U. ^{13}C MR Spectroscopy Study of Lactate as Substrate for Rat Brain. Developmental neuroscience. 2000; **22**(5-6): 429-36.

Quick AJ, Cooper MA. The synthesis of hippuric acid: a new test of liver function. The American Journal of the Medical Sciences. 1933; **185**(5): 630.

Quistorff B, Secher NH, Van Lieshout JJ. Lactate fuels the human brain during exercise. The FASEB Journal. 2008; **22**(10): 3443.

Rabi II, Zacharias JR, Millman S, Kusch P. A New Method of Measuring Nuclear Magnetic Moment. Physical Review. 1938; **53**(4): 318.

Raine CS, Scheinberg LC. On the immunopathology of plaque development and repair in multiple sclerosis. Journal of neuroimmunology. 1988; **20**(2-3): 189.

Rajendran JG, Mankoff DA, O'Sullivan F, Peterson LM, Schwartz DL, Conrad EU, *et al.* Hypoxia and Glucose Metabolism in Malignant Tumors. Clinical cancer research. 2004; **10**(7): 2245.

Rak K, Rader DJ. Cardiovascular disease: The diet-microbe morbid union. Nature. 2011; **472**(7341): 40-1.

Ramagopalan SV, Handel AE, Giovannoni G, Rutherford Siegel S, Ebers GC, Chaplin G. Relationship of UV exposure to prevalence of multiple sclerosis in England. Neurology. 2011; **76**(16): 1410-4.

Ramautar R, Demirci A, Jong GJd. Capillary electrophoresis in metabolomics. TrAC Trends in Analytical Chemistry. 2006; **25**(5): 455-66.

Ratering D, Baltes C, Nordmeyer-Massner J, Marek D, Rudin M. Performance of a 200-MHz cryogenic RF probe designed for MRI and MRS of the murine brain. Magnetic resonance in medicine. 2008; **59**(6): 1440-7.

Reisberg B, Doody R, Stöffler A, Schmitt F, Ferris S, Möbius HJ. Memantine in Moderate-to-Severe Alzheimer's Disease. New England Journal of Medicine. 2003; **348**(14): 1333-41.

Rivers TM, Sprunt D, Berry G. Observations on attempts to produce acute disseminated encephalomyelitis in monkeys. The Journal of experimental medicine. 1933; **58**(1): 39.

Robinet G, Thomas P, Breton J, Lena H, Gouva S, Dabouis G*, et al.* Results of a phase III study of early versus delayed whole brain radiotherapy with concurrent cisplatin and vinorelbine combination in inoperable brain metastasis of non-small-cell lung cancer: Groupe Français de Pneumo-Cancérologie (GFPC) Protocol 95–1*. Annals of oncology. 2001; **12**(1): 59.

Rogers J. Inflammation as a pathogenic mechanism in Alzheimer's disease. Arzneimittel-Forschung. 1995; **45**(3A): 439.

Rolan P, Atkinson AJ, Lesko LJ. Use of biomarkers from drug discovery through clinical practice: report of the Ninth European Federation of Pharmaceutical Sciences Conference on Optimizing Drug Development. Clinical Pharmacology and Therapeutics. 2003; **73**(4): 284-91.

Románb TCGC. Multiple Sclerosis in Latin America. Neuroepidemiology. 2006; **26**: 1-3.

Rosati G. The prevalence of multiple sclerosis in the world: an update. Neurological sciences. 2001; **22**(2): 117-39.

Ross JM, Öberg J, Brené S, Coppotelli G, Terzioglu M, Pernold K*, et al.* High brain lactate is a hallmark of aging and caused by a shift in the lactate dehydrogenase A/B ratio. Proceedings of the National Academy of Sciences. 2010; **107**(46): 20087-92.

Rovaris M, Confavreux C, Furlan R, Kappos L, Comi G, Filippi M. Secondary progressive multiple sclerosis: current knowledge and future challenges. The Lancet Neurology. 2006; **5**(4): 343-54.

Rovira A, Swanton J, Tintore M, Huerga E, Barkhof F, Filippi M*, et al.* A single, early magnetic resonance imaging study in the diagnosis of multiple sclerosis. Archives of neurology. 2009; **66**(5): 587.

Ruderman NB, Hall TC. Use of glucocorticoids in the palliative treatment of metastatic brain tumors. Cancer. 1965; **18**(3): 298-306.

Rudin M, Weissleder R. Molecular imaging in drug discovery and development. Nature Reviews Drug Discovery. 2003; **2**(2): 123-31.

Runmarker B, Andersen O. Prognostic factors in a multiple sclerosis incidence cohort with twenty-five years of follow-up. Brain. 1993; **116**(1): 117.

Sacktor NC, Wong M, Nakasujja N, Skolasky RL, Selnes OA, Musisi S*, et al.* The International HIV Dementia Scale: a new rapid screening test for HIV dementia. Aids. 2005; **19**(13): 1367.

Sadovnick A, Remick R, Allen J, Swartz E, Yee I, Eisen K*, et al.* Depression and multiple sclerosis. Neurology. 1996; **46**(3): 628.

Sahu P, Pinkalwar N, Dubey RD, Paroha S, Chatterjee S, Chatterjee T. Biomarkers: An Emerging Tool for Diagnosis of a Disease and Drug Development. Asian J Res Pharm Sci. 2011; **1**(1): 09-16.

Salek R, Colebrooke R, Macintosh R, Lynch P, Sweatman B, Emson P*, et al.* A Metabolomic Study of Brain Tissues from Aged Mice with Low Expression of the Vesicular Monoamine Transporter 2 (VMAT2) Gene. Neurochemical Research. 2008; **33**(2): 292-300.

Salek RM, Xia J, Innes A, Sweatman BC, Adalbert R, Randle S*, et al.* A metabolomic study of the CRND8 transgenic mouse model of Alzheimer's disease. Neurochemistry international. 2010; **56**(8): 937-47.

Sand T, Stovner LJ, Dale L, Salvesen R. Side effects after diagnostic lumbar puncture and lumbar iohexol myelography. Neuroradiology. 1987; **29**(4): 385-8.

Saude EJ, Adamko D, Rowe BH, Marrie T, Sykes BD. Variation of metabolites in normal human urine. Metabolomics. 2007; **3**(4): 439-51.

Saunders NR, Ek CJ, Habgood MD, Dziegielewska KM. Barriers in the brain: a renaissance? Trends in neurosciences. 2008; **31**(6): 279-86.

Sawcer S, Ban M, Maranian M, Yeo T, Compston A, Kirby A*, et al.* A high-density screen for linkage in multiple sclerosis. American journal of human genetics. 2005; **77**(3): 454.

Sawcer S, Hellenthal G, Pirinen M, Spencer CCA, Patsopoulos NA, Moutsianas L*, et al.* Genetic risk and a primary role for cell-mediated immune mechanisms in multiple sclerosis. Nature. 2011; **476**(7359): 214-9.

Scalfari A, Neuhaus A, Degenhardt A, Rice GP, Muraro PA, Daumer M*, et al.* The natural history of multiple sclerosis, a geographically based study 10: relapses and long-term disability. Brain. 2010; **133**(7): 1914-29.

Schaefer DJ, Bourland JD, Nyenhuis JA. Review of Patient Safety in Time-Varying Gradient Fields. Journal of Magnetic Resonance Imaging. 2000; **12**(1): 20-9.

Schaefer P, Budzik Jr R, Gonzalez R. Imaging of cerebral metastases. Neurosurgery Clinics of North America. 1996; **7**(3): 393.

Schellinger PD, Meinck HM, Thron A. Diagnostic accuracy of MRI compared to CCT in patients with brain metastases. Journal of neuro-oncology. 1999; **44**(3): 275-81.

Schifitto G, Navia BA, Yiannoutsos CT, Marra CM, Chang L, Ernst T*, et al.* Memantine and HIV-associated cognitive impairment: a neuropsychological and proton magnetic resonance spectroscopy study. Aids. 2007; **21**(14): 1877.

Schouten LJ, Rutten J, Huveneers HAM, Twijnstra A. Incidence of brain metastases in a cohort of patients with carcinoma of the breast, colon, kidney, and lung and melanoma. Cancer. 2002; **94**(10): 2698-705.

Schumacher GA, Beebe G, Kibler RF, Kurland LT, Kurtzke JF, McDowell F*, et al.* Problems of experimental trials of therapy in multiple sclerosis: report by the panel on the evaluation of experimental trials of therapy in multiple sclerosis. Annals of the New York Academy of Sciences. 1965; **122**(1): 552-68.

Schweitzer B, Kingsmore SF. Measuring proteins on microarrays. Current opinion in biotechnology. 2002; **13**(1): 14-9.

Serber Z, Richter C, Moskau D, Böhlen J-M, Gerfin T, Marek D*, et al.* New Carbon-Detected Protein NMR Experiments Using CryoProbes. Journal of the American Chemical Society. 2000; **122**(14): 3554-5.

Serres S, Balathasan L, Hamilton A, Wessiensteiner T, Carbonell WS, McAteer MA*, et al.* Early detection of brain metastasis using novel MRI contrast agent targeting VCAM-1. Proceedings of the World Molecular Imaging Congress. 2010.

Serres S, Mardiguian S, Campbell SJ, McAteer MA, Akhtar A, Krapitchev A*, et al.* VCAM-1-targeted magnetic resonance imaging reveals subclinical disease in a mouse model of multiple sclerosis. The FASEB Journal. 2011.

Shank R, Aprison M. Present status and significance of the glutamine cycle in neural tissues. Life Sciences. 1981; **28**(8): 837-42.

Shapshak P, Kangueane P, Fujimura RK, Commins D, Chiappelli F, Singer E*, et al.* Editorial NeuroAIDS review. Aids. 2011; **25**(2): 123.

Sharief MK, Hentges R. Association between Tumor Necrosis Factor-α and Disease Progression in Patients with Multiple Sclerosis. New England Journal of Medicine. 1991; **325**(7): 467-72.

Shaykhutdinov RA, MacInnis GD, Dowlatabadi R, Weljie AM, Vogel HJ. Quantitative analysis of metabolite concentrations in human urine samples using 13 C {1 H} NMR spectroscopy. Metabolomics. 2009; **5**(3): 307-17.

Shields JA, Shields CL, Brotman HK, Carvalho C, Perez N, Eagle RCJ. Cancer Metastatic to the Orbit: The 2000 Robert M. Curts Lecture. Ophthalmic Plastic & Reconstructive Surgery. 2001; **17**(5): 346-54.

Shoghi-Jadid K, Small GW, Agdeppa ED, Kepe V, Ercoli LM, Siddarth P*, et al.* Localization of neurofibrillary tangles and beta-amyloid plaques in the brains of living patients with Alzheimer disease. American Journal of Geriatric Psych. 2002; **10**(1): 24.

Shortreed MR, Li H, Huang WH, Yeung ES. High-throughput single-molecule DNA screening based on electrophoresis. Analytical chemistry. 2000; **72**(13): 2879-85.

Shrimpton P, Hillier M, Lewis M, Dunn M. National survey of doses from CT in the UK: 2003. British journal of radiology. 2006; **79**(948): 968.

Simpson DM, Tagliati M. Neurologic manifestations of HIV infection. Annals of Internal Medicine. 1994; **121**(10): 769.

Sloka J, Pryse-Phillips WEM, Stefanelli M. The relation of ultraviolet radiation and multiple sclerosis in Newfoundland. The Canadian Journal of Neurological Sciences. 2008; **35**(1): 69-74.

Smith-Bindman R, Lipson J, Marcus R, Kim KP, Mahesh M, Gould R*, et al.* Radiation dose associated with common computed tomography examinations and the associated lifetime attributable risk of cancer. Archives of internal medicine. 2009; **169**(22): 2078.

Solís J, Herranz AS, Herreras O, Lerma J, del Río RM. Does taurine act as an osmoregulatory substance in the rat brain? Neuroscience Letters. 1988; **91**(1): 53-8.

Song H, Li J, Shi S, Yan L, Zhuang H, Li K. Thermal stability and inactivation of hepatitis C virus grown in cell culture. Virol J. 2010; **7**: 40.

Soto MS, Serres S, Dickens AM, Larkin J, Anthony DC, Sibson N. Endothelial activation in brain metastasis. NCRI conference abstract. 2011.

Spain R, Cameron M, Bourdette D. Recent developments in multiple sclerosis therapeutics. BMC medicine. 2009; **7**(1): 74.

Sperduto PW, Berkey B, Gaspar LE, Mehta M, Curran W. A New Prognostic Index and Comparison to Three Other Indices for Patients With Brain Metastases: An Analysis of 1,960 Patients in the RTOG Database. International Journal of Radiation Oncology Biology Physics. 2008; **70**(2): 510-4.

Staels B, Auwerx J. Perturbation of developmental gene expression in rat liver by fibric acid derivatives: lipoprotein lipase and alpha-fetoprotein as models. Development. 1992; **115**(4): 1035.

Stephen R R. Neuronal expression of glutamine synthetase in Alzheimer's disease indicates a profound impairment of metabolic interactions with astrocytes. Neurochemistry international. 2000; **36**(4-5): 471-82.

Stokkel M, Ten Broek F, Van Rijk P. The role of FDG PET in the clinical management of head and neck cancer. Oral oncology. 1998; **34**(6): 466-71.

Strachan DP. Family size, infection and atopy: the first decade of the'hygiene hypothesis'. Thorax. 2000; **55**(suppl 1): S2.

Stuve O, Leussink VI, Frohlich R, Hemmer B, Hartung HP, Menge T*, et al.* Long-term B-lymphocyte depletion with rituximab in patients with relapsing-remitting multiple sclerosis. Archives of neurology. 2009; **66**(2): 259.

Styles P, Soffe NF, Scott CA, Crag DA, Row F, White DJ*, et al.* A high-resolution NMR probe in which the coil and preamplifier are cooled with liquid helium. Journal of Magnetic Resonance (1969). 1984; **60**(3): 397-404.

Sugimoto M, Wong D, Hirayama A, Soga T, Tomita M. Capillary electrophoresis mass spectrometry-based saliva metabolomics identified oral, breast and pancreatic cancer-specific profiles. Metabolomics. 2010; **6**(1): 78-95.

Surma-aho O, Niemelä M, Vilkki J, Kouri M, Brander A, Salonen O*, et al.* Adverse long-term effects of brain radiotherapy in adult low-grade glioma patients. Neurology. 2001; **56**(10): 1285.

Swanton JK, Fernando K, Dalton CM, Miszkiel KA, Thompson AJ, Plant GT*, et al.* Modification of MRI criteria for multiple sclerosis in patients with clinically isolated syndromes. Journal of Neurology, Neurosurgery & Psychiatry. 2006; **77**(7): 830-3.

Swanton JK, Rovira A, Tintore M, Altmann DR, Barkhof F, Filippi M*, et al.* MRI criteria for multiple sclerosis in patients presenting with clinically isolated syndromes: a multicentre retrospective study. The Lancet Neurology. 2007; **6**(8): 677-86.

Takeuchi H, Jin S, Wang J, Zhang G, Kawanokuchi J, Kuno R*, et al.* Tumor Necrosis Factor-α Induces Neurotoxicity via Glutamate Release from Hemichannels of Activated Microglia in an Autocrine Manner. Journal of Biological Chemistry. 2006; **281**(30): 21362-8.

Tao K, Fang M, Alroy J, Sahagian GG. Imagable 4T1 model for the study of late stage breast cancer. BMC Cancer. 2008; **8**(1): 228.

Taylor BV, Pearson JF, Clarke G, Mason DF, Abernethy DA, Willoughby E*, et al.* MS prevalence in New Zealand, an ethnically and latitudinally diverse country. Multiple Sclerosis. 2010; **16**(12): 1422-31.

Thauer RK. Citric acid cycle, 50 years on. European Journal of Biochemistry. 1988; **176**(3): 497-508.

Thompson A, Montalban X, Barkhof F, Brochet B, Filippi M, Miller D*, et al.* Diagnostic criteria for primary progressive multiple sclerosis: a position paper. Annals of neurology. 2000; **47**(6): 831-5.

Tintore M, Rovira A, Martinez MJ, Rio J, Diaz-Villoslada P, Brieva L*, et al.* Isolated demyelinating syndromes: comparison of different MR imaging criteria to predict conversion to clinically definite multiple sclerosis. American journal of neuroradiology. 2000; **21**(4): 702.

Togo T, Akiyama H, Iseki E, Kondo H, Ikeda K, Kato M*, et al.* Occurrence of T cells in the brain of Alzheimer's disease and other neurological diseases. Journal of neuroimmunology. 2002; **124**(1-2): 83-92.

Trapp BD, Bö L, Mörk S, Chang A. Pathogenesis of tissue injury in MS lesions. Journal of neuroimmunology. 1999; **98**(1): 49-56.

Tsang TM, Woodman B, McLoughlin GA, Griffin JL, Tabrizi SJ, Bates GP*, et al.* Metabolic Characterization of the R6/2 Transgenic Mouse Model of Huntington's Disease by High-Resolution MAS 1H NMR Spectroscopy. Journal of Proteome Research. 2006; **5**(3): 483-92.

Tullman M, Oshinsky R, Lublin F, Cutter G. Clinical characteristics of progressive relapsing multiple sclerosis. Multiple Sclerosis. 2004; **10**(4): 451.

Tur C, Tintoré M, Rovira Á, Nos C, Río J, Téllez N*, et al.* Very early scans for demonstrating dissemination in time in multiple sclerosis. Multiple Sclerosis. 2008; **14**(5): 631-5.

Ubogu EE, Cossoy MB, Ransohoff RM. The expression and function of chemokines involved in CNS inflammation. Trends in pharmacological sciences. 2006; **27**(1): 48-55.

Underwood BR, Broadhurst D, Dunn WB, Ellis DI, Michell AW, Vacher C*, et al.* Huntington disease patients and transgenic mice have similar pro-catabolic serum metabolite profiles. Brain. 2006; **129**(4): 877-86.

Usenius J-PR, Kauppinen RA, Vainio PA, Hernesniemi JA, Vapalahti MP, Paljärvi LA*, et al.* Quantitative Metabolite Patterns of Human Brain Tumors: Detection by 1H NMR Spectroscopy In Vivo and In Vitro. Journal of computer assisted tomography. 1994; **18**(5): 705-13.

Usenius JP, Tuohimetsä S, Vainio P, Ala-Korpela M, Hiltunen Y, Kauppinen RA. Automated classification of human brain tumours by neural network analysis using in vivo H magnetic resonance spectroscopic metabolite phenotypes. Neuroreport. 1996; **7**(10): 1597.

Van Broeck B, Van Broeckhoven C, Kumar-Singh S. Current Insights into Molecular Mechanisms of Alzheimer Disease and Their Implications for Therapeutic Approaches. Neurodegenerative Diseases. 2007; **4**(5): 349-65.

van de Pol M, Twijnstra A, ten Velde GPM, Menheere PPCA. Neuron-specific enolase as a marker of brain metastasis in patients with small-cell lung carcinoma. Journal of neuro-oncology. 1994; **19**(2): 149-54.

van den Bent MJ. The diagnosis and management of brain metastases. Current Opinion in Neurology. 2001; **14**(6): 717.

van den Berg R, Hoefsloot H, Westerhuis J, Smilde A, van der Werf M. Centering, scaling, and transformations: improving the biological information content of metabolomics data. BMC genomics. 2006; **7**(1): 142.

van Kasteren SI, Kramer HB, Jensen HH, Campbell SJ, Kirkpatrick J, Oldham NJ*, et al.* Expanding the diversity of chemical protein modification allows post-translational mimicry. Nature. 2007; **446**(7139): 1105-9.

Vecht CJ, Haaxma Reiche H, Noordijk EM, Padberg GW, Voormolen JHC, Hoekstra FH*, et al.* Treatment of single brain metastasis: radiotherapy alone or combined with neurosurgery. Annals of neurology. 1993; **33**(6): 583-90.

Venneri A, Shanks MF, Staff RT, Pestell SJ, Forbes KE, Gemmell HG*, et al.* Cerebral blood flow and cognitive responses to rivastigmine treatment in Alzheimer's disease. Neuroreport. 2002; **13**(1): 83.

Venter JC, Adams MD, Myers EW, Li PW, Mural RJ, Sutton GG*, et al.* The Sequence of the Human Genome. Science. 2001; **291**(5507): 1304-51.

Vidal-Vanaclocha F, Fantuzzi G, Mendoza L, Fuentes AM, Anasagasti MJ, Martín J*, et al.* IL-18 regulates IL-1 -dependent hepatic melanoma metastasis via vascular cell adhesion molecule-1. Proceedings of the National Academy of Sciences. 2000; **97**(2): 734.

Villalba S, Salvucci O, Aoki Y, Sierra MDLL, Gupta G, Davis D*, et al.* Serum inactivation contributes to the failure of stromal-derived factor-1 to block HIV-I infection in vivo. Journal of leukocyte biology. 2003; **74**(5): 880.

Virley DJ. Developing therapeutics for the treatment of multiple sclerosis. NeuroRx. 2005; **2**(4): 638-49.

Vogeser M, Seger C. A decade of HPLC–MS/MS in the routine clinical laboratory — Goals for further developments. Clinical Biochemistry. 2008; **41**(9): 649-62.

Voltz R, Starck M, Zingler V, Strupp M, Kolb HJ. Mitoxantrone therapy in multiple sclerosis and acute leukaemia: a case report out of 644 treated patients. Multiple Sclerosis. 2004; **10**(4): 472.

Vukusic S, Van Bockstael V, Gosselin S, Confavreux C. Regional variations in the prevalence of multiple sclerosis in French farmers. Journal of Neurology, Neurosurgery & Psychiatry. 2007; **78**(7): 707.

Walsh M, Brennan L, Malthouse J, Roche H, Gibney M. Effect of acute dietary standardization on the urinary, plasma, and salivary metabolomic profiles of healthy humans. American Journal of Clinical Nutrition. 2006; **84**(3): 531.

Wang LP, Schmidt JF. Central nervous side effects after lumbar puncture. A review of the possible pathogenesis of the syndrome of postdural puncture headache and associated symptoms. Danish medical bulletin. 1997; **44**(1): 79.

Want EJ, Cravatt BF, Siuzdak G. The Expanding Role of Mass Spectrometry in Metabolite Profiling and Characterization. ChemBioChem. 2005; **6**(11): 1941-51.

Warburg O, Wind F, Negelein E. The metabolism of tumors in the body. The Journal of general physiology. 1927; **8**(6): 519.

Wasinger VC, Cordwell SJ, Cerpa Poljak A, Yan JX, Gooley AA, Wilkins MR*, et al.* Progress with gene product mapping of the Mollicutes: Mycoplasma genitalium. Electrophoresis. 1995; **16**(1): 1090-4.

Waterman C, Currie R, Cottrell L, Dow J, Wright J, Waterfield C*, et al.* An integrated functional genomic study of acute phenobarbital exposure in the rat. BMC genomics. 2010; **11**(1): 9.

Wei T, Lightman SL. The neuroendocrine axis in patients with multiple sclerosis. Brain. 1997; **120**(6): 1067.

Weigelt B, Peterse JL, van't Veer LJ. Breast cancer metastasis: markers and models. Nat Rev Cancer. 2005; **5**(8): 591-602.

Weinshenker BG, Bass B, Rice GPA, Noseworthy J, Carriere W, Baskerville J*, et al.* The Natural-History of Multiple-Sclerosis - a Geographically Based Study. Brain. 1989; **112**: 133-46.

Weiss RA. How does HIV cause AIDS? Science. 1993; **260**(5112): 1273.

Weljie AM, Newton J, Mercier P, Carlson E, Slupsky CM. Targeted profiling: quantitative analysis of 1H NMR metabolomics data. Analytical chemistry. 2006; **78**(13): 4430-42.

Weller M, Fontana A. The failure of current immunotherapy for malignant glioma. Tumor-derived TGF-[beta], T-cell apoptosis, and the immune privilege of the brain. Brain research reviews. 1995; **21**(2): 128-51.

Whitaker JN, McKeehan A, Freeman DW. Monoclonal and polyclonal antibody responses to the myelin basic protein epitope present in human urine. J Neuroimmunol. 1994; **52**(1): 53-60.

Whitaker JN, Kachelhofer RD, Bradley EL, Burgard S, Layton BA, Reder AT*, et al.* Urinary myelin basic protein-like material as a correlate of the progression of multiple sclerosis. Ann Neurol. 1995; **38**(4): 625-32.

White MB. Jean-Martin Charcot's contributions to the interface between neurology and psychiatry. The Canadian journal of neurological sciences Le journal canadien des sciences neurologiques. 1997; **24**(3): 254.

Williams RJ. Individual metabolomic patterns and human disease: an exploratory study utlizing predominatly paper chromatographic methods. University of Texas Publications. 1951; **5109**: 15.

Williams RT. Detoxication mechanisms. The metabolism and detoxication of drugs, toxic substances and other organic compounds. Detoxication mechanisms The metabolism and detoxication of drugs, toxic substances and other organic compounds. 1959; (2nd ed. 2nd).

Wishart DS, Tzur D, Knox C, Eisner R, Guo AC, Young N*, et al.* HMDB: the Human Metabolome Database. Nucleic Acids Research. 2007; **35**(suppl 1): D521-D6.

Wishart DS, Knox C, Guo AC, Eisner R, Young N, Gautam B*, et al.* HMDB: a knowledgebase for the human metabolome. Nucleic Acids Research. 2009; **37**(suppl 1): D603.

Wolf A, Kabat EA, Bezer ADAE. The pathology of acute disseminated encephalomyelitis produced experimentally in the rhesus monkey and its resemblance to human demyelinating disease. Journal of Neuropathology & Experimental Neurology. 1947; **6**(4): 333.

Wolfensohn S, Lloyd M, Corporation E. Handbook of laboratory animal management and welfare: Wiley Online Library; 2003.

Wolinsky JS. The diagnosis of primary progressive multiple sclerosis. Journal of the Neurological Sciences. 2003; **206**(2): 145-52.

Woo HK, Northen TR, Yanes O, Siuzdak G. Nanostructure-initiator mass spectrometry: a protocol for preparing and applying NIMS surfaces for high-sensitivity mass analysis. Nature Protocols. 2008; **3**(8): 1341-9.

Wright CE, Tallan HH, Lin YY. Taurine: biological update. Annual review of biochemistry. 1986; **55**(1): 427-53.

Xi Y, Rocke DM. Baseline correction for NMR spectroscopic metabolomics data analysis. BMC bioinformatics. 2008; **9**(1): 324.

Zamvil S, Nelson P, Trotter J, Mitchell D, Knobler R, Fritz R*, et al.* T-cell clones specific for myelin basic protein induce chronic relapsing paralysis and demyelination. 1985.

Zhang M, Olsson Y. Reactions of astrocytes and microglial cells around hematogenous metastases of the human brain Expression of endothelin-like immunoreactivity in reactive astrocytes and activation of microglial cells. Journal of the Neurological Sciences. 1995; **134**(1-2): 26-32.

Zimm S, Wampler GL, Stablein D, Hazra T, Young HF. Intracerebral metastases in solid tumor patients: Natural history and results of treatment. Cancer. 1981; **48**(2): 384-94.